MOLECULAR COORDINATION OF ZEBRAFISH FIN DEVELOPMENT, REGENERATION, AND RAY PATTERNING

By

AMY ELIZABETH ROBBINS

A DISSERTATION
Presented to the Department of Biology
and the University of Oregon Division of Graduate Studies
in partial fulfillment of the requirements
for the degree of
Doctor of Philosophy
June 2023

DISSERTATION APPROVAL PAGE

Student: Amy Robbins

Title: Molecular Coordination of Zebrafish Fin Development, Regeneration, and Ray Patterning

This dissertation has been accepted and approved in partial fulfillment of the requirements for the Doctor of Philosophy degree in the Department of Biology by:

Karen Guillemin	Chairperson
Kryn Stankunas	Advisor
Judith Eisen	Core Member
Charles Kimmel	Core Member
Robert Guldberg	Institutional Representative

and

Krista Chronister	Vice Provost for Graduate Studies

Original approval signatures are on file with the University of Oregon Division of Graduate Studies.

Degree awarded June 2023

DISSERTATION ABSTRACT

Amy Elizabeth Robbins

Doctor of Philosophy

Department of Biology

June 2023

Title: Molecular Coordination of Zebrafish Fin Development, Regeneration, and Ray Patterning

Danio rerio zebrafish fins and human limbs, although outwardly dissimilar, develop using conserved genetic modules. However, unlike humans, zebrafish can perfectly regenerate their fins following amputation or injury. Therefore, understanding the mechanisms underlying fin development and regeneration may improve our understanding of human limb abnormalities and aid the rational design of therapeutics for injury repair. In this dissertation, I use the branched zebrafish caudal fin skeleton as a model system to explore the fundamental question of how appendages form a precisely patterned skeleton. Our lab previously discovered Sonic hedgehog (Shh) signaling is specifically required for fin ray branching during regeneration. In Chapter II, I extend this understanding to demonstrate Shh mediates ray branching during development of all seven zebrafish fins. Further, I find Shh slows the migration of basal epidermal cells as they pass over immature bone in the distal outgrowing fin. This reinforces a potential heterotypic cell association mechanism by which the Shh+ basal epidermis directs branching during ray formation. In Chapter III, I further detail the development of the caudal fin skeleton. I describe how a subset of fin rays, the peripheral principal rays, differs in ontogeny from other fin rays and propose three organizing centers together produce caudal fin symmetry. Chapter IV uses a zebrafish model of Fraser Syndrome to explore how basement membrane-mediated epithelial-mesenchymal associations contribute to ray branching morphogenesis in development and

regeneration. In addition to describing the first adult zebrafish model of Fraser Syndrome, I characterize dramatic fin ray patterning abnormalities including but not limited to unbranched rays. I demonstrate the skeletal patterning abnormalities are Shh signaling-independent, showing the basement membrane (and likely additional extracellular structures) establishes a permissive environment for robust skeletal patterning. Turning back to which signals direct ray branching, I identify *wnt10a*, which is known to be expressed during fin regeneration, as a putative upstream activator of localized basal epidermal *shha.* In Chapter V, I generate fin-deficient *wnt10a* mutants and describe the temporal requirements of Wnt10a for median fin development and regeneration. In Chapter VI, I use the *wnt10a* mutants to demonstrate Wnt10a activates basal epidermal *shha* expression and thereby initiates the cooperative cell behaviors underlying ray branching morphogenesis. Collectively, this dissertation advances our understanding of the molecular control of zebrafish fin development, regeneration, and skeletal patterning.

CIRRICULUM VITAE

NAME OF AUTHOR: Amy Elizabeth Robbins

GRADUATE AND UNDERGRADUTE SCHOOLS ATTENDED:

University of Oregon, Eugene OR
University of Michigan, Ann Arbor MI

DEGREES AWARDED:

Doctor of Philosophy, Biology, 2023, University of Oregon
Bachelor of Science, Evolutionary Anthropology and Japanese Language dual concentration, 2015, University of Michigan

AREAS OF SPECIAL INTEREST:

Developmental Biology
Molecular Genetics
Skeletal Biology
Organogenesis and Regeneration

PROFESSIONAL EXPERIENCE:

Laboratory Manager/ Research Technician Intermediate, Dr. Maureen Devlin Research Group, Murine Skeletal Development, Dept. of Anthropology, University of Michigan, 2015-2017

Undergraduate Research Assistant, Dr. Alon Kahana Research Group, Zebrafish Orbital Development, Dept. of Ophthalmology and Visual Sciences, University of Michigan Kellogg Eye Center 2011-2015

Undergraduate Research Assistant, Dr. Hiroyuki Sasaki Research Group, Murine Epigenetic Regulation, Medical Institute of Bioregulation, Kyushu University, Japan 2013-2014.

Summer Intern, Dr. Hiroyuki Takeda Laboratory, Medaka Polycystic Kidney Disease, Dept. of Biology, University of Tokyo, Japan 2013.

GRANTS, AWARDS, AND HONORS:

2023	Raymond-Stevens Fellow
2022	Pete von Hippel Senior Graduate Award – Research and Service Institute of Molecular Biology, University of Oregon
2020-22	F31-Diversity NRSA Fellow

NIH/NIGMS 5F31GM139343-02, *Mechanisms of Sonic Hedgehog Mediated Skeletal Patterning in Zebrafish Fin Appendages*

2020 Basic Research Pitch Competition Winner and Audience Favorite Winner
Oregon Biosciences Association Digital Conference

2020 Conference Travel Award Recipient – Donald Wimber Fund

2019 Outstanding Graduate Poster Presentation
Institute of Molecular Biology, University of Oregon

2018-20 T32 NRSA Predoctoral Trainee
NIH/University of Oregon Genetics Training Program, T32 GM 007413

2019 First Place Graduate Student Poster Presentation
Society for Developmental Biology, Northwest Meeting

2018 Outstanding New Grad Student Adamson Foundation Endowment Award,
Institute of Molecular Biology, University of Oregon

2015 Japanese National Honors Society
2015 Language Award, University of Michigan Asian Languages & Cultures
2013-15 University of Michigan Academic Honors
2013-14 Heiwa-Nakajima Foundation Sponsored Foreign Scholar
2013 University of Tokyo Research Internship Program Award
2012 University of Michigan Biomedical & Life Sci Summer Research Fellow

PUBLICATIONS:

1. Robbins AE, Braunstein JA, O'Hara-Smith J, Square TA, Miller CT, Stewart S, Stankunas K. Wnt10a activates basal epidermal Sonic hedgehog a expression to initiate zebrafish fin ray branching. *In preparation.*

2. Robbins AE, O'Hara-Smith J, Square TA, Miller CT, Stewart S, Stankunas K. Wnt10a promotes zebrafish median fin development and caudal fin regeneration. *In preparation.*

3. Robbins AE, Horst SG, Lewis VM, Stewart S, Stankunas K. The Fraser Complex interconnects tissue layers to support basal epidermis and osteoblast integrated morphogenesis underlying fin skeletal patterning. *In preparation.*

4. Lewis VM, Le Bleu HK, Henner AL, Markovic H, Robbins AE, Stewart S, Stankunas K. Insulin-like growth factor receptor / mTOR signaling elevates global translation to accelerate zebrafish fin regenerative outgrowth. Dev Biol. 2023 Jun 6: S0012-1606(23)00092-1. doi: 10.1016/j.ydbio.2023.05.008

5. Desvignes, T*, Robbins, AE*, Carey, AZ, Bailon-Zambrano, R, Nichols, JT, Postlethwait, JH, Stankunas, K, 2022. Coordinated patterning of zebrafish caudal fin symmetry by a central and two peripheral organizers. *Developmental Dynamics*. 251, 1306–1321. https://doi.org/10.1002/dvdy.475

   * Indicates co-first authorship

6. Braunstein, JA*, Robbins, AE*, Stewart, S, Stankunas, K, 2021. Basal epidermis collective migration and local Sonic hedgehog signaling promote skeletal branching morphogenesis in zebrafish fins. Dev. Biol. 477, 177–190. https://doi.org/10.1016/J.YDBIO.2021.04.010

   * Indicates co-first authorship

7. Stewart, S, Le Bleu, HK, Yette, GA, Henner, AL, Robbins, AE, Braunstein, JA, Stankunas, K., 2021. longfin causes cis-ectopic expression of the kcnh2a ether-a-go-go K+ channel to autonomously prolong fin outgrowth. *Development*. https://doi.org/10.1242/DEV.199384

8. Robbins, AE, Tom, CATMB, Cosman, MN, Moursi, C, Shipp, L, Spencer, TM, Brash, T, Devlin, MJ, 2018. Low temperature decreases bone mass in mice: Implications for humans. *American Journal of Physical Anthropology*. https://doi.org/10.1002/ajpa.23684

9. Devlin, M., Robbins, AE, Cosman, MN, Moursi, CA, Cloutier, AM, Louis, L, Vliet, M Van, Conlon, C, Bouxsein, M.L., 2018. Differential effects of high fat diet and diet-induced obesity on skeletal acquisition in female C57BL/6J vs. FVB/NJ Mice. *Bone Reports*. https://doi.org/10.1016/j.bonr.2018.04.003

10. Goetz, TG, Mamillapalli, R, Devlin, MJ, Robbins, AE, Majidi-Zolbin, M, Taylor, HS, 2017. Cross-sex testosterone therapy in ovariectomized mice: addition of low-dose estrogen preserves bone architecture. *American Journal of Physiology-Endocrinology and Metabolism.* https://doi.org/10.1152/ajpendo.00161.2017

11. Grzegorski, SJ, Chiari, EF, Robbins, AE, Kish, PE, Kahana, A, 2014. Natural variability of Kozak sequences correlates with function in a zebrafish model. *PLoS One*. https://doi.org/10.1371/journal.pone.0108475

ACKNOWLEDGEMENTS

This dissertation was made possible through the guidance of many advisors and mentors as I found my way. To Dr. Kryn Stankunas, I am fortunate to have done my graduate training in your lab. Thank you for believing in me as my projects waxed, waned, and wandered into uncharted territory. I have grown magnitudes as a scientist. To Dr. Scott Stewart for always pushing me to think critically and for setting an example of discipline for the sake and reward of doing good science. To my incredible dissertation committee, Drs. Karen Guillemin, Charles Kimmel, Judith Eisen, and Robert Guldberg. I am honored to have had the chance to learn under your advisement. To Dr. John Postlethwait, who alongside Dr. Kimmel, welcomed me to the wonderful tradition of zebrafish at UO back in 2018. Completing a Ph.D. in zebrafish biology here is a dream fulfilled.

Thank you to my colleagues, collaborators, and mentees who have assisted directly and indirectly in my research pursuits. Thank you to past and present lab members, especially Dr. Victor Lewis, Astra Henner, Joshua Braunstein, Bryson Ricamona, and Hannah Markovic. You have each taught me so much. Thank you to my collaborators, particularly Drs. Thomas Desvignes and Tyler Square, for your willingness to share your science so we can do cooler stuff than we could alone. I am grateful to my funding sources, which have allowed me to pursue research full time for nearly 5 years. They are as follows: NIH T32 Genetics Training Program GM007413 (2018-20), NIH NIGMS F31 5F31GM139343 (2020-22), and the Raymond-Stevens Fund (2023).

Thank you to my scientific mentors prior to graduate school. To Dr. Alon Kahana, for giving an 18-year-old freshman with no scientific experience a chance and sparking my passion for biomedical research. To Phil, Steve, Alfonso, Bahaar, and Ke'ale for helping me find my

scientific footing, which was not always graceful. To Drs. Hiroyuki Takeda and Sasaki, who let an American undergrad poke around their incredible labs and soak in as much as possible. And finally, to Dr. Maureen Devlin, whose brilliance, enthusiasm, and trust made an independent scientist out of me. This dissertation is influenced by all of you. I try to pay it forward.

I must acknowledge the non-scientific support that has enabled me to complete this work. Thank you to my partner and my dog for being my home, support, and refuge. I love you very much. Thank you to my many circles of idiot friends who help me to never take things too seriously – the M&Bs, Adventure Crabs, Syncytium. You all feed my soul. To the friends who never stop checking in on with even when I don't feel like I have anything to offer, especially Ian, Bootsy, Ryan, and Katie. To my new friends at ACE, who help me to reconnect with parts of myself grad school put on hiatus; to Jojo, who in meeting me as I cross the finish line, reminds me life is full of chaos and wonder. To my family, close and extended, for your support even as you have no frame of reference for what exactly it is that I do. It has been a special experience to get to show you all, at the end of this Ph.D. adventure, what kind of scientist I have become. To Chris, who is nowhere, and everywhere.

So long and thanks for all the fish.

Dedicated to the wonderful, frustrating, beautiful pursuit of the unknown

TABLE OF CONTENTS

TABLE OF FIGURES

CHAPTER I: INTRODUCTION

A fundamental question in biology is how appendages develop the correct size, shape, and pattern. Zebrafish can robustly regenerate fin appendages after injury or amputation, including re-establishing an elaborately branched skeleton of bony rays (Figure 1.1). Defects in signaling dynamics are known to cause skeletal patterning disorders (e.g., polydactyly) in humans (Takamiya et al., 2004; Zhang et al., 2010) . Thus, identifying how zebrafish fins direct skeletal patterning will show how signaling networks control appendage development and facilitate the discovery of therapeutics for congenital bone disorders and skeletal regenerative medicine.

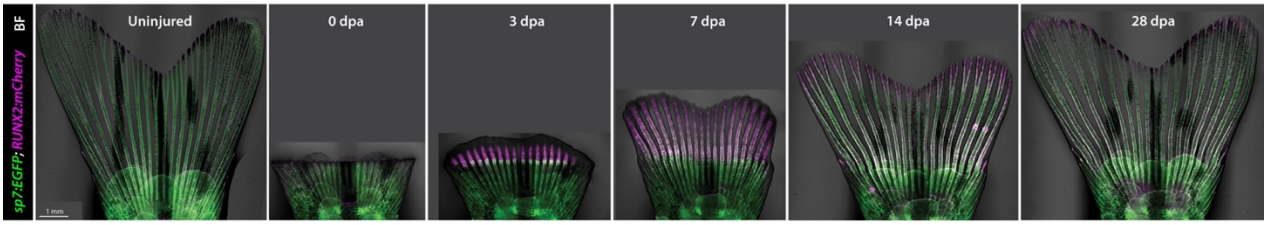

Figure 1.1. Zebrafish caudal fin regeneration time series.

A representative fin at uninjured, 0, 3, 7, 14, and 28 days-post amputation (dpa). Double transgenic fluorescence shows mature osteoblast bone cells in green *Tg(sp7:EGFP)* and immature pre-osteoblasts in magenta *Tg(RUNX2:mCherry)* overlayed with brightfield (BF).

The zebrafish caudal fin has become a leading model of vertebrate appendage regeneration (Grotek et al., 2013; Lee et al., 2009; Poss et al., 2000; Quint et al., 2002; Sehring et al., 2022; Shibata et al., 2018). The caudal fin offers many advantages, such as ease of manipulation, availability of transgenics, and a highly stereotyped skeleton. The caudal fin typically has 18 dermal bony rays called lepidotrichia arranged symmetrically on dorsal and ventral lobes to form a V-shaped fin. The rays are hollow inside, formed by two hemi-rays. The intra-ray space contains blood, immune cells, fibroblasts, and bone-producing osteoblasts among other cell

types. Rays branch as the fin grows, providing a simple but robust skeletal pattern. Older adults form secondary and tertiary branchpoints as the fin isometrically scales with the size of the fish (Arratia et al., 2008; Marí-Beffa et al., 1999; Marí-Beffa and Murciano, 2010).

Upon amputation or injury, the fin initiates a regenerative program that precisely restores its' uninjured size, shape, and pattern. A wound epidermis forms within the first 24 hours-post-amputation (hpa). Next, a highly proliferative regenerative blastema emerges. During blastema establishment and subsequent outgrowth comparmentalized signaling centers form, expressing Wingless-related integration (Wnt), Fibroblast growth factor (Fgf), Bone morphogenic protein (Bmp), and Hedgehog (Hh) signals (Grotek et al., 2013; Nechiporuk and Keating, 2002; Poss et al., 2000a, 2000b). These signaling networks tightly coordinate the regenerative outgrowth phase, during which de-differentiated mature bone cells proximal to the amputation plane re-differentiate back to a mature state and re-populate the regenerating fin (Knopf et al., 2011; Singh et al., 2012; Stewart and Stankunas, 2012). Fin regeneration slows by 14 dpa and is complete by 21-28 dpa.

The signaling families involved in fin regeneration are highly conserved across the animal kingdom (Cass et al., 2021). One pathway, Sonic hedgehog (Shh), has been known since the 1960's as a morphogen specifier of limb digit identity (Riddle et al., 1993; Saunders and Gasseling, 1983, 1968). Perturbations to the Shh signaling pathway cause congenital limb deformities including absent digits, as well as disease states such as cancers (Anderson et al., 2012; Chen et al., 2013; Chiang et al., 2001; Letelier et al., 2021; Zeng et al., 2017). The zebrafish ortholog of Shh expressed in fins, Shha, is expressed in basal epidermal domains at the

distal end of each fin ray (Laforest et al., 1998; Quint et al., 2002). Our lab previously discovered inhibition of Shha by chemical inhibition of its downstream effector Smoothened (Smo) prevents ray branching in regenerating fins but does not impact outgrowth (Armstrong et al., 2017). This finding was made more surprising as *shha*-expressing basal epidermal cells are immediately adjacent to immature bone cells (pre-osteoblasts, pObs), in contrast to its well-characterized role as a long-range morphogen in limb buds. Thus, ray branching morphogenesis provides an accessible skeletal patterning model to study short-range Shh signaling.

In Chapter II, I first sought to determine if regenerative Shh-mediated ray branching is conserved developmentally. This study was completed in collaboration with Mr. Joshua Braunstein and evaluated the assumption that developmental mechanisms were re-deployed during regeneration with ray branching as no exception. We not only confirm *shha* enables caudal fin ray branching during development, we also found this mechanism is conserved in all seven zebrafish fin appendages. Additionally, we leveraged the small size of the developing caudal fin relative to regenerating adults to pioneer new time-lapse imaging techniques. These assays revealed *shha*-expressing cells slow their migration as they pass over pOb regions, apparently "pulling" pObs into a branch point (Braunstein et al., 2021). This exciting finding has opened a new area of research seeking to identify the exact mechanisms in which skin cells manipulate immature bone into position.

Chapter III is a deep dive into the development of the caudal fin, focusing on the ontogeny of caudal fin rays. This collaborative project, utilizing many transgenic lines and musculoskeletal markers, offered a unique opportunity for collaboration as it spanned multiple departments and

institutions. The resulting work was conducted in collaboration with Dr. Thomas Desvignes with support from Dr. James T. Nichols, Mr. Andrew Carey, and Ms. Raisa Bailion-Zombrano and supervision by Drs John Postelthwait and Kryn Stankunas. In this paper we characterized a subset of the caudal fin's 18 principal rays, that we term the peripheral principal rays, which differ in their ontogeny and musculoskeletal connections from the other central principal rays. Once again, I developed new imaging techniques for this study to visualize caudal fin ray development in immobilized larvae real time. Ultimately, we propose a central and two peripheral organizers pattern the caudal fin rays (Desvignes et al., 2022).

Chapter VI focuses on the contribution of the extracellular matrix environment during fin ray branching. I used a zebrafish genetic model of Fraser Syndrome, *fras1*^{te262}, to investigate how disrupted adhesion between epithelial and mesenchymal tissue layers impact caudal fin development and regeneration. I describe adult *fras1* mutants for the first time and characterize striking fin ray abnormalities reminiscent of digit mispatterning in human Fraser Syndrome. This work demonstrates the extracellular matrix environment supports robust fin skeletal patterning independent of Shh signaling. Additionally, we promote a new model in which to study Fraser Syndrome-related mechanisms.

Chapters V and VI were inspired by a key unresolved question in fin ray branching: how is *shha* transcription transiently activated in a subset of basal epidermal cells only in close proximity to pObs? This answer ultimately would identify the upstream regulator of ray branching. We first confirmed Wnt/β-catenin signaling functions upstream of *shha,* extending previous reports (Wehner et al., 2014). I next identified *wnt10a* as a promising activator of *shha* due to its

expression levels and location (Grotek et al., 2013; Stewart et al., 2019; Stoick-Cooper et al., 2007a; Wehner et al., 2014). I then mutagenized *wnt10a* using CRISPR/Cas9 technology, predicting fin ray patterning abnormalities and/or a reduction in *shha* expression. Unexpectedly, the resulting mutants were strikingly fin-reduced with no dorsal or anal fins and variably truncated caudal fins. Chapter V details the developmental and regenerative contributions of *wnt10a* to median fin development. I identified a critical window of 1-2 days-post-fertilization as highly dependent on *wnt10a* activity for development of the median fin fold from which the dorsal, anal, and caudal fins develop. I then characterized regenerative defects in *wnt10a* mutants that form partial caudal fins. Finally, I demonstrated ectopic *wnt10a* induction using a heat-shock inducible transgene rescues the median fin fold, partially rescues both median fin development and regenerative capacity.

Finally, Chapter VI focuses on *shha* expression and branching morphogenesis in the *wnt10a* mutants. I found *shha* expression is specifically disrupted in the partial caudal fins of *wnt10a* mutants but not in other organs known to be patterned by Shh. Consistent with our hypothesized *wnt10a-shha* interaction, I found the caudal fin rays of *wnt10a* mutants rarely branched. Heat shock induction of *wnt10a* during regeneration rescued both *shha* expression and ray branching in *wnt10a* mutants with partial caudal fins. The work presented in my dissertation details caudal development and regeneration, presents novel imaging techniques, considers how the extracellular environment impacts bone morphogenesis in a disease model, generates genetic fin loss mutants, and rescues fin phenotypes using transgenics. Taken together, this research expands our understanding of fin ray branching and leaves exciting new questions of study.

REFERENCES

Anderson, E., Peluso, S., Lettice, L.A., Hill, R.E., 2012. Human limb abnormalities caused by disruption of hedgehog signaling. Trends Genet. 28, 364–373. https://doi.org/10.1016/j.tig.2012.03.012

Armstrong, B.E., Henner, A., Stewart, S., Stankunas, K., 2017. Shh promotes direct interactions between epidermal cells and osteoblast progenitors to shape regenerated zebrafish bone. Dev. 144, 1165–1176. https://doi.org/10.1242/dev.143792

Arratia, G., Schultze, H.-P., Wilson, M.V.H., 2008. Actinopterygian postcranial skeleton with special reference to the diversity of fin ray elements, and the problem of identifying homologies, in: Mesozoic Fishes 4 – Homology and Phylogeny. pp. 49–101.

Braunstein, J.A., Robbins, A.E., Stewart, S., Stankunas, K., 2021. Basal epidermis collective migration and local Sonic hedgehog signaling promote skeletal branching morphogenesis in zebrafish fins. Dev. Biol. 477, 177–190. https://doi.org/10.1016/J.YDBIO.2021.04.010

Cass, A.N., Elias, A., Fudala, M.L., Knick, B.D., Davis, M.C., 2021. Conserved mechanisms, novel anatomies: The developmental basis of fin evolution and the origin of limbs. Diversity 13, 1–17. https://doi.org/10.3390/d13080384

Chen, J.-S., Huang, X., Wang, Q., Huang, J.-Q., Zhang, L., Chen, X.-L., Lei, J., Cheng, Z.-X., 2013. Sonic hedgehog signaling pathway induces cell migration and invasion through focal adhesion kinase/AKT signaling-mediated activation of matrix metalloproteinase (MMP)-2 and MMP-9 in liver cancer. Carcinogenesis 34, 10–19. https://doi.org/10.1093/carcin/bgs274

Chiang, C., Litingtung, Y., Harris, M.P., Simandl, B.K., Li, Y., Beachy, P.A., Fallon, J.F., 2001. Manifestation of the Limb Prepattern: Limb Development in the Absence of Sonic Hedgehog Function. Dev. Biol. 236, 421–435. https://doi.org/10.1006/dbio.2001.0346

Desvignes, T., Robbins, A.E., Carey, A.Z., Bailon-Zambrano, R., Nichols, J.T., Postlethwait, J.H., Stankunas, K., 2022. Coordinated patterning of zebrafish caudal fin symmetry by a central and two peripheral organizers. Dev. Dyn. 251, 1306–1321. https://doi.org/10.1002/dvdy.475

Grotek, B., Weidinger, G., Wehner, D., 2013. Notch signaling coordinates cellular proliferation with differentiation during zebrafish fin regeneration. Development 140, 1412–1423. https://doi.org/10.1242/dev.087452

Knopf, F., Hammond, C., Chekuru, A., Kurth, T., Hans, S., Weber, C.W., Mahatma, G., Fisher, S., Brand, M., Schulte-Merker, S., Weidinger, G., 2011. Bone regenerates via dedifferentiation of osteoblasts in the zebrafish fin. Dev. Cell 20, 713–724. https://doi.org/10.1016/j.devcel.2011.04.014

Laforest, L., Brown, C.W., Poleo, G., Géraudie, J., Tada, M., Ekker, M., Akimenko, M.A., 1998. Involvement of the sonic hedgehog, patched 1 and bmp2 genes in patterning of the zebrafish dermal fin rays. Development 125, 4175–4184.

Lee, Y., Hami, D., Val, S. De, Kagermeier-Schenk, B., Wills, A.A., Black, B.L., Weidinger, G., Poss, K.D., 2009. Maintenance of blastemal proliferation by functionally diverse epidermis in regenerating zebrafish fins. Dev. Biol. 331, 270–280. https://doi.org/10.1016/j.ydbio.2009.05.545

Letelier, J., Naranjo, S., Sospedra-Arrufat, I., Ramon Martinez-Morales, J., Lopez-Rios, J., Shubin, N., Gomez-Skarmeta, J.L., 2021. The Shh/Gli3 gene regulatory network precedes the origin of paired fins and reveals the deep homology between distal fins and digits. Proc. Natl. Acad. Sci. U. S. A. 118, 1–7. https://doi.org/10.1073/pnas.2100575118

Marí-Beffa, M., Palmqvist, P., Marín-Girón, F., Montes, G.S., Becerra, J., 1999. Morphometric study of the regeneration of individual rays in teleost tail fins. J. Anat. 195, 393–405. https://doi.org/10.1017/S0021878299005464

Marí-Beffa, M., Murciano, C., 2010. Dermoskeleton morphogenesis in zebrafish fins. Dev. Dyn. 239, 2779–2794. https://doi.org/10.1002/dvdy.22444

Nechiporuk, A., Keating, M.T., 2002. A proliferation gradient between proximal and msxb - expressing distal blastema directs zebrafish fin regeneration. Development 129, 2607–2617. https://doi.org/10.1242/dev.129.11.2607

Poss, K.D., Shen, J., Keating, M.T., 2000. Induction of lef1 during zebrafish fin regeneration. Dev. Dyn. 219, 282–286. https://doi.org/10.1002/1097-0177(2000)9999:9999<::AID-DVDY1045>3.3.CO;2-3

Poss, K.D., Shen, J., Nechiporuk, A., McMahon, G., Thisse, B., Thisse, C., Keating, M.T., 2000. Roles for Fgf signaling during zebrafish fin regeneration. Dev. Biol. 222, 347–358. https://doi.org/10.1006/dbio.2000.9722

Quint, E., Smith, A., Avaron, F., Laforest, L., Miles, J., Gaffield, W., Akimenko, M.-A., 2002. Bone patterning is altered in the regenerating zebrafish caudal fin after ectopic expression of sonic hedgehog and bmp2b or exposure to cyclopamine. Proc. Natl. Acad. Sci. 99, 8713–8718. https://doi.org/10.1073/pnas.122571799

Riddle, R.D., Johnson, R.L., Laufer, E., Tabin, C.J., 1993. Sonic hedgehog mediates the polarizing activity of the ZPA. Cell 75, 1401–1416.

Saunders, J.W., Gasseling, M., 1968. Ectodermal-mesenchymal interaction in the origin of limb symmetry. Ep. Interact. 78–97.

Saunders, J.W., Gasseling, M., 1983. New insights into the problem of pattern regulation in the limb bud of the chick embryo. Limb Dev. Regul. 67–76.

Sehring, I., Mohammadi, H.F., Haffner-Luntzer, M., Ignatius, A., Huber-Lang, M., Weidinger, G., 2022. Zebrafish fin regeneration involvgeneric and regeneration-specifiosteoblast injury responses. Elife 11, 1–28. https://doi.org/10.7554/eLife.77614

Shibata, E., Ando, K., Murase, E., Kawakami, A., 2018. Heterogeneous fates and dynamic rearrangement of regenerative epidermis-derived cells during zebrafish fin regeneration. Development 145, dev.162016. https://doi.org/10.1242/dev.162016

Singh, S.P., Holdway, J.E., Poss, K.D., 2012. Regeneration of Amputated Zebrafish Fin Rays from De Novo Osteoblasts. Dev. Cell 22, 879–886. https://doi.org/10.1016/j.devcel.2012.03.006

Stewart, S., Gomez, A.W., Armstrong, B.E., Henner, A., Stankunas, K., 2014. Sequential and Opposing Activities of Wnt and BMP Coordinate Zebrafish Bone Regeneration. Cell Rep. 6, 482–498. https://doi.org/10.1016/j.celrep.2014.01.010

Stewart, S., Stankunas, K., 2012. Limited dedifferentiation provides replacement tissue during zebrafish fin regeneration. Dev. Biol. 365, 339–349. https://doi.org/10.1016/j.ydbio.2012.02.031

Stewart, S., Yette, G.A., Le Bleu, H.K., Henner, A.L., Braunstein, J.A., Chehab, J.W., Harms, M.J., Stankunas, K., 2019. Skeletal geometry and niche transitions restore organ size and shape during zebrafish fin regeneration. bioRxiv. https://doi.org/https://doi.org/10.1101/606970

Stoick-Cooper, C.L., Weidinger, G., Riehle, K.J., Hubbert, C., Major, M.B., Fausto, N., Moon, R.T., 2007. Distinct Wnt signaling pathways have opposing roles in appendage regeneration. Development 134, 479–489. https://doi.org/10.1242/dev.001123

Takamiya, K., Kostourou, V., Adams, S., Jadeja, S., Chalepakis, G., Scambler, P.J., Huganir, R.L., Adams, R.H., 2004. A direct functional link between the multi-PDZ domain protein GRIP1 and the Fraser syndrome protein Fras1. Nat. Genet. 36, 172–177. https://doi.org/10.1038/ng1292

Wehner, D., Cizelsky, W., Vasudevaro, M.D., Özhan, G., Haase, C., Kagermeier-Schenk, B., Röder, A., Dorsky, R.I., Moro, E., Argenton, F., Kühl, M., Weidinger, G., 2014. Wnt/β-Catenin Signaling Defines Organizing Centers that Orchestrate Growth and Differentiation of the Regenerating Zebrafish Caudal Fin. Cell Rep. 6, 467–481. https://doi.org/10.1016/j.celrep.2013.12.036

Zeng, C., Chen, T., Zhang, Y., Chen, Q., 2017. Hedgehog signaling pathway regulates ovarian cancer invasion and migration via adhesion molecule CD24. J. Cancer 8, 786–792. https://doi.org/10.7150/jca.17712

Zhang, J., Wagh, P., Guay, D., Sanchez-Pulido, L., Padhi, B.K., Korzh, V., Andrade-Navarro, M.A., Akimenko, M.A., 2010. Loss of fish actinotrichia proteins and the fin-to-limb transition. Nature 466, 234–237. https://doi.org/10.1038/nature09137

CHAPTER II: BASAL EPIDERMIS COLLECTIVE MIGRATION AND LOCAL SONIC HEDGEHOG SIGNALING PROMOTE SKELETAL BRANCHIING MORPHOGENESIS IN ZEBRAFISH FINS

Published in *Developmental Biology* May 2021

Joshua A. Braunstein[1, 2, #], Amy E. Robbins[1, 2, #], Scott Stewart[1], Kryn Stankunas[1, 2, *]

# Equal contributions

[1]Institute of Molecular Biology
[2]Department of Biology
University of Oregon
273 Onyx Bridge
1318 Franklin Blvd
Eugene, OR 97403-1229
Office: (541) 346-7416
Fax: (541) 346-4854

* Correspondence: kryn@uoregon.edu

INTRODUCTION

The diversity and beauty of fish fins has long captivated aquarists while providing compelling models to consider morphological evolution and organ patterning. Fins' intricate skeletons, comprised of elongated dermal bony rays and body-proximal endochondral bones, support swimming biomechanics and define appendage shape. Most rays, or lepidotrichia, branch one or more times to elaborate the skeletal network. Fin rays, as well as ancestral unpaired medial fins, were lost during the fish-to-tetrapod transition (Freitas et al., 2014). Paired pectoral and pelvic fins and their endochondral bones evolved into tetrapod limbs. However, fin rays and limb digits may share deep evolutionary homology (Nakamura et al., 2016). Comparing skeletal patterning

between paired and unpaired fins, including the prominent caudal fin, can reveal core appendicular development mechanisms and those underlying evolutionary innovations.

Danio rerio zebrafish are widely studied teleost fish with branched rays in all paired and unpaired fins. For example, zebrafish caudal fins typically have 18 rays of which the central 16 branch into "daughter" rays (Figure S2.1A). Juvenile fish form primary branches around 30 days post fertilization (dpf) followed by secondary and tertiary branches. Individual rays comprise two opposed hemi-rays that form cylindrical skeletal units segmented by joints and enveloped by a multilayered epidermis (Figure S2.1B). Zebrafish fully regenerate adult fins including restoring a branched ray skeleton within two weeks of injury. Empowered by versatile genetic and other tools, zebrafish have become a leading model for appendage regeneration research. Collective studies implicate many of the same signaling pathways, including Wnt, Bmp, Fgf, retinoic acid, and Hh, involved in tetrapod limb development (Reviewed in Sehring and Weidinger, 2019). Therefore, zebrafish fin development and regeneration provide complementary contexts to understand how cell signaling patterns the appendicular skeleton and how the same pathways are reactivated for repair. Further, zebrafish fins and their rays enable studies of fundamental developmental questions, including how branched networks form – a common property of many organs including vasculature, lungs, kidneys, mammary glands, and pancreas.

Sonic hedgehog (Shh) signaling through its Smoothened (Smo) effector is one pathway dually involved in fin regeneration and appendage development. Shh is associated closely with tetrapod limb skeletal patterning (Zuniga, 2015) and Shh/Smo pathway perturbations cause syndactyly and polydactyly (Anderson et al., 2012; Malik, 2012). Shh is the Zone of Polarizing Activity

(ZPA) morphogen that pre-patterns the limb bud into distinct skeletal units, including digits (Chiang et al., 2001; Riddle et al., 1993; Saunders and Gasseling, 1968). Zebrafish *shha* expression studies suggest a ZPA patterns pectoral and other paired fins but not unpaired fins including the caudal fin (Hadzhiev et al., 2007; Laforest et al., 1998). Nevertheless, *shha* is expressed in distal epidermal domains overlying each forming ray during caudal fin development and regeneration (Armstrong et al., 2017; Hadzhiev et al., 2007; Laforest et al., 1998; Lee et al., 2009; Zhang et al., 2012). At least during regeneration, each *shha*-expressing domain splits prior to ray branching. We leveraged the highly specific Smo inhibitor BMS-833923 (BMS) to show Shh/Smo specifically promotes ray branching during zebrafish caudal fin regeneration (Armstrong et al., 2017). However, a potentially similar Shh/Smo role during developmental ray branching of all fins and underlying mechanisms are unresolved.

During caudal fin regeneration, distal-moving basal epidermal cells (bEps) adjacent to bony rays upregulate *shha* at the distal "progenitor zone" (Armstrong et al., 2017; Figure S2.1C). Shh-expressing bEps activate Hedgehog/Smoothened (Hh/Smo) signaling in themselves and immediately adjacent pre-osteoblasts (pObs) as marked by *patched2* (*ptch2*), which encodes a Hh receptor and universal negative feedback regulator (Alexandre et al., 1996; Goodrich et al., 1996; Lorberbaum et al., 2016; Marigo et al., 1996). This short-range Hh/Smo signaling is required to split pOb pools and therefore ray branching without impacting proliferation or differentiation. While Hh/Smo signaling is active continuously, *shha*-expressing basal epidermal domains split laterally prior to pOb partitioning (Figure S2.1D). We proposed Shh/Smo signaling might enhance physical associations between moving epidermal cells and pObs to enable the progressive partition of pOb pools (Armstrong et al., 2017). However, this model has not been

assessed during fin development or expanded on by visualization of cell movement dynamics in live animals.

Here, we explore the mechanisms underlying developmental fin ray branching in both paired and unpaired fins of juvenile zebrafish. We show basal epidermal dynamics as well as Shh/Smo activity and function are largely the same as during regeneration. We use transgenic reporter lines for *shha* and its target gene *ptch2* to refine developmental expression profiles. Kaede photoconversion of *TgBAC(ptch2:Kaede)* fish reveals continuous Shh/Smo signaling in distal ray Shh+ basal epidermal domains and neighboring pObs. We inhibit Shh/Smo signaling using the small molecule BMS-833923 to show the pathway is largely dedicated to ray branching in all fins, including paired fins. Shh+ bEps and pObs are closely apposed at the site of Shh/Smo signaling where a basement membrane is incompletely assembled. bEps constantly move distally, trafficking through while contributing to *shha*-expressing domains that split laterally prior to ray branching. We use live time-lapse imaging to demonstrate Shh/Smo signaling restrains basal epidermal distal migration, possibly by transiently coupling *shha*+ bEps to distal ray pObs. We conclude the collective migration of bEps, constantly distal with progressive lateral domain splitting, and their atypical use of local Shh/Smo signaling re-positions pObs for skeletal branching during both fin development and regeneration. This reflects a unique branching morphogenesis process whereby movements of a neighboring cell type – the bEps – guides the tissue-forming cells – the pObs – into split pools.

RESULTS

Shha expression is progressively restricted to distal ray basal epidermal domains that split preceding ray branching

Developing fins express *sonic hedgehog a* (*shha*) in single basal epidermal domains adjacent to the tip of each hemi-ray up to 20 days post fertilization (dpf) (Hadzhiev et al., 2007; Laforest et al., 1998). During caudal fin regeneration, similar *shha*-positive basal epidermal domains split into distinct domains around 4 days post amputation (dpa) immediately preceding ray branching (Armstrong et al., 2017; Laforest et al., 1998; Lee et al., 2009; Quint et al., 2002; Zhang et al., 2012). We expected a comparable pattern during fin development if branching during fin regeneration recapitulates developmental processes. We used the reporter line *Tg(-2.4shha:gfpABC)*^{sb15}, which mimics endogenous *shha* expression (*shha:GFP*; (Ertzer et al., 2007; Zhang et al., 2012), to monitor *shha* expression in live zebrafish from its emergence through primary ray branching in juveniles around 30 dpf. *shha:GFP* expression in the caudal region was restricted to the developing floor plate and notochord through 5 dpf, as previously established (Krauss et al., 1993). From 5-9 dpf, *shha:GFP* expression expanded into the caudal fin fold primordium through a ventral gap of melanophores (Figure 2.1A, white arrowhead). By 9-10 dpf, *shha:GFP*+ cells were enriched along emerging immature rays (Figure 2.1B). At 10-12 dpf, *shha:GFP* expression became specifically associated with the distal aspect of maturing central rays while remaining along the lengths of immature peripheral rays (Figure 2.1C). *shha:GFP* was restricted to ray tips by 14 dpf, when all rays contained maturing, segmented bone (Figure 2.1D).

The *shha:GFP* domains began splitting around 30 dpf, immediately prior to branching of the corresponding ray (Figure 2.1I, I', white brackets). We used whole mount immunostaining for

GFP and the basal epidermal marker Tp63 (Lee and Kimelman, 2002) and 3D confocal reconstructions to confirm *shha*-driven GFP was expressed exclusively in basal epidermal cells (bEps) (Figure 2.1K, L; expanded data in Figure S2.2). Where Tp63-marked cells were multi-layered (magenta dashed line, Figure 2.1K), only the innermost cells expressed GFP. Similar *shha* expression patterns, including *shha*+ bEp domain splitting, support a common Shh/Smo-dependent mechanism for both developmental and regenerative ray branching.

Zebrafish have 3 unpaired (dorsal, anal, and caudal) and 4 paired (pectoral and pelvic) fin appendages, each with a branched dermoskeleton. We explored if *shha:GFP* domains split ahead of developmental ray branching in all fins. We imaged dissected fins from 51 dpf juvenile fish carrying *shha:GFP* and *Tg(runx2:mCherry)* (*runx2:mCherry*; Shannon Fisher Lab, unpublished; Barske et al., 2020), which marks *runx2*+ pre-osteoblasts (pObs) and then perdures in differentiated Obs along ray lengths. *shha:GFP* was expressed at and slightly distal to the *runx2:mCherry*+ pOb-defined fin boundary in all seven fins, including paired pectoral and pelvic fins (Figure S2.3). In all cases, branching rays were tipped with two distinct *shha:GFP*+ domains, suggesting shared Shh/Smo-promoted ray branching regardless of fin evolutionary or morphological divergence.

Ptch2 expression indicates Hh/Smo activity in basal epidermis and pre-osteoblasts

We next assessed expression of *ptch2*, a Hh/Smo negative feedback regulator and activity marker (Alexandre et al., 1996; Goodrich et al., 1996; Lorberbaum et al., 2016; Marigo et al., 1996). Hh/Smo signaling induces *ptch2* in pObs and neighboring bEps during caudal fin regeneration (Armstrong et al., 2017; Quint et al., 2002). *ptch2* is also expressed in distal regions of late larval

caudal fins, although cell-level expression is unresolved (Laforest et al., 1998). We imaged the *TgBAC(ptch2:kaede)*^{a4596} reporter line (*ptch2:Kaede*; Huang et al., 2012) at the same developmental time points we examined *shha:GFP*. *ptch2:Kaede* expression was confined to the notochord and floor plate until ~9 dpf (Figure 2.1E). By 9-10 dpf, *ptch2:Kaede* was associated with nascent rays in the ventrally expanding fin primordium (Figure 2.1F). At 10-12 dpf, *ptch2:Kaede* was detected along the entire length of each ray (Figure 2.1G). This pattern, which includes past *ptch2* expression due to prolonged Kaede stability, persisted through 14 dpf with notably higher *ptch2:Kaede* expression associated with joints and distal ray tips, matching its pattern in regenerating fins (Figure 2.1H; Armstrong et al., 2017). As with *shha:GFP*, *ptch2:Kaede*+ domains split as ray branching initiated in 30-33 dpf juvenile fish (Figure 2.1J, J').

To define the cell types expressing *ptch2* during caudal fin development, we combined *ptch2:Kaede* with *runx2:mCherry* and *shha:GFP* to mark *runx2*+ pObs and *shha*+ bEps, respectively (Figure 2.1M-P and expanded data with single channel images in Figure S4). Confocal imaging of live 19 dpf double transgenic larval fish showed *ptch2:Kaede* co-localized with distal fin *runx2:mCherry*-expressing pObs (Figure 2.1M, N). Only adjacent and further distal presumptive bEps additionally expressed *ptch2:Kaede.* We used photoconversion to discern Kaede from GFP and reveal non-pOb *ptch2:Kaede* co-localized with *shha:GFP*-expressing and nearby bEps (Figure 2.1O, P). Therefore, *ptch2* defines autocrine (in bEps) and short-range (in pObs and non-*shha*+ bEps) Shh/Smo signaling during caudal fin development.

Active Shha/Smo signaling is restricted to outgrowing distal ray regions

We photoconverted distal ray ends of 25 dpf *ptch2:Kaede* caudal fins (Figure 2.2A-C) and re-imaged 24 hours later (Figure 2.2D-F) to distinguish actively produced Kaede from perduring reporter fluorescence (experimental schematic in Figure 2.2G). New, unconverted Kaede was produced exclusively in short, discrete domains at the ray tips (Figure 2.2D, F). Therefore, active Shh/Smo signaling appears narrowly focused in close proximity with *shha*-expressing bEps. We also observed a stretch of photoconverted Kaede+ cells distal to the ray tips in tissue newly formed over the 24-hour post-conversion period (Figure 2.2F'). We saw a similar pattern during fin regeneration and likewise identify the cells as distal-moving bEps given their broader domain and more distal location than ray-forming osteoblasts (Armstrong et al., 2017). Therefore, previously Shh-responsive bEps rapidly cease *ptch2* expression as they collectively move beyond the Shh/Smo active zone.

We used the potent Smo inhibitor BMS-833923 (Armstrong et al., 2017; Lin and Matsui, 2012; henceforth abbreviated BMS) to confirm *ptch2:Kaede* reports Shh/Smo activity during fin development. As expected, caudal fins of 25 dpf fish treated with 1.25 μM BMS and photoconverted 3 hours later produced no new Kaede 24 hours post-conversion (hpc; Figure 2.2G-L). Curiously, we no longer observed distally displaced photoconverted Kaede+ bEps with the remaining photoconverted Kaede narrowly associated with ray tips and therefore likely pObs (Figure 2.2F', L'). We surmise the 24-hour Shh/Smo-inhibition led distal-moving Kaede+ bEps to shed prematurely, leaving only photoconverted Kaede+ pObs. As such, Shh/Smo signaling may retard distal bEp collective movements.

Sustained Shh/Smo signaling promotes ray branching during fin development

We next investigated if Shh/Smo is required for ray branching during fin development. Treating *Tg(sp7:EGFP)*^{b1212} osteoblast reporter fish (*sp7:EGFP*; DeLaurier et al., 2010) with 0.63 μM BMS from 25 to 42 dpf blocked caudal fin ray branching (Figure 2.3A-D, *n*=5 per BMS and DMSO control groups). In contrast, Shh/Smo-inhibition did not disrupt caudal fin outgrowth or skeletal maturation, indicated by well-defined cylindrical bony ray segments complete with joints, of the central 16 rays (Figure S2.5). Curiously, the non-branching principal peripheral rays uniquely were shorter in BMS-treated fish (Figure 2.3A, C white arrows and Figure S2.5). BMS-treatment of 29 dpf *shha:GFP* fish exposed to EdU for 12 hours did not change the fraction of EdU+ intra-ray cells, i.e. pObs and mesenchyme nestled between the epidermal Shh+ domains of each hemi-ray (Figure S2.6, *n*=5 per group). We conclude Shh/Smo signaling is largely dedicated to ray branching with minimal proliferation or bone maturation effects during both fin development and, as shown previously, regeneration (Armstrong et al., 2017).

Shh/Smo signaling may act transiently to initiate ray branching or continuously during the branching process. To distinguish between these possibilities, we staggered the start of BMS treatment to "before", "during", or "after" branching (Figure 2.3E), identified by *a priori* screening 24-35 dpf *sp7:EGFP* clutchmate fish. Expectedly, BMS-exposure initiated prior to ray branching prevented said rays from branching ("before" group, Figure 2.3F, G, G', *n*=4/4) and rays that had already fully branched remained so after BMS treatment ("after" group, J, K, K', *n*=4/4). However, rays that recently initiated branching ("during" group, Figure 2.3H) re-fused upon BMS exposure, forming "gapped" ray segments (Figure 2.3I, I', *n*=4/5). Therefore, sustained Shh signaling acts throughout ray branching morphogenesis rather than as a switch that initiates branching.

Shh/Smo signaling does not substantially contribute to initial fin ray patterning

shha and *ptch2* expression during early stages of caudal fin formation (Figure 2.1B, E), while non-polarized, is reminiscent of Shh's ZPA role in paired appendages. This pattern suggests Shh/Smo may influence early caudal fin skeletal patterning in addition to promoting later, juvenile-stage ray branching. To explore this possibility, we inhibited Shh/Smo signaling from as early as 2 dpf, when the larval fin fold entirely comprises soft tissue absent of any ray structures. As expected, *ptch2:Kaede*-marked Shh/Smo signaling was restricted to the notochord and floor plate at this stage (Figure S2.7A-C). Photoconversion experiments confirmed BMS fully inhibited production of new *ptch2:Kaede* in 14 dpf larval caudal fins (Figure S2.7D-E', total *n*=33-44 per group), as with embryos, juvenile fins, and regenerating adult fins (Figure 2.2G-L; (Armstrong et al., 2017). We treated *sp7:EGFP;runx2:mCherry* fish with 1.25 μM BMS from 2 until 14 dpf, when all 18 rays were clearly established. Their caudal fins developed the standard complement of 18 rays with a central diastema and apparently normal length distribution across the dorsal-ventral axis to define typical "V-shaped" fins (Figure S2.7F-G'). As such, Shh/Smo may have limited or no role in pre-patterning the caudal fin field despite early *shha* and *ptch2* expression.

Shh/Smo signaling supports ray branching in all fins

We tested if Shh/Smo signaling promotes ray branching in all seven fins, paired and unpaired, by treating *shha:GFP;runx2:mCherry* fish with BMS starting at 21 dpf, prior to asynchronous ray branching across fins. As expected, both DMSO control and BMS-treated fish showed *shha:GFP+* domains at the distal end of every ray of all fins at 42 dpf (Figure 2.4). However, BMS-treated fish showed no or, at best, severely delayed branching in all fins (*n*=6 per group). The rare, delayed branching likely reflects incomplete Shh/Smo inhibition due to the challenge of sustaining

effective drug concentrations across a multi-week treatment. Nevertheless, the near absence of branchpoints confirms all fins employ a common Shh/Smo signaling-dependent mechanism for ray branching irrespective of their evolutionary divergence, including the apparent *shha*-defining ZPA in paired fins (Hadzhiev et al., 2007; Laforest et al., 1998).

Shha+ basal epidermis and pre-osteoblasts are intimately associated in developing caudal fins

We next aimed to identify how sustained, local Shh/Smo signaling affects bEp and/or pOb cell behaviors to promote ray branching morphogenesis. The close proximity of these two Shh-responsive cell types suggested their movements might be physically coupled in a Shh/Smo-dependent manner to promote branching. To assess potential physical contacts between bEps and pObs, we first stained longitudinal sections of 32 dpf juvenile fin rays from *shha:GFP* fish with GFP, the osteoblast marker Zns-5, and Laminin, a component of the epidermal-osteoblast separating basement membrane. As expected, Shha:GFP+ bEps were directly adjacent to pObs (Figure S8). A thin Laminin-containing basement membrane separated pObs and the proximal-most Shha:GFP+ bEps that had recently arrived in the active zone and initiated *shha* expression. More distally, the double staining for Shha:GFP+ bEps and Zns-5+ pObs produced even partially overlapping signal (Figure S2.8D and D'), suggesting the two cell types are intimately associated. Here, the Laminin+ basement membrane was less dense and sometimes fragmented, likely reflecting its nascent production (Figure S2.8 asterisks, D').

We further explored the relative positioning of bEps and pObs at the onset of ray branching by 3D confocal reconstructions of live imaged fins of 28 dpf *shha:GFP;runx2:mCherry* fish (Figure

2.5A-C). *shha:GFP*+ bEps and *runx2:mCherry*+ pObs were tightly juxtaposed in both hemi-rays of a single lepidotrichia (Movie 2.1). Focusing on one hemi-ray, we observed extensive apparent heterotypic contacts, including areas where *shha:GFP*+ bEps enshrouded a ridge of pObs (Movie 2.2). Single sagittal optical slices and reconstructed slice equivalents examined multi-dimensionally (Figure 2.5D-F) confirmed closely juxtaposed bEps and pObs.

We considered if Shh/Smo signaling promotes the juxtaposition of bEps and pObs. However, BMS treatment of *shha:GFP;runx2:mCherry* fish from 24-34 dpf did not alter the intimate association between Shh+ bEps and Runx2+ pObs in static images of live fins even though the same drug exposure prevented ray branching to 42 dpf (Figure S2.9). As expected, Runx2+ pOb pools failed to split upon BMS exposure, even when *shha:GFP* domains still did. The *shha:GFP* domains of BMS-treated fish variably appeared to remain as one cluster per hemi-ray (Figure S9E, J; 4/10 split for dorsal ray 3). In contrast, our fin regeneration study indicated Shha-domain splitting is always Shh/Smo-independent (Armstrong et al., 2017). The difference could reflect difficulty visualizing the initial splitting of the smaller *shha:GFP* domains of juvenile fins. Further, constant *shha* production throughout fin growth, not just at branching, seemingly precludes a direct Shh/Smo role in periodically splitting bEp domains. Regardless, Shh/Smo signaling does not support ray branching by promoting close proximity between bEps and pObs per se.

Shh/Smo signaling restrains basal epidermal collective movements while adjacent to pObs

Shh/Smo inhibition appeared to increase the rate of bEp shedding due to accelerated distal collective movements (Figure 2.2I, L). Therefore, we considered if Shh/Smo transiently couples bEps and pObs by direct cell-to-cell adhesion or through intermediary connections that impede

bEp movements while they neighbor relatively stable pObs. Such regulated heterotypic associations, which may not be evident by static imaging, coupled with force-generating bEp collective movements during *shha*+ domain splitting, could re-position pOb pools over time. We time-lapse imaged caudal fins of *ptch2:Kaede* fish at late larval stages (22-24 dpf) to assess heterotypic cellular dynamics in outgrowing rays. *ptch2:Kaede*+ bEps moved distally over *ptch2:Kaede*+ pObs, which remained stationary over the 30 minute imaging period, and in more distal fin tissue (Movie 2.3, Figure S2.10A-C). We used semi-automated tracking of individual *ptch2:Kaede*+ bEps to determine *ptch2:Kaede*+ bEps of BMS treated fish moved significantly faster (3-6 cells per fish and *n*=8 fish per group) (Figure S2.10D). Therefore, Shh/Smo signaling restrains the distal movement of Shh/Smo-responsive bEps.

We imaged caudal fins of *shha:GFP*;*runx2:mCherry* larval fish with and without Shh/Smo inhibition to monitor movement dynamics of *shha:GFP*-expressing bEps relative to Runx2+ pObs (representative fish in Figure 2.6A-D' and Movie 2.4; all fish shown in Figure S2.11). We resolved individual cells at higher detail in distal ray regions by capturing full confocal z-stacks every 2 minutes over 30 minutes. Assisted by semi-automated cell tracking, we noted bEps moved faster when beyond the field of pObs in DMSO-treated control fins. We observed slow moving bEps in contact with pObs rapidly increased in speed after distally moving past the pObs. In contrast, BMS exposure caused rapid distal bEp movement irrespective of proximal-to-distal position or proximity to pObs.

We quantified positional dynamics of individual bEps and plotted their average normalized speed compared to starting position relative to the end of ray-forming Runx2+ pObs (DMSO: *n*=5 fish,

26-38 cells per fish, total of 159 cells; BMS: *n*=4 fish, 26-41 cells per fish, total of 135 cells). *shha:GFP*-expressing bEps located distal to pObs moved faster than pOb-associated bEps in control animals, producing a clear upward velocity shift at the pOb border (Figure 2.6E). In contrast, BMS treatment caused evenly distributed bEp velocities before and after the pOb-containing region. Taken together, we propose local Shh/Smo signaling enhances heterotypic cell associations that transiently restrain the continuous distal movement of bEps while they pass directly over pObs. For ray branching morphogenesis, Shh/Smo-enhanced cell interactions between pObs and successive waves of bEps could enable the pOb pool to gradually follow laterally splitting *shha*-expressing bEp domains. Eventually, the divided pOb pools would then form separate daughter rays connected at a branch point.

DISCUSSION

Basal epidermal movements and Shh/Smo signaling direct skeletal branching morphogenesis during zebrafish fin ray development and regeneration

Zebrafish fin ray branching provides an accessible context to define ancestral mechanisms of appendicular skeletal morphogenesis. Our current and earlier study (Armstrong et al., 2017) extends previous research to demonstrate the same Shh-dependent branching morphogenesis mechanism branches developing and regenerating rays. In both contexts, a gradually splitting domain of Shh-expressing basal epidermal cells (bEps) at the distal aspect of each outgrowing fin ray partitions the immediately adjacent pre-osteoblast (pOb) pool. Highly localized, continuous Shh/Smo activity allows a given ray's distal pOb population to gradually follow the separating Shha+ basal epidermal domains. Eventually fully split, divided pOb pools continue to promote

outgrowth of now two rays connected at a branch point. The shared mechanism of pOb positioning for ray branching underscores that fin regeneration re-activates developmental mechanisms. We show Shh/Smo-promoted ray branching morphogenesis acts in unpaired and paired fins, distinct from the paired fins' presumptive earlier use of *shha* in a ZPA-like patterning role (Hadzhiev et al., 2007; Laforest et al., 1998). Smo-dependent Shh signaling appears largely dedicated to ray branching in unpaired fins as pathway inhibition minimally disrupts initial fin patterning, outgrowth, or skeletal differentiation during caudal fin development or regeneration.

Live imaging of the developing caudal fin highlights how collective movement of Shha+ bEps positions pObs to generate branched rays (model in Figure S2.12 and Movie 2.5). Our Kaede photoconversion and time-lapse imaging show bEps continuously move distally in developing fins, activating *shha* expression upon reaching the distal zone that includes pObs. Individual bEps pass through the *shha*-expressing domain, down-regulate *shha* when moving beyond the pObs, and then are seemingly shed from the end of the fin. In turn, proximal bEps enter the distal zone and activate *shha* to replenish the *shha*-expressing basal epidermal domain adjacent to pObs. Shha produces a constant Smo-dependent response in neighboring pObs and an autocrine, transient response in *shha*-producing bEps as represented by upregulated *ptch2* in both cell types. This continuous, localized Hh/Smo signaling restrains bEp collective movement dynamics and promotes ray branching by enabling concomitant separation of pOb pools with lateral splitting *shha* basal epidermal domains.

The directly observed distal movement and likely shedding of fins' basal epidermis, as surmised during regeneration (Armstrong et al., 2017; Shibata et al., 2018) is intriguing both functionally

and mechanistically. Functionally, continuous bEp replacement may enable rapid recovery from frequent environmental insults. Further, we propose bEp collective movements, distal and lateral, contribute the force that maintains pOb alignment (Armstrong et al., 2017) and enables splitting of physically coupled pOb pools for ray branching. Distal epidermal movements are likely promoted by distributed proliferation across the fin, as seen during regeneration for the basal epidermis (Shibata et al., 2018) and overlying superficial epidermis (Chen et al., 2016; Shibata et al., 2018). In contrast, the cause of periodic lateral *shha*-expressing bEp movements that split *shha*-defined bEp domains and thereby instruct ray branching is unknown.

Shh/Smo signaling is involved in branching morphogenesis of other organs, including the lung (Bellusci et al., 1997; Fernandes-Silva et al., 2017; Pepicelli et al., 1998) and submandibular salivary gland (Jaskoll et al., 2004). In the lung, Shh/Smo mediates interactions between mesenchymal and epithelial populations although likely by promoting local proliferation and/or differentiation (Kim et al., 2015). Collective cell migration also is broadly implicated in branching morphogenesis, including for renal tubes, mammary glands and blood vessels (Ewald et al., 2008; Riccio et al., 2016; Spurlin and Nelson, 2017). Unlike those contexts, we propose a neighboring cell type – basal epidermis – that does not directly contribute to the final tissue provides the instructive collective movements. This unusual arrangement may reflect regenerating fin pObs having a mesenchymal state during patterning before returning to their differentiated epithelial state (Stewart et al., 2014).

Shh/Smo signaling may position pre-osteoblasts by physical coupling to moving basal epidermal cells

Continuous Shh/Smo signaling through fin development and retained splitting of Shh-expressing basal epidermal domains when the pathway is inhibited indicate Shh/Smo has a permissive role in ray branching. We favor a model whereby Shh/Smo's function is to promote transient associations between bEps and pObs (Figure S2.12). The transient nature may result from the moving bEps rapidly terminating their *shha* expression and *ptch2*-defined Shh/Smo activity. A slight lateral component to bEp movements away from the midline of each forming ray would then successively tug interconnected pObs to follow. Over the course of several days, pObs eventually are pulled into two pools. The pOb pools become sufficiently and irreversibly separated to now generate branched daughter rays.

Our 3-D reconstructions showing Shh-expressing bEps and Runx2-expressing pObs likely share extensive physical contacts are consistent with this heterotypic cell association model. Importantly, bEps and pObs would remain adjacent but not necessarily physically coupled when Shh/Smo signaling is blocked. As such, our novel time-lapse imaging of developing caudal fins provides key functional support by showing Shh/Smo signaling impedes bEp distal movements (Movie 5). Notably, Shh-expressing bEps accelerate when they pass beyond Shh-responding pObs. Chemical inhibition of Shh/Smo signaling significantly increases overall Ptch2-positive bEp migration rates and equalizes velocities whether Shh-expressing bEps are adjacent to or beyond pObs. While inhibiting Shh/Smo signaling accelerates individual bEp cell movements, a steady-state Shh-expressing basal epidermal domain persists and at least partially splits. However, we propose the pObs cannot follow without Shh/Smo signaling to couple them with bEps and therefore remain as a single pOb pool that forms an unbranched ray. Longer-term live imaging monitoring lateral movements of both bEps and pObs would help test this model.

We favor the model that Shh/Smo physically couples bEps and pObs movements for ray branching over alternative hypotheses for additional reasons. First, we did not observe Shh/Smo-dependent cell proliferation during development (this study) or regeneration (Armstrong et al., 2017), arguing against a model whereby Shh promotes localized proliferation at the margins of a given pOb pool to progressively divide it. Notably, previous conclusions that Shh/Smo signaling is a pro-proliferative factor in regenerating fins (Lee et al., 2009; Quint et al., 2002) may reflect off-target cyclopamine effects (Armstrong et al., 2017). In contrast, fins develop and regenerate to normal size when using BMS-833923 to block Shh/Smo signaling with the intriguing exception of the two principal peripheral rays. Second, all Shh/Smo-responsive cells remain outwardly specified upon Shh/Smo inhibition, including osteoblasts that still differentiate to produce ray skeletal units complete with joints. Any additional Shha or other Hedgehog ligand roles appear minor or may be Smo-independent, as with Indian Hedgehog A (Ihha) and bone maturation during fin regeneration (Armstrong et al., 2017). Third, we use chemical genetics to map the Shh/Smo time-of-function and show ray branching requires persistent Shh/Smo signaling from initial hints of Shh-expressing basal epidermal domain splitting until daughter rays are fully separated. Therefore, Shh/Smo signaling seemingly promotes a continuously emergent process and not a periodic switch-like event for either distal bEp movement or Shha-expressing bEp domain splitting.

Short range Shh promoting cell associations may be a common Shh/Smo signaling mode

Our proposed short range Shh/Smo signaling mode promoting heterotypic cell association differs from Hh's more typical role as a gradient-forming morphogen. Providing precedence, Hh acts on neighboring cells in several well-established contexts. For example, Hh mediates interactions

between directly adjacent cells during *Drosophila* embryo segment boundary formation (Ingham, 1993). Short-range Shh/Smo signaling also occurs in vertebrates, including mammalian hair follicle development (Sato et al., 1999; Woo et al., 2012), avian limb patterning (Sanders et al., 2013), and zebrafish retina development (Shkumatava, 2004). Perhaps most germane, *shha+* epidermal cells organize closely associated Hh-responsive dermal cells during zebrafish scale morphogenesis (Aman et al., 2018).

Shh/Smo has also been tied to cell associations in other settings. For example, Hh's archetypal role in *Drosophila* wing disc compartment boundary establishment (Ayers et al., 2010) may be through increased "cell bonding" (Rudolf et al., 2015). Shh alters neural crest cell adhesion and migration during avian neural tube morphogenesis (Fournier-Thibault et al., 2009; Jarov et al., 2003; Testaz et al., 2001). Further, misregulated Shh/Smo signaling is linked to invasive cell migration associated with liver, breast, ovarian, and skin cancers (Chen et al., 2013, 2014; Hanna and Shevde, 2016; Zeng et al., 2017).

Identification, characterization, and manipulation of Shh/Smo-upregulated molecules effecting bEp and pOb interactions would strengthen our ray branching model. Such Shh/Smo targets could directly promote cell adhesion, as for neural tube morphogenesis (Jarov et al., 2003; Tsai et al., 2020), or indirectly as extracellular matrix intermediaries. Alternatively, Shh/Smo activity could alter cell features (e.g. shape, polarity, or interconnectivity) that indirectly favor heterotypic association. A third intriguing possibility is that Shh/Smo-upregulated Patched directly binds to membrane-retained Shh on bEp surfaces to increase high-affinity contacts between pObs and bEps. This mechanism could apply elsewhere given Patched is an evolutionary-conserved Shh/Smo-

target gene (Alexandre et al., 1996; Goodrich et al., 1996; Lorberbaum et al., 2016; Marigo et al., 1996) while placing Patched in the curious position as both a Shh/Smo effector and negative feedback regulator.

Fin ray branching as an ancestral mechanism of Shh-mediated appendage patterning and skeletal morphogenesis

How vertebrates pattern skeletal appendages (fins, limbs) is a fundamental question of evolutionary and developmental biology. Rays were lost in tetrapod lineages although fin dermal skeleton and tetrapod digits may share deep homology (Nakamura et al., 2016). If so, our demonstration Shh/Smo signaling supports developmental ray branching morphogenesis is intriguing given Shh's long-appreciated but mechanistically distinct role in vertebrate digit patterning. Shh is the secreted morphogen produced by the zone of polarizing activity (ZPA) at the posterior edge of developing limb buds that directs anterior-to-posterior patterning of skeletal elements including digits (Tickle and Towers, 2017), Polarized *shha* expression in zebrafish pectoral fin buds indicates paired fins employ ZPA-like skeletal patterning (Akimenko and Ekker, 1995; Krauss et al., 1993; Neumann et al., 1999). In contrast, caudal fin primordia lack polarized *shha* (Hadzhiev et al., 2007; Laforest et al., 1998; our results). Consistently, we found disrupting Shh/Smo signaling even prior to formation of the caudal fin field does not alter the initial complement of 18 rays. Moreover, we demonstrate Shh/Smo signaling is required for ray branching in all fins, whether paired or unpaired. The unpaired medial fins (dorsal, caudal, anal) evolved prior to paired fin appendages (Dahn et al., 2006; Desvignes et al., 2018; Freitas et al., 2006; Larouche et al., 2017). Therefore, Shh-dependent ray branching may reflect an ancestral skeletal morphogenesis mechanism that predates emergence of ZPA-based appendage patterning.

The waning fitness demand for a ray branching mechanism during the water-to-land transition then may have released selective pressure on the Shh/ZPA module to facilitate terrestrial limb adaptations. Classic models postulating a branching component to endochondral limb skeleton patterning (Oster et al., 1988; Shubin and Alberch, 1986) further inspire exploring if aspects of Shh/Smo's function during ray branching endure in ZPA-dependent limb patterning.

Shh/Smo signaling promotes skeletal morphogenesis in many contexts beyond limbs. In zebrafish, Shh/Smo patterns craniofacial dermal bones, as illustrated by the opercle (Huycke et al., 2012), and both developing and regenerating scales (Aman et al., 2018; Iwasaki et al, 2018). Shh/Smo signaling also impacts mesenchymal cell movements to pattern bird feathers, a non-ossified, scale-related dermal skin appendage (Li et al., 2018). Shh further supports patterning of the axial skeleton (Chiang et al., 1996; Choi et al., 2012; Dworkin et al., 2016; Hu et al., 2015; Hu and Helms, 1999; Jeong et al., 2004; Swartz et al., 2012) as well as teeth (Ahn et al., 2010; Dassule et al., 2000; Seppala et al., 2017). Our discovery Shh/Smo signaling enables neighboring cells to position pObs during fin ray branching suggests similar mechanisms act in other skeletal patterning contexts. If so, manipulating Shh/Smo pathway to position therapeutically delivered or endogenous progenitor cells could enhance skeletal regenerative medicine.

MATERIALS AND METHODS

Zebrafish

Danio rerio zebrafish were maintained in 28-29°C circulating fish water within the University of Oregon Aquatic Animal Care Services (UO AqACS) fish facility. Adult zebrafish were housed in

Techniplast polycarbonate containers and fed with dry pellets ("Zebrafish Juvenile Diet", #388765-134-684, Zeigler Bros., Inc.). Early larvae ~4-10 dpf were fed live rotifers (*Brachionus plicatilis,* Reed Mariculture, Campbell, CA), mid-larvae ~10-21 dpf were fed rotifers and *Artemia nauplii* brine shrimp (Great Salt Lake strain *Artemia franciscana*, Artemia International, LLC, Fairview, TX), late larvae ~21-30 dpf were fed brine shrimp, and juveniles ~30-60 dpf were fed brine shrimp and dry pellets. AqACS facility staff performed feedings twice daily

Standard housing densities were *n*=25/3.5-liter tank for fish aged > 21 dpf, *n*=25/1.1-liter tank for larvae 4-21 dpf, and *n*=25/100 mL petri dish for < 4 dpf larvae. The following lines were used: wildtype AB, *Tg(sp7:EGFP)*^{b1212} (DeLaurier et al., 2010), *TgBAC(ptch2:Kaede)*^{a4596} (Huang et al., 2012), *Tg(-2.4shha:gfp:ABC)*^{sb15} [previously known as *Tg(-2.2shh:gfp:ABC)*] (Ertzer et al., 2007; Shkumatava, 2004), (*Tg(runx2:mCherry)* (From Shannon Fisher Lab; Barske et al., 2020). The University of Oregon Institutional Animal Care and Use Committee (IACUC) approved zebrafish experiments.

Fish were staged by days post fertilization (dpf) and visually screened to identify stages of ray branching morphogenesis development (i.e. pre-branching, semi-branched, branched). Approximate standard lengths (SL, as described in Parichy et al., 2009) for the developmental stages used are listed below:

Approx. SL (mm)	**Approx. dpf**	**Developmental stage**	**Caudal fin state**
3	2	Larval	Fin fold
5-6	14	Mid-larval	Unbranched rays
9-11	24-28	Late larval	Unbranched rays
11.5-13.5	28-33	Juvenile	Active ray branching
14-15	35	Juvenile	Branched rays
20	42	Juvenile	Branched rays

Microscopy

Larval and juvenile fish were anesthetized with 74 μg/ml tricaine (MS-222, Syndel) in fish facility system water. Fish or dissected fins were transferred immediately to a 35 mm glass bottom FluoroDish plate (World Precision Instruments). Two or three drops of 1% low-melt agarose, stored at 38°C and cooled before application, were placed on the caudal fin. Fins were quickly flattened to the FluoroDish with a single-hair paintbrush before the agarose hardened. The following microscopes were used: Nikon Eclipse T*i*-E widefield and Nikon Eclipse T*i2*-E with Yokogawa CSU-W1 spinning disk attachments, and Zeiss LSM 880 laser scanning confocal microscope. Confocal image stacks were processed using Imaris software to generate single optical slice digital sections, surface renderings, and 3D reconstructions. Adobe Photoshop was used to adjust levels with identical image acquisition and processing settings for a given experiment. Live fish promptly were euthanized or returned to tanks after imaging.

Kaede photoconversion and imaging

ptch2:Kaede fish were anesthetized and placed on FluoroDish plates as described above. Fins were viewed with a Nikon Eclipse T*i*-E widefield microscope or Nikon T*i*2-E/ Yokogawa CSU-W1 spinning disk confocal microscope. Kaede-expressing regions of interest (ROIs) were photoconverted using a metal halide light source and DAPI excitation filter or with 405 nm laser illumination from 10 seconds to 2 minutes, depending on ROI size and fish age. Before and after images were acquired to ensure complete photoconversion of Kaede from green (518 nm) to red (580 nm) emission. Fish were returned to system water and then similarly re-imaged after defined periods. *ptch2:Kaede* expression in different cell types was discerned by fin cells' distinctive

relative positions and morphologies confirmed by co-marker staining (Figure 1M-P and Figure S4).

BMS-833923 treatments

BMS-833923 ("BMS", Cayman Chemicals) was dissolved in DMSO to a concentration of 50 mM, single-use aliquots of 6.3-12.5 mM were prepared from stock for each experiment, and stored at -20ºC until time of use. Aliquots were diluted to a final concentration of 0.63-1.25 μM in system fish water for both larval and juvenile zebrafish treatments. Equal volumes of DMSO were used for control group treatments. Concentrations varied due to batch-dependent drug potency. Each batch of BMS was validated and optimized using photoconversion experiments on *ptch2:Kaede* fish to define a drug concentration that fully inhibited production of Hh/Smo activity-marking new Kaede.

To test Hh/Smo requirements for caudal fin ray branching, 25 dpf *sp7:EGFP* fish (*n*=6 per group) with unbranched rays were treated initially for 24 hours in BMS or DMSO-alone still water (at a minimum volume of 100 mL per fish) and then returned to standard housing with circulating system water. Fish were exposed to BMS for 4 hours every other day until the experimental end point at 42 dpf. BMS was made fresh for each treatment from previously prepared aliquots and not replenished during treatment times. To assess Hh/Smo roles in all fin appendages, *shha:GFP;runx2:mCherry* fish were treated with 1.25 μM BMS or DMSO (*n*= 6 per group) from 21 to 42 dpf. Fins were dissected and imaged as described above.

For staggered-start juvenile fish treatments, 25 dpf *sp7:EGFP* fish were anesthetized, fluorescently screened, and sorted into groups of those having caudal fins with "unbranched" rays or fins in which branching had initiated but was incomplete ("during"). Fish from the two groups were then treated with BMS as described above. Untreated clutchmate *sp7:EGFP* fish were returned to standard housing and screened every other day until all fish had developed branched rays. Drug treatment of the "branched" group of fish was started at 35 dpf. All treatments ended at 42 dpf, when fins were mounted and imaged as described. For BMS-treated fish (unbranched, during branching, and branched), *n*=4 or 5 fish per group with *n*=2 or 3 for DMSO-treated control groups.

For early larval development studies, *sp7:EGFP;runx2:mCherry* and *ptch2:Kaede* fish were bathed in 1.25 μM BMS starting at 2 dpf alongside DMSO-treated controls (*n*=33-44 fish per group, per clutch). The same drug exposure regiment described for juvenile fish was used. From 2-4 dpf, larvae were treated in 40 mL embryo media in petri dishes. From 5-14 dpf, fish were drug-exposed in beakers containing 125 mL embryo media. Drug efficacy on larval fish was assessed by photoconverting distal fin ROIs of *ptch2:Kaede* fins (photoconversion methods described above) at 13 dpf and re-imaging those regions at 14 dpf (*n*=3-5 per group). All fish were screened for skeletal patterning phenotypes by widefield microscopy. Across clutches, 35/44 (79.5%) BMS-treated larvae developed normally (9/44 or 20.5% were runted) compared to 26/33 (78.8%) DMSO-treated larvae (7/33 or 21.2% were runted). The ~20% incidence of developmentally delayed larvae was likely caused by extended periods in 250 mL beakers instead of larger nursery tanks. Regardless, nearly all larvae irrespective of size in both groups developed the normal complement of 18 caudal fin rays.

Ray morphometrics

Ray lengths were assessed for *sp7:EGFP* clutch mates treated from 25-42 dpf with BMS-833923 or DMSO (experiment described above, *n*=6 per group). Using Fiji-ImageJ software, the Principal Peripheral Ray (unbranching lateral ray) and Dorsal Ray 3 (longest branching ray) were measured from 42 dpf endpoint caudal fin images from the proximal base of the fin to the distal fin end. Fin widths were used to normalize for body size but did not differ between DMSO and BMS groups. Raw and normalized data were graphed with GraphPad Prism V8 and significance assessed with a Student's unpaired t-test.

Whole mount immunostaining

shha:GFP caudal fins were harvested at 22-23 dpf and immediately fixed in 4% PFA/PBS overnight at 4°C or for 4 hours at room temperature. Fins were washed extensively in PBS + 0.1% Tween-20 and blocked in 1x PBS, 1% Triton X-100, 5% Normal Goat Serum, and 10% DMSO buffer overnight at 4°C. Fins were incubated with primary antibodies in blocking buffer overnight at 4°C. Primary antibodies were anti-GFP (1:1000; AVES, GFP-1020), anti-Tp63 (1:100; Thermo Fisher, PA5-36069) and anti-Runx2 (1:100; Santa Cruz Biotechnology, sc-101145). Fins were washed in a high-salt 500 mM NaCl buffer for 30 min followed by extensive washes in PBS + 0.1% Tween-20. Secondary antibody incubations using Alexa Fluor conjugates (Thermo Fisher) were performed overnight protected from light at 4°C at a concentration of 1:1000 in blocking buffer. Fins were then washed extensively in PBS + 0.1% Tween-20, nuclei stained with Hoechst (Thermo Fisher) and mounted with SlowFade Diamond Antifade (Thermo Fisher).

Paraffin section immunostaining

Dissected 32 dpf *shha:GFP* caudal fins were fixed in 4% PFA/PBS overnight at 4°C. After extensive PBS washing, fins were decalcified for 4 days in 0.5M EDTA, pH 8.0 with daily solution changes. Fins then were dehydrated in an ethanol series and tissue cleared with xylenes prior to longitudinal embedding in paraffin wax. 7 μm sections were cut on a Leica RM255 microtome. Antigen retrieval was performed on rehydrated sections using 1 mM EDTA + 0.1% Tween-20 for 5 minutes in a Cuisinart electric pressure cooker set on high. Following PBS washes, sections were blocked in 1x PBS, 10% nonfat dry milk, 2% normal goat serum, and 4% fetal bovine serum for a minimum of 1 hour. Sections were incubated overnight at 4°C with primary antibodies in blocking solution. Primary antibodies were: anti-GFP (1:3000; AVES, GFP-1020), anti-Tp63 (1:100; Thermo Fisher, PA5-36039), anti-Laminin (1:40; Sigma, L9393), and anti-Zns5 (1:5, ZIRC). Sections were washed in PBS containing 500 mM NaCl + 0.1% Tween-20. Alexa Fluor conjugated secondary antibodies (Thermo Fisher) were diluted 1:1000 in blocking buffer and incubated for 1 hour at room temperature protected from light. Sections were washed, nuclei stained with Hoechst, and mounted with SlowFade Gold Antifade (Thermo Fisher). Images were acquired on a Zeiss LSM 880 laser scanning confocal microscope and images processed with Fiji-ImageJ, Imaris, and Adobe Photoshop.

In vivo EdU incorporation assays

29 dpf *shha:GFP* juvenile fish were treated with DMSO or 1.25 μM BMS for 4 hours in groups of *n*=5. Anesthetized fish were injected intraperitoneally with 5 μl of 1 mg/mL EdU (Thermo Fisher) in sterile PBS, monitored for recovery for 10 minutes in fresh facility water, and then returned to treatment tanks. 12 hours post-injection, caudal fins were amputated and fixed for 4 hours at room temperature in 4% PFA/PBS. Fins were washed thoroughly with PBS and blocked

overnight at 4ºC in PBS/1% Triton X-100/5% Normal Donkey Serum/10% DMSO. EdU signal was detected with Click-iT Plus Alexa Fluor 647 Picolyl Azide (ThermoFisher) at 2.5 µl/ mL according to the manufacturer's protocol. Following EdU detection, whole-mount GFP immunostaining and Hoechst nuclear staining was performed as described below. Whole mount confocal images were acquired using a Zeiss 880 LSM and 3D reconstructions prepared using Imaris. EdU+ and total intra-ray nuclei, i.e. from cells located in between the epidermal Shh domains of each hemi-ray, were identified and scored for Rays 2 and 3 using the Imaris "Spots" function and the following parameters: ROI around length of Shha:GFP+ domain, Quality Threshold 0.642, cell diameter 3 microns. Quantification of EdU+ cells is expressed as the number of EdU+ intra-ray cells over total number of Hoechst-stained nuclei.

Cell migration imaging and analysis

Fish were anesthetized sequentially in freshly prepared 74 µg/ml tricaine solution for 3 minutes and monitored for slowed opercular movements. Anesthetized fish were transferred to a 35 mm FluroDish plate and mounted in 3% low melt agarose as described earlier. Set agarose was carefully removed from the most distal region of the caudal fin to allow for free movement of the epidermis while the trunk remained adhered to the FluoroDish. 74 µg/ml of tricaine solution was added to maintain anesthesia and cover the fin. After imaging, fish were returned to system water to confirm recovery and then promptly euthanized. Fish that did not recover were excluded from downstream cell migration analyses. We occasionally observed extremely rapid epidermal movements in which entire *shha:GFP+* domains would be shed from rays in <15 min. We suspect this phenomenon results from elevated stress, anesthesia intolerance, and/or damage from plate surface contact or agarose application. We excluded these animals from analyses.

For bulk cell migration assays, 22-24 dpf *ptch2:Kaede* fish were treated with 0.63 μM BMS or DMSO (*n*=8 per group). 24 hours later, fish were mounted and imaged with a Nikon Eclipse T*i*-E widefield microscope every 1 minute for 30 minutes. Imaris was used to automatically track cells for 3-6 single *ptch2:Kaede*+ basal epidermal cells on dorsal rays 2-5 for each fish. All tracks were quality checked to confirm individual cell tracking. Individual cell speeds (arbitrary units, *n*=38 cells per group) and then average speed for each animal were determined. Statistical significance was assessed by Student's unpaired *t*-tests for all cells tracked (*n*=38 cells per group) and average cell speed per fish (*n*=8 fish per group).

For position-dependent cell migration assays, 21-24 dpf *shha:GFP;runx2:mCherry* fish were treated with DMSO or 1.25 μM BMS for 24 hours prior to imaging. Fish were imaged every 2 minutes for 30 minutes with full z-stacks using a Nikon Ti2-E with a Yokogawa CSU-W1 SoRa spinning disk confocal unit. A single hemi-ray of Ray 2 or Ray 3 was analyzed for each time-lapse video. If both rays were captured, the ray with more pObs in frame was analyzed to avoid oversampling individuals. GFP+ cells were automatically tracked using Imaris software "Spots" algorithms with the following parameters: estimated cell diameter 5 microns, maximum distance between frames 6 microns, maximum gap between frames 3 time points. Each cell track was quality checked using 3D reconstructions and edited if Imaris assigned multiple cells to one track or fragmented the track of a given cell. 26-41 cells were tracked across 9 fish (*n*=5 for DMSO and *n*=4 for BMS groups, respectively) for a total of *n*=159 for DMSO-treated and *n*=135 for BMS-treated fish. Data was normalized for each fish by dividing the track speed of a single cell by the average of all cells tracked for that fish. Positional data was determined by setting the X-

position of the most distal Runx2+ pOb as "0" and assigning a relative initial X-position for each *shha:GFP+* cell. Cells with a negative starting position were therefore pOb-associated while those with a positive starting position had already migrated beyond the pOb pool when video acquisition began. Imaris was used to determine each cell's total X-displacement and track speed. Graphs were generated using GraphPad Prism V8. Fourth-order best-fit polynomial curves were added to position/speed graphs to help visualize data trends.

REFERENCES

Crotwell, P.L., Mabee, P.M., 2007. Gene expression patterns underlying proximal-distal skeletal segmentation in late-stage zebrafish, Danio rerio. Dev. Dyn. 236, 3111–3128. https://doi.org/10.1002/dvdy.21352

Lin, T.L., Matsui, W., 2012. Hedgehog pathway as a drug target: Smoothened inhibitors in development. Onco. Targets. Ther. 5, 47–58. https://doi.org/10.2147/ott.s21957

Jarov, A., Williams, K.P., Ling, L.E., Koteliansky, V.E., Duband, J.-L., Fournier-Thibault, C., 2003. A dual role for Sonic hedgehog in regulating adhesion and differentiation of neuroepithelial cells. Dev. Biol. 261, 520–536. https://doi.org/10.1016/s0012-1606(03)00351-8 PMID - 14499657

Armstrong, B.E., Henner, A., Stewart, S., Stankunas, K., 2017. Shh promotes direct interactions between epidermal cells and osteoblast progenitors to shape regenerated zebrafish bone. Dev. 144, 1165–1176. https://doi.org/10.1242/dev.143792

Riddle, R.D., Johnson, R.L., Laufer, E., Tabin, C.J., 1993. Sonic hedgehog mediates the polarizing activity of the ZPA. Cell 75, 1401–1416.

Hanna, A., Shevde, L.A., 2016. Hedgehog signaling: modulation of cancer properies and tumor mircroenvironment. Mol. Cancer 15, 24. https://doi.org/10.1186/s12943-016-0509-3

Chiang, C., Litingtung, Y., Lee, E., Young, K.E., Corden, J.L., Westphal, H., Beachy, P.A., 1996. Cyclopia and defective axial patterning in mice lacking Sonic hedgehog gene function. Nature 383, 407–413. https://doi.org/10.1038/383407a0

Ertzer, R., Müller, F., Hadzhiev, Y., Rathnam, S., Fischer, N., Rastegar, S., Strähle, U., 2007. Cooperation of sonic hedgehog enhancers in midline expression. Dev. Biol. 301, 578–589. https://doi.org/10.1016/j.ydbio.2006.11.004

Anderson, E., Peluso, S., Lettice, L.A., Hill, R.E., 2012. Human limb abnormalities caused by disruption of hedgehog signaling. Trends Genet. 28, 364–373. https://doi.org/10.1016/j.tig.2012.03.012

Spurlin, J.W., Nelson, C.M., 2017. Building branched tissue structures: from single cell guidance to coordinated construction. Philos. Trans. R. Soc. B Biol. Sci. 372, 20150527. https://doi.org/10.1098/rstb.2015.0527

Li, A., Cho, J.-H., Reid, B., Tseng, C.-C., He, L., Tan, P., Yeh, C.-Y., Wu, P., Li, Y., Widelitz, R.B., Zhou, Y., Zhao, M., Chow, R.H., Chuong, C.-M., 2018. Calcium oscillations coordinate feather mesenchymal cell movement by SHH dependent modulation of gap junction networks. Nat. Commun. 9, 5377. https://doi.org/10.1038/s41467-018-07661-5

Larouche, O., Zelditch, M.L., Cloutier, R., 2017. Fin modules: an evolutionary perspective on appendage disparity in basal vertebrates. BMC Biol. 15, 32. https://doi.org/10.1186/s12915-017-0370-x

Barske, L., Fabian, P., Hirschberger, C., Jandzik, D., Square, T., Xu, P., Nelson, N., Yu, H.V., Medeiros, D.M., Gillis, J.A., Crump, J.G., 2020. Evolution of vertebrate gill covers via shifts in an ancient Pou3f3 enhancer. Proc. Natl. Acad. Sci. 117, 24876–24884. https://doi.org/10.1073/pnas.2011531117 PMID - 32958671

Huycke, T.R., Eames, B.F., Kimmel, C.B., 2012. Hedgehog-dependent proliferation drives modular growth during morphogenesis of a dermal bone. Development 139, 2371–2380. https://doi.org/10.1242/dev.079806

Woo, W.-M., Zhen, H.H., Oro, A.E., 2012. Shh maintains dermal papilla identity and hair morphogenesis via a Noggin–Shh regulatory loop. Genes Dev. 26, 1235–1246. https://doi.org/10.1101/gad.187401.112

Shkumatava, A., 2004. Sonic hedgehog, secreted by amacrine cells, acts as a short-range signal to direct differentiation and lamination in the zebrafish retina. Development 131, 3849–3858. https://doi.org/10.1242/dev.01247

Chen, Q., Xu, R., Zeng, C., Lu, Q., Huang, D., Shi, C., Zhang, W., Deng, L., Yan, R., Rao, H., Gao, G., Luo, S., 2014. Down-Regulation of Gli Transcription Factor Leads to the Inhibition of Migration and Invasion of Ovarian Cancer Cells via Integrin β4-Mediated FAK Signaling. PLoS One 9, e88386. https://doi.org/10.1371/journal.pone.0088386

Shubin, N.H., Alberch, P., 1986. A morphogenetic approach to the origin and basic organization of the tetrapod limb. Evol. Biol. 319–387. https://doi.org/10.1007/978-1-4615-6983-1_6

Iwasaki, M., Kuroda, J., Kawakami, K., Wada, H., 2018. Epidermal regulation of bone morphogenesis through the development and regeneration of osteoblasts in the zebrafish scale. Dev. Biol. 437, 105–119. https://doi.org/10.1016/j.ydbio.2018.03.005 PMID - 29524434

Freitas, R., Zhang, G., Cohn, M.J., 2006. Evidence that mechanisms of fin development evolved in the midline of early vertebrates. Nature 442, 1033–1037. https://doi.org/10.1038/nature04984

Stewart, S., Gomez, A.W., Armstrong, B.E., Henner, A., Stankunas, K., 2014. Sequential and Opposing Activities of Wnt and BMP Coordinate Zebrafish Bone Regeneration. Cell Rep. 6, 482–498. https://doi.org/10.1016/j.celrep.2014.01.010

DeLaurier, A., Eames, B.F., Blanco-Sánchez, B., Peng, G., He, X., Swartz, M.E., Ullmann, B., Westerfield, M., Kimmel, C.B., 2010. Zebrafish sp7:EGFP: A transgenic for studying otic vesicle formation, skeletogenesis, and bone regeneration. genesis 48, 505–511. https://doi.org/10.1002/dvg.20639

Alexandre, C., Jacinto, A., Ingham, P.W., 1996. Transcriptional activation of hedgehog target genes in Drosophila is mediated directly by the cubitus interruptus protein, a member of the GLI family of zinc finger DNA-binding proteins. Genes Dev. 10, 2003–2013. https://doi.org/10.1101/gad.10.16.2003

Tickle, C., Towers, M., 2017. Sonic Hedgehog Signaling in Limb Development. Front. Cell Dev. Biol. 5, 14. https://doi.org/10.3389/fcell.2017.00014 PMID - 28293554

Dworkin, S., Boglev, Y., Owens, H., Goldie, S.J., 2016. The Role of Sonic Hedgehog in Craniofacial Patterning, Morphogenesis and Cranial Neural Crest Survival. J. Dev. Biol. 4, 24. https://doi.org/10.3390/jdb4030024

Zeng, C., Chen, T., Zhang, Y., Chen, Q., 2017. Hedgehog signaling pathway regulates ovarian cancer invasion and migration via adhesion molecule CD24. J. Cancer 8, 786–792. https://doi.org/10.7150/jca.17712

Jeong, J., McMahon, A.P., 2004. Growth and pattern of the mammalian neural tube are governed by partially overlapping feedback activities of the hedgehog antagonists patched 1 and Hhip1. Development 132, 143–154. https://doi.org/10.1242/dev.01566

Marigo, V., Scott, M.P., Johnson, R.L., Goodrich, L. V, Tabin, C.J., 1996. Conservation in hedgehog signaling: induction of a chicken patched homolog by Sonic hedgehog in the developing limb. Development 122, 1225–1233.

Nakamura, T., Gehrke, A.R., Lemberg, J., Szymaszek, J., Shubin, N.H., 2016. Digits and fin rays share common developmental histories. Nature 537, 225–228. https://doi.org/10.1038/nature19322

Huang, P., Xiong, F., Megason, S.G., Schier, A.F., 2012. Attenuation of Notch and Hedgehog Signaling Is Required for Fate Specification in the Spinal Cord. PLoS Genet. 8, e1002762. https://doi.org/10.1371/journal.pgen.1002762

Dassule, H.R., Lewis, P., Bei, M., Maas, R., McMahon, A.P., 2000. Sonic hedgehog regulates growth and morphogenesis of the tooth. Development 127, 4775–4785.

Fernandes-Silva, H., Correia-Pinto, J., Moura, R.S., 2017. Canonical Sonic Hedgehog Signaling in Early Lung Development. J. Dev. Biol. 5, 3. https://doi.org/10.3390/jdb5010003

Riccio, P., Cebrian, C., Zong, H., Hippenmeyer, S., Costantini, F., 2016. Ret and Etv4 Promote Directed Movements of Progenitor Cells during Renal Branching Morphogenesis. PLOS Biol. 14, e1002382. https://doi.org/10.1371/journal.pbio.1002382

Freitas, R., Gómez-Skarmeta, J.L., Rodrigues, P.N., 2014. New frontiers in the evolution of fin development. J. Exp. Zool. Part B Mol. Dev. Evol. 322, 540–552. https://doi.org/10.1002/jez.b.22563 PMID - 24677573

Desvignes, T., Carey, A., Postlethwait, J.H., 2018. Evolution of caudal fin ray development and caudal fin hypural diastema complex in spotted gar, teleosts, and other neopterygian fishes. Dev. Dyn. 247, 832–853. https://doi.org/10.1002/dvdy.24630

Fournier-Thibault, C., Blavet, C., Jarov, A., Bajanca, F., Thorsteinsdóttir, S., Duband, J.-L., 2009. Sonic Hedgehog Regulates Integrin Activity, Cadherin Contacts, and Cell Polarity to Orchestrate Neural Tube Morphogenesis. J. Neurosci. 29, 12506–12520. https://doi.org/10.1523/jneurosci.2003-09.2009

Quint, E., Smith, A., Avaron, F., Laforest, L., Miles, J., Gaffield, W., Akimenko, M.-A., 2002. Bone patterning is altered in the regenerating zebrafish caudal fin after ectopic expression of sonic hedgehog and bmp2b or exposure to cyclopamine. Proc. Natl. Acad. Sci. 99, 8713–8718. https://doi.org/10.1073/pnas.122571799

Hadzhiev, Y., Lele, Z., Schindler, S., Wilson, S.W., Ahlberg, P., Strähle, U., Müller, F., 2007. Hedgehog signaling patterns the outgrowth of unpaired skeletal appendages in zebrafish. BMC Dev. Biol. https://doi.org/10.1186/1471-213X-7-75

Krauss, R.S., Concordet, J., Ingham, P.W., 1993. A functionally conserved homolog of the Drosophila segment polarity gene hh is expressed in tissues with polarizing activity in zebrafish embryos. Cell 75, 1431–1444.

Hu, D., Helms, J.A., 1999. The role of sonic hedgehog in normal and abnormal craniofacial morphogenesis. Development 126, 4873–4884.

Testaz, S., Jarov, A., Williams, K.P., Ling, L.E., Koteliansky, V.E., Fournier-Thibault, C., Duband, J.-L., 2001. Sonic hedgehog restricts adhesion and migration of neural crest cells independently of the Patched- Smoothened-Gli signaling pathway. Proc. Natl. Acad. Sci. 98, 12521–12526. https://doi.org/10.1073/pnas.221108698

Ayers, K.L., Gallet, A., Staccini-Lavenant, L., Thérond, P.P., 2010. The Long-Range Activity of Hedgehog Is Regulated in the Apical Extracellular Space by the Glypican Dally and the Hydrolase Notum. Dev. Cell 18, 605–620. https://doi.org/10.1016/j.devcel.2010.02.015

Sato, N., Leopold, P.L., Crystal, R.G., 1999. Induction of the hair growth phase in postnatal mice by localized transient expression of Sonic hedgehog. J. Clin. Invest. 104, 855–864. https://doi.org/10.1172/jci7691

Lorberbaum, D.S., Ramos, A.I., Peterson, K.A., Carpenter, B.S., Parker, D.S., De, S., Hillers, L.E., Blake, V.M., Nishi, Y., McFarlane, M.R., Chiang, A.C.Y., Kassis, J.A., Allen, B.L., McMahon, A.P., Barolo, S., 2016. An ancient yet flexible cis-regulatory architecture allows localized Hedgehog tuning by patched/Ptch1. Elife 5, e13550. https://doi.org/10.7554/elife.13550

Sehring, I.M., Weidinger, G., 2020. Recent advancements in understanding fin regeneration in zebrafish. Wiley Interdiscip. Rev. Dev. Biol. 9, 1–16. https://doi.org/10.1002/wdev.367

Oster, G.F., Shubin, N., Murray, J.D., Alberch, P., 1988. EVOLUTION AND MORPHOGENETIC RULES: THE SHAPE OF THE VERTEBRATE LIMB IN ONTOGENY AND PHYLOGENY. Evolution (N. Y). 42, 862–884. https://doi.org/10.1111/j.1558-5646.1988.tb02508.x

Laforest, L., Brown, C.W., Poleo, G., Géraudie, J., Tada, M., Ekker, M., Akimenko, M.A., 1998. Involvement of the sonic hedgehog, patched 1 and bmp2 genes in patterning of the zebrafish dermal fin rays. Development 125, 4175–4184.

Saunders, J.W., Gasseling, M., 1968. Ectodermal-mesenchymal interaction in the origin of limb symmetry. Ep. Interact. 78–97.

Hu, D., Young, N.M., Li, X., Xu, Y., Hallgrimsson, B., Marcucio, R.S., 2015. A dynamic Shh expression pattern, regulated by SHH and BMP signaling, coordinates fusion of primordia in the amniote face. Development 142, 567–574. https://doi.org/10.1242/dev.114835

Seppala, M., Fraser, G.J., Birjandi, A.A., Xavier, G.M., Cobourne, M.T., 2017. Sonic Hedgehog Signaling and Development of the Dentition. J. Dev. Biol. 5, 6. https://doi.org/10.3390/jdb5020006

Kim, H.Y., Pang, M.-F., Varner, V.D., Kojima, L., Miller, E., Radisky, D.C., Nelson, C.M., 2015. Localized Smooth Muscle Differentiation Is Essential for Epithelial Bifurcation during Branching Morphogenesis of the Mammalian Lung. Dev. Cell 34, 719–726. https://doi.org/10.1016/j.devcel.2015.08.012

Lee, H., Kimelman, D., 2002. A Dominant-Negative Form of p63 Is Required for Epidermal Proliferation in Zebrafish. Dev. Cell 2, 607–616.

Shibata, E., Ando, K., Murase, E., Kawakami, A., 2018. Heterogeneous fates and dynamic rearrangement of regenerative epidermis-derived cells during zebrafish fin regeneration. Development 145, dev.162016. https://doi.org/10.1242/dev.162016

Dahn, R.D., Davis, M.C., Pappano, W.N., Shubin, N.H., 2006. Sonic hedgehog function in chondrichthyan fins and the evolution of appendage patterning. Nature 445, 311–314. https://doi.org/10.1038/nature05436

Marí-Beffa, M., Santamaría, J.A., Murciano, C., Santos-Ruiz, L., Andrades, J.A., Guerado, E., Becerra, J., 2007. Zebrafish fins as a model system for skeletal human studies. ScientificWorldJournal. 7, 1114–1127. https://doi.org/10.1100/tsw.2007.190

Rudolf, K., Umetsu, D., Aliee, M., Sui, L., Jülicher, F., Dahmann, C., 2015. A local difference in Hedgehog signal transduction increases mechanical cell bond tension and biases cell intercalations along the Drosophila anteroposterior compartment boundary. Development 142, 3845–3858. https://doi.org/10.1242/dev.125542

Neumann, C.J., Grandel, H., Gaffield, W., Schulte-Merker, S., Nüsslein-Volhard, C., 1999. Transient establishment of anteroposterior polarity in the zebrafish pectoral fin bud in the absence of sonic hedgehog activity. Development 126, 4817–4826.

Jaskoll, T., Leo, T., Witcher, D., Ormestad, M., Astorga, J., Bringas, P., Carlsson, P., Melnick, M., 2004. Sonic hedgehog signaling plays an essential role during embryonic salivary gland epithelial branching morphogenesis. Dev. Dyn. 229, 722–732. https://doi.org/10.1002/dvdy.10472

Choi, K.-S., Lee, C., Harfe, B.D., 2012. Sonic hedgehog in the notochord is sufficient for patterning of the intervertebral discs. Mech. Dev. 129, 255–262. https://doi.org/10.1016/j.mod.2012.07.003

Zuniga, A., 2015. Next generation limb development and evolution: old questions, new perspectives. Development 142, 3810–3820. https://doi.org/10.1242/dev.125757

Goodrich, L. V, Johnson, R.L., Milenkovic, L., McMahon, J.A., Scott, M.P., 1996. Conservation of the hedgehog/patched signaling pathway from flies to mice: induction of a mouse patched gene by Hedgehog. Genes Dev. 10, 301–312. https://doi.org/10.1101/gad.10.3.301

Pepicelli, C. V., Lewis, P.M., McMahon, A.P., 1998. Sonic hedgehog regulates branching morphogenesis in the mammalian lung. Curr. Biol. 8, 1083–1086. https://doi.org/10.1016/S0960-9822(98)70446-4

Chen, J.-S., Huang, X., Wang, Q., Huang, J.-Q., Zhang, L., Chen, X.-L., Lei, J., Cheng, Z.-X., 2013. Sonic hedgehog signaling pathway induces cell migration and invasion through focal adhesion kinase/AKT signaling-mediated activation of matrix metalloproteinase (MMP)-2 and MMP-9 in liver cancer. Carcinogenesis 34, 10–19. https://doi.org/10.1093/carcin/bgs274

Aman, A.J., Fulbright, A.N., Parichy, D.M., 2018. Wnt/β-catenin regulates an ancient signaling network during zebrafish scale development. Elife 7, e37001. https://doi.org/10.7554/elife.37001

Tsai, T.Y.-C., Sikora, M., Xia, P., Colak-Champollion, T., Knaut, H., Heisenberg, C.-P., Megason, S.G., 2020. An adhesion code ensures robust pattern formation during tissue morphogenesis. Science (80-.). 370, 113–116. https://doi.org/10.1126/science.aba6637 PMID - 33004519

Zhang, J., Jeradi, S., Strähle, U., Akimenko, M.A., 2012. Laser ablation of the sonic hedgehog-a-expressing cells during fin regeneration affects ray branching morphogenesis. Dev. Biol. 365, 424–433. https://doi.org/10.1016/j.ydbio.2012.03.008

Lee, Y., Hami, D., Val, S. De, Kagermeier-Schenk, B., Wills, A.A., Black, B.L., Weidinger, G., Poss, K.D., 2009. Maintenance of blastemal proliferation by functionally diverse epidermis in regenerating zebrafish fins. Dev. Biol. 331, 270–280. https://doi.org/10.1016/j.ydbio.2009.05.545

Swartz, M.E., Nguyen, V., McCarthy, N.Q., Eberhart, J.K., 2012. Hh signaling regulates patterning and morphogenesis of the pharyngeal arch-derived skeleton. Dev. Biol. 369, 65–75. https://doi.org/10.1016/j.ydbio.2012.05.032

Ewald, A.J., Brenot, A., Duong, M., Chan, B.S., Werb, Z., 2008. Collective epithelial migration and cell rearrangements drive mammary branching morphogenesis. Dev. Cell 14, 570–581. https://doi.org/10.1016/j.devcel.2008.03.003

Figures 2.1 – 2.6
Figures S2.12

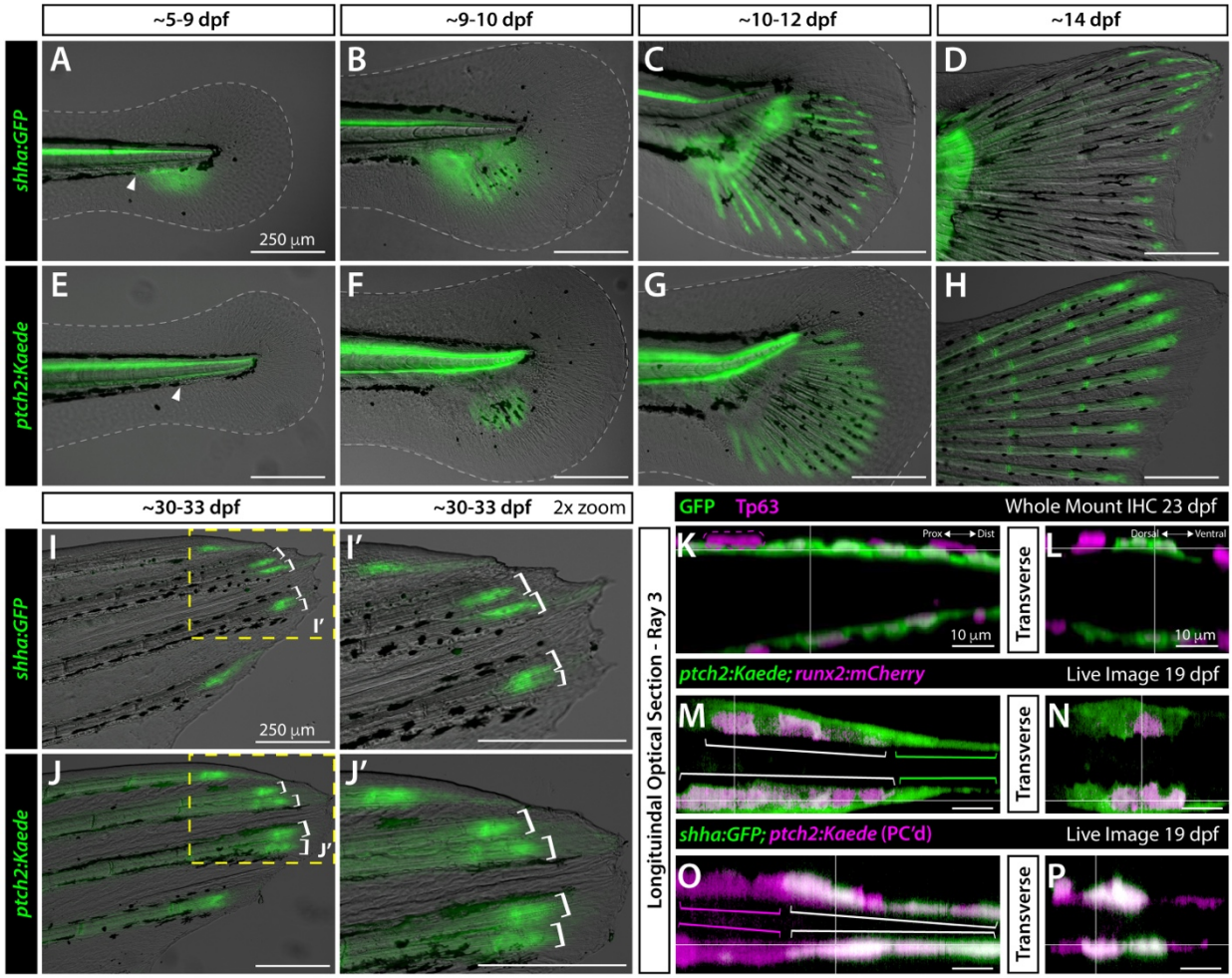

Figure 2.1. Basal epidermal *shha* and *ptch2*-defined responses in basal epidermis and pre-osteoblasts become progressively distally restricted during caudal fin development.

Figure 2.1. Basal epidermal *shha* and *ptch2*-defined responses in basal epidermis and pre-osteoblasts become progressively distally restricted during caudal fin development.

(A-J') Differential interference contrast and fluorescent overlay images of developing caudal fins of *shha:GFP* (A-D, I, I') and *ptch2:Kaede* (E-H, J, J') fish of indicated ages. White dotted lines outline the fin fold (A-F). The white arrowhead indicates the gap in melanophores where *shha:GFP* expression emerges. Yellow boxes in (I, J) indicate the 2x zoom fields in (I', J'). White brackets (I-J') mark branched reporter domains in dorsal rays 2 and 3 preceding overt ray branching. (K-P) Single optical slices of caudal fin dorsal ray 3 in longitudinal (K, M ,O) and transverse (L, N, P) planes derived from 3D-reconstructed whole mount confocal images of fluorescent reporter fish of indicated ages. (K, L) 23 dpf *shha:GFP* fin whole mount antibody stained for GFP (green) and the basal epidermis marker Tp63 (magenta). The orange dashed line outlines a representative Tp63+, GFP- cell that occasionally overlay the innermost basal epidermal layer. (M-P) Single optical slice reconstructed equivalents from live whole mount-imaged 19 dpf *ptch2:Kaede;runx2:mCherry* and *shha:GFP;ptch2:Kaede* caudal fins. (M, N) *ptch2:Kaede* (green) is in distal *runx2*-marked pre-osteoblasts (magenta; white brackets) and a thin layer of tightly associated adjacent and further distally-extending basal epidermis (green brackets). (O, P) *ptch2:Kaede* (photoconverted; magenta) in pre-osteoblasts (magenta brackets) and co-localized with *shha:GFP*-expressing basal epidermis (green, white brackets). Scale bars are 250 μm in (A-J') and 10 μm in (K-P).

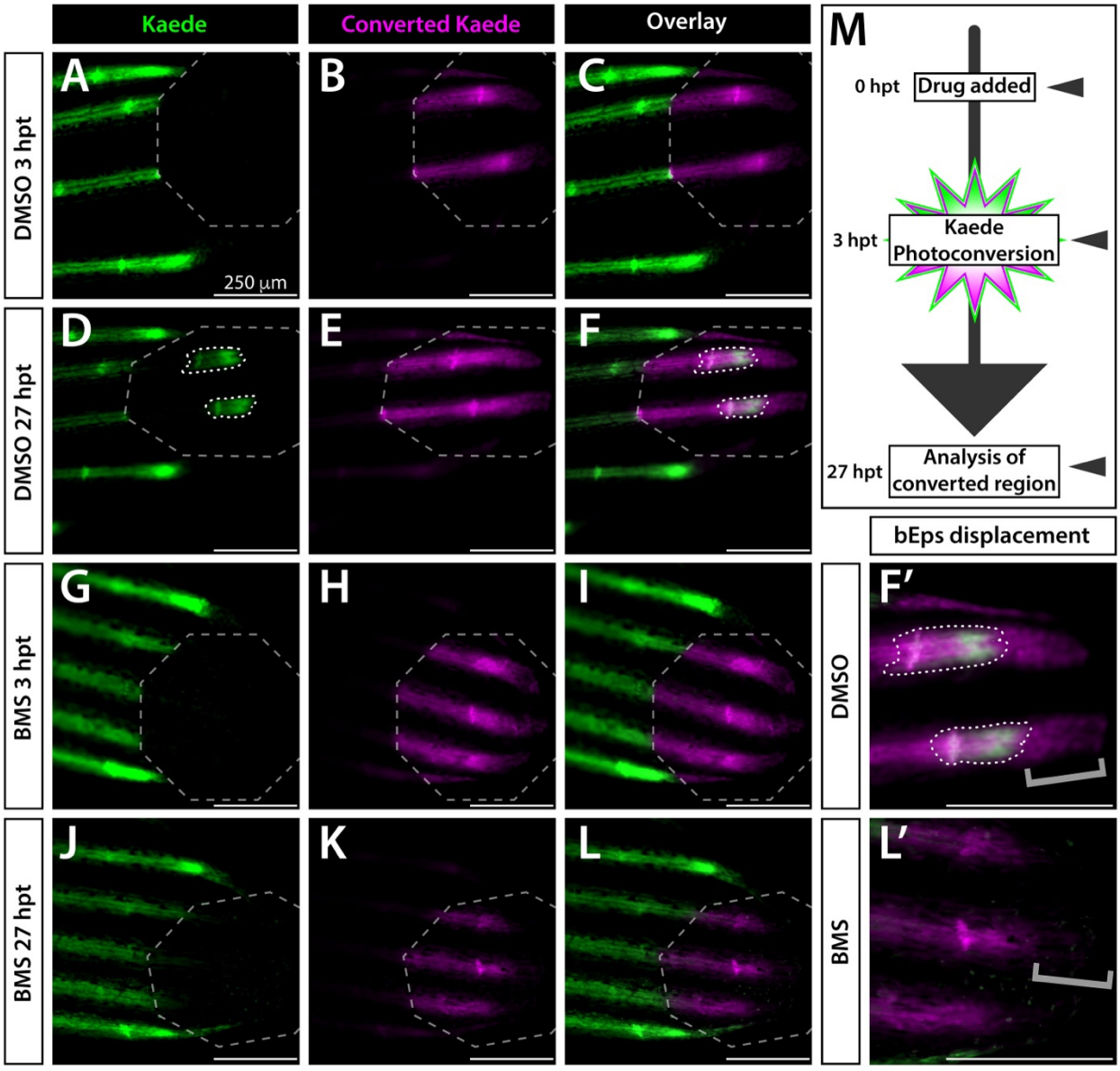

Figure 2.2. Active Shh/Smo signaling is restricted to a narrow distal stretch of each developing fin ray.

Figure 2.2. Active Shh/Smo signaling is restricted to a narrow distal stretch of each developing fin ray.

(A-L) Whole mount fluorescence images of the distal aspect of the caudal fin of 25 dpf *ptch2:Kaede* fish treated with DMSO (A-F) or BMS-833923 (BMS; G-L). Images are from the time of Kaede photoconversion from green to red (false colored magenta) fluorescence (0 hours post conversion (hpc); A-C, G-I) and 24 hours later (24 hpc, D-F, J-L). Grey dashed octagons mark photoconverted regions of interest (ROIs). The 0 hpc overlay (C) demonstrates complete Kaede photoconversion. The same fish at 24 hpc displays a small patch of newly produced green Kaede (white dotted outlines in D, F) within the ROI. Slight splitting of the new green Kaede domain indicates the onset of ray branching. The BMS-treated fish shows no new Kaede within the ROI (J-L). (F', L') Zoom view of distal ray regions. Grey brackets mark presence or absence of distally displaced basal epidermis retaining photoconverted Kaede. These cells are missing in BMS-treated fish (L'), possibly due to accelerated movement and therefore shedding. The few green Kaede+ basal epidermal cells in (J, L) moved into the photoconverted region without producing new Kaede. (M) Schematic of the time course for drug treatment, photoconversion, and imaging. Imaged fish represent groups of n=8. Scale bars are 250 μm.

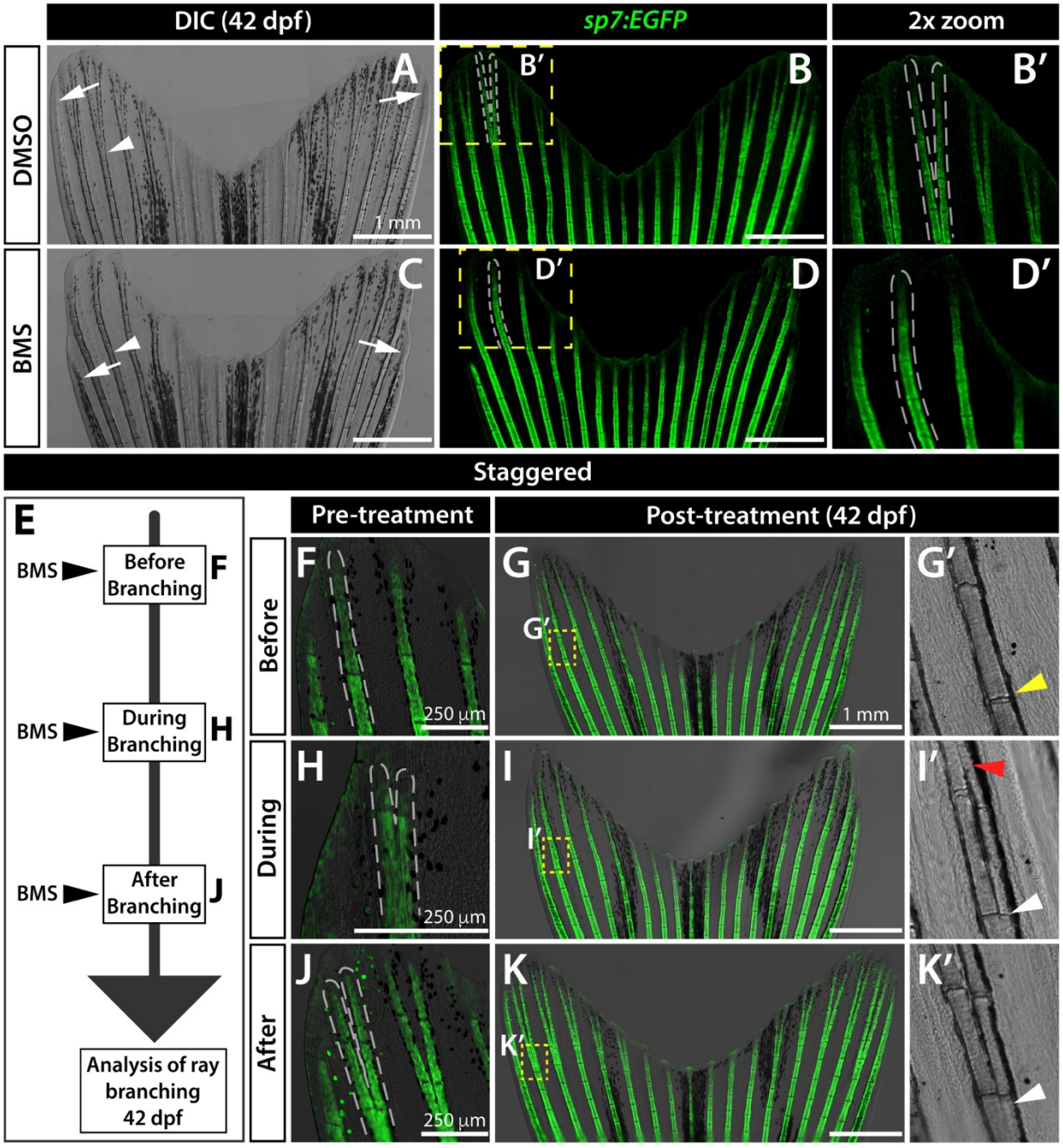

Figure 2.3. Sustained Shh/Smo signaling is required for ray branching in developing caudal fins.

Figure 2.3. Sustained Shh/Smo signaling is required for ray branching in developing caudal fins.

(A-D) Differential interference contrast (DIC) and fluorescence images of caudal fins from DMSO (A, B) and BMS-833923 (BMS)-treated (C, D) 42 dpf *sp7:EGFP* osteoblast reporter fish. Dashed white lines outline dorsal ray 3 and daughter rays, when present. White arrowheads designate a present (A) or absent (B) branch point. White arrows mark ends of the principal peripheral rays. (E-K) Experimental schematic of (E) and resulting caudal fin images of 42 dpf *sp7:EGFP* fish from (F-K') staggering the start of BMS treatment to before (F-G'), during (H-I'), and after branch initiation (J-K'). Yellow dashed boxes outline dorsal ray 2 regions shown in (G', I' and K'). The yellow arrowhead in (G') designates where branching would have occurred without Shh/Smo-inhibition. The red arrowhead in (I') marks where a ray re-fused when BMS was added after branching had initiated. White arrowheads in (I' and K') indicate ray branch points. Images represent treatment groups (before, during, and after) of n=4 or 5 BMS-treated and n =2 or 3 DMSO controls. Ray re-fusions occur in 4 of 5 fish treated with BMS "during" ray branching in rays 2, 3, and 16. Scale bars are 250 μm or 1 mm, as indicated.

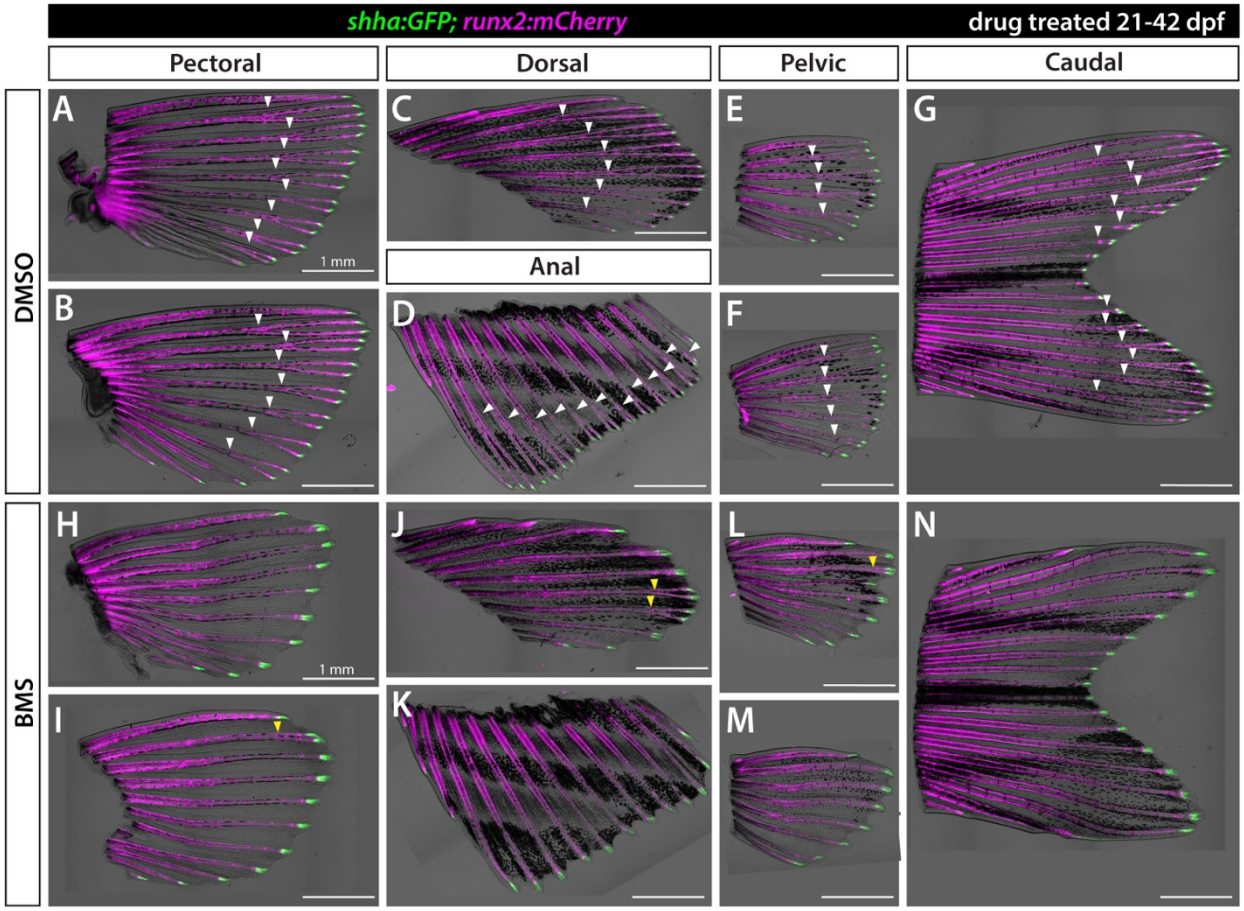

Figure 2.4. Shh/Smo signaling promotes ray branching in all paired and unpaired fins.

Brightfield and fluorescence overlay images of isolated fins from *shha:GFP;runx2:mCherry* juvenile fish treated with DMSO (A-G) or 1.25 µM BMS-822923 (BMS; H-N) from 21-42 dpf. *runx2:mCherry*-labeled rays branch (white arrowheads) in all fins whereas rays of BMS-treated fish mostly fail to branch or have severely delayed branching (yellow arrowheads). *shha:GFP+* basal epidermal cells are restricted to distal ray tips under both conditions. *n*=6 for each group. Scale bars are 1 mm.

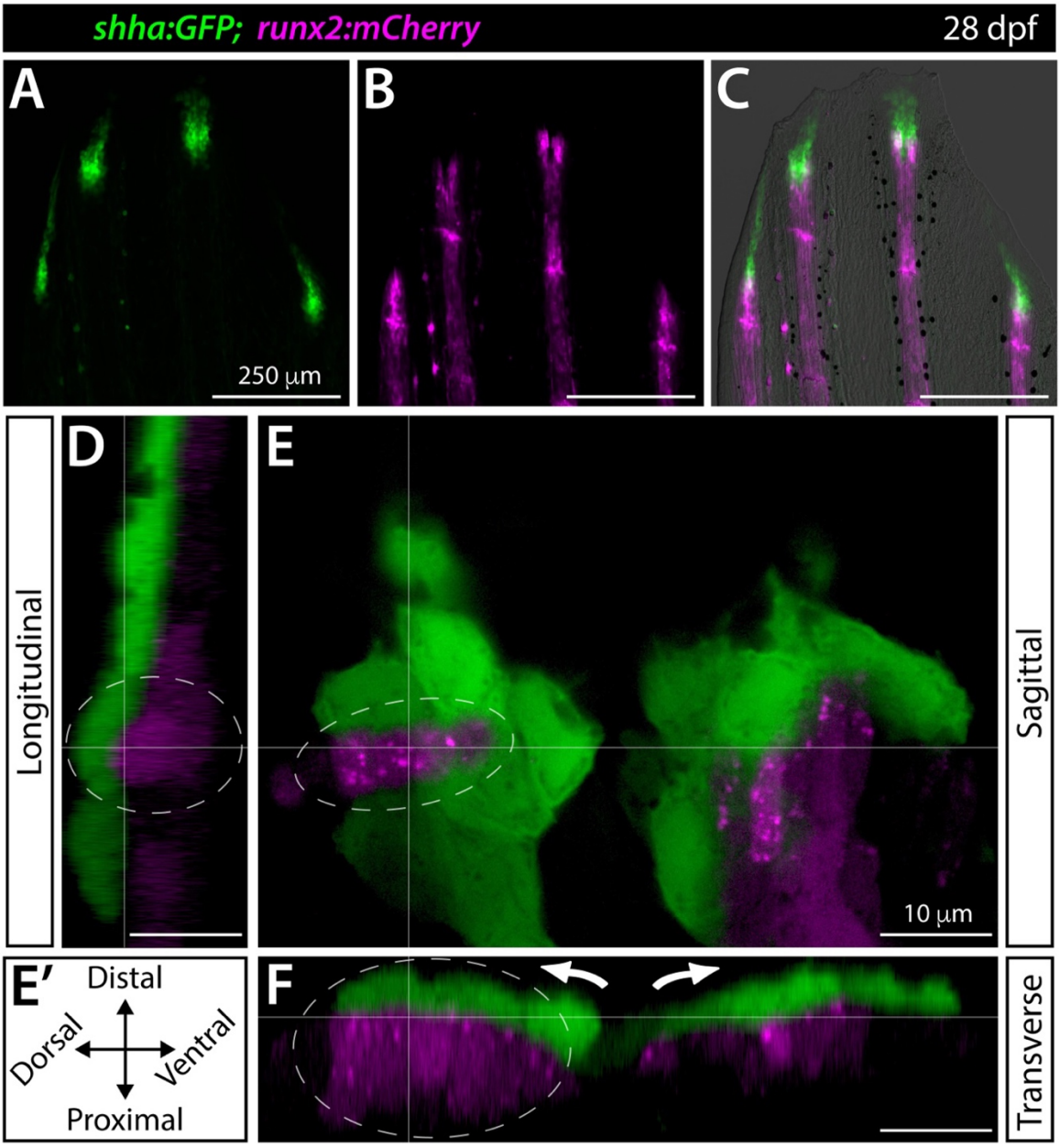

Figure 2.5. Shha+ basal epidermis and pre-osteoblasts are intertwined in developing fins.

(A-F) Fluorescence widefield (A-C) or confocal (D-F) images of the dorsal caudal fin lobe of a 28 dpf *shha:GFP;runx2:mCherry* fish. (A-C) *shha:GFP*-expressing basal epidermal cells (green) overlay and extend distally from *runx:mCherry*-high pre-osteoblast (magenta). The overlay in (C) includes a brightfield image for context. (D-F) A single optical slice (E; sagittal; orientation key in E') and reconstructed longitudinal (D) and transverse (F) views of a distal ray region undergoing ray branching. *shha:GFP*+ basal epidermis (green) and *runx2:mCherry*+ pre-osteoblasts (magenta) have overlapping signal at interfaces, indicating their tight juxtaposition. Basal epidermis and pre-osteoblasts tandemly separate into split pools during branching (white arrows). The grey dotted oval highlights a ridge of pre-osteoblasts nestled into a *shha:GFP*+ basal epidermal groove (Movie 2). Scale bars are 250 μm (A-C) and 10 μm (D-F).

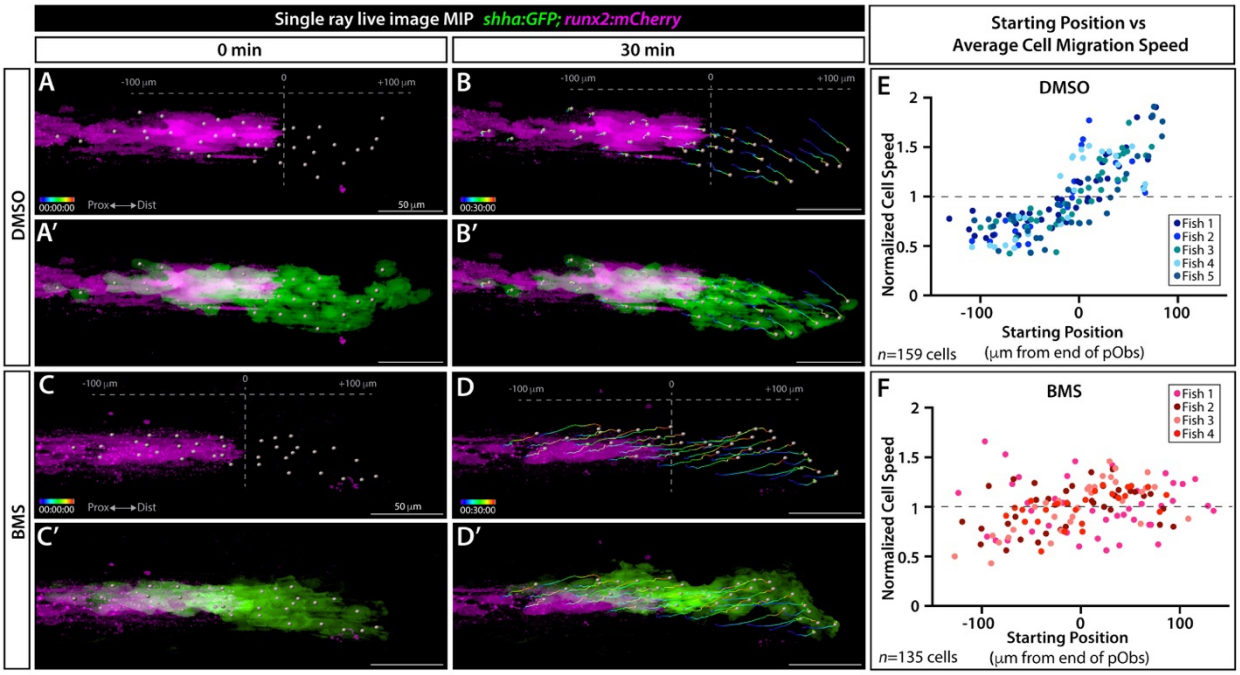

Figure 2.6.Shh/Smo signaling slows collective migration of shha-expressing basal epidermal cells associated with pre-osteoblasts.

(A-D') Frames from a time lapse movie showing dorsal ray 3 of the caudal fin from live mounted 24 dpf *shha:GFP;runx2:mCherry* fish treated with DMSO or BMS-833923 (BMS) for 24 hours prior to imaging. Images are maximum intensity projections (MIP) and show the start (0 min; A, A', C, C') and end (30 min; B, B', D, D') points. The Imaris-generated colored tracks show the progressive displacement of individual *shha:GFP+* basal epidermal cells (green). Grey spheres show the starting or final positions of all tracked basal epidermal cells. Grey dashed vertical lines in (A, B, C, D) indicate the distal most Runx2+ pre-osteoblast (magenta), defined as position "0". (E, F) Scatter plot graphs showing the average speed of individual basal epidermal cells, considering their net X-displacement and normalized to all scored cells of the given fish, relative to starting position for DMSO- (159 individual cells from five fish) and BMS-exposed fish (135 cells from four fish). Dot colors correspond to cells from a given fish. Scale bars are 50 µm.

CHAPTER II: SUPPLEMENTARY MATERIAL

Figures S2.1-S2.12.

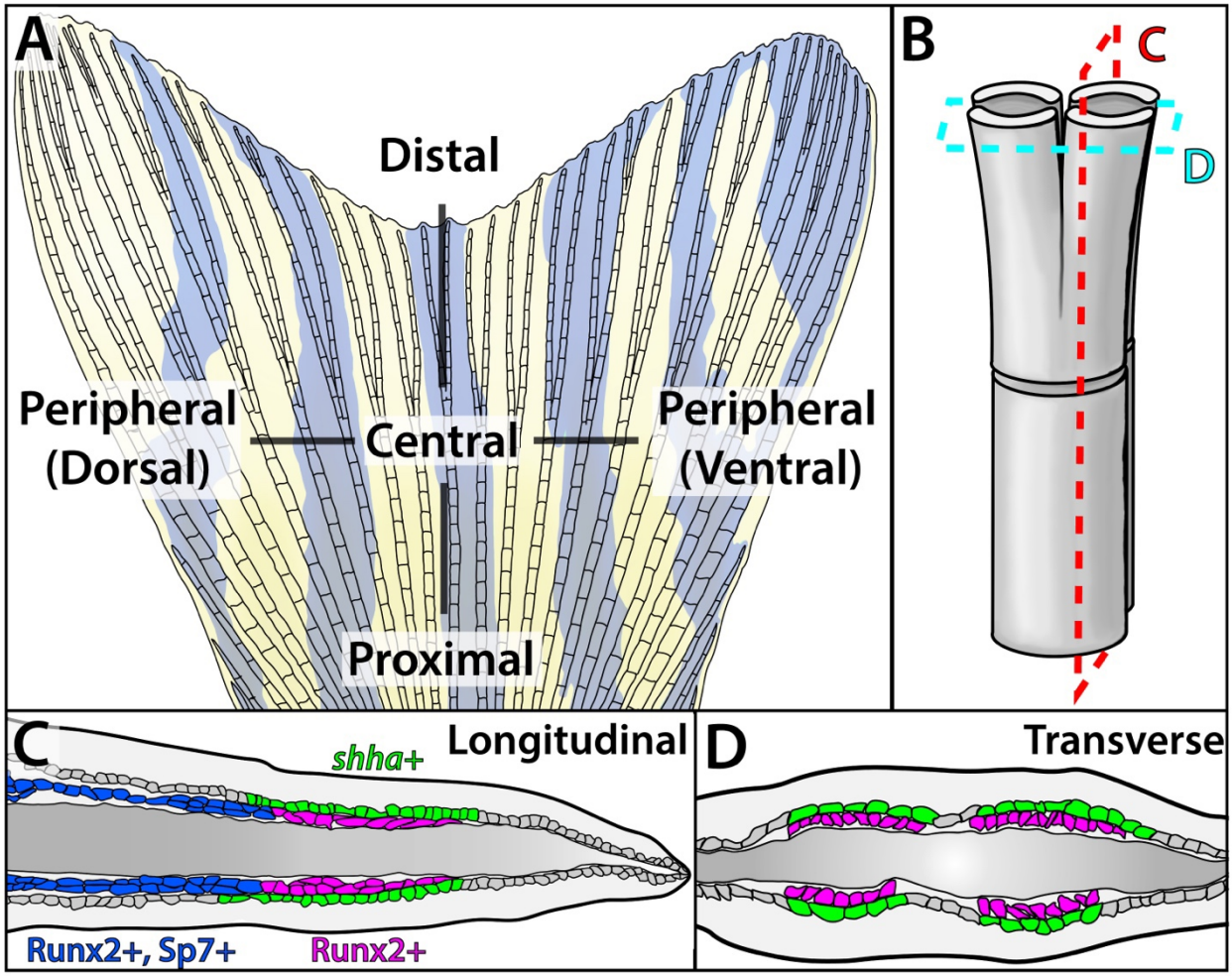

Figure S2.1. Schematic of caudal fin skeletal anatomy.

(A) Schematic of an adult zebrafish caudal fin. The caudal fin skeleton comprises 18 bony rays (lepidotrichia), of which the inner 16 branch at least once. (B) Cartoon rendering of a skeletal ray branch point. Two opposed hemi-cylindrical calcified hemi-rays form each ray. Branching produces two equally sized daughter rays. (C, D) Colored tracings of longitudinal (C) and transverse (D) sections through a branching lepidotrichia. Distal domains of *shha*-expressing basal epidermal cells (basal epidermis, green) directly neighbor Runx2+ pre-osteoblasts (magenta). Those basal epidermal cells distally beyond pre-osteoblast pools lose *shha* expression. *shha*+ basal epidermis and pre-osteoblast domains both split peripherally as branching initiates. As the fin extends, the distal Runx2+ pre-osteoblast pool generates differentiating Runx2/Sp7+ osteoblasts (purple) that eventually mature into proximal sp7+ bone-forming cells (blue).

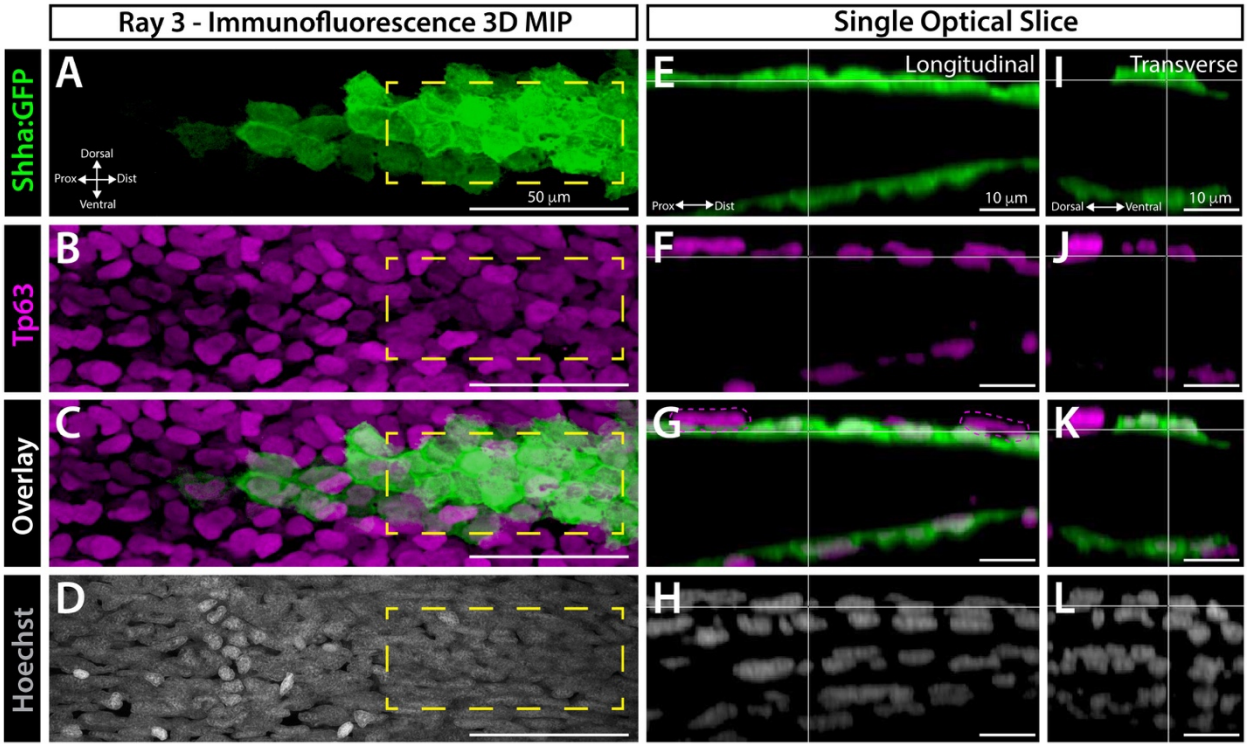

Figure S2.2. *shha* is expressed in a single layer of distal basal epidermal cells in developing caudal fins.

3D reconstructed sectional views of dorsal ray 3 from a whole mount immunostained 23 dpf *shha:GFP* caudal fin. Panels show GFP (green, A, E, I), the basal epidermal marker Tp63 (magenta, B, F, J), GFP and Tp63 overlays (C, G, K; G and K are reproduced in Figure 1), and Hoechst-stained nuclei (white, D, H, I). (A-D) Maximum intensity projection (MIP) of the "native" frontal view. (E-L) Reconstructed single optical slice equivalents showing longitudinal (E-H) and transverse (I-L) planar views of the dashed yellow boxed regions in (A-D). Shha-expressing cells (as marked by GFP) define the innermost basal epidermal cell layer and all co-express Tp63. An occasional single-positive Tp63+ basal epidermis (representative cell in magenta dashed lines, G) is found in the suprabasal layer. Scale bars and orientations are indicated.

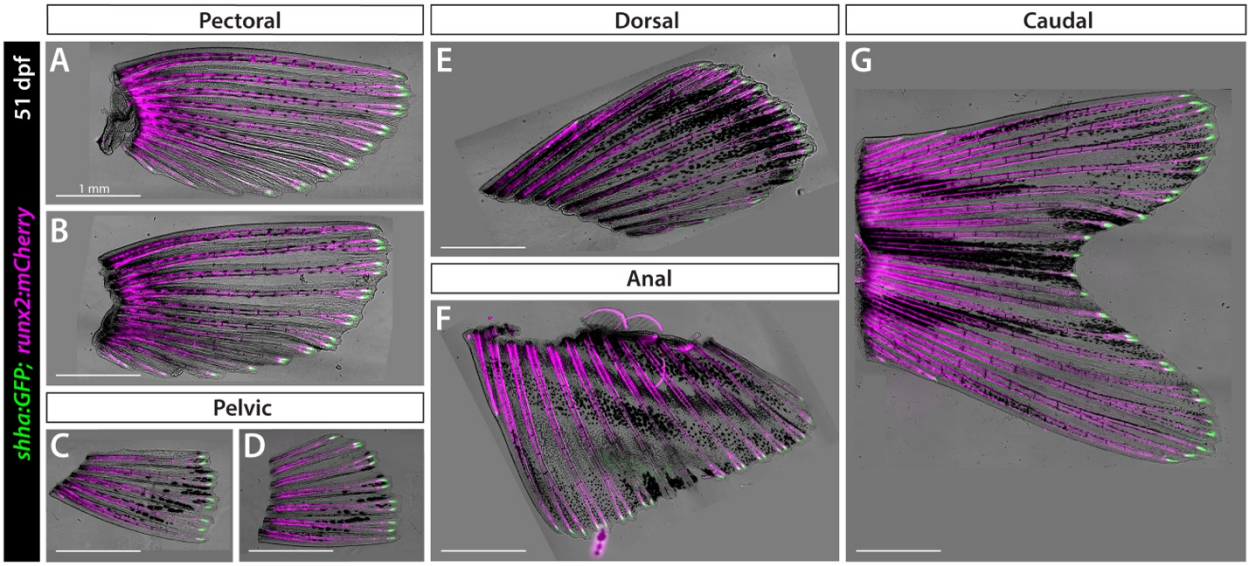

Figure S2.3 Distal *shha* expression is conserved across developing fins.

Dissected fins from a representative 51 dpf *shha:GFP;runx2:mCherry* fish. Zebrafish have 7 fin appendages: the paired pectoral (A, B) and pelvic (C, D) fins and unpaired dorsal (E), anal (F), and caudal (F) fins. All have branched rays marked by *runx2:mCherry* (magenta) with *shha:GFP+* domains (green) at the distal end of each developing ray. All images are brightfield/GFP/mCherry overlays and sized to the same scale (1 mm scale bars).

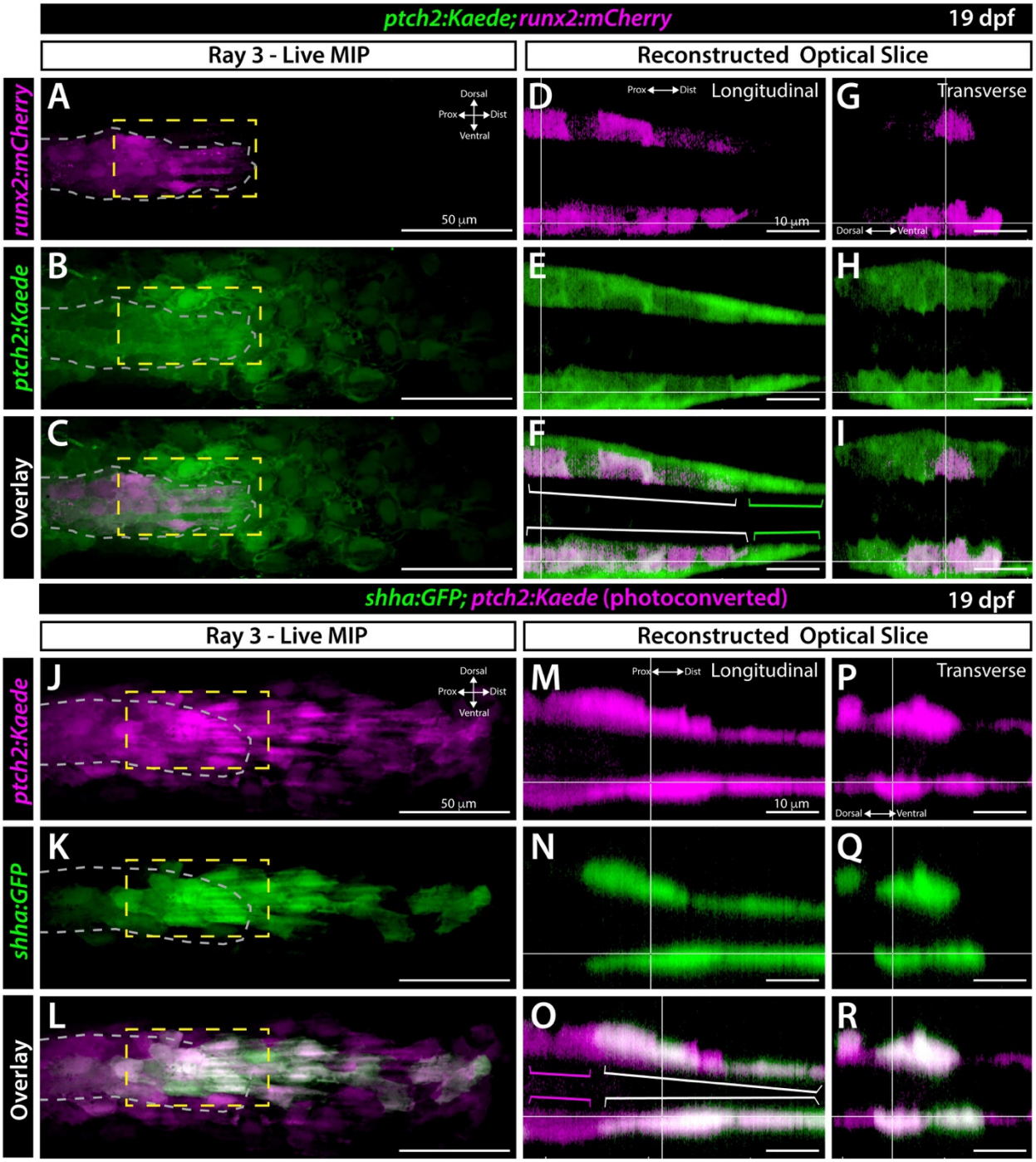

Figure S2.4. *ptch2* is expressed in tightly associated layers of distal basal epidermal cells and pre-osteoblasts in developing caudal fins.

Figure S2.4. *ptch2* is expressed in tightly associated layers of distal basal epidermal cells and pre-osteoblasts in developing caudal fins.

(A-I) Whole mount confocal imaging of dorsal ray 3 from a live 19 dpf *ptch2:Kaede; runx2:mCherry* caudal fin. (A-C) Maximum intensity projection (MIP) of a frontal view. The pre-osteoblast pool is outlined with grey dashed lines. *runx2:mCherry*-marked pre-osteoblasts are in magenta (A) and *ptch2:Kaede* is in green (B). The overlay is shown in (C). (D-I) Reconstructed optical slice views of the region marked by yellow dashed lines in A-C. Overlays (F, I; reproduced in main Figure 1) show relatively proximal regions of *ptch2:Kaede* and *runx2:mCherry*+ co-expressing pre-osteoblasts (white brackets) and an adjacent thin layer of *ptch2:Kaede*+ basal epidermal cells. These basal epidermal cells extend further distally from the pre-osteoblast pool (green brackets). (J-R) Confocal images of dorsal ray 3 from a 19 dpf *shha:GFP;ptch2:Kaede* caudal fin in which the Kaede protein has been photoconverted from green to red fluorescence emission. (J-L) Frontal view MIP with osteoblast-populated region outlined with grey dashed lines. *shha:GFP* basal epidermis (green) co-express *ptch2:Kaede* (magenta). (M-R) Reconstructed optical slices of the yellow dashed boxes in J-L. Overlays (O, R; reproduced in main Figure 1) demonstrate proximal regions contain single-positive *ptch2:Kaede*+ pre-osteoblasts (magenta brackets) whereas distal regions include co-expressing *shha:GFP* and *ptch2:Kaede* basal epidermis (white brackets). Scale bars are 50 μm in A-C, J-L and 10 μm in D-I, M-R.

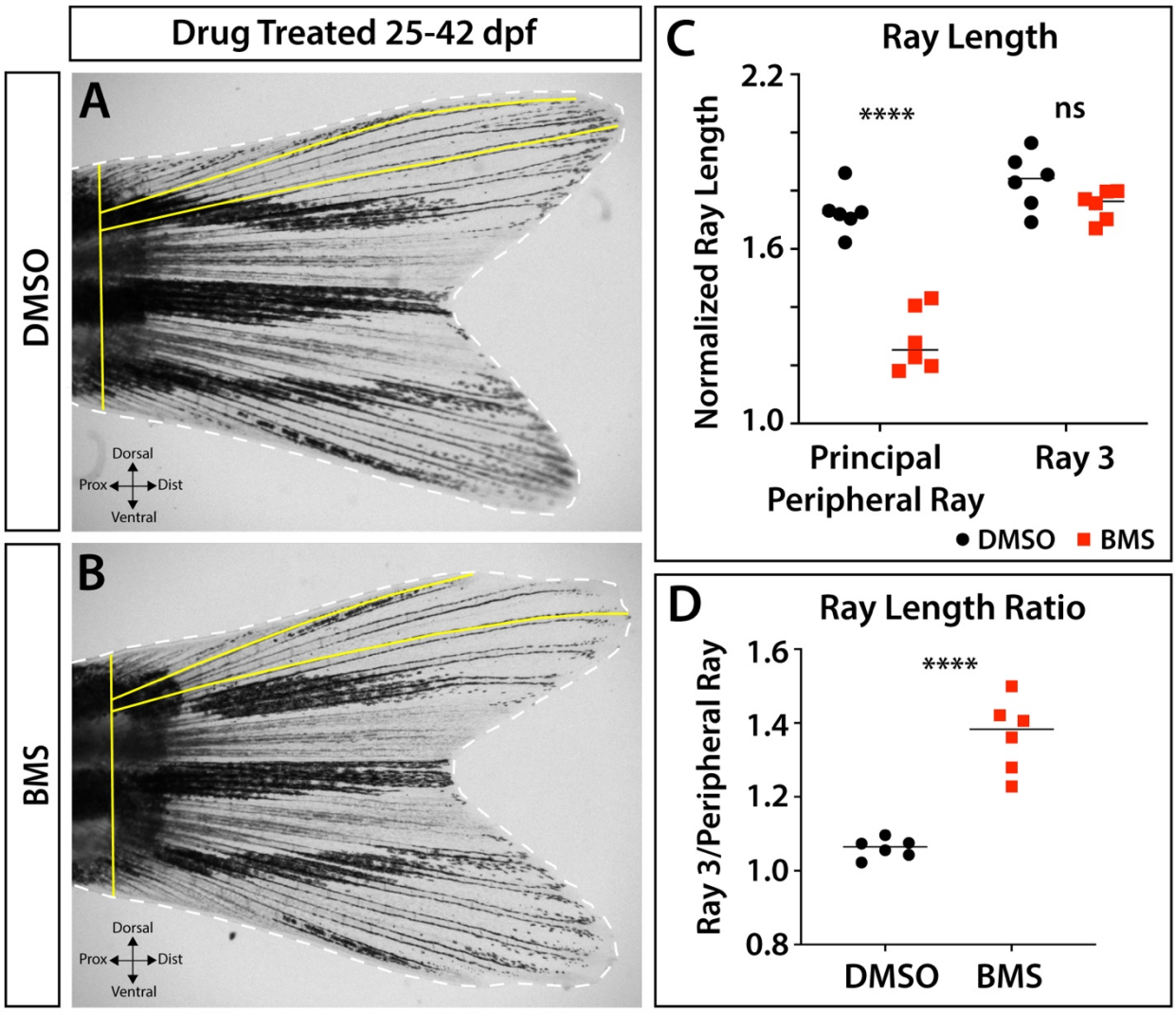

Figure S2.5. Shh/Smo signaling contributes to principal peripheral ray outgrowth.

Whole mount caudal fin images of (A) DMSO- and (B) BMS-treated juvenile fish (exposed from 25-42 days post fertilization (dpf)) and (C) graphs of ray morphometrics. Yellow lines indicate measured ray lengths and fin widths. Dorsal ray 3 does not significantly differ in length between treatment groups ($p = 0.09$). In contrast, the non-branching principal peripheral ray 1 is uniquely shorter in BMS-treated versus DMSO control fish ($p < 0.0001$). As such, the ray length ratio between ray 3 and principal peripheral ray 1 is higher in BMS-treated fish ($p < 0.0001$). Images are representatives of experimental groups of $n=6$. Ray length measurements are from the base of the fin and are normalized to fin width, which did not differ between groups. Statistical significance was determined using Student's unpaired t-tests.

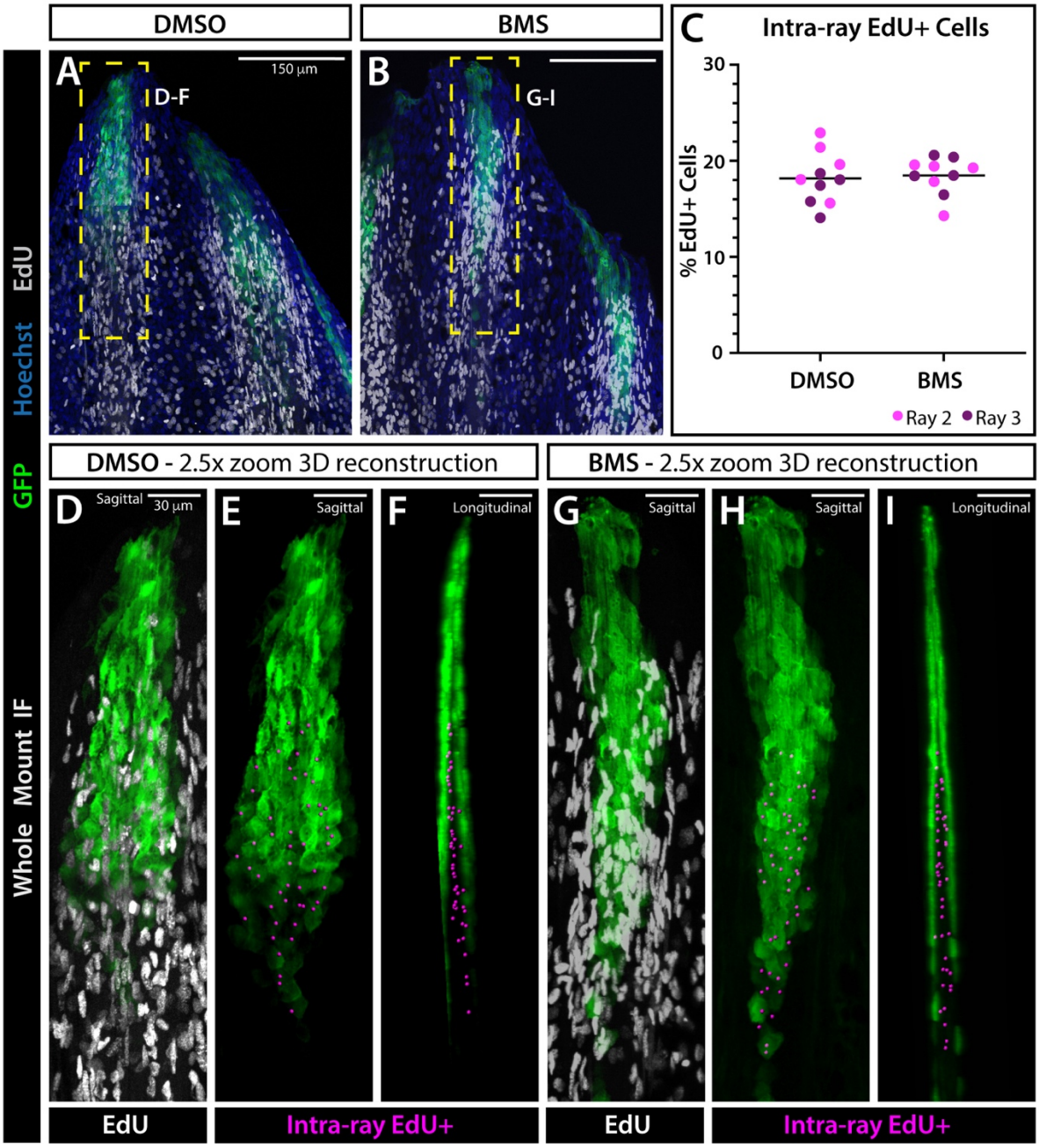

Figure S2.6. Shh/Smo signaling does not impact proliferation in developing fin rays.

Figure S2.6. Shh/Smo signaling does not impact proliferation in developing fin rays.

(A, B) Confocal maximum intensity projection images of whole mount immunostained 29 dpf developing *shha:GFP* caudal fins. Fish were treated with DMSO (A) or BMS-833923 (BMS) (B) for 4 hours, IP injected with EdU, returned to drug, and fins harvested 12 hours later. GFP is in green, Hoechst nuclear stain in blue, and EdU as detected with Click-iT Plus in white. (C) Dot plot graph showing the percent of intra-ray EdU+ cells, i.e. those located in between the epidermal Shh domains of each hemi-ray, does not significantly differ between DMSO controls and BMS-treated fish. n=5 for each group. (D-I) 3D reconstructions of ray 3 domains marked by yellow dashed boxes in (A, B). (D, G) Overlay of GFP and EdU, sagittal view. (E, H) GFP with magenta spheres marking EdU+ cells located within the intra-ray space, detected and quantified with Imaris software. (F, I) Longitudinal view of (E, H). Intra-ray EdU+ cells are located in between Shh+ domains with epidermal cells excluded from automated scoring. Scale bars are 150 μm or 30 μm, as indicated.

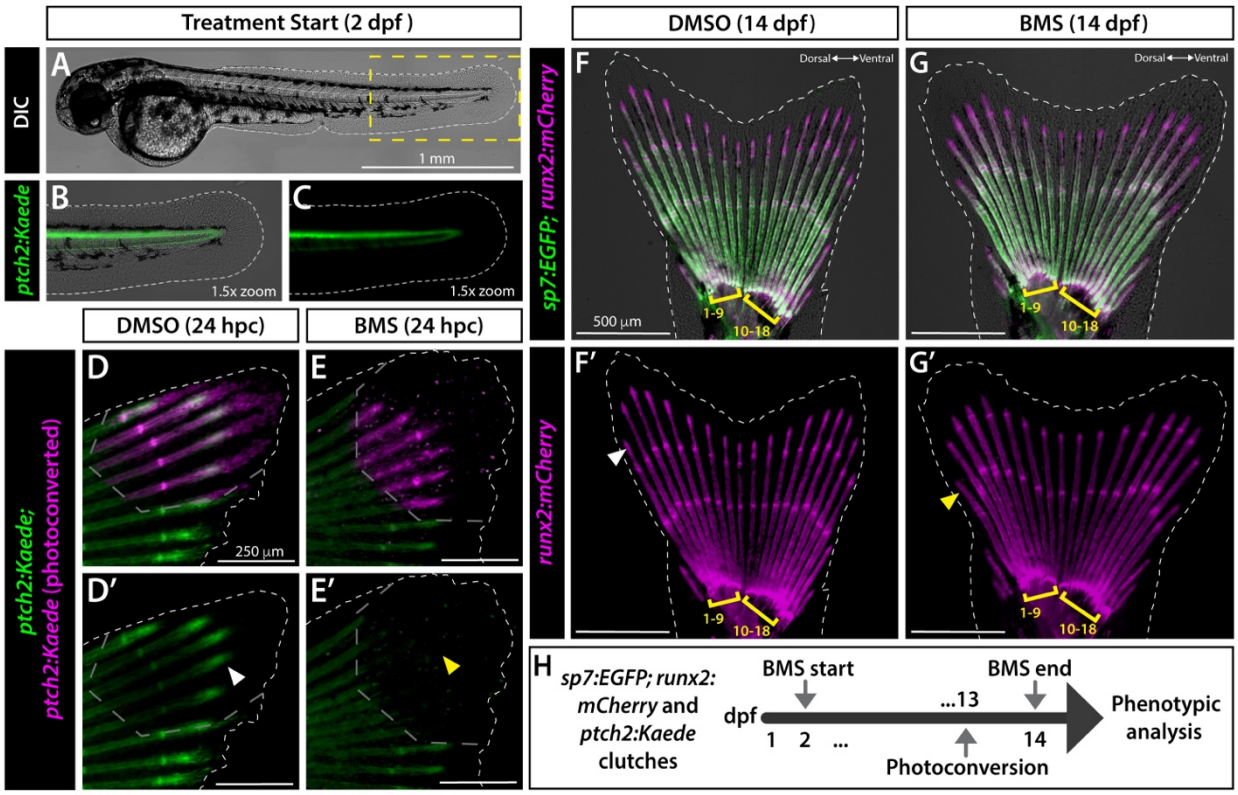

Figure S2.7. Shh/Smo signaling does not influence initial caudal fin patterning.

(A-C) Whole mount differential interference contrast (DIC) and/or fluorescence images of a 2 dpf *ptch2:Kaede* embryo. The dashed yellow box marks the 1.5x zoomed region shown in (B, C). The primordial fin fold lacks rays or structural ray precursors. *ptch2:Kaede* expression is restricted to the notochord and does not expand into the fin fold. (D-E'). *ptch2:Kaede* larvae treated with DMSO or BMS-833923 (BMS) from 2 dpf, photoconverted distal fin regions at 13 dpf (grey dashed lines), and imaged 24 hours later (*n*=3-5 per group). BMS treatment blocked production of new green Kaede (yellow arrowhead, E') compared to controls (white arrowhead, D'). (F-G') Whole mount fluorescence images of *sp7:EGFP;runx2:mCherry* larvae treated with DMSO (F) or BMS (G) from 2-14 dpf. Both groups have caudal fins with the standard complement of 18 segmented rays, with 9 rays each on the dorsal and ventral lobes (yellow brackets). BMS-treated fins exhibit shortened principal peripheral rays (yellow arrowhead, G') compared to DMSO controls (white arrowhead, F'). *n*=33 DMSO- and *n*=44 BMS-treated larvae from 2-14 dpf. Scale bars are 1 mm, 250 µm, or 500 µm, as marked.

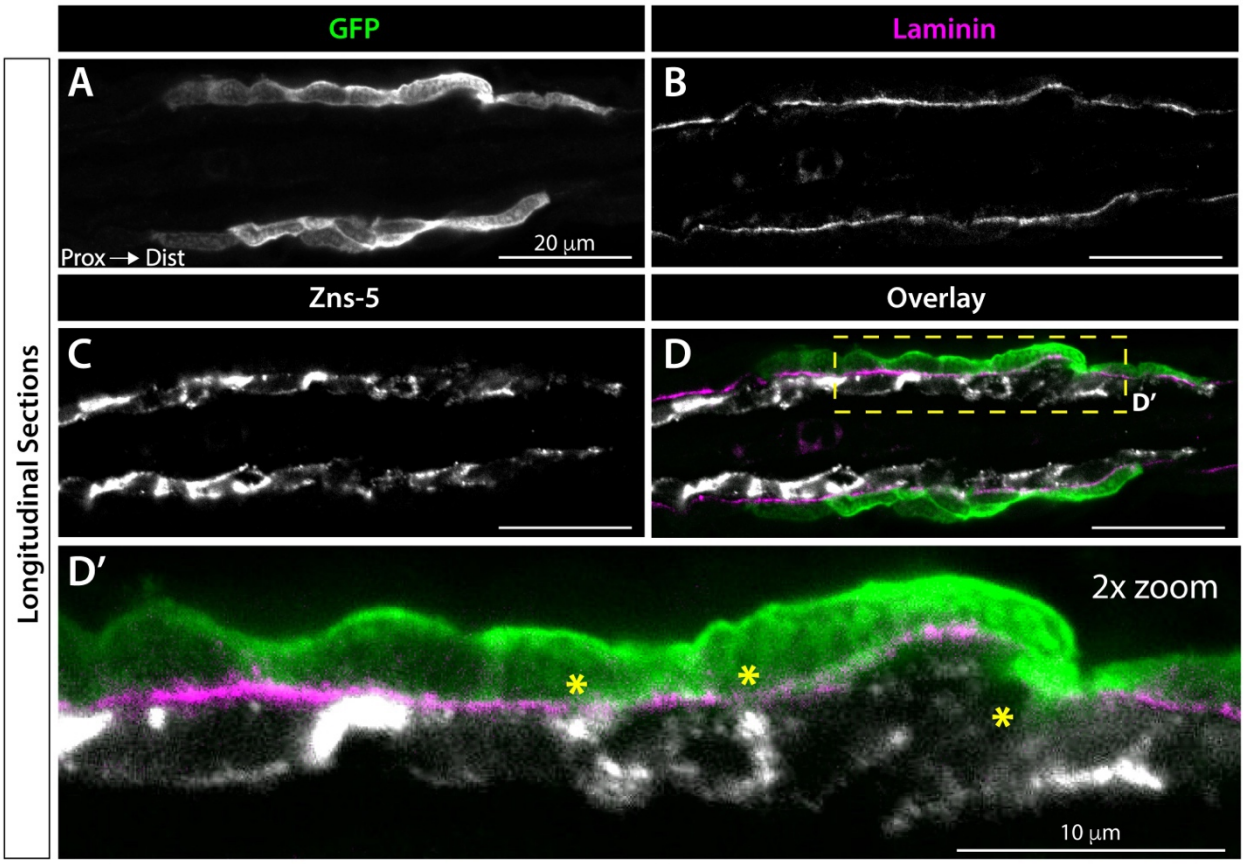

Figure S2.8. Shha+ basal epidermal cells are tightly associated with pre-osteoblasts in distal regions of incomplete basement membrane assembly.

(A-D) Confocal images of the distal ray regions from immunostained longitudinal caudal fin sections of 32 dpf *shha:GFP* fish. GFP-expressing basal epidermal cells (green) and Zns-5-marked osteoblasts (white) are separated by a Laminin-defined basement membrane (BM; magenta). (D') 2x magnification of the yellow dashed box region in the (D) overlay. Asterisks mark areas where Laminin signal is less dense, indicating an incompletely assembled BM, and GFP and Zns-5 partially overlap (D'). Scale bars are 20 μm.

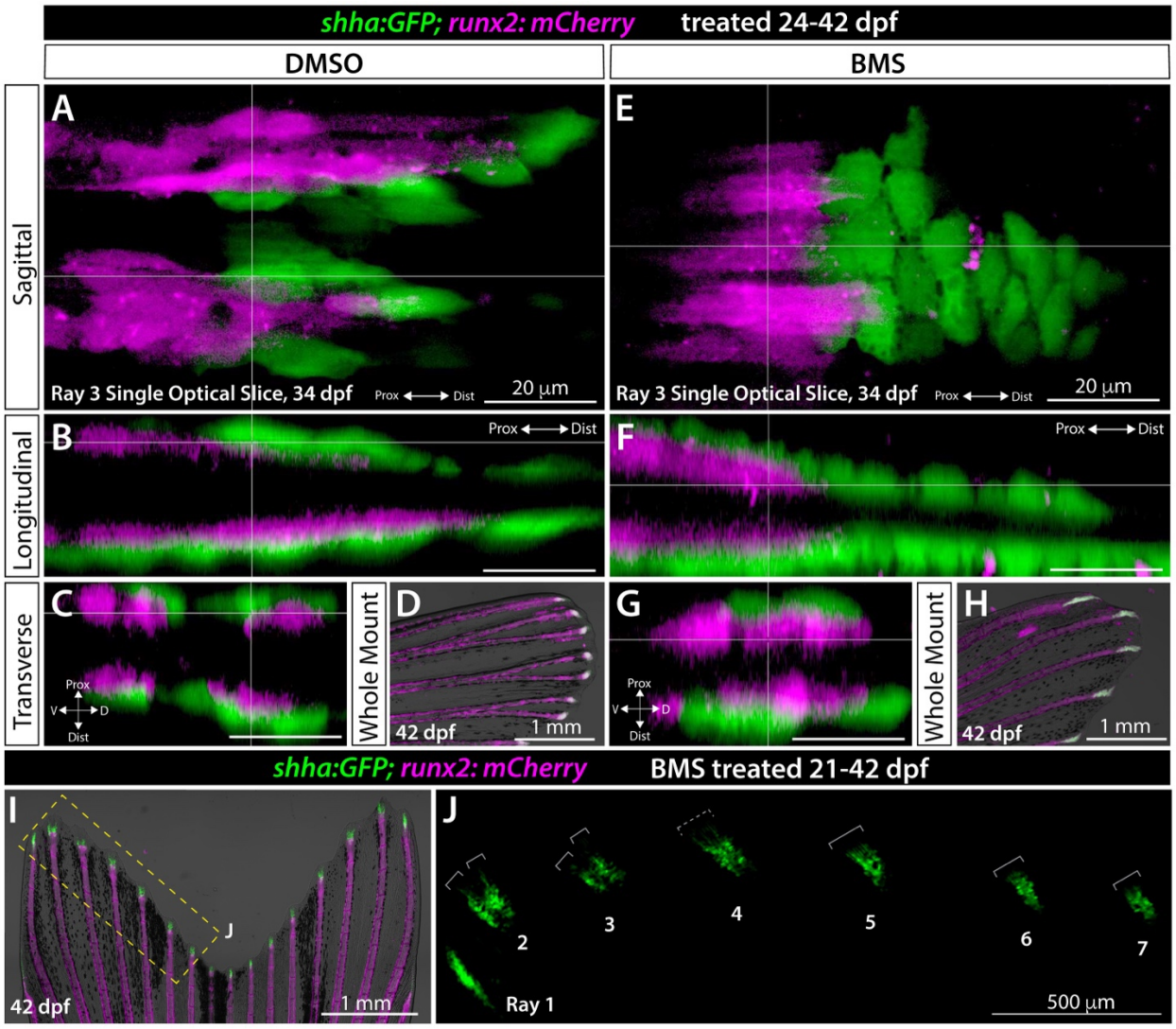

Figure S2.9. Shh/Smo signaling does not influence Shh+ basal epidermis and pre-osteoblast juxtaposition.

Figure S2.9. Shh/Smo signaling does not influence Shh+ basal epidermis and pre-osteoblast juxtaposition.

(A-J) Confocal or widefield fluorescence caudal fin images from *shha:GFP;runx2:mCherry* fish treated with DMSO (control) or 1.25 μM BMS-833923 (BMS) starting at 24 dpf (*n*=8 per group). (A-C, E-G) Single optical slices or equivalent 3D-reconstructed views of 34 dpf mid-treatment fish, imaged concurrently with active ray branching morphogenesis. *shha:GFP+* basal epidermal cells (green, A) are closely associated with *runx2:mCherry*-expressing pre-osteoblasts (magenta). BMS-treated fish (E-G) maintain close Shh+ basal epidermal and Runx2+ pre-osteoblast contacts while lacking clear *shha:GFP* domain-splitting (*n*=4 per group). (D, H, I, J) Caudal fin images of *shha:GFP;runx2:mCherry* fish continued on drug treatment until 42 dpf (*n*=4 per group). (D, H, I) Widefield fluorescence and brightfield overlay caudal fin images. Unlike DMSO controls (D), BMS-treated fish do not develop branched rays, confirming drug efficacy (H). (I, J) Fin of a 21-42 dpf BMS-treated fish. The yellow dashed box indicates the GFP-alone magnified panel in (J). *shha:GFP* domains are variably split (two grey brackets, rays 2, 3), partially split (dashed grey bracket, ray 4) or unsplit (one grey bracket, rays 5-7). Scale bars are 20 μm (A-C, E-G), 1 mm (G, H, I) and 500 μm (J).

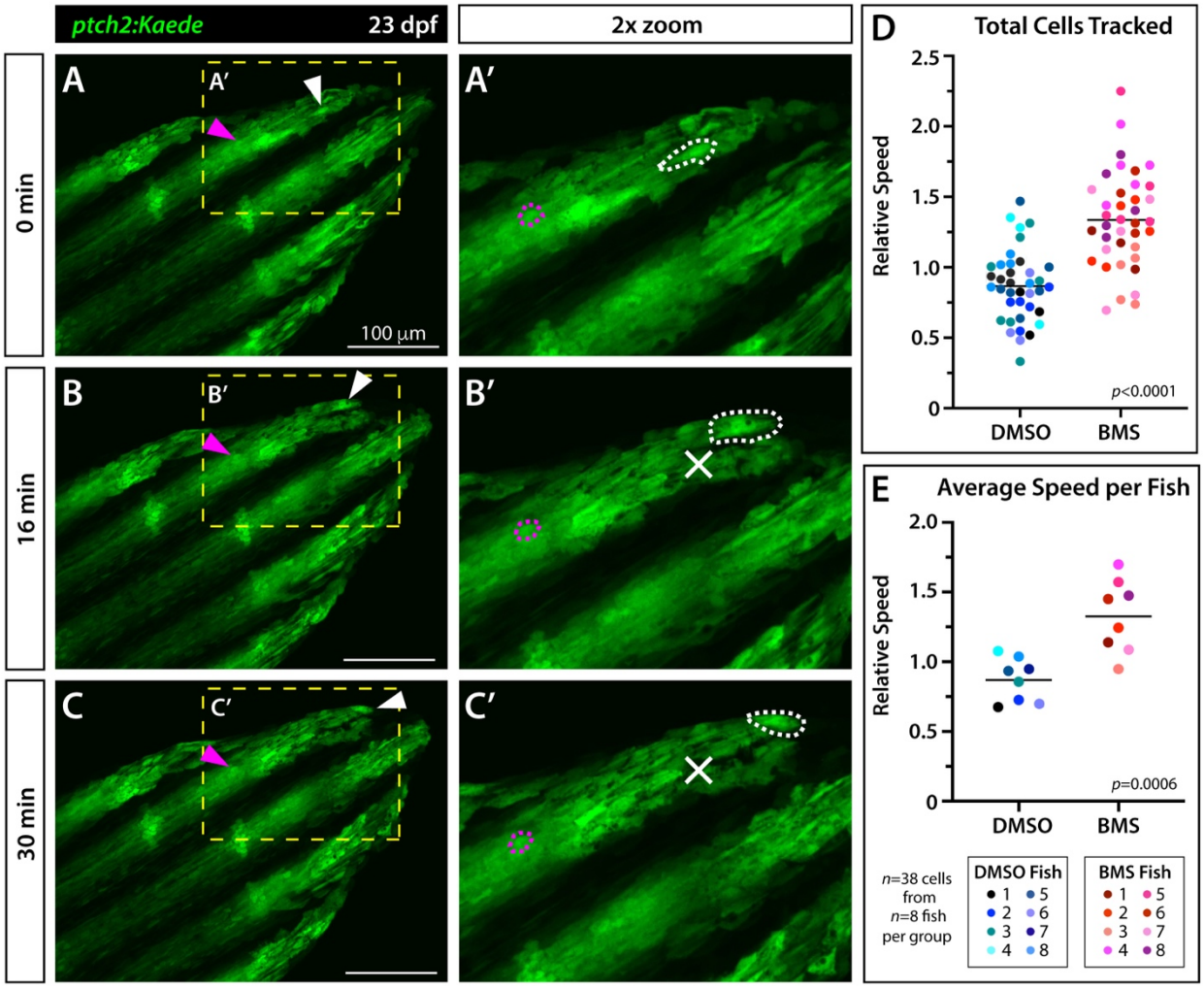

Figure S2.10. Shh/Smo signaling restrains the distal migration of basal epidermal cells.

(A-C) Still frames from 30 minute time lapse movies capturing basal epidermal distal migration in a caudal fin of a live mounted 23 dpf *ptch2:Kaede* fish. The fish was DMSO-treated as a control group member for quantitative studies. Maximum intensity projections of a fin's dorsal lobe are shown at 0 minutes (A, start position), 16 minutes (B, halfway through video), and 30 minutes (C, end position). White and magenta arrowheads indicate a *ptch2:Kaede*+ basal epidermis and pre-osteoblast, respectively. Yellow dashed boxes mark the 3x magnified distal ray region in (A'-C'). The representative basal epidermis (white) and pre-osteoblast (magenta) are outlined with dashed lines. The white Xs in (B', C') indicate the basal epidermal cell's starting position at 0 minutes. Scale bars are 100 μm. (D) Dot plot graph showing average speeds (arbitrary units) of individual *ptch2:Kaede*+ basal epidermal cells from fish treated with DMSO or BMS-833923 (BMS) for 24 hours and then imaged over 30 minutes. Cells of BMS-treated fish migrate faster than DMSO controls ($p < 0.0001$, Student's t-test). (E) Graph showing basal epidermal migration averaged by individual animal (as indicated by different colors) is significantly faster ($p < 0.0006$, Student's t-test) in BMS-treated fish. n=3-6 cells per fish with 8 fish per treatment for a total of 38 tracked cells per group. Colors represent single basal epidermal cells from the same animal.

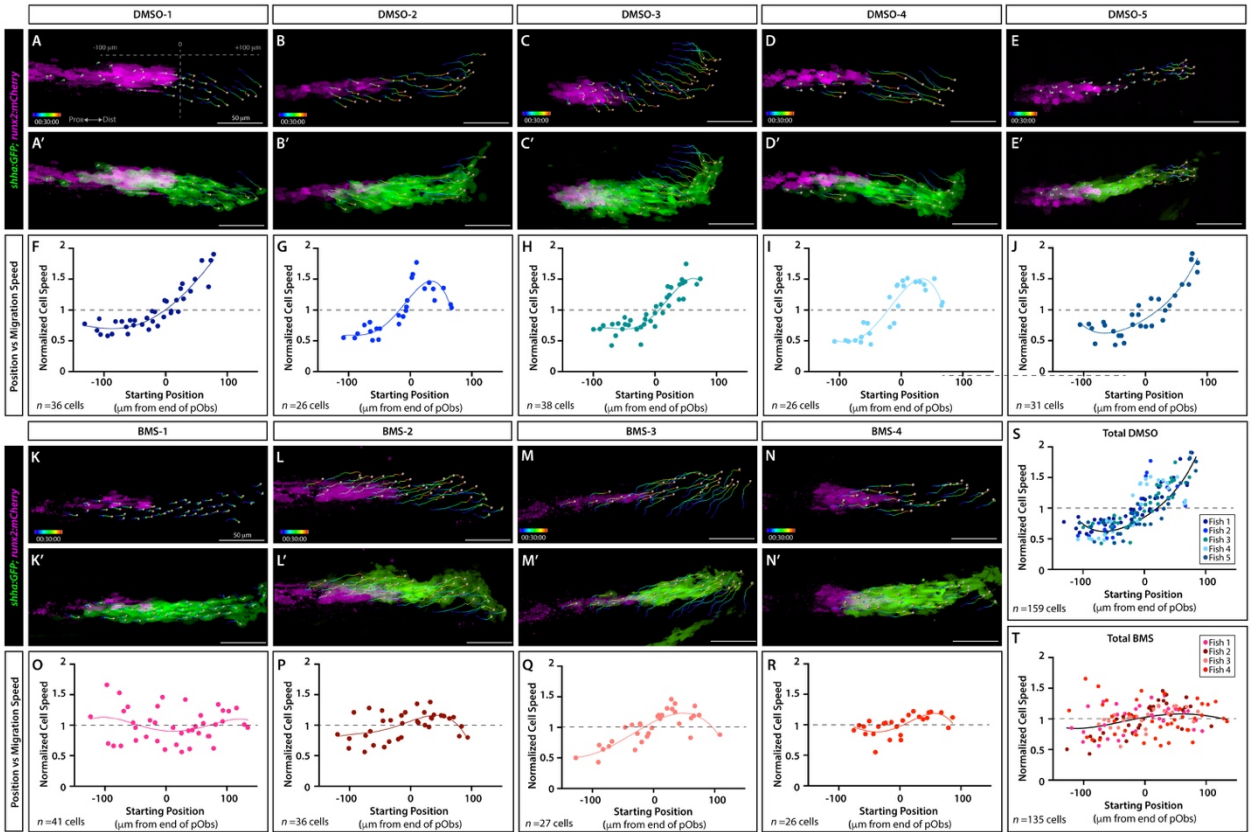

Figure S2.11. Position- and Shh/Smo-dependent shha:GFP+ basal epidermal migration rates of individual fish.

Expanded data from Figure 6. (A-E', K-N') Maximum intensity projections of the final 30 minute frame of time lapse-imaged *shha:GFP;runx2:mCherry* fish (21-24 dpf) treated with DMSO (*n*=5) or BMS-833923 (BMS; *n*=4) for 24 hours. Panels show *runx2:mCherry* pre-osteoblasts only (A-E, K-N; magenta) or both pre-osteoblasts and *shha:GFP*+ basal epidermal cells (A'-E', K'-N'; green). Grey spheres mark semi-automatically tracked basal epidermal cells with their cell displacement over 30 minutes indicated by multicolor tracks. (F-J, O-T) Normalized cell speed vs. starting position scatter plot graphs for each fish. Data points represent individual cell speeds. Non-parametric best-fit curves provide a visual guide. (S, T) Summary graphs reproduced from Figure 6 show combined data with added overall trends. Scale bars are 50 μm.

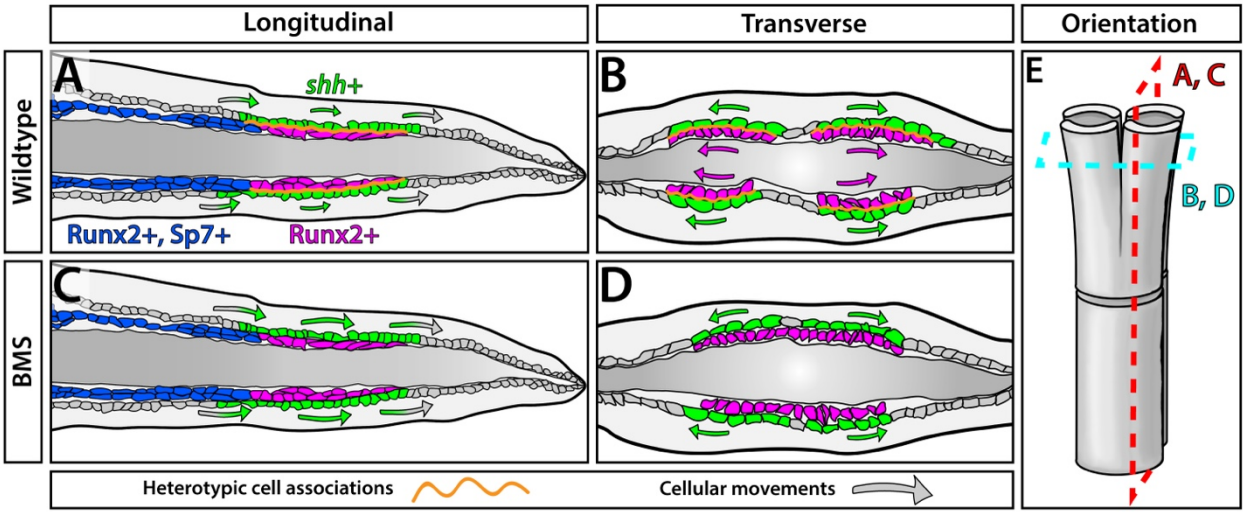

Figure S2.12. Basal epidermis collective movements and Shh/Smo-driven heterotypic associations with pre-osteoblasts direct fin ray branching morphogenesis.

(A-D) Schematics depicting the organization and cell movements of basal epidermal cells and osteoblasts during ray branching of outgrowing fins. Wildtype (A, B) and Shh/Smo-inhibited (C, D) conditions are shown. Longitudinal views (A, C) illustrate basal epidermal distal cell movements and transverse views (B, D) highlight lateral movements of both basal epidermal cells and Runx2+ pre-osteoblasts. **(E)** Schematic of a mature branched ray to orient the equivalent sectional views in (A-D). (A, C) Distal-moving basal epidermal cells (grey) enter the Shh/Smo active zone and upregulate *shha* to activate a Shh/Smo response in themselves and juxtaposed pre-osteoblasts. Shh/Smo-inhibition using the small molecule BMS-833923 increases and steadies the rate of basal epidermal distal migration (see animation in Movie 5). This suggests Shh/Smo activity normally slows the distal march of transiently Shh-expressing basal epidermal cells by enhancing cell associations (orange lines) with relatively static Runx2+ pre-osteoblasts. Basal epidermal cells downregulate *shha* and lose their Shh/Smo response as they move beyond the pre-osteoblasts. (B, D) The *shha*-expressing basal epidermal domain laterally divides, closely followed by underlying pre-osteoblast pools, prior to ray branching. BMS-833923 prevents pre-osteoblasts from following the lateral-splitting *shha*-expressing basal epidermis and thereby blocks ray branching. Shh/Smo-promoted heterotypic cell associations may transfer lateral forces from successively passaging basal epidermal cells to progressively re-position pre-osteoblasts into split pools. Each pre-osteoblast pool and their derived Runx2+/sp7+ osteoblasts now form separate daughter rays joined at a branch point.

MOVIES

Movies associated with this chapter can be downloaded at the following link:

https://www.sciencedirect.com/science/article/pii/S0012160621001135?via%3Dihub#appsec1

Movie Legends 2.1-2.5.

Movie 2.1. A dynamic 3-D visualization of confocal-imaged caudal fin dorsal ray 3 from a 28 dpf *shha:GFP;runx2:mCherry* fish. *shha:GFP+* basal epidermis (green) of both hemi-rays are beginning to branch. Underlying pre-osteoblasts (magenta) are pressed against basal epidermis. 3D reconstruction of live confocal microscopy. Surfaces added with Imaris to visualize domain boundaries.

Movie 2.2. 3-D space exploration of the distal region of a confocal-imaged caudal fin hemi-ray from a 28 dpf *shha:GFP;runx2:mCherry* fish. The *shha:GFP+* basal epidermis (green) domain has started splitting ahead of ray branching. A ridge of pre-osteoblasts (magenta) is nestled in a hollow of *shha:GFP+* basal epidermis. Imaris-generated surfaces help visualize domain boundaries. Single optical slices of the same region are shown in Figure 2.5.

Movie 2.3. Time lapse movie of the dorsal lobe of the caudal fin of a live-mounted 23 dpf *ptch2:Kaede* fish treated with DMSO (control group) for 24 hours prior to imaging. Widefield fluorescence images were collected every 2 minutes over a 30-minute period. Still images and data analysis are in Figure S2.11.

Movie 2.4. Time lapse movie of caudal fin dorsal lobes of representative live-mounted *shha:GFP;runx2:mCherry* fish treated with DMSO (upper panel) or BMS-833923 (lower panel) for 24 hours prior to imaging. Shh+ basal epidermis in green and Runx2+ pre-osteoblasts in magenta were imaged by fluorescence confocal microscopy. Multicolor lines indicate cell migration tracks for individual Shh+ basal epidermal cells (marked by grey spheres) over time. Images were acquired every 2 minutes for 30 minutes. Still images and data analysis are in Figure 2.6.

Movie 2.5. Heterotypic cell associations decrease the rate of basal epidermal distal movements while adjacent to pre-osteoblasts. This animation related to Figure S2.13 highlights the distal transit of single basal epidermal cells (red) in longitudinal section views of outgrowing caudal fins. (A) Basal epidermal cells constantly and collectively move distally as an interconnected epithelium, upregulating *shha* to sustain a distal Shh/Smo active zone including tightly associated pre-osteoblasts. Normally, Shh/Smo-promoted associations between basal epidermal cells and pre-osteoblasts transiently restrain the passage of basal epidermal cells. Basal epidermal cells then accelerate once passing beyond the pre-osteoblasts and losing Shh/Smo-dependent heterotypic associations. (B) Shh/Smo inhibition using BMS-833923 likely tempers associations between bEps and pObs, increasing and producing a now constant rate of basal epidermis distal migration. Basal epidermal lateral movements preceding ray branching and Shh/Smo-dependent tight associations may confer the physical force that progressively splits underlying pOb pools for ray branching morphogenesis.

BRIDGE TO CHAPTER III

This chapter demonstrates Shh/Smo-mediated ray branching is a developmental mechanism re-deployed during adult fin regeneration. We additionally demonstrate Shh is required for ray branching in all zebrafish fins, in support of fin ray patterning mechanisms evolving prior to paired fins. Finally, we develop new imaging techniques to assay cell migration in live juvenile fish and uncover Shh restrains the rate of migrating basal epidermal cells as they pass over pre-osteoblasts. This chapter therefore confirms the findings of Armstrong et al. 2017 are developmentally conserved and provides new mechanistic insights for further study. In Chapter III, we further characterize the musculoskeletal patterning of the developing caudal fin. Detailed understanding of the developing and regenerating caudal fin enables comparative mechanistic studies, including within subsequent chapters.

CHAPTER III: COORDINATED PATTERNING OF ZEBRAFISH CAUDAL FIN SYMMETRY BY A CENTRAL HYPURAL DIASTEMA AND TWO PERIPHERAL ORGANIZERS

Published in *Developmental Dynamics* August 2022

Thomas Desvignes[1, *, †], Amy E. Robbins[2, *], Andrew Z. Carey[1], Raisa Bailon-Zambrano[3], James T. Nichols[3], John H. Postlethwait[1], Kryn Stankunas[2, †]

[*] Equal contributions

[1]Institute of Neuroscience, University of Oregon, Eugene OR 97403, USA

[2]Institute of Molecular Biology, University of Oregon, Eugene OR 97403, USA

[3]Department of Craniofacial Biology, University of Colorado Anschutz Medical Campus, Aurora CO 80045, USA

[†]Corresponding authors:

Thomas Desvignes, Ph.D.
Institute of Neuroscience
University of Oregon
Eugene, OR 97403
Phone: 541-346-4495
Email: tdesvign@uoregon.edu

Kryn Stankunas, Ph.D.
Institute of Molecular Biology
Department of Biology
University of Oregon
273 Onyx Bridge
1318 Franklin Blvd
Eugene, OR 97403
Phone: 541-346-7416
Email: kryn@uoregon.edu

INTRODUCTION

The homocercal and externally symmetric caudal fin of teleost fishes likely contributes to their evolutionary success by increasing maneuverability and thrust relative to the heterocercal and asymmetric caudal fin of most non-teleost fishes (Giammona, 2021; Gosline, 1997; Lauder, 2000). The 'tail' of early diverging actinopterygians is hypothesized to result from "two outgrowths with distinct organizers and growth trajectories" (Sallan, 2016). In teleost, however, the "upper vertebrae-bearing tail, equivalent to that of tetrapods" is stunted or absent, thus the teleost 'tail' is composed of only the "lower median fin turned caudal fin". The teleost caudal fin skeleton comprises highly modified and often fused pre-ural and ural vertebrae, endochondral skeletal elements (i.e., haemal spines and hypurals ventrally, and epurals dorsally), and intramembranous fin rays (Figure 3.1A). Fin rays, or lepidotrichia, articulate with the distal ends of endochondral elements on two "plates of connective tissue" (Figure 3.1B) (Schultze and Arratia, 1989) composed of elastic cartilage (Bensimon-Brito et al., 2012; Desvignes et al., 2018b). Endochondral skeletal elements provide robust attachments to the vertebral column while rays associate with muscles and confer support and flexibility for efficient swimming. The number, types, and patterning of caudal fin endochondral elements and rays varies across species and provide diagnostic meristic characters for the classification of actinopterygian fishes (e.g., Arratia, 2008; Arratia, 2015; Fricke, 1983; Schultze and Arratia, 2013).

Teleost homocercal caudal fins typically are externally symmetric, with equal dorsal and ventral lobes. The fin's axis of symmetry aligns with the body axis following the upward bending of the notochord that rotates fin skeletal elements that formed earlier along the anterior-posterior body axis (e.g., Bird and Mabee, 2003; Desvignes et al., 2018b; Fujita, 1992; Huxley, 1859;

Konstantinidis and Johnson, 2012; Li et al., 2015; Thieme et al., 2021). The hypural diastema, a "space positioned between hypurals 2 and 3 or a notch positioned at the distal regions of hypurals 2 and 3" (Schultze and Arratia, 2013; Figure 3.1) aligns with the fin's dorsoventral axis of symmetry and has been considered a teleost exclusivity, or synapomorphy. We previously compared teleost and non-teleost species to define the hypural diastema complex (HDC) as: 1) a gap between hypurals 2 and 3 (i.e., the hypural diastema), that 2) separates two plates of connective tissue at 3) the branching of the caudal vasculature (Desvignes et al., 2018a; Desvignes et al., 2018b). Living gars have an HDC and some extinct non-teleost ray-finned fish lineages with heterocercal and asymmetric caudal fins have hypural diastemas but may lack other features of the complex. Only in teleosts, however, does the HDC align with the body axis and separate the earliest two developing caudal fin rays. Therefore, an accentuated HDC and its alignment with the body and caudal fin axes of symmetry rather than the HDC itself is likely the teleost synapomorphy. As such, external symmetry of the adult teleost caudal fin may represent an exaptation of the developmental processes forming an ancestral hypural diastema complex (Desvignes et al., 2018b). However, roles for HDC-associated ontogenies in the symmetrical patterning of the plates of connective tissue and the entire set of caudal fin rays in teleosts remain to be addressed.

Traditionally, teleost caudal fin rays are classified as principal or procurrent (Arratia, 2008). Principal rays are defined as rays supported by endoskeletal elements (i.e., hypurals, parhypural, and haemal spines of pre-ural centra 1 and 2). Principal caudal fin ray 1 is supported by the most posterior hypural and is positioned underneath the notochord while the last principal ray (principal ray 18 in zebrafish) is the anterior-most principal ray supported by the parhypural or

haemal spines of pre-ural centra 1 and 2, depending on the species (Figure 3.1B) (Arratia, 2008). Procurrent rays located along the fin's dorsal and ventral edges are shorter than principal rays, unbranched, and usually unsegmented with occasional exception of segmented posterior rays in adults. In contrast, all principal caudal fin rays are segmented and branched, except for the unbranched peripheral-most ray of each lobe referred to as the "long leading principal caudal rays" (Figure 3.1, principal rays 1 and 18 in zebrafish) (Arratia, 2008). It is largely unknown how developing rays adopt unique characteristics including their differential features and sizes associated with caudal fin symmetry.

We tracked the development of the zebrafish caudal fin endoskeleton and fin rays relative to the hypural diastema using staining methods and transgenic reporters to explore the developmental origins of teleost caudal fin symmetry. Our observations suggest that symmetry largely arises from an organizing center established at or before the onset of caudal skeleton formation and positioned at the future HDC. This proposed hypural diastema organizing center (HDOC) may pattern several elements bi-directionally and symmetrically by 1) forming the gap between hypurals 2 and 3 that 2) separates the two plates of connective tissue and 3) two sets of seven central principal rays. Further, we propose that two peripheral organizing centers (POCs) equidistant from the HDOC each pattern similar sets of two peripheral principal rays and thereby contribute to overall fin symmetry. Distinct muscle connections for the central principal rays and the two peripheral principal ray sets further reveal each set's distinctive identity, morphology, and biomechanical properties for swimming. Our model that zebrafish caudal fin symmetry originates from three organizers and responding fields contextualizes studies of caudal fin

developmental mechanisms and sources of morphological variation among zebrafish genotypes and across teleost species.

RESULTS

Zebrafish caudal fin rays emerge as mirrored sets on each side of an early-forming hypural diastema

We monitored the emergence of the zebrafish caudal fin skeleton throughout larval development using Alcian Blue and Alizarin Red staining to visualize hyaline cartilage and calcified bone, respectively. Caudal skeletal elements had not yet formed at 3.37 mm (7 dpf) (Figure 3.2A). By 4.36 mm (8 dpf), the anlagen of hypurals 1, 2, and 3 had formed ventrally along the anterior-to-posterior axis (Figure 3.2B). The relatively wide gap between hypurals 2 and 3 already demarcated the hypural diastema (Figure 3.2B). The parhypural anlage appeared anterior to hypural 1 (Figure 3.2B). At 5.27 mm (8 dpf), the parhypural began to fuse proximally with hypural 1, hypural 4 started condensing posterior to hypural 3, and haemal spine 2 formed anterior to the parhypural (Figure 3.2C). Two sets of three principal caudal fin rays, faintly stained by Alcian Blue, emerged on each side of the hypural diastema (Figure 3.2C, vCPR and dCPR). At 5.31 mm (8 dpf), the parhypural and hypural 1 were fused proximally (Figure 2D, circled) and the notochord started to flex dorsally posterior to the site of contact with the parhypural and hypural 1 (Figure 3.2D). Four rays were present on each side of the hypural diastema (Figure 3.2D). By 5.34 mm (9 dpf), the extending hypurals and haemal elements pivoted dorsally with the upward bending of the notochord (Figure 3.2E). Ten fin rays were apparent and symmetrically arranged around the hypural diastema (Figure 3.2E). At 5.50 mm (10 dpf), hypural 5 formed posterior to hypural 4 (Figure 3.2F). The ten central-most rays, five on

each side of the hypural diastema, were mineralized at their proximal ends as visualized by Alizarin Red (Figure 3.2F). Eight additional ray anlagen – four on each side – were labelled faintly with Alcian Blue (Figure 3.2F). By 5.99 mm (11 dpf), all 18 principal caudal rays showed proximal-to-distal graded mineralization (Figure 3.2G). At 8.44 mm (15 dpf), four of each ventral and dorsal procurrent rays were present and mineralized (Figure 3.2H). These results show that zebrafish caudal fin endochondral elements form earlier than caudal fin rays but without obvious dorsoventral symmetry. In contrast, fin rays are symmetrically arranged throughout caudal fin development, emerging as dorsal and ventral mirrored sets on each side of an early-forming hypural diastema.

Two plates of connective tissue develop symmetrically from twin cartilage precursor pools on each side of the hypural diastema

The two "plates of connective tissue" (Schultze and Arratia, 1989) at the junction between caudal fin endochondral elements and bony rays also develop symmetrically on each side of the hypural diastema. We followed their formation using cartilage-marking transgenic reporters derived from *sox10*, *trps1*, and *sox9a* regulatory sequences. The transgenic line *sox10:mRFP* labels cell membranes within caudal fin endochondral skeletal elements (e.g., haemal spines and hypurals) (Kirby et al., 2006) (Figure 3.3A-E). The *trps1:EGFP* transgene marks joint precursor cells and skeletal joints (Talbot et al., 2010). Double transgenic *sox10:mRFP;trps1:EGFP* fish showed specific *trps1*-driven GFP in precursor cells of the plates of connective tissue at the distal epiphyses of mRFP-positive hypurals and haemal spines (Figure 3.3A-F). Two patches of *trps1:EGFP*-expressing progenitor cells first appeared on each side of the hypural diastema at the epiphyses of hypurals 2 and 3 at ~4.80 mm (7 dpf) (Figure 3.3A, white arrows in A'). The

two differentiating plates of connective tissue remained distinct at ~5.45 mm (9 dpf, Figure 3.3B, B'). The anterior plate spanned the epiphyses of the parhypural and hypurals 1 and 2 (Figure 3.3B, B'), while the posterior plate extended across the epiphyses of hypurals 3 and 4 (Figure 3.3B, B'). At later stages, each cartilaginous plate condensed where proximal endochondral skeletal elements (haemal spine 2, parhypural, and hypurals 1 and 2 for the ventral plate, and hypurals 3 to 5 for the dorsal plate) articulated with distal principal caudal fin rays (Figure 3.3C-F).

We combined the *sox10:mRFP* transgene with the pan-cartilage marker *sox9a:EGFP* (Eames et al., 2013) to further resolve plates of connective tissue formation. Expression of *sox9a:EGFP* reinforced the plates' cartilaginous nature and their distinct ontogenies on each side of the hypural diastema (Figure 3.3G-H). The combination of *sox10* and *sox9a* reporters further revealed differences in cartilage subtypes. The *sox10* and *sox9a* reporters were co-expressed in endochondral skeletal elements (i.e., haemal spine, parhypural, and hypurals) made of hyaline cartilage, while only *sox9a:EGFP* was expressed in the plates of connective tissue (Figure 3.3G-H) made of elastic cartilage (Bensimon-Brito et al., 2012; Desvignes et al., 2018b). The *sox9a:EGFP* expression pattern in the developing caudal fin thus corresponds to the combined *sox10:mRFP* and *trps1:EGFP* expression patterns. Together, we conclude that cartilaginous plates of connective tissue emerge independently from one another and distal to endochondral skeletal elements from twin precursor pools located on each side of the hypural diastema.

Transgenic markers show distinct emergence of two sets of two peripheral principal rays

We used the transgenic markers *RUNX2:mCherry* (from S. Fisher lab, Barske et al., 2020) and *sp7:EGFP* (DeLaurier et al., 2010) to follow the pattern of emergence of caudal fin rays in individual larvae starting at 4.57 mm (8 dpf). Pre-osteoblasts express *runx2*, differentiating osteoblasts strongly express both *runx2* and *sp7*, and mature osteoblasts express *sp7* with decreased *runx2* expression (Komori, 2019; Sinha and Zhou, 2013; Stewart et al., 2014). Hence, *RUNX2:mCherry* and *sp7:EGFP* double reporter fish enable tracking osteoblast states and transitions prior to ray calcification. We first observed *RUNX2:mCherry* expression at 4.57 mm (8 dpf) in two developing principal caudal fin rays, one on each side of the hypural diastema (Figure 3.4A). These rays would become the central-most rays 9 and 10 of the adult fin (see Figure 3.1, Movie 3.1). Ten hours later, at 4.60 mm (8.5 dpf), a second mirrored pair of *RUNX2:mCherry*-expressing rays emerged while the first pair now co-expressed *sp7:EGFP* proximally, indicating initial pre-osteoblast differentiation (Figure 3.4B). At 5.21 mm (9 dpf), four mirrored pairs of rays had formed with the inner two pairs co-expressing *RUNX2:mCherry* and *sp7:EGFP* (Figure 3.4C). By 5.42 mm (9 dpf), five mirrored pairs of principal rays symmetrically emerged around the hypural diastema. The central-most six rays, three on each side, co-expressed *RUNX2:mCherry* and *sp7:EGFP* proximally while *RUNX2:mCherry* single positive pre-osteoblasts were restricted to the most recently added principal rays and the distal ends of all developing rays (Figure 3.4D, Movie 3.1).

At 5.56 mm, principal ray 2 and principal ray 17 emerged simultaneously but asynchronously from the central group of principal rays and with a notable gap separating each from the central ray field (Figure 3.4E-E”, Movie 3.1). These separate rays and the most recently developed mirrored pair of now 10 central rays (rays 5 and 14) expressed *RUNX2:mCherry* but not

sp7:EGFP (Figure 4E-E"). A few *RUNX2:mCherry*-expressing precursors of principal ray 18 also appeared anterior to principal ray 17 (Figure 3.4E-E'). By 5.71 mm, a sixth mirrored pair of central principal rays and principal ray 1 emerged (Figure 3.4F-F"). The four peripheral rays (principal rays 1, 2, 17 and 18), organized as dorsal and ventral sets of two rays each, remained distinctly separated from the central principal ray field, which now comprised rays 4 to 15 (Figure 3.4F-F", Movie 3.1). Rays 2, 5, and 14 now co-expressed *RUNX2:mCherry* and *sp7:EGFP* (Figure 3.4F, F"). By 5.99 mm, all 18 principal rays were present (Figure 3.4G-G", Movie 3.1). The last rays to emerge, mirrored central principal rays 3 and 16, were slightly shorter than their respective flanking rays (Figure 3.4G-G"). By 6.01 mm, the continuous, fan-like caudal fin comprised 18 outgrowing rays, segmented by joints, mirrored on dorsal and ventral lobes, and centered around the hypural diastema (Figure 3.4H-H", Movie 3.1). Thus, while central principal rays (CPRs, rays 3-16) emerge synchronously, sequentially, and symmetrically by mirrored pairs around the hypural diastema, peripheral principal rays (PPRs, rays 1-2 and 17-18) emerge independently and earlier than adjacent CPRs (rays 3, 4, 15 and 16). PPRs, like CPRs, emerge in outward progression.

To further discern the developmental mechanisms of peripheral and central principal rays, we used the transgenic line *alx4a:DsRed2,* which expresses a red fluorescent reporter in fin fibroblasts and osteoblasts in position-specific manners, including in the anterior-most rays of paired and median fins (Nachtrab et al., 2013). In adults, *alx4a:DsRed2* is distinctly expressed in the ventral-most caudal fin ray, but its pattern has not been described throughout caudal fin development (Nachtrab et al., 2013). At 4.43 mm (9 dpf), the fin fold had not yet developed rays and expressed *alx4a* mostly in iridophore pigment cells (Figure 3.5A) (Jang et al., 2021). By 5.41

mm (12 dpf), we observed strong *alx4a:DsRed2* expression at the posterior end of the ventral melanophore stripe before the caudal fin condensation region (Figure 3.5B) (Parichy et al., 2009) and faint expression just below the notochord distal tip (Figure 3.5B, white arrowhead). By 5.74 mm (13 dpf), ventral and dorsal *alx4a:DsRed2* expression intensity increased (Figure 3.5C). By 5.97 mm (14 dpf), dorsal *alx4a:DsRed2* expanded along the length of developing principal rays 1, 17, and 18, and faintly at the base of ray 2 (Figure 3.5D, yellow arrowheads). At 6.48 mm (15 dpf), *alx4a:DsRed2* was clearly expressed in principal rays 1-2 and 17-18 (Figure 3.5E, yellow arrowheads) and in the developing ventral and dorsal procurrent ray regions (Figure 3.5E, orange brackets and arrowheads). The *alx4a:DsRed2* was also expressed along the leading peripheral rays of the emerging dorsal and anal fins, consistent with a previous report (Nachtrab et al., 2013) (Figure 3.5E, green and blue arrows). At 6.80 mm (16 dpf), *alx4a:DsRed2* expression persisted along each peripheral-most principal ray (rays 1 and 18) and in the developing ventral and dorsal procurrent ray regions but was now faint along principal rays 2 and 17 (Figure 3.5F, yellow arrowheads). The *alx4a:DsRed2* also became visible in emerging ray joints (Figure 3.5F, yellow dashed zoom box). By 8.69 mm (21 dpf), *alx4a:DsRed2* was expressed most intensely in peripheral principal rays 1 and 18, was present but more muted in rays 2 and 17 (Figure 3.5G, G' yellow arrowheads), highly expressed in dorsal and ventral procurrent rays (Figure 3.5G, G' orange brackets), and remained restricted to the ray joints in central principal rays (Figure 3.5G, G', dashed yellow zoom inset). Only later, in reproductive adults, did *alx4a:DsRed2* expression become mainly restricted to the ventral-most peripheral principal ray 18, as previously reported (data not shown; Nachtrab et al., 2013). Expression of *alx4a:DsRed2* restricted to developing PPRs (and procurrent rays) reinforces the conclusion that the PPRs have different developmental mechanisms, and potential different identities, compared to the symmetrically-emerging CPRs.

Each set of central and peripheral principal rays associates with distinct caudal muscles

Caudal fin rays attach to the caudal muscles conferring thrust and maneuverability during swimming. We explored if ray symmetry was reflected in musculoskeletal attachments by combining muscle staining with transgenic markers. Phalloidin staining of actin filaments (F-actin) in ~8.00 mm *alx4a:DsRed2* fish (27 dpf) showed that inerfilamenti caudalis dorsalis (ICD) and inerfilamenti caudalis ventralis (ICV) muscles connected to central principal rays (rays 3-16) but not to *alx4a:dsRed2*-expressing peripheral principal rays (rays 1-2 and 17-18) (Figure 3.6A, A') (Siomava et al., 2018). Confirming previous observations (Chen and Galloway, 2014; Kague et al., 2019), the tendon-labeling *scxa:mCherry* line (McGurk et al., 2017) was expressed strongly in myosepta between myomeres and at caudal fin ray joints (Figure 3.6B, B'). In addition, we observed robust *scxa:mCherry* expression along a proximal stretch of all principal and procurrent fin rays, reinforcing that caudal musculature anchors to the base of all fin rays (Figure 3.6B-B'). Finally, the proximal, central ends of ICD and ICV appeared attached to rays 7-9 and 10-12, respectively while the distal, peripheral ends of ICD and ICV associated with rays 3-6 and 13-16, respectively (Figure 3.6A-A', C). This ICD and ICV attachment pattern to CPRs may confer undulating movement capacities. These studies demonstrate that the ICD and ICV muscles attach to the central principal rays 3 to 16 with a matching symmetrical arrangement around the hypural diastema (Siomava et al., 2018).

Myosin heavy chain (Mhc) staining of *sp7:EGFP* fish further highlighted the symmetric organization of similarly shaped ICD and ICV muscles around the hypural diastema and their attachment to respective dorsal and ventral central ray sets (Figure 3.6C-D). Dorsally, the adductor caudalis ventralis (ACV) attached to the base of peripheral principal rays 1 and 2

(Figure 3.6D, E) (Siomava et al., 2018). Ventrally, the flexor caudalis ventralis superior (sFCV) attached to the base of peripheral principal rays 17 and 18. Further, the flexor caudalis ventralis inferior (iFCV) attached to the base of ventral procurrent rays (Figure 3.6D, F) (Siomava et al., 2018). Together, these observations reveal that dorsal and ventral sets of central rays and both peripheral principal ray sets attach to distinct caudal muscles. Fin symmetry extends to the pairing of mirrored ICD and ICV muscles with respective dorsal and ventral CPR sets on each side of the hypural diastema. In contrast, muscles attached to the dorsal and ventral peripheral principal rays are not symmetrically organized and display morphological differences in shape, length, and ray attachments.

DISCUSSION

Our study of the emergence of zebrafish caudal fin skeletal elements from progenitor cell states reveals potential patterning mechanisms underlying external fin symmetry of adults. Our results indicate that caudal fin symmetry largely arises from the synchronous emergence of mirrored sets of central principal rays (CPRs) forming around an early-developing hypural diastema – the gap between hypurals 2 and 3 at the caudal fin's dorsoventral axis of symmetry (Figure 3.7). Similarly, the two plates of connective tissue develop symmetrically around the hypural diastema. In contrast, the two peripheral principal rays (PPRs) of each fin lobe develop asynchronously from the central principal rays. Each CPR and PPR set also connects to distinct swimming muscles. Collectively, we propose that zebrafish fin symmetry arises from the action of three organizers: a central hypural diastema organizing center (HDOC) and two peripheral organizing centers (POC). By this model, the HDOC patterns the surrounding field bi-directionally into mirrored plates of connective tissue and sets of CPRs. The two POCs, spaced

equidistant from the HDOC along the anterior-posterior body axis, form sets of two PPRs each. By this model, the caudal fin composite appendage is assembled from at least three organizers and responding fields, defining developmental modules. Unique anterior-posterior-defined positional identities of each module could confer distinct muscle attachments, ray morphologies, and growth properties to each ray set for optimized fin shape, swimming biomechanics, and life history traits. Further, genetic changes affecting one module or another could explain symmetry-breaking morphological variations observed in several teleost groups.

The hypural diastema reflects an early developmental organizing center that determines the axis of external symmetry of the adult zebrafish caudal fin

Endoskeletal caudal fin elements do not develop symmetrically and the earliest forming elements (i.e., the two hypurals H1 and H2) are located anterior to the future hypural diastema so that the diastema becomes visible only when hypural 3 initially forms posterior to it, as previously described (Bensimon-Brito et al., 2012; Desvignes et al., 2018b; Wiley et al., 2015). Therefore, an HDOC influence on endoskeletal elements would appear restricted to establishing the extra space between hypurals 2 and 3. Instead, endoskeletal element emergence and morphogenesis likely is regulated by distinct regulatory modules, potentially including antero-posterior patterning genes (e.g., *hox* genes) and hedgehog signaling (Hadzhiev et al., 2007). In contrast, we propose that an HDOC regulates the symmetrical emergence of distal caudal fin skeletal elements. Plates of connective tissue develop distal to the endochondral elements, forming elastic cartilage joints at the articulation between the endochondral elements and fin rays in the adult caudal fin (Bensimon-Brito et al., 2012; Desvignes et al., 2018b). The ventral plate of connective tissue spans haemal spine 2, the parhypural, and hypurals 1 and 2. The dorsal plate of connective

tissue spans hypurals 3 to 5. The *trps1* and *sox9a* transgenic lines demonstrate that the two plates of connective tissue develop simultaneously but separately and persist as two independent plates through adulthood. Thus, we propose that the HDOC patterns both plates of connective tissue and maintains their separation. Our muscle staining, matching a developmental series of zebrafish caudal muscle formation (Siomava et al., 2018), shows that ICD and ICV caudal muscles also develop symmetrically on each side of the hypural diastema in association with respective dorsal and ventral CPRs and thus may also be patterned by the HDOC. In addition, the HDOC may also influence the branching of the caudal vasculature and caudal nerve axons that each ramify dorsally and ventrally at the hypural diastema (Bump et al., 2022; Desvignes et al., 2018b; Schultze and Arratia, 1989). Together, the HDOC likely broadly patterns the surrounding mesoderm and its innervating axons.

We propose that the central HDOC also drives the symmetric patterning of the CPRs. Mirrored CPRs emerge synchronously and symmetrically on each side of the hypural diastema, consistent with previous observations in zebrafish (Desvignes et al., 2018b; Parichy et al., 2009) and medaka (Iida et al., 2014). Thus, the HDOC may be a source of unknown morphogens that bidirectionally and progressively specify ray emergence, befitting our proposed "organizer" designation. Further, the regularly-spaced specification of ray pre-osteoblasts in a stripe-like pattern suggests a Turing reaction/diffusion process, as proposed for a Bmp-Sox9-Wnt network in tetrapod limb and pectoral fin endoskeleton patterning (Onimaru et al., 2016; Raspopovic et al., 2014). Greater distance from the HDOC correlates with larger and longer rays. This pattern could reflect morphogen-specified, differential ray outgrowth properties (e.g., population sizes or cell-level positional identities). Regardless, the HDOC seemingly patterns 14 of the 18 principal

rays and establishes much of external caudal fin symmetry, including the axis of symmetry. Meanwhile, the upward bending of the notochord rotates the anterior-posterior specified appendage into its caudal position in dorsoventral alignment with the body axis.

Two early-forming peripheral organizing centers may pattern the caudal fin peripheral rays

Our time course monitoring *RUNX2:mCherry*-expressing pre-osteoblasts tracks the earliest onset of caudal fin ray emergence. Notably, in all observed specimens across many clutches, rays 1-2 and 17-18 emerge separately from rays 3-16 and earlier than neighboring CPRs (rays 3, 4 and 15, 16) within a 24-hour period from 9-10 dpf (5.5-5.7 mm). The neighboring CPRs (rays 3, 4 and 15, 16) then quickly bridge the gaps such that the separate emergence of the peripheral rays is no longer apparent. We call these rays (1, 2, 17, and 18) peripheral principal rays (PPRs) as a subtype of principal caudal fin ray ontogenetically distinct from the CPRs. The lag between osteoblast specification and tissue mineralization likely prevented detection of this ray emergence pattern in earlier studies (e.g., Bensimon-Brito et al., 2012; Bird and Mabee, 2003; Desvignes et al., 2018b; Parichy et al., 2009). Principal rays therefore develop in one of three groups separated by developmental time and anterior-posterior body axis position – the central CPRs plus what become dorsal and ventral sets of PPRs.

Expression of an *alx4a*-driven transgene shows that all four developing PPRs express a distinct transcription factor from the CPRs, reinforcing the different ontogeny and potential identities of PPRs compared to CPRs. Further, *alx4a:DsRed2* expression at the site of the later-developing ventral PPRs (vPPRs) predates the appearance of *RUNX2:mCherry*-expressing PPR pre-

osteoblasts. Likewise, but later in development, *alx4a:DsRed2* expression at the site of the future dorsal PPRs (dPPRs) precedes the emergence of *RUNX2:mCherry*-marked corresponding PPRs. Therefore, the caudal mesenchyme fields forming PPRs may be distinct from that of the CPRs. We favor a model whereby peripheral organizing centers (POCs) within these fields specify the two peripheral-most principal rays of each caudal fin lobe. In contrast, a single organizing center (the HDOC) seems unlikely to produce developmentally staggered waves of rays, unless mesenchymal cells at the future PPRs differentiate under lower levels of a hypothetical HDOC-originating morphogen. The temporal delay between the establishment of the vPOC (more anterior) and dPOC (posterior) may reflect the progressive anterior-posterior differentiation of caudal mesenchyme, as seen with endochondral elements. POCs may limit the number of principal rays by restricting the continued bi-directional advance of sequentially forming central rays. Later developing procurrent rays also may be specified by the POCs or by additional, procurrent ray-specific organizers. These hypotheses tying organizers to sets of rays (e.g., the HDOC to all CPRs) with cross-organizer interfering effects could be tested by combinatorial transplantations and ablations of to-be-identified HDOC and POC cells prior to ray emergence.

The formation of two POCs approximately equal distance from the HDOC along the anterior-posterior body axis seemingly is necessary for overall adult fin symmetry. Further, the POCs appear largely equivalent given they produce the same number of PPRs with each mirrored pair of approximately equal length and morphology. Small deviations in POC position, timing of emergence, or potency relative to the HDOC would readily explain the occasional variation in numbers of principal rays in zebrafish ventral and dorsal caudal fin lobes (Bird and Mabee, 2003; Parichy et al., 2009). Ray radius measurements indicate PPRs are proportionately wider than

CPRs (Stewart et al., 2019). Therefore, PPR-comprising cells may have distinct growth properties reflective of independent ontogenies and potentially different positional identities. CPR, vPPR, and dPPR positional identities, shared across cells comprising each set of rays and established by anterior-posterior body axis position, could then influence regenerative responses that robustly restore the caudal fin's homocercal and externally symmetry shape even following diagonal or other asymmetric amputations. Regardless, all three organizers would have to be precisely "tuned" to collectively provide external fin symmetry – a teleost innovation seemingly under strong selective pressure.

Distinct muscles attach to central and peripheral principal caudal fin ray sets

The different ontogeny, morphology, and positional identity of CPRs and PPRs likely underlie different biomechanical roles for each principal caudal fin ray type. Transgenic *alx4a* expression, thought to label a subset of fibroblasts, osteoblasts, and/or ligaments (Nachtrab et al., 2013; Nichols et al., 2016), and tendon marker *scxa* (McGurk et al., 2017) combined with myosin heavy chain and phalloidin muscle staining reveal that CPRs and PPRs connect to different caudal swimming muscles (Flammang and Lauder, 2008; Flammang and Lauder, 2009; Gosline, 1997). CPRs attach to inerfilamenti caudalis dorsalis (ICD) and inerfilamenti caudalis ventralis (ICV) muscles that develop and are positioned symmetrically around the hypural diastema (Siomava et al., 2018). In contrast, dPPRs and vPPRs associate with the peripheral abductor caudalis ventralis (ACV) and superior flexor caudalis ventralis (sFCV) muscles, respectively. Therefore, different muscles can independently move the ventral PPRs, dorsal PPRs, and both CPR sets, contributing to complex swimming dynamics (Flammang and Lauder, 2009; Giammona, 2021; Lauder, 2000). The most peripheral, sturdier, and unbranched PPRs (principal rays 1 and

18) likely provide stiffness to the caudal fin by framing the ray field to enhance caudal fin thrust. Indeed, in fluid-structure interaction models, a "cupping" stiffness pattern for caudal fins (similar to the pattern seen in zebrafish; highest rigidity at the boundaries and lowest in the center) requires the least energy expenditures to generate the largest thrust (Esposito et al., 2012; Luo et al., 2020; Shi et al., 2019). Similar to the observed muscle-to-ray set pairings, PPRs and CPRs show distinct innervation (Bump et al., 2021). Together, the different ontogeny of PPRs and CPRs under the control of three organizing centers may provide each ray set with distinct identities altering ray morphology as well as muscle and nerve targeting, collectively optimizing biomechanical properties for efficient thrust and maneuverability.

Evolutionary conservation of caudal fin organization

Our model that an HDOC and two POCs pattern the symmetric zebrafish caudal fin suggests that similar organizers are conserved across teleosts with externally symmetric fins and that altered organizers underlie symmetry-breaking forms. Further, our model raises questions about the organizers' evolutionary origins and lineage-specific variations. While not specifically observed in the ontogeny of all teleost species, the hypural diastema defined as a gap between hypural 2 and 3 or a notch between hypural plates is a teleost hallmark (Arratia, 2013; Arratia, 2015), although also observed in gars (Desvignes et al., 2018a; Desvignes et al., 2018b). Further, in documented teleost species, the sequential and symmetrical emergence of CPRs around the hypural diastema appears to be conserved (e.g., Desvignes et al., 2018b; Fujita, 1992; Huxley, 1859; Konstantinidis and Johnson, 2012; Li et al., 2015; Metscher and Ahlberg, 2001; Thieme et al., 2021). In contrast, in spotted gar, the first rays to form are not located around the hypural diastema but instead adjacent to hypurals 1 and 2 (Desvignes et al., 2018b). In both gars and

teleosts, however, the gap between hypural 2 and 3 coincides with the separation of the connective tissue plates and the branching of the caudal vasculature (Desvignes et al., 2018b). Therefore, an HDOC may pattern the hypural diastema, each plate of connective tissue, and the caudal vasculature in both gars and teleosts. As such, the exaptation of an HDOC to additionally pattern CPRs and establish external symmetry may be a synapomorphy of the teleost group, extending our previous hypothesis (Desvignes et al., 2018b). Alternatively, the putative gar HDOC may pattern surrounding rays but without symmetry due to uneven bi-directional morphogens, pre-existing field asymmetry in size or cell sensitivity to diffusible morphogens, or the interference of nearby ray organizing centers. Additional targeted work on non-teleost actinopterygian species is also needed to evaluate the relatedness of our hypothesized teleost HDOC to other hypothesized actinopterygians 'tail' organizers (Sallan, 2016).

Studying the conservation of PPRs and POCs across teleost and non-teleost species is difficult because traditional methods such as Alcian Blue and Alizarin Red stain differentiated tissue rather than progenitor cells. However, in teleosts, a similar pattern of asynchronous emergence of CPRs and PPRs in goldfish detected using calcein to label forming bones (Figs. 22 and 33 in Li et al., 2015) suggests conservation of POCs among cyprinids. Transgenic reporter lines and molecular labeling techniques in other teleost and non-teleost fish groups would further explore the conservation of PPRs, and thus likely POCs, and reveal their evolutionary origin as an ancestral ray-finned fish character, a teleost innovation, or a derived character in some teleost lineages. Nonetheless, we hypothesize that altered POC modules could explain strikingly asymmetric caudal fin forms. For example, the ornamental sword of male swordtail *Xiphophorus* spp. contributing to mate choice is characterized by disproportionately extended ventral PPRs

(Darwin, 1871). Thus, the hypothesized *Xiphophorus* "sword organizer" (Eibner et al., 2008; Schartl et al., 2021) may correspond to the zebrafish ventral peripheral organizing center (vPOC) and confer distinct growth properties to ventral PPRs. The elongation of dorsal PPRs in female swordtails treated with testosterone (Eibner et al., 2008) suggests the conservation of the dorsal POC and its relatedness with the vPOC. Flying fishes and tripodfishes (*Bathypterois* spp.) also have dramatically elongated ventral caudal fin lobes, again with particularly long ventral PPRs possibly specified by a specialized vPOC. In flying fishes, elongated ventral PPRs enable propulsion while the rest of the body is out of the water (Davenport, 1994). In tripodfishes, the extremely long caudal fin ventral PPRs that match pelvic fin ray length enable a posture parallel to the substrate (Davis and Chakrabarty, 2011). Altered POC modules may also drive the remarkable extension of the peripheral-most principal caudal fin rays of some whiptail catfishes (Loricariinae) (e.g., Paixão and Toledo-Piza, 2009; Rojas-Molina et al., 2019; Terán et al., 2019; Thomas and Pérez, 2010). Co-characterizing caudal fin ray ontogeny, morphologies, and muscle attachments in these groups would help elucidate if and how changes to vPOC/vPPR modules cause caudal fin symmetry-breaking and ray elongation phenotypes.

Studies identifying the genetic mechanisms underlying PPR elongation can inform on the specificity of POC modules. The elongated rays of the swordtail *Xiphophorus helleri*'s ventral caudal fin lobe are promoted by the potassium channel *kcnh8* (Schartl et al., 2021), a paralog of *kcnh2a*, of which ectopic expression causes dramatic fin ray overgrowth in *longfin*^{t2} (*lof*^{dlt2}) mutant zebrafish (Daane et al., 2021; Stewart et al., 2021). Similarly, the *kcnk5a* and *kcnk9* potassium channels may promote ventral lobe elongation in flying fish caudal fins (Daane et al., 2021). Gain-of-function mutations in the related potassium channel *kcnk5b* extend fin rays of the

zebrafish *another longfin* (*alf*) mutant (Perathoner et al., 2014) and cause the *long-tail* phenotype in goldfish (Kon et al., 2020). Overexpression of additional potassium channels also cause zebrafish caudal fin overgrowth (Silic et al., 2020). Therefore, organizer- or field-specific variations in ion channel expression could readily alter fin morphology under evolutionary selection. Expression studies of potassium channel genes and downstream ion signaling driving teleost caudal fin variation will help decipher these evolutionary and ray outgrowth mechanisms. Genetic changes that add, remove, or reposition organizers and alter their developmental influence could produce additional types of symmetry-breaking caudal fin forms. Collectively, our model provides a framework to explore the existence and function of developmental organizers in the caudal and other fins and their roles in fin shape evolution.

MATERIALS AND METHODS

Zebrafish lines

Zebrafish (*Danio rerio*) were maintained in 28-29°C circulating fish water within the University of Oregon Aquatic Animal Care Services (UO AqACS) fish facility and the University of Colorado Anschutz Medical Campus. The following lines were used: wildtype AB, *Tg(trps1:EGFP)*^{j1271aGt} (Talbot et al., 2010), *Tg(sox10:mRFP)*^{vu234} (Kirby et al., 2006), *Tg(sox9a:EGFP)*^{zc81Tg} (Eames et al., 2013), *Tg(RUNX2:mCherry)* (Shannon Fisher Lab, (Barske et al., 2020)), *Tg(sp7:EGFP)*^{b1212} (DeLaurier et al., 2010), *Tg(alx4a:DsRed2)*^{pd52} (Nachtrab et al., 2013), and *Tg(scxa:mCherry)*^{fb301Tg} (McGurk et al., 2017). Zebrafish experiments were approved by the Institutional Animal Care and Use Committees (IACUC) of the University of Oregon and the University of Colorado Anschutz Medical Campus.

Zebrafish developmental stages are described primarily by standard length (SL). SL was measured using ImageJ (Schneider et al., 2012) from the snout to the tip of the notochord in pre-flexion larvae and from the snout to the caudal peduncle in post-flexion larvae. The age of all animals is also reported as days post fertilization (dpf). However, some discrepancies in SL and dpf exist between fish lines because fish were reared in different facilities with differing developmental rates. SL could not always be accurately measured by stereomicroscopy for older, larger specimens. In these instances, SL (denoted by ~) was estimated based on skeletal element development, pigmentation patterns, and degree of notochordal flexion (Kimmel et al., 1995; Parichy et al., 2009).

Alcian Blue and Alizarin Red staining

Briefly, fish were euthanized with an overdose of MS-222 (Syndel), fixed in 4% paraformaldehyde (PFA), washed, and serially transferred into 80% ethanol for storage or immediate staining. Fish were stained first with Alcian Blue for cartilage, enzymatically cleared using 1% trypsin, bleached in 3% hydrogen peroxide, differentially stained with Alizarin Red for calcified bone, and finally cleared with increasingly concentrated glycerol solutions (Desvignes et al., 2018a; Walker and Kimmel, 2007). Specimens of various sizes were prepared and stained following the same method but the length of each step was adjusted according to the size of the fish.

Whole mount fluorescent staining

Fish were euthanized by MS-222 overdose, fixed in 4% PFA, and washed in PBS. Phalloidin staining (AlexaFluor 647 Phalloidin, Thermo Fisher #A22287) was performed at 1:1000 in PBS

+ 0.1% Triton X-100 for 30 minutes. For myosin heavy chain skeletal muscle immunostaining, fish were blocked overnight at 4ºC in 1x PBS/ 1% Triton X-100/ 5% NGS/ 10% DMSO. Anti-Myh (myosin heavy chain) monoclonal antibody (DSHB Hybridoma Product MF-20) was used at 1:250 in blocking solution overnight at 4ºC and visualized with Alexa Fluor 647 anti-mouse secondary antibody (Thermo Fisher). Specimens were mounted on a FluroDish in SlowFade Gold prior to imaging.

Imaging

Alcian Blue and Alizarin Red stained fish were observed using a Leica M165 FC stereomicroscope equipped with a Leica DFC425 C camera. Widefield images of *trps1:EGFP* and *sox10:mRFP* larval transgenic fish were acquired on the same stereomicroscope. Confocal images of larval transgenic *trps1:EGFP*, *sox10:mRFP*, *sox9a:EGFP* were acquired on a Zeiss LSM5 Pascal confocal. A Nikon Eclipse T*i* microscope equipped with a Yokogawa CSU-W1 spinning disk confocal attachment was used to observe larval transgenic *RUNX2:mCherry;sp7:EGFP, alx4a:DsRed2* fish and MF-20 immunostained specimens. For longitudinal tracking of individual *RUNX2:mCherry;sp7:EGFP* larvae, *n=5* larvae were singly housed in petri dishes in standard nursery conditions and imaged 2-3x daily from 7-11 dpf until all principal fin rays developed, then 1x daily until 16 dpf. For expression profiling of *alx4a:DsRed2* fish, a group of *n=6* larvae were housed together in standard nursery conditions and imaged 1x daily from 12-16 dpf. Additional *alx4a:DsRed2* and *scxa:mCherry* fluorescent images in juveniles were captured using a Leica DMi8 equipped with an Andor Dragonfly 301 spinning disk confocal system. All confocal images are maximum intensity projections of sagittal Z-stacks.

REFERENCES

Arratia G. 2008. Actinopterygian postcranial skeleton with special reference to the diversity of fin ray elements, and the problem of identifying homologies. In: Arratia, G, Schultze, H-P, Wilson, MVH, editors. Mesozoic Fishes 4 – Homology and Phylogeny. Verlag Dr. Friedrich Pfeil, pp. 49–101.

Arratia G. 2013. Morphology, Taxonomy, and Phylogeny of Triassic Pholidophorid Fishes (Actinopterygii, Teleostei). Journal of Vertebrate Paleontology 33:1–138.

Arratia G. 2015. Complexities of Early Teleostei and the Evolution of Particular Morphological Structures through Time. Copeia 103:999–1025.

Barske L, Fabian P, Hirschberger C, Jandzik D, Square T, Xu P, Nelson N, Yu HV, Medeiros DM, Gillis JA, Crump JG. 2020. Evolution of vertebrate gill covers via shifts in an ancient Pou3f3 enhancer. PNAS 117:24876–24884.

Bensimon-Brito A, Cancela ML, Huysseune A, Witten PE. 2012. Vestiges, rudiments and fusion events: the zebrafish caudal fin endoskeleton in an evo-devo perspective. Evol Dev 14:116–127.

Bird NC, Mabee PM. 2003. Developmental morphology of the axial skeleton of the zebrafish, Danio rerio (Ostariophysi: Cyprinidae). Dev Dyn 228:337–357.

Bump RG, Goo CEA, Horton EC, Rasmussen JP. 2021. Osteoblasts pattern endothelium and somatosensory axons during zebrafish caudal fin organogenesis. https://www.biorxiv.org/content/10.1101/2021.09.28.462226v1.

Bump RG, Goo CEA, Horton EC, Rasmussen JP. 2022. Osteoblasts pattern endothelium and somatosensory axons during zebrafish caudal fin organogenesis. Development 149:dev200172.

Chen JW, Galloway JL. 2014. The development of zebrafish tendon and ligament progenitors. Development 141:2035–2045.

Daane JM, Blum N, Lanni J, Boldt H, Iovine MK, Higdon CW, Johnson SL, Lovejoy NR, Harris MP. 2021. Modulation of bioelectric cues in the evolution of flying fishes. Current Biology. https://www.sciencedirect.com/science/article/pii/S0960982221011908.

Darwin C. 1871. The Descent of Man, and Selection in Relation to Sex. The Descent of Man, and Selection in Relation to Sex. John Murray. https://www.degruyter.com/document/doi/10.1515/9781400820061/html.

Davenport J. 1994. How and why do flying fish fly? Rev Fish Biol Fisheries 4:184–214.

Davis MP, Chakrabarty P. 2011. Tripodfish (Aulopiformes: Bathypterois) locomotion and landing behaviour from Movie observation at bathypelagic depths in the Campos Basin of Brazil. Marine Biology Research 7:297–303.

DeLaurier A, Eames BF, Blanco-Sanchez B, Peng G, He X, Swartz ME, Ullmann B, Westerfield M, Kimmel CB. 2010. Zebrafish sp7:EGFP: a transgenic for studying otic vesicle formation, skeletogenesis, and bone regeneration. Genesis 48:505–511.

Desvignes T, Carey A, Braasch I, Enright T, Postlethwait JH. 2018a. Skeletal development in the heterocercal caudal fin of spotted gar (lepisosteus oculatus) and other lepisosteiformes. Developmental Dynamics 247:724–740.

Desvignes T, Carey A, Postlethwait JH. 2018b. Evolution of caudal fin ray development and caudal fin hypural diastema complex in spotted gar, teleosts, and other neopterygian fishes. Developmental Dynamics 247:832–853.

Eames BF, DeLaurier A, Ullmann B, Huycke TR, Nichols JT, Dowd J, McFadden M, Sasaki MM, Kimmel CB. 2013. FishFace: interactive atlas of zebrafish craniofacial development at cellular resolution. BMC Developmental Biology 13:23.

Eibner C, Pittlik S, Meyer A, Begemann G. 2008. An organizer controls the development of the "sword," a sexually selected trait in swordtail fish. Evolution & Development 10:403–412.

Esposito CJ, Tangorra JL, Flammang BE, Lauder GV. 2012. A robotic fish caudal fin: effects of stiffness and motor program on locomotor performance. Journal of Experimental Biology 215:56–67.

Flammang BE, Lauder GV. 2009. Caudal fin shape modulation and control during acceleration, braking and backing maneuvers in bluegill sunfish, Lepomis macrochirus. Journal of Experimental Biology 212:277–286.

Flammang BE, Lauder GV. 2008. Speed-dependent intrinsic caudal fin muscle recruitment during steady swimming in bluegill sunfish, Lepomis macrochirus. Journal of Experimental Biology 211:587–598.

Fricke R. 1983. A method of counting caudal fin rays of actinopterygian fishes. Braunschweiger Naturkundliche Schriften 1:729–733.

Fujita K. 1992. Caudal skeleton ontogeny in the adrianichthyid fish, Oryzias latipes. Japanese Journal of Ichthyology 39:107–109.

Giammona FF. 2021. Form and Function of the Caudal Fin Throughout the Phylogeny of Fishes. Integrative and Comparative Biology 61:550–572.

Gosline WA. 1997. Functional morphology of the caudal skeleton in teleostean fishes. Ichthyological Research 44:137–141.

Hadzhiev Y, Lele Z, Schindler S, Wilson SW, Ahlberg P, Strähle U, Müller F. 2007. Hedgehog signaling patterns the outgrowth of unpaired skeletal appendages in zebrafish. BMC Developmental Biology 7:75.

Huxley TH. 1859. Observations on the Development of some parts of the Skeleton of Fishes. Transactions of The Microscopical Society & Journal 7:33–46.

Iida Y, Hibiya K, Inohaya K, Kudo A. 2014. Eda/Edar signaling guides fin ray formation with preceding osteoblast differentiation, as revealed by analyses of the medaka all-fin less mutant afl. Developmental Dynamics 243:765–777.

Jang HS, Chen Y, Ge J, Wilkening AN, Hou Y, Lee HJ, Choi YR, Lowdon RF, Xing X, Li D, Kaufman CK, Johnson SL, Wang T. 2021. Epigenetic dynamics shaping melanophore and iridophore cell fate in zebrafish. Genome Biology 22:282.

Kague E, Hughes SM, Lawrence EA, Cross S, Martin-Silverstone E, Hammond CL, Hinits Y. 2019. Scleraxis genes are required for normal musculoskeletal development and for rib growth and mineralization in zebrafish. The FASEB Journal 33:9116–9130.

Kimmel CB, Ballard WW, Kimmel SR, Ullmann B, Schilling TF. 1995. Stages of embryonic development of the zebrafish. Developmental Dynamics 203:253–310.

Kirby BB, Takada N, Latimer AJ, Shin J, Carney TJ, Kelsh RN, Appel B. 2006. In vivo time-lapse imaging shows dynamic oligodendrocyte progenitor behavior during zebrafish development. Nature Neuroscience 9:1506–1511.

Komori T. 2019. Regulation of Proliferation, Differentiation and Functions of Osteoblasts by Runx2. International Journal of Molecular Sciences 20:1694.

Kon T, Omori Y, Fukuta K, Wada H, Watanabe M, Chen Z, Iwasaki M, Mishina T, Matsuzaki SS, Yoshihara D, Arakawa J, Kawakami K, Toyoda A, Burgess SM, Noguchi H, Furukawa T. 2020. The Genetic Basis of Morphological Diversity in Domesticated Goldfish. Current Biology 30:2260-2274.e6.

Konstantinidis P, Johnson GD. 2012. A comparative ontogenetic study of the tetraodontiform caudal complex: Caudal complex of tetraodontiforms. Acta Zoologica 93:98–114.

Lauder GV. 2000. Function of the Caudal Fin During Locomotion in Fishes: Kinematics, Flow Visualization, and Evolutionary Patterns. American Zoologist 40:101–122.

Li I-J, Chang C-J, Liu S-C, Abe G, Ota KG. 2015. Postembryonic staging of wild-type goldfish, with brief reference to skeletal systems. Developmental Dynamics 244:1485–1518.

Luo Y, Xiao Q, Shi G, Wen L, Chen D, Pan G. 2020. A fluid–structure interaction solver for the study on a passively deformed fish fin with non-uniformly distributed stiffness. Journal of Fluids and Structures 92:102778.

McGurk PD, Swartz ME, Chen JW, Galloway JL, Eberhart JK. 2017. In vivo zebrafish morphogenesis shows Cyp26b1 promotes tendon condensation and musculoskeletal patterning in the embryonic jaw. PLOS Genetics 13:e1007112.

Metscher BD, Ahlberg PE. 2001. Origin of the teleost tail: phylogenetic frameworks for developmental studies. In: Ahlberg, PE, Systematics Association, editors. Major events in early vertebrate evolution: palaeontology, phylogeny, genetics, and development. London ; New York: Taylor & Francis, pp. 343–349.

Nachtrab G, Kikuchi K, Tornini VA, Poss KD. 2013. Transcriptional components of anteroposterior positional information during zebrafish fin regeneration. Development 140:3754–3764.

Nichols JT, Blanco-Sánchez B, Brooks EP, Parthasarathy R, Dowd J, Subramanian A, Nachtrab G, Poss KD, Schilling TF, Kimmel CB. 2016. Ligament versus bone cell identity in the zebrafish hyoid skeleton is regulated by mef2ca. Development 143:4430–4440.

Onimaru K, Marcon L, Musy M, Tanaka M, Sharpe J. 2016. The fin-to-limb transition as the re-organization of a Turing pattern. Nat Commun 7:11582.

Paixão A de C, Toledo-Piza M. 2009. Systematics of Lamontichthys Miranda-Ribeiro (Siluriformes: Loricariidae), with the description of two new species. Neotrop ichthyol 7:519–568.

Parichy DM, Elizondo MR, Mills MG, Gordon TN, Engeszer RE. 2009. Normal table of postembryonic zebrafish development: Staging by externally visible anatomy of the living fish. Dev Dyn 238:2975–3015.

Perathoner S, Daane JM, Henrion U, Seebohm G, Higdon CW, Johnson SL, Nüsslein-Volhard C, Harris MP. 2014. Bioelectric Signaling Regulates Size in Zebrafish Fins. PLOS Genet 10:e1004080.

Raspopovic J, Marcon L, Russo L, Sharpe J. 2014. Digit patterning is controlled by a Bmp-Sox9-Wnt Turing network modulated by morphogen gradients. Science. https://www.science.org/doi/abs/10.1126/science.1252960.

Rojas-Molina YA, Provenzano-Rizzi F, Ramírez-Gil H. 2019. A new species of whiptail armored catfish, genus Pseudohemiodon (Siluriformes: Loricariidae) from the Orinoco River basin, Llanos region of Colombia and Venezuela. Neotrop ichthyol 17. http://www.scielo.br/j/ni/a/FT8nC4Tym6SjcgbP33dLgkD/abstract/?lang=en.

Sallan L. 2016. Fish ‘tails’ result from outgrowth and reduction of two separate ancestral tails. Current Biology 26:R1224–R1225.

Schartl M, Kneitz S, Ormanns J, Schmidt C, Anderson JL, Amores A, Catchen J, Wilson C, Geiger D, Du K, Garcia-Olazábal M, Sudaram S, Winkler C, Hedrich R, Warren WC, Walter R, Meyer A, Postlethwait JH. 2021. The Developmental and Genetic Architecture of the Sexually Selected Male Ornament of Swordtails. Current Biology 31:911-922.e4.

Schneider CA, Rasband WS, Eliceiri KW. 2012. NIH Image to ImageJ: 25 years of image analysis. Nature Methods 9:671–675.

Schultze H-P, Arratia G. 1989. The composition of the caudal skeleton of teleosts (Actinopterygil: Osteichthyes). Zoological Journal of the Linnean Society 97:189–231.

Schultze H-P, Arratia G. 2013. The caudal skeleton of basal teleosts, its conventions, and some of its major evolutionary novelties in a temporal dimension. In: Wilson, MVH, Arratia, G, Schultze, H-P, editors. Mesozoic fishes 5 - Global diversity and evolution. München: F. Pfeil, pp. 187–246.

Shi G, Xiao Q, Zhu Q, Liao W. 2019. Fluid-structure interaction modeling on a 3D ray-strengthened caudal fin. Bioinspir Biomim 14:036012.

Silic MR, Wu Q, Kim BH, Golling G, Chen KH, Freitas R, Chubykin AA, Mittal SK, Zhang G. 2020. Potassium Channel-Associated Bioelectricity of the Dermomyotome Determines Fin Patterning in Zebrafish. Genetics 215:1067–1084.

Sinha KM, Zhou X. 2013. Genetic and molecular control of osterix in skeletal formation. Journal of Cellular Biochemistry 114:975–984.

Siomava N, Shkil F, Voronezhskaya E, Diogo R. 2018. Development of zebrafish paired and median fin musculature: basis for comparative, developmental, and macroevolutionary studies. Scientific Reports 8:14187.

Stewart S, Gomez AW, Armstrong BE, Henner A, Stankunas K. 2014. Sequential and Opposing Activities of Wnt and BMP Coordinate Zebrafish Bone Regeneration. Cell Reports 6:482–498.

Stewart S, Le Bleu HK, Yette GA, Henner AL, Robbins AE, Braunstein JA, Stankunas K. 2021. longfin causes cis-ectopic expression of the kcnh2a ether-a-go-go K+ channel to autonomously prolong fin outgrowth. Development. https://doi.org/10.1242/dev.199384.

Stewart S, Yette GA, Bleu HKL, Henner AL, Braunstein JA, Chehab JW, Harms MJ, Stankunas K. 2019. Skeletal geometry and niche transitions restore organ size and shape during zebrafish fin regeneration. https://www.biorxiv.org/content/10.1101/606970v3.

Talbot JC, Johnson SL, Kimmel CB. 2010. hand2 and Dlx genes specify dorsal, intermediate and ventral domains within zebrafish pharyngeal arches. Development 137:2507–2517.

Terán GE, Ballen GA, Alonso F, Aguilera G, Mirande JM. 2019. A new species of Farlowella (Siluriformes: Loricariidae) from the upper Bermejo River, La Plata River basin, northwestern Argentina. Neotrop ichthyol 17. http://www.scielo.br/j/ni/a/gBDB4cBBd36sjgwTXfvhrdD/?lang=en.

Thieme P, Warth P, Moritz T. 2021. Development of the caudal-fin skeleton reveals multiple convergent fusions within Atherinomorpha. Frontiers in Zoology 18:20.

Thomas MR, Pérez MHS. 2010. A New Species of Whiptail Catfish, Genus Loricaria (Siluriformes: Loricariidae), from the Rio Curuá (Xingu Basin), Brazil. cope 2010:274–283.

Walker M, Kimmel C. 2007. A two-color acid-free cartilage and bone stain for zebrafish larvae. Biotechnic & Histochemistry 82:23–28.

Wiley EO, Fuiten AM, Doosey MH, Lohman BK, Merkes C, Azuma M. 2015. The Caudal Skeleton of the Zebrafish, Danio rerio, from a Phylogenetic Perspective: A Polyural Interpretation of Homologous Structures. Copeia 103:740–750.

FIGURES

Figures 3.1 – 3.7

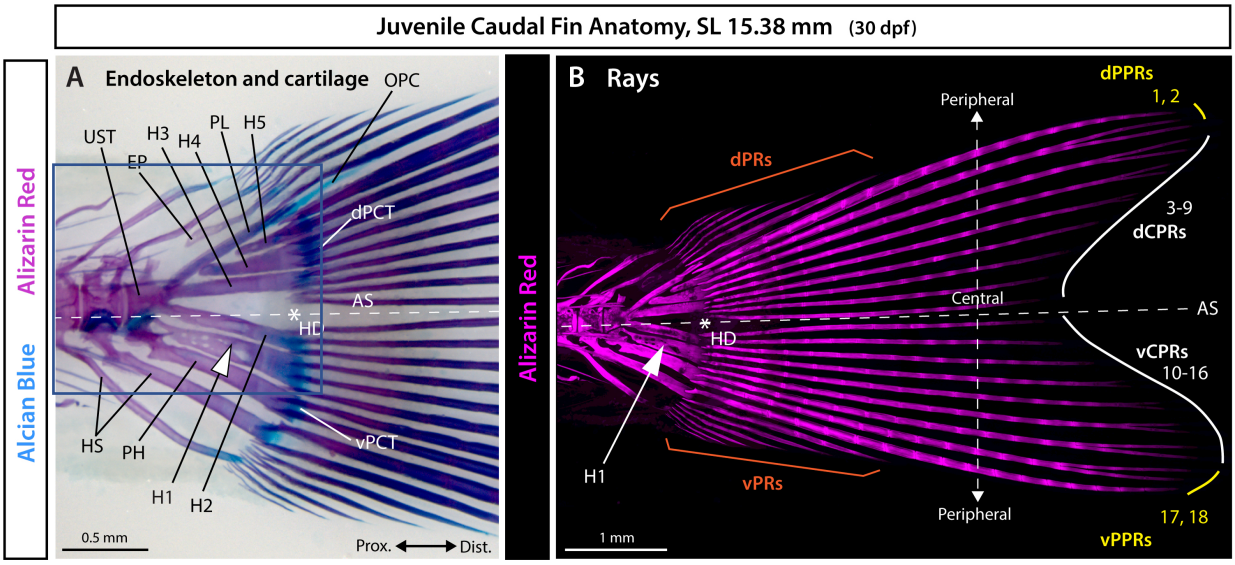

Figure 3.1. Anatomy of the zebrafish caudal skeleton.

A: Whole mount brightfield and B: maximum intensity projection of confocal fluorescent images of a juvenile zebrafish caudal fin stained with Alcian Blue and Alizarin Red. The white asterisk denotes the hypural diastema (HD), the white arrow indicates the hypural 1 (H1), and the white dashed line marks the axis of external dorsoventral symmetry (AS). Abbreviations: CPRs (white), central principal rays; dPCT and vPCT, dorsal and ventral plates of connective tissue, respectively; dPPRs and vPPRs (yellow), dorsal and ventral peripheral principal rays, respectively; dPRs and vPRs (orange), dorsal and ventral procurrent rays, respectively; EP, epural; H1-H5, hypurals 1 to 5; HS, haemal spine; OPC, opisthural cartilage; PH, parhypural; PL, pleurostyle; UST, urostyle.

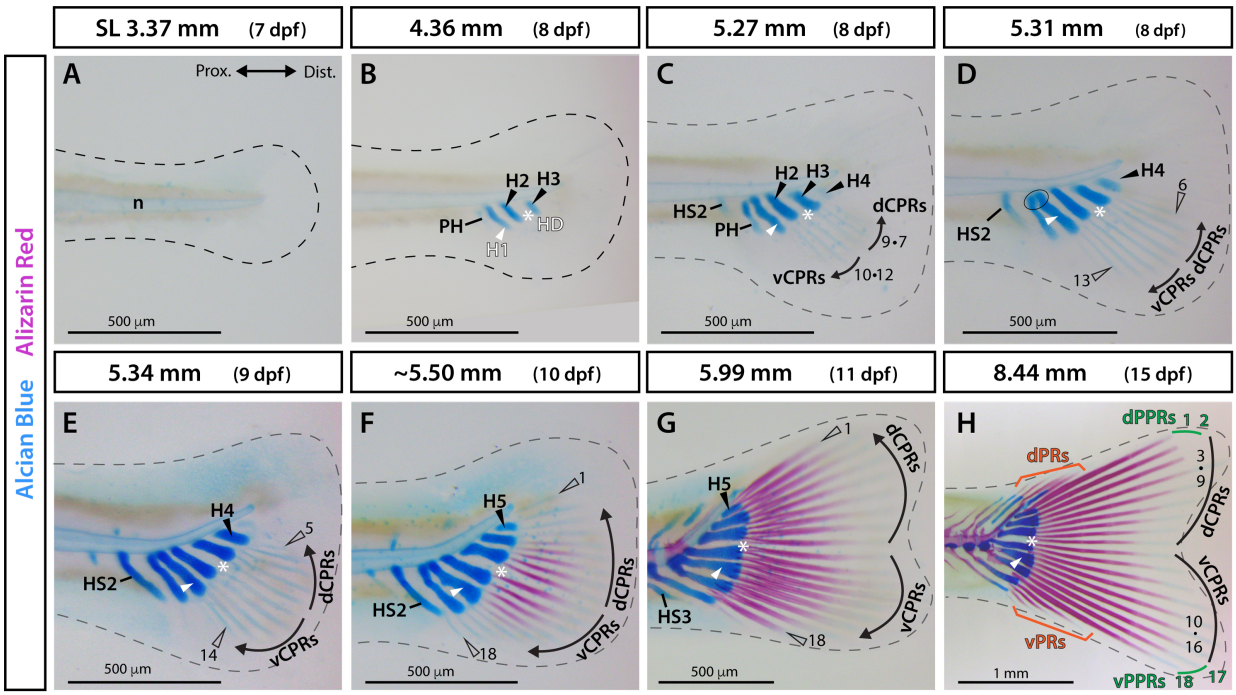

Figure 3.2. Alcian Blue and Alizarin Red visualization of caudal fin symmetry establishment and body axis alignment anchored by the hypural diastema.

A-H: Whole-mount images of Alcian Blue (cartilage) and Alizarin Red (calcified bone) stained caudal fin skeletons across a zebrafish larval developmental sequence. The dashed line marks the border of the fin fold. The ellipse in D indicates fusion of the parhypural and hypural 1. Abbreviations: dCPR and vCPR, dorsal and ventral central principal rays, black); dPPR and vPPR, dorsal and ventral peripheral principal rays (green); dPR and vPR, dorsal and ventral procurrent rays (orange); H1 and white arrowhead, hypural 1; H2-5 and black arrowheads, hypurals 2-5; HD and white asterisk, hypural diastema; HS2-3, haemal spine 2-3; n, notochord; PH, parhypural.

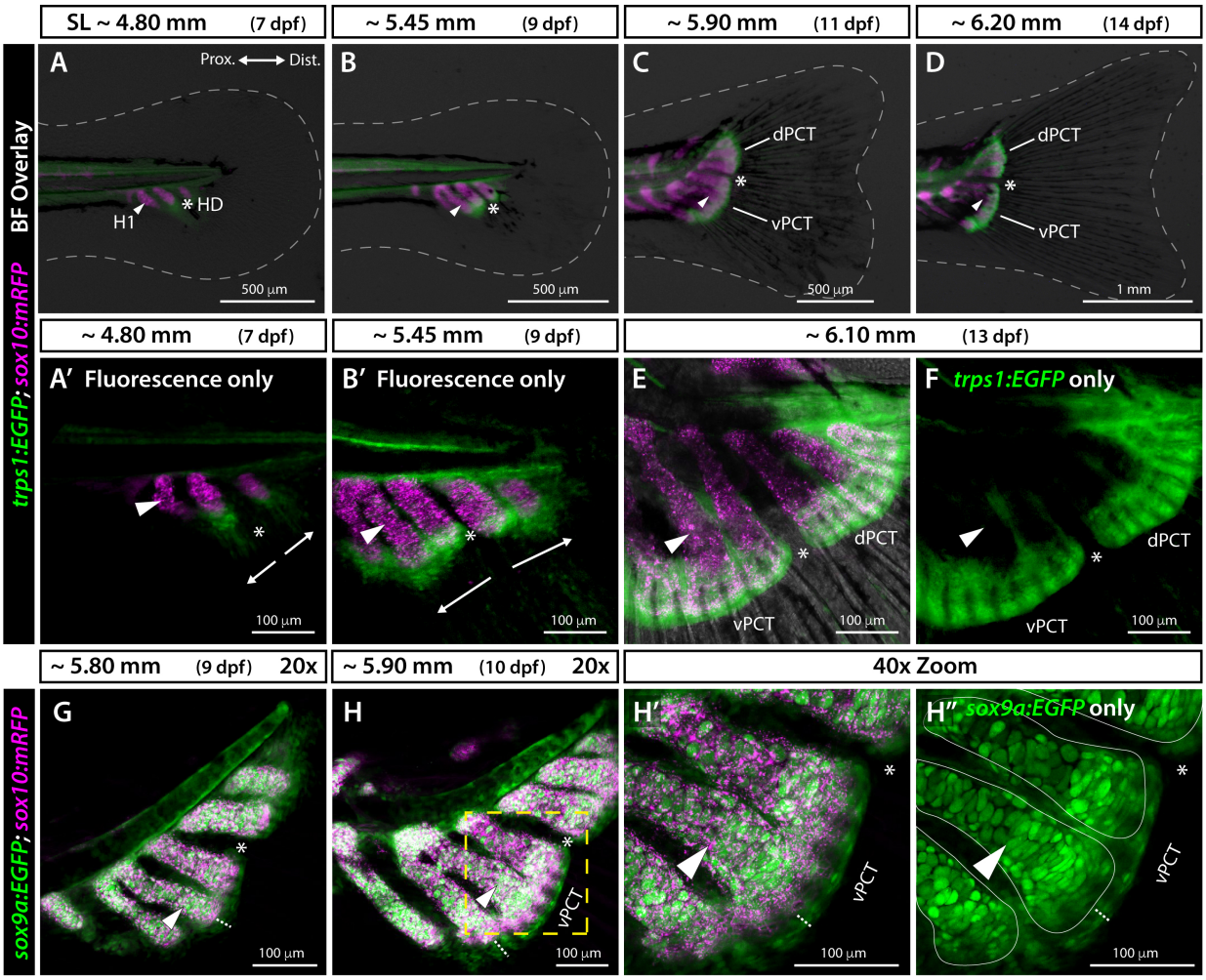

Figure 3.3. Transgene reporters reveal that plates of connective tissue develop symmetrically around the hypural diastema.

Figure 3.3. Transgene reporters reveal that plates of connective tissue develop symmetrically around the hypural diastema.

A-D: Widefield and A', B', E, F: confocal whole mount images of the caudal region of *trps1:EGFP*;*sox10:mRFP* larval zebrafish. White dashed line indicates fin boundaries. The *sox10:mRFP* (magenta) transgene labels endochondral elements, including hypurals, parhypural, and haemal spines. The *trps1:EGFP* marker labels precursor cells of the two plates of connective tissue located at the distal end of endochondral elements and on which caudal fin rays articulate. The hypural diastema lies between hypurals 2 and 3 and separates the two developing plates of connective tissue. Arrows in A' and B' indicate the directions of outgrowth of the plates of connective tissue. G-H": Confocal images of combined *sox9a:EGFP* and *sox10:mRFP* expression patterns in ~5.80 mm and 5.90 mm specimens. The *sox9a:EGFP* and *sox10:mRFP* transgenes are co-expressed in endochondral elements with additional *sox9a:EGFP* expressed in the two developing plates of connective tissue separated at the hypural diastema. The thickness of the plates of connective tissue marked by the *sox9a* reporter but not by the *sox10* reporter is highlighted by a white dotted line in H-H''. The yellow dashed line in H is blown up in H' and H". Solid white lines in H" denote the borders of the endochondral skeletal elements as judged by *sox10:mRFP* expression in H'. Abbreviations: dPCT and vPCT, dorsal and ventral plates of connective tissue, respectively; H1 and white arrowhead, Hypural 1; HD and white asterisk, hypural diastema.

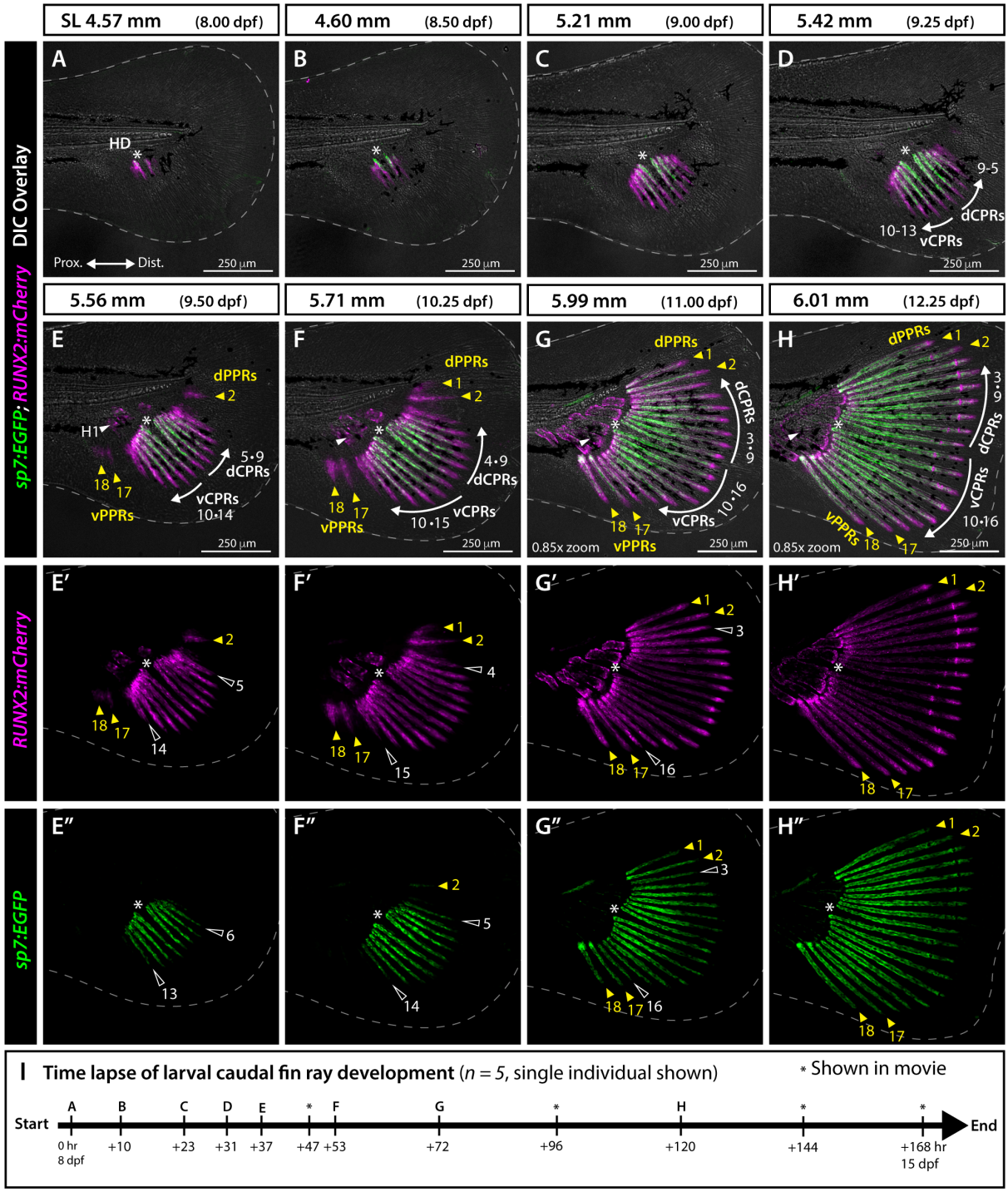

Figure 3.4. Osteoblast developmental state markers demonstrate synchronous and symmetric central principal ray formation and distinct emergence of peripheral principal caudal fin rays.

Figure 3.4. Osteoblast state markers demonstrate synchronous and symmetric central principal ray formation and distinct emergence of peripheral principal caudal fin rays.

A-H”: Whole mount confocal images of a representative *RUNX2:mCherry*;*sp7:EGFP* larva (from $n = 5$) followed from SL 4.57 mm to 6.01 mm (8-12.25 dpf) and imaged following the schedule in I. Differential interference contrast overlays in A-H; *RUNX2:mCherry* (pre-osteoblasts, magenta) single channel in E’-H’; and *sp7:EGFP* (differentiating osteoblasts, green) single channel in E”-H”. White dashed line indicates fin boundaries. A: At 4.57 mm, the first two central principal rays (CPRs) marked by *RUNX2:mCherry* form around the hypural diastema (HD, white asterisk). B: At 4.60 mm, two mirrored CPR pairs are apparent with the original pair now expressing *sp7:EGFP*. C: Four mirrored pairs of CPRs emerge by 5.21 mm. D: At 5.42 mm, five CPR mirrored pairs are evident. CPR direction of outgrowth is indicated by white arrows. E: At 5.56 mm, dorsal peripheral principal ray 2 (dPPR) and ventral peripheral principal rays 17 and 18 (vPPRs) emerge asynchronously (yellow arrowheads) and physically separated from the ten symmetrically organized CPRs. E’-E’’: Newly formed PPRs express *RUNX2:mCherry* but not *sp7:EGFP*, as with the most recently formed CPRs (rays 5 and 14, white open arrowheads). F: At 5.71 mm, a sixth mirrored pair of CPRs is present. All four peripheral rays comprising the two PPR sets are formed (yellow arrowheads) with a retained gap to the central rays. F”: Maturing dPPR 2, CPR 5, and CPR 14 express *sp7:EGFP*. G: By 5.99 mm, all 18 principal rays are present. The last CPR mirrored pair to emerge, rays 3 and 16 (open arrowheads in G’ and G”) are slightly shorter than the rays that flank them. H: By 6.01 mm, the full complement of principal rays, now segmented by joints, form a continuous, fan-like ray field comprised of 18 rays symmetrically organized around the hypural diastema. I: Timing of time lapse image acquisition points shown in the corresponding panels (letters) or in Movie 1 (asterisks).

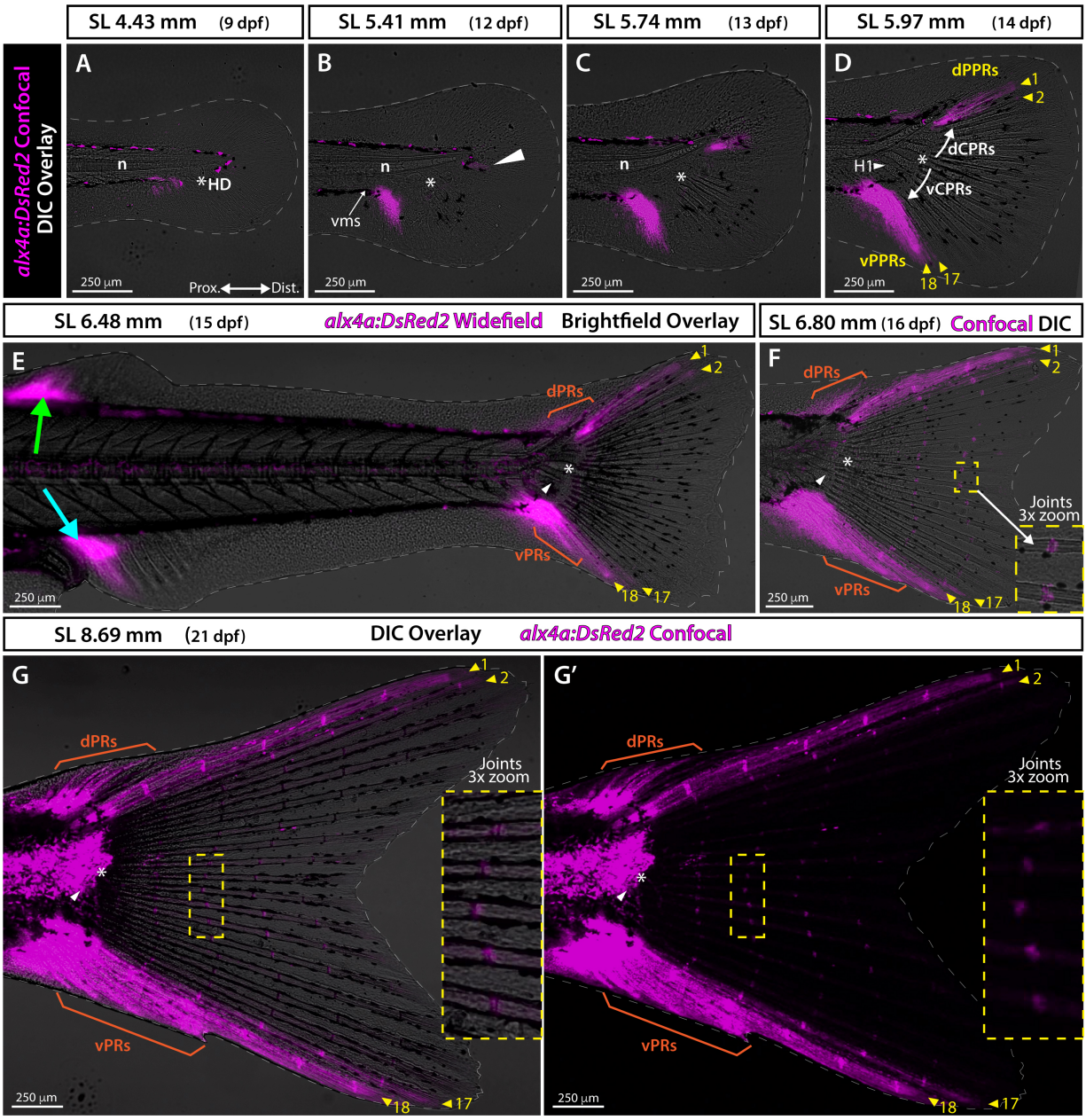

Figure 3.5. *alx4a* transgenic expression indicates the distinct nature of peripheral principal rays.

Figure 3.5. *alx4a* transgenic expression indicates the distinct nature of peripheral principal rays.

Developing caudal fin of *alx4a:DsRed2* zebrafish at indicated larval stages. A-D and F-G' are confocal maximum intensity projections (MIP) overlaid with DIC. G' is a single channel confocal MIP. E is a widefield fluorescence and brightfield overlay. White asterisks mark the hypural diastema (HD) and white arrowheads indicate hypural 1 (H1). Gray dashed line indicates fin boundaries. White arrows in Dmark the sequence of central principal ray specification. A: At 4.43 mm, *alx4a:DsRed2* expression was limited to pigment cells and a few cells in the ventral fin fold. B: At 5.41 mm, *alx4a:DsRed2* was expressed in a ventral patch at the posterior end of the ventral melanophore stripe (vms) before the caudal fin condensation region and faintly just below the notochord distal tip. C By 5.74 mm, *alx4a:DsRed2* ventral expression had increased and the small posterior patch expressing *alx4a:DsRed2* became clear. D: At 5.97 mm, dorsal and ventral central principal ray sets (dCPRs and vCPRs) continued forming symmetrically around the HD. The *alx4a:DsRed2* reporter was strongly expressed ventrally along ray 18 and faintly around ray 17 (vPPRs, yellow arrowheads), and dorsally around ray 1 and faintly along ray 2 (dPPRs, yellow arrowheads). E By 6.48 mm, *alx4a:DsRed2* expression persisted along PPRs with elevated levels in forming ventral and dorsal procurrent ray regions (vPRs and dPRs, orange arrowheads and brackets). Expression is also seen on one peripheral side of the developing dorsal fin (green arrow) and anal fin (cyan arrow). F: At 6.80 mm, vPRs and vPPRs 18 and 17 showed strong *alx4a:DsRed2* expression. Dorsal expression comprised emerging dPRs and the length of dPPRs 1 and 2, as well as in newly formed joints (dashed yellow box with 3x zoom inset) . G: By 8.69 mm, *alx4a:DsRed2* was strongly expressed by dPRs and vPRs, and by the most peripheral rays 1 and 18, with clear but reduced expression in rays 2 and 18. Joints (dashed yellow box with 3x zoom inset) also continued to express the transgene. G': Single channel *alx4a:DsRed2* expression.

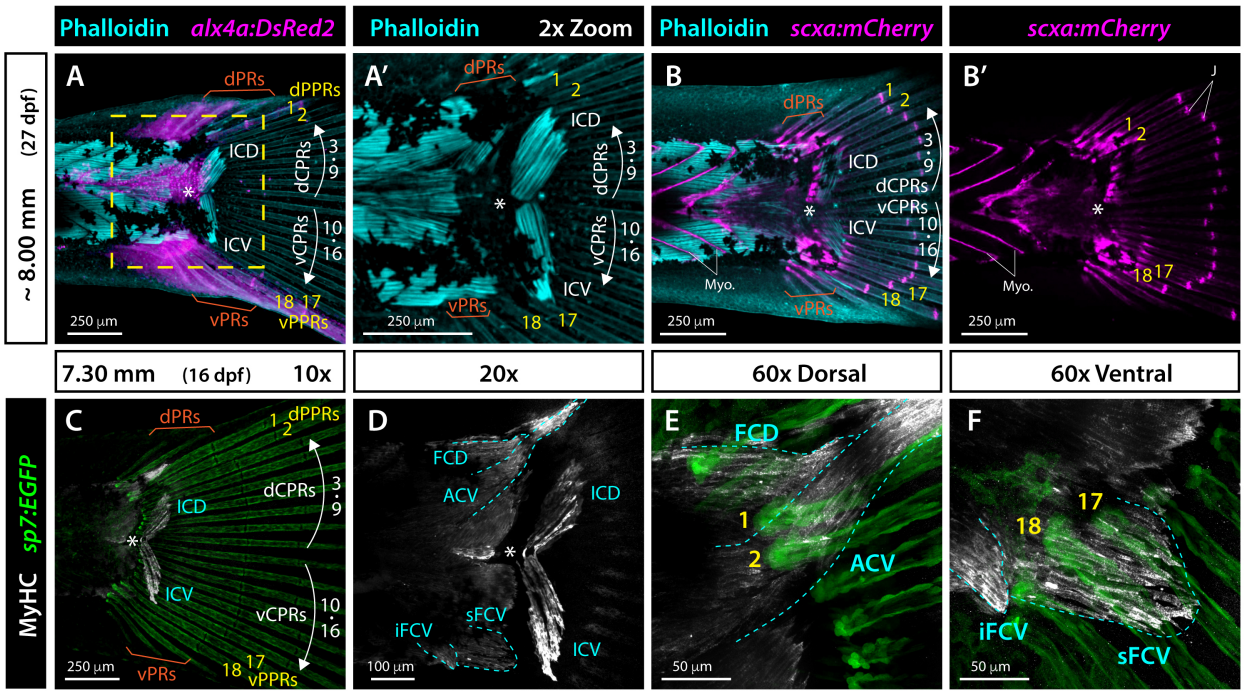

Figure 3.6. Muscle staining combined with *alx4a* and *scxa* reporters revealed that each set of central principal rays and peripheral principal rays is associated with distinct swimming muscles.

Whole mount widefield fluorescent images of the caudal region of zebrafish larvae. A, A': Phalloidin-stained ~8.00 mm *alx4a:DsRed2* larval zebrafish. F-actin (phalloidin) is cyan and DsRed2-expressing cells, including peripheral principal rays (PPRs), are magenta. B-B': Phalloidin-stained (cyan) ~8.00 mm *scxa:RFP* larval zebrafish. The mCherry fluorescent marker labels tendons, myosepta (Myo.), and caudal fin ray joints (J). C-F: Whole mount immunostained 7.30 mm *sp7:EGFP* larva. Myosin heavy chain (Myh) antibody labels skeletal muscles (white). EGFP fluorescence is green. Muscles are outlines in cyan dashed line. Abbreviations: ACV, abductor caudalis ventralis; dCPR and vCPR, dorsal and ventral central principal rays, respectively; dPPR and vPPR (yellow), dorsal and ventral peripheral principal rays, respectively; dPR and vPR, dorsal and ventral procurrent rays, respectively; FCD, flexor caudalis dorsalis; ICD, inerfilamenti caudalis dorsalis; ICV, inerfilamenti caudalis ventralis; iFCV, inferior flexor caudalis ventralis; sFCV, superior flexor caudalis ventralis; white asterisk, hypural diastema.

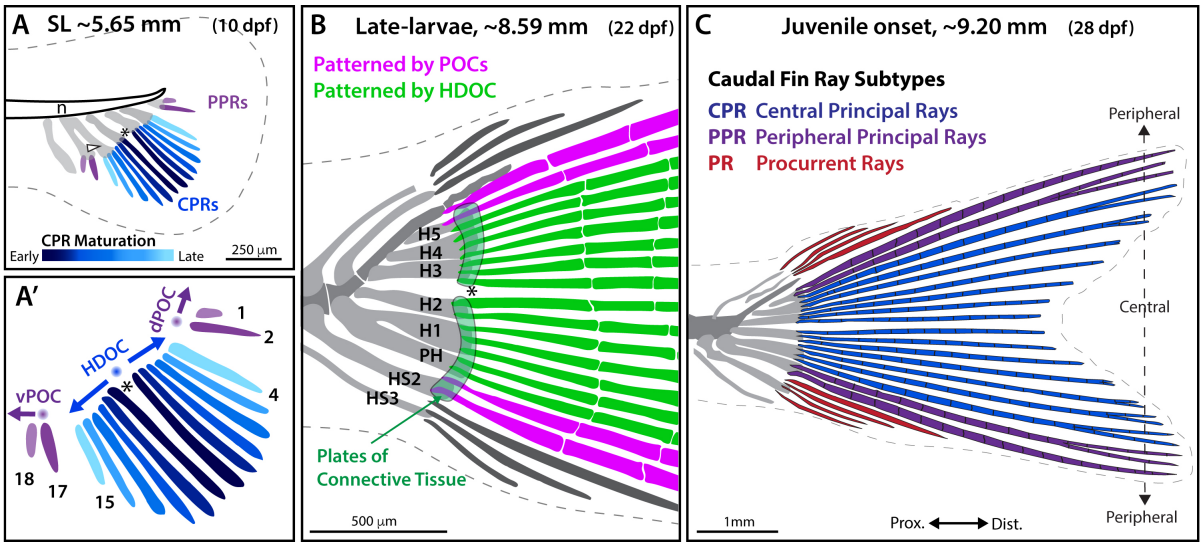

Figure 3.7. Schematic representation of zebrafish caudal fin skeletal patterning.

Schematic drawings of staged zebrafish caudal fins showing a model for the origins of external symmetry. The caudal fin comprises three subtypes of fin rays differing in their ontogeny, morphology, and identity: central principal rays (CPRs), two sets of peripheral principal rays (ventral and dorsal PPRs), and procurrent rays (PRs). A-A': CPRs (blue, with dark-to-light color gradient representing the first-to-last forming rays) are specified by a hypothetical bidirectional hypural diastema organizing center (HDOC; blue sphere) triggering the sequential and synchronous addition of mirrored pairs of rays (14 total) symmetrically distributed around the hypural diastema (asterisk). Two sets of PPRs (principal rays 1, 2 and 17, 18; purple) develop separately from the CPRs, unidirectionally specified by two hypothetical peripheral organizer centers (POCs, purple spheres). (B) Two plates of connective tissue (light green) are specified on each side of the HDOC along with CPRs (green), while PPRs are specified by POCs. H1-H5, Hypurals 1-5; HS2 and HS3, haemal spines 2 and 3. (C) CPRs (blue) are segmented and branched. Among the PPRs (purple), the two most peripheral (principal rays 1 and 18) are segmented but unbranched, while PPR 2 and 17 are segmented and branched. Unbranched PRs (red) emerge after the formation of all principal rays. This model suggests that the caudal fin is then a "compound" appendage with body axis-aligned external symmetry arising from 1) HDOC-initiated, symmetrically specified CPRs and plates of connective tissue, 2) two similar PPR sets specified by two POCs equally spaced from the HDOC, and 3) upward bending of the notochord that rotates skeletal elements from an anterior-posterior to a dorsal-ventral position, aligning the hypural diastema with the body axis. Morphological variation including loss of symmetry could be readily achieved by genetic changes impacting gene expression or activity in these developmental modules.

BRIDGE TO CHAPTER IV

This chapter details the specific ontogeny of fin rays during caudal fin development. We describe how central principal rays (CPRs, rays 3-16) are added sequentially and symmetrically to the dorsal and ventral fin lobes around a hypural diastema organizing center. We term a previously uncharacterized subset of the principal rays, peripheral principal rays (PPRs, rays 1, 2, 17, and 18) which differ in their ontogeny, order of emergence, and musculoskeletal connections from CPRs. We propose two peripheral organizing centers coordinate the patterning of PPRs separately from CPRs. In Chapters IV and V, we use both caudal fin development and regeneration as models to explore skeletal patterning.

CHAPTER IV: THE FRASER COMPLEX INTERCONNECTS TISSUE LAYERS TO SUPPORT BASAL EPIDERMIS AND OSTEOBLAST INTEGRATED MORPHOGENESIS UNDERLYING FIN SKELETAL PATTERNING

In preparation (style of *Developmental Biology*)

Co-authored material to be published as Amy E. Robbins[1, 2], Samuel G. Horst[1, 2], Victor M. Lewis[1], Scott J. Stewart[1], and Kryn Stankunas[1, 2], *

AUTHOR CONTRIBUTIONS

Amy E. Robbins conceived of the study and experimental design. Samuel G. Horst assisted with experiments. Victor M. Lewis contributed transcriptomic data analyses. Kryn Stankunas supervised the project with support from Scott Stewart. Amy E. Robbins drafted the manuscript with contributions and edits from Kryn Stankunas. Victor M. Lewis provided editorial assistance. The manuscript was approved with input from all authors.

[1]Institute of Molecular Biology
[2]Department of Biology
University of Oregon
273 Onyx Bridge
1318 Franklin Blvd
Eugene, OR 97403-1229
Office: (541) 346-7416
Fax: (541) 346-4854

* Correspondence: kryn@uoregon.edu

INTRODUCTION

Fraser Syndrome is a rare autosomal recessive disorder characterized by a wide range of variable abnormalities across organ systems within (e.g., fluctuating asymmetry between left and right limbs) and between affected individuals. Limb and digit abnormalities, including cutaneous syndactyly (webbed digits), clinodactyly/camptodactyly (curved or bent digits, respectively), brachydactyly (short digits), and polydactyly (extra digits) are common (Slavotinek & Tifft, 2002; van Haelst et al., 2008; Pasu et al., 2011; Butt et al., 2014; Mahadevan et al., 2002). The hands and feet of individuals with Fraser Syndrome are as unique as the individuals themselves, reflecting the exceptional variability in penetrance and expressivity of Fraser Syndrome alleles.

Teleost fins represent evolutionary precursors of mammalian limbs (Coates, 1994; Shubin et al., 2006). Even fin rays (lepidotrichia), while dermal bone, share a deeply conserved gene regulatory network with tetrapod digit endochondral elements (Woltering et al., 2014 Nakamura et al., 2016). Zebrafish fins provide a particularly tractable model to study core mechanisms of digit skeletal patterning relevant to human disease. The zebrafish caudal fin and its rays is particularly well studied, including as a leading model of robust, epimorphic regeneration. The caudal fin typically has eighteen principal rays, of which the central sixteen branch during development and regeneration (Arratia et al., 2008). Individual rays comprise two calcified and osteoblast-lined hemirays encasing intra-ray fibroblasts, nerves, vasculature and other cell types. Mesenchymal state pre-osteoblasts (pObs) proliferate within an outgrowth zone distal to each ray, then epithelialize to a bone-depositing differentiated state to extend forming rays. A laminin-containing basement membrane separates mature osteoblasts from a multi-layered epidermis that surrounds and interconnects the rays (Chen et al., 2015).

Sonic hedgehog (Shh) signaling from basal epidermal cells to adjacent pre-osteoblasts (pObs) promotes ray branching during development and regeneration (Armstrong et al., 2017; Braunstein et al., 2021; Zhang et al., 2012). Distally moving basal epidermal cells activate *sonic hedgehog a* (*shha)* expression while passing over pObs in the distal growth zone. The *shha*-expressing basal epidermal domain gradually splits during outgrowth, with *shha*-positive basal epidermal cells seemingly "pulling" pObs into divided pools to form a ray branch point. These signaling and potentially physical cell-cell interactions between epithelial (basal epidermal) and mesenchymal (pOb) state cells occur where the basement membrane remains immature. The contributions of this distinct extracellular environment to enable and/or modulate such cell interactions underlying ray branching morphogenesis are unresolved.

In Fraser Syndrome, disruptions to the basement membrane-localized Fraser Complex compromise epithelial-mesenchymal signaling, adhesion, and basement membrane rigidity (Smyth and Scambler, 2005). The Fraser Complex accumulates in the sublamina densa layer of the basement membrane separating epithelial from mesenchymal tissue layers, and Fraser Complex proteins are highly expressed in the embryonic zebrafish caudal fin (Dalezios et al., 2007; Gautier et al., 2008; Kiyozumi et al., 2006). Mouse forward genetic screens identified pathogenic variants of Fraser Complex genes *Fraser extracellular matrix complex subunit* (*Fras1*) and *Fras1-related extracellular matrix protein 2* (*Frem2*), along with *Glutamate receptor interacting protein 1* (*Grip1*), a scaffold protein required for Fras1/Frem trafficking (Jadeja et al., 2005; McGregor et al., 2003; Takamiya et al., 2004; Vrontou et al., 2003). Loss of *Fras1* in mice results in subepidermal blistering of embryonic limb buds and digit syndactyly

(Hines et al., 2016; Miller et al., 2013; Vrontou et al., 2003). Blistering is also observed in the zebrafish caudal fin fold of *fras1* and other Fraser Syndrome-related mutant larvae, along with craniofacial abnormalities recapitulating Fraser Syndrome characteristic phenotypes (Carney et al., 2010; Talbot et al., 2012; Talbot et al., 2016)..However, adult phenotypes including any affecting fins have not been examined due to frequent larval lethality.

We explored Fraser Complex roles during fin formation using zebrafish *fras1*^{te262} loss-of-function mutants (Carney et al., 2010; Talbot et al., 2016, 2012). We found ~10% of *fras1* homozygous mutants survived to adulthood. All fins of surviving *fras1* mutant adults had variable skeletal defects reminiscent of tetrapod limb syndactyly, including intermittent ray branching, ray fusions, and overall fewer rays. Focusing on the caudal fin, we found abnormalities extended to the endochondral skeleton, including poor articulation of hypurals and radials and ectopic cartilaginous structures. *fras1* mutants regenerated amputated caudal fins to their original length. However, the regenerated fins acquired additional skeletal defects including further disrupted ray branching. Single-cell RNA-seq and *in situ* expression studies localized Fraser Complex transcripts and proteins to the distal-most basal epidermis and its mesenchyme-facing, basal side. Shh signaling between basal epidermis and pre-osteoblasts that promotes ray branching was retained in *fras1* mutant regenerating fins. However, the Fraser Complex did not assemble and extensive sub-epidermal blistering disrupted the normally tight association between the basal epidermis epithelium and underlying blastema mesenchyme, including pre-osteoblasts. We propose Fraser Complex is upregulated in distal outgrowing fins to establish a robust environment supporting interactions between basal epidermis and pre-osteoblasts that underlie skeletal patterning. Zebrafish *fras1* mutant fins and their regeneration provide a

compelling context to explore Fraser complex functions at epithelial-mesenchymal interfaces during tissue morphogenesis and uncover deeply conserved mechanisms that may underlie Fraser Syndrome-associated syndactyly in tetrapods.

RESULTS

Fras1 promotes robust fin skeletal patterning including ray branching

The *fras1*^{te262} mutant allele is reported as lethal around 10-12 days-post-fertilization (dpf) (Carney et al., 2010). However, we found 10.4% (n = 110/1057) of homozygous *fras1*^{te262} mutants (hereafter referred to as *fras1*$^{-/-}$) were viable to adulthood under careful rearing conditions. Surviving adults required no special care and lived well over a year in standard housing conditions, albeit with reduced breeding efficiency. *fras1*$^{-/-}$ adults exhibited varied phenotypes, such as a protruding lower jaw, fin abnormalities including uneven pigment striping, particularly evident in the caudal fin (Figure 4.1A). We noted differences in ray number between the matched paired fins (i.e, pectoral fins) of the same fish (Figure S4.1C, D), consistent with fluctuating left-right asymmetry associated with human Fraser Syndrome. Both paired (pectoral and pelvic) and median (dorsal, anal, caudal) fins showed extensive but highly variable fin and ray skeletal patterning defects, including asymmetrical fin shapes, reduced ray number associated with smaller fins, curved or warped rays, and decreased ray branching (Figure 4.1A, Figure S4.1).

We focused on the caudal fin as an accessible model to further study Fraser complex roles in fin and fin ray development. Wildtype caudal fins typically have 18 principal, full length rays with 9 rays each symmetrically arranged on dorsal and ventral fin lobes. At least three shorter

procurrent rays, sometimes called rudimentary rays, lie peripherally on each side of the peripheral rays. The inner 16 principal rays branch at least once, while the peripheral principal rays 1 and 18 remain unbranched. (Figure 4.1B; Arratia et al., 2008; Coates, 1994). The caudal fin skeleton of *fras1*$^{-/-}$ fish (Figure 4.1C-F) showed a range of abnormalities (Figure 4.1B). *fras1*$^{-/-}$ caudal fins developed with fewer principal (count 5-18, n = 38) and procurrent rays (count 2-6, n= 37). Ray branching varied from normal (all central 16 of 18 rays) to completely absent (Figure 4.1G-I). Additional abnormalities included overall fin asymmetry (Figure 4.1D, E), ray fusions (Figure 4.1C', F'), precocious branching (Figure 4.1C'), ectopic branching of peripheral principal rays (Figure 4.1D'), unevenly positioned branch points, misaligned and wavy hemi-rays, and poorly articulated joints (Figure 4.1E'). Therefore, Fras1 is required for fin skeletal patterning with variable expressivity and incomplete penetrance reminiscent of distal limb defects in humans with Fraser Syndrome.

Fras1 contributes to endochondral and dermal bone patterning during fin development

Fin rays are dermal bone, unlike the fully endochondral skeleton of extant tetrapod limbs (Arratia et al., 2008; Coates, 1994). Therefore, we examined if zebrafish *fras1* also was required for endochondral fin skeletal pattering. We visualized the developing caudal skeleton of *fras1*$^{-/-}$ mutants by Alcian Blue and Alizarin Red staining of cartilage and calcified bone, respectively, at late larval stages. A representative heterozygote sibling control at 22 dpf (out of n = 7) (Figure 4.2A) had five clearly defined hypurals, centered around a hypural diastema (the gap between hypurals 2 and 3 around which principal rays symmetrically emerge; Desvignes et al., 2018; Desvignes et al, 2022). Age- (22 dpf, Figure 4.2C) and size-matched (28 dpf, Figure 4.2E, G) *fras1*$^{-/-}$ mutants showed variable caudal skeletal abnormalities including fusions between

endochondral elements (Figure 4.2C, E) and ectopic cartilaginous structures (Figure 4. 2C, E, G). Further, *fras1*$^{-/-}$ fish often displayed an extra dorsal hypural despite having fewer fin rays (Figure 4.2C, E). As forementioned, while caudal fin rays normally are evenly spaced and segmented by joints (Figure 4.1A), *fras1*$^{-/-}$ rays frequently were unaligned (Figure 4.2C, G) and had poorly articulated joints (Figure 4.2E, G). The hypural diastema was missing. The anal and dorsal median fins also showed endochondral skeletal defects. Control siblings had evenly spaced radials (Figure 4.2B) whereas *fras1*$^{-/-}$ radials were variably truncated and/or contorted (Figure 4.2D, F, H). The dorsal fin frequently had supernumerary posterior radials. We conclude Fras1 supports patterning of both endochondral and dermal bone fin skeletal elements.

Fras1 stabilizes fin ray pattering without contributing to outgrowth during fin regeneration

Rapid and robust adult fin regeneration enables studying active roles of Fras1 during fin formation spanning wound healing through bone maturation (Reviewed in Sehring & Weidinger, 2020). We tracked heterozygote control (n = 6) and *fras1*$^{-/-}$ (n = 9) siblings throughout caudal fin regeneration, imaging fins at uninjured, 3, 7, and 28 days-post-amputation (dpa) (Figure 4.3). Control caudal fins progressively and robustly regenerated to their original size and bilobed shape with long peripheral rays, shorter central rays, and a branched ray field (Figure 4.3B-D). *fras1*$^{-/-}$ fins at 3 dpa exhibited blistering between distal ray and epidermal boundaries (Figure 4.3F, F', N, N') and excess distal epidermis (Figure 4.3F', J', N'). Outwardly evident blisters at 3 dpa receded by 7 dpa (Figure 4.3G, G', K, K', O, O'). By 28 dpa, *fras1*$^{-/-}$ caudal fins (n = 9/9) restored the same extent of fin tissue as controls (control ray length recovery from uninjured to 28 dpa for longest ray +/- 5%; *fras1*$^{-/-}$ longest ray recovery +/-4%; shortest ray length recovery

+/-8% for both groups) (Figure 4.3S) but with notable skeletal patterning defects including fewer branched rays than their uninjured pattern (*n* = 9/9, Figure 4.3H, L, P, R) and a different number of principal fin rays (*n* = 8/9, Figure 4.3I, L, M, P).

We additionally noted *fras1*$^{-/-}$ caudal fins exhibited a shallower bi-lobed "V" shape compared to controls in both uninjured and regenerated states. The ratio of the longest ray to the shortest ray was not significantly different in uninjured vs. 28 dpa control fish, indicating fin proportions are restored after regeneration (Ratio1.665 vs. 1.662, One-Way ANOVA P = 0.99, *n* = 6) or uninjured vs. 28 dpa *fras1*$^{-/-}$ (1.338 vs. 1.270, P = 0.34, *n* = 8). However, the fin length ratios for the controls vs *fras1*$^{-/-}$ groups were significantly different for both uninjured at 28 dpa timepoints (P = 0.0009 by t-test) (Figure 4.3E, I, M, Q), reflecting the less pronounced bilobed shape of *fras1*$^{-/-}$ caudal fins. Moreover, we noted the longest ray switched from dorsal (uninjured, Figure 4.3M) to ventral (*n* = 1/9) (28 dpa, Figure 4.3P) in one *fras1*$^{-/-}$ individual. Taken together, the worsened and still variable phenotypes seen in regenerated fins indicates Fras1 stabilizes tissue patterning during both developmental and regenerative fin outgrowth.

Fraser Complex transcripts and proteins are enriched in distal fin regenerates and support pre-osteoblasts alignment

The subepidermal blistering in early *fras1*$^{-/-}$ fin regenerates characterizes Fraser syndrome-associated defects in other contexts. Therefore, zebrafish fin regeneration provides a new and compelling model to explore Fraser Complex function in modulating interactions between adjacent epithelial and mesenchymal cells. We examined Fraser Complex transcript and protein localization during fin regeneration, anticipating expression in cells adjacent to the basement

membrane separating basal epidermis from blastema (Figure 4.4A, B). We mined our existing single-cell RNA-Seq dataset of 3 and 7 dpa regenerating fin cells, focusing on the unique clusters for superficial epidermis, basal epidermis, and combined mesenchyme, fibroblast and osteoblast-lineage cells (Figure 4.4C; Lewis et al., 2022). As reported by bulk RNA-Seq analyses (Nauroy et al., 2019), Fraser Complex transcripts *frem2a, frem2b*, and *frem3* were highly expressed in the basal epidermal cluster cells, and *fras1* was highest enriched basal epidermal specific marker in our scRNA-Seq dataset (Figure 4.4D, Figure S4.2). The Fraser complex transcripts *frem1a* was expressed sparsely in basal epidermal and mesenchyme/fibroblast/osteoblast clusters, and *frem1b* showed lower levels in the fibroblast/osteoblast cluster and scarce expression in superficial epidermis (Figure 4.4D, Figure S4.2). These data are consistent with findings from mouse studies showing Fraser Complex transcripts are expressed in nearby epithelial and mesenchymal tissue while the proteins translocate and complex in the basement membrane (Jadeja et al., 2005; McGregor et al., 2003; Takamiya et al., 2004; Vrontou et al., 2003).

We antibody-stained 4 dpa regenerating fin sections to define Fras1protein spatial expression *in situ*. Fras1 was highly enriched in distal-most tissue separating basal epidermis from blastemal mesenchyme. Fras1 was also present in proximal, re-formed tissue, in association with the mature basement membrane separating basal epidermis from bone-lining osteoblasts (Figure 4. 4E, E'; Armstrong et al., 2017; Chen et al., 2015). Fluorescent *in situ* hybridization demonstrated *frem2a* transcripts were highest in far distal basal epidermis with lower expression in blastemal mesenchyme and superficial epidermis. The *frem2b* pattern was similar but more specific to basal epidermal cells (Figure 4.4F-G'). We conclude Fraser Complex transcripts are upregulated in distal basal epidermis of regenerating fins to produce locally accumulating Fraser Complex.

We examined expression of Fras1 relative to pre-osteoblasts in 4 dpa regenerating fin sections given skeletal defects in *fras1*$^{-/-}$ mutants. Fras1 protein mostly accumulated distal to blastema-lining Runx2-expressing pre-osteoblasts (Figure 4.5A). Lower Fras1 was found lateral to the most distal pre-osteoblasts. Fras1 protein was unsurprisingly absent in *fras1*$^{-/-}$ mutants (n = 6) (Figure 4.5B). Runx2+ pre-osteoblasts were clumped and multi-layered rather than evenly spaced along the basal epidermis (Figure 4.5A, B). We also examined Frem2 protein localization relative to Runx2+ pre-osteoblasts. Like Fras1, Frem2 was highly enriched distally between basal epidermis and blastema mesenchyme and largely distal to pre-osteoblasts (Figure 4.5C, C'). Frem2 was also present extracellularly within the superficial epidermis layer enveloping distal basal epidermal cells (Figure 4.5C", n = 6). In *fras1*$^{-/-}$ mutants, Frem2 protein was almost completely absent (Figure 4.5D, D') and what protein remained appeared intracellularly retained within basal epidermal cells (Figure 4.5D", n = 6). We conclude Fras1 supports Frem2 secretion and assembly into Fraser Complex-containing basement membrane. Further, we find that Fras1 promotes pre-osteoblast alignment, albeit likely indirectly given the Fraser Complex minimally associated with pre-osteoblasts.

Fras1-mediated skeletal patterning functions independently of Shh/Smo signaling.

Fin ray branching requires basal epidermal Sonic hedgehog/Smoothened (Shh/Smo) signaling to divide underlying pre-osteoblast pools during development and regeneration (Armstrong et al., 2017; Braunstein et al., 2021; Cardeira-da-Silva et al., 2022; Quint et al., 2002). We considered if this epithelial-mesenchymal signaling was disrupted in *fras1*$^{-/-}$ mutants given frequent ray branching defects and disorganized Runx2+ pre-osteoblasts. *shha* is transcriptionally activated in

distal basal epidermal cells as they collectively move distally and pass over pre-osteoblasts of the outgrowth zone (Braunstein et al., 2021; Zhang et al., 2012). *shha*-expressing basal epidermal domains progressively divide during fin outgrowth, likely driving the subsequent Shh/Smo-dependent splitting of pre-osteoblast pools. We assessed if *shha* expression during fin regeneration was Fras1-dependent using *Tg(-2.4shha:gfpABC)* (Ertzer et al., 2007; henceforth referred to as *shha:GFP*). *shha:GFP* was expressed in distal ray-associated domains in both heterozygote control (n = 3) and *fras1*$^{-/-}$ mutants (n = 3). Likewise, the *shha:GFP* domains of *fras1*$^{-/-}$ regenerating fins still split into two pools by 8 dpa, when ray branching is well underway, even though many *fras1*$^{-/-}$ fin rays did not branch (Figure 4.6A, A', C, C'). Therefore, Fraser complex is not required for *shha* induction nor the *shha*-expressing basal epidermal domain splitting underlying ray branching.

We next considered if Fras1 facilitates Shh/Smo signal transduction to pre-osteoblasts. We photoconverted the well-established Shh/Smo activity reporter *Tg(ptch2:Kaede)* (Huang et al., 2012; henceforth *ptch2:Kaede*) in distal ray regions at 4 dpa from green to red (false colored magenta) (Figure 4.6E, G). Both heterozygote controls and *fras1*$^{-/-}$ mutants (n = 6 each) produced new domains of green Kaede protein at 24 hours post-conversion, even in clearly abnormal *fras1*$^{-/-}$ mutant fins (Figure 4.6F, H). *ptch2:Kaede* photoconversion assays during fin development yielded similar results (Figure S4.3). We conclude Shh/Smo signal transduction in zebrafish fins does not require Fraser Complex. However, the Fraser Complex at least supports the Shh/Smo downstream cell behaviors that split pre-osteoblasts given frequent ray branching defects in *fras1*$^{-/-}$ mutants. The variable phenotypes in *fras1*$^{-/-}$ mutants and predominant

expression of the Fraser complex distal to the Shh/Smo signaling zone, including pre-osteoblasts, suggest an indirect and/or supporting role.

Fras1 maintains epidermal-mesenchymal continuity in regenerating caudal fin rays.

The morphological changes to *fras1*$^{-/-}$ regenerating rays (e.g., blistering, blunted ends, disorganized bone) led us to investigate how Fras1 contributes to tissue organization during caudal fin regeneration. We hematoxylin and eosin (H&E)-stained 4 dpa regenerating caudal fin sections of heterozygote control (n = 7) and *fras1*$^{-/-}$ animals (n = 8). The blastema mesenchyme of control fins was continuously associated with a surrounding single-cell layer of basal epidermis (bEps) further encased by superficial epidermis (sEp) (Figure 4.7A). *fras1*$^{-/-}$ regenerates variably exhibited an uneven shape and acellular gaps and pockets (or, "blisters") concentrated distally (Figure 4.7B-D). Single confocal optical slices of eosin-stained fins (Figure 4.7E-H) revealed fully penetrant but variable blistering with both intra-epidermal acellular pockets and tissue separations between the basal epidermis and underlying blastema mesenchyme. We frequently also observed excess "flaps" of epidermal tissue distal to the blastema (Figure 4.7F-H). We conclude Fras1 maintains tissue continuity in the distal ray outgrowth region of regenerating fins to enable robust restoration of skeletal pattern.

DISCUSSION

We show that *fras1* loss-of-function zebrafish develop variably abnormal fins affecting both endochondral and dermal skeletons. These skeletal patterning defects, including supernumerary cartilages, fin asymmetry with aberrant ray numbers, and deficient ray branching resemble variable limb/digit abnormalities seen in Fraser Syndrome. The most common limb defect in

Fraser Syndrome is cutaneous syndactyly (webbed digits, frequency 54%-79%; (Slavotinek and Tifft, 2002; van Haelst et al., 2008), a phenotype also observed in mouse models (Jadeja et al., 2005; McGregor et al., 2003; Miller et al., 2013; Smyth et al., 2004; Takamiya et al., 2004; Vrontou et al., 2003). However, Fraser syndrome syndactyly also includes digit skeletal fusions and ectopic skeletal elements ((Butt et al., 2014; Mahadevan et al., 2002; Pasu et al., 2011). Fish fin dermal bone rays and tetrapod limb digits may share deep evolutionary homology, yet divergence in their anatomy (Boisvert et al., 2008; Freitas et al., 2012; Letelier et al., 2018; Nakamura et al., 2016a; Sordlno et al., 1995). For example, whereas tetrapod digits separate by controlled interdigital apoptosis (Hines et al., 2016; Kashgari et al., 2020), fin rays are epidermally webbed together. Therefore, the fin endochondral and ray patterning defects in *fras1*^{te262} homozygous zebrafish provide new models to understand origins of Fraser syndrome limb abnormalities affecting skeletal pattern (i.e., complex syndactyly, loss of digits) rather than cutaneous syndactyly. Centrally, our results indicate Fraser complex establishes an environment supporting cooperative epidermal and adjacent mesenchymal, including pre-osteoblast, interactions for robust skeletal patterning (Figure 4.8).

Fraser Syndrome occurs in approximately 1:10,000 stillbirths and 1:200,000 live births, suggesting ~ 5% survival of Fraser Syndrome-afflicted fetuses (Divya et al., 2014; Martínez-Frías et al., 1994; Thomas et al., 1986). Fraser Syndrome patients that survive adolescence can achieve normal life spans (Impallomeni et al., 2006). While *fras1*$^{-/-}$ mice are mostly embryonic lethal, they likewise can survive to adulthood depending on their genetic background (McGregor et al., 2003; Miller et al., 2013; Vrontou et al., 2003). Similarly, we find 10.4% viability for *fras1*^{te262} homozygous zebrafish under careful rearing conditions. These homozygous survivors

live over a year under standard care. This phenotypic variability suggests the influence of background genetic modifiers, supported by clutch-specific differences in *fras1*^{te262} jaw features (Talbot et al., 2012; Talbot et al., 2016) and the exacerbation of *fras1*^{te262} phenotypes by site-independent transgene sequences (Kimmel et al., 2021). Alternatively, characteristic variability across species including humans could arise from the Fraser complex largely providing robustness to organ development. Fraser complex loss-of-function phenotypes then variably manifest depending on stochastic or environmental perturbations with development often even proceeding normally. Long-term viability through adulthood amongst *fras1* loss-of-function escapers suggests Fraser complex functions are particularly important during organ patterning and morphogenesis and are less essential once organs are established.

The naturally regenerative zebrafish enables exploring and comparing gene function during the establishment of skeletal pattern during initial fin development and pattern re-establishment during fin regeneration. We find Fras1 is not necessary for fin regeneration in general, including outgrowth extent. However, skeletal patterning, including ray branching, defects worsen in regenerated fins lacking Fras1. Therefore, the Fraser Complex both helps establish the overall number and distribution of rays during early fin development and actively supports ray morphogenesis during fin outgrowth.

The ray branching morphogenesis defects and mis-aligned pre-osteoblasts in *fras1* mutants tie the Fraser complex to the maintenance of a well-organized environment supporting pre-osteoblast positioning. For Shh/Smo-mediated ray branching, intercellular signaling remains intact but downstream cell behaviors, which could include basal epidermal and pre-osteoblast

heterotypic associations and co-movements (Braunstein et al., 2021b), likely are perturbed. Frequent blistering distal to the rays in *fras1* mutants suggest the Fraser Complex serves a permissive role sustaining a robustly layered epidermis closely associated with underlying blastema mesenchyme. Similar blistering defects in Fraser complex mutants are observed during development, including for craniofacial patterning (Talbot et al., 2016, 2012). Further, parallel genetic studies in mice describe extensive *in utero* blistering of eye, limb bud, and kidneys which typically become hemorrhagic associated with poor outcomes (McGregor et al., 2003; Reviewed in Smyth and Scambler, 2005; Vrontou et al., 2003). Adult fin regeneration provides an accessible model to pursue conserved Fraser Complex-dependent epidermal-mesenchymal organization across forming organs.

We find *fras1* is highly enriched in distal basal epidermis of regenerating fins while the *frem* family Fraser Complex subunits are expressed in basal epidermis and fibroblast and osteoblast lineage cells of the blastemal mesenchyme. Immunohistochemistry and *in situ* hybridization revealed Fras1 protein and *frem2a/b* transcripts are most highly localized to the distalmost basement membrane separating the intra-ray blastemal mesenchyme from the encasing stratified epidermis. We show that *fras1*$^{-/-}$ mutants exhibit diminished Frem2 at the basement membrane but maintain distal basal epidermis intra-cellular expression. Similarly, Frem2 is unable to localize to the basement membrane lamina densa and is instead retained intracellularly in epithelial cells upon *Fras1* loss-of-function in mice (Petrou et al., 2007). Therefore, zebrafish regenerating fins provide a new context to examine mechanisms of Fraser Complex transcription upregulation as well as protein synthesis, processing, and assembly.

The Fraser complex-enriched distal basal epidermis of regenerating fins has an immature basement membrane compared with the thicker and well-defined laminin-containing layer that separates the basal epidermis from mature bone-lining osteoblasts more proximally (Armstrong et al., 2017; Chen et al., 2015). We propose the Fraser complex may serve as a scaffold stabilizing tissue organization during basement membrane formation to enable morphogenetic epithelial-mesenchymal interactions. Extending this idea, the Fraser complex may even template efficient basement membrane assembly. Such general, permissive roles could explain strikingly variable phenotypes across organs that characterize Fraser Syndrome and animal models thereof. Similarly, a transient function while organs are forming could explain why the Fraser Complex seems more critical during embryonic developmental windows or epimorphic organ regeneration rather than for organ homeostasis (Talbot et al., 2016). Regardless, zebrafish fins provide a new context to explore Fraser Complex mechanisms during epithelial-mesenchymal interactions and, potentially, conserved origins of Fraser Syndrome syndactylism.

MATERIALS & METHODS

Zebrafish husbandry and lines

Danio rerio zebrafish were housed at the University of Oregon with husbandry as described (Westerfield, 2007) overseen by the Aquatic Animal Care Services (AqACS) . Protocols were approved by the Institutional Care and Use Committee (IACUC). The following mutant and transgenic lines were used: *fras1*^{te262} line (Carney et al., 2010)*, Tg(-2.4shha:gfpABC)* (Ertzer et al., 2007a) and *Tg(ptch2:Kaede)* (Huang et al., 2012).

fras1^{te262} homozygous mutants were screened by embryonic fin fold blistering at 24 hpf. Larvae were reared in beakers with lower water volume, a reduced concentration of rotifer feed, and health-checked more frequently compared to standard care. At 30 dpf, healthier juveniles were moved to standard housing with no further exceptional care. *fras1*^{te262} heterozygote adults were identified by fin clip PCR and subsequent SspI-HF restriction enzyme digest (F: 5' GGAAGATTTTCTTTATTTAGCAGTCTCT R: 5' TTGGAACTAGGTCCTCTTTGGTGTGCTATAAAATA).

Skeletal Staining

Live adult fish were stained with Alizarin Red S (LabChem, Zelienople, PA) at 0.01% concentration in fish facility system water for 15 minutes (Bensimon-Brito et al., 2016), followed by 3 x 5 minute washes in fresh system water. Live adult fish were anesthetized in 0.6 mM tricaine (MS222, Syndel) in system water and imaged on a Nikon T*i*-E inverted microscope with a Yokogawa CSU spinning disc confocal unit. Images of all fins (n = 5 controls, n = 8 *fras1*^{te262} mutants) were acquired by tricaine overdose euthanasia of Alizarin-stained fish and subsequent dissection of fins, followed by imaging with dual Brightfield and Widefield fluorescence on a Nikon T*i*-E inverted microscope. Larval fish less than 30 dpf were stained with Alcian Blue (Anatech, Batte Creek, MI) and Alizarin Red S using a modified double-stain protocol (Walker and Kimmel, 2007) whereby the clearing step of 20% glycerol and 0.25% KOH was increased to 4 days with daily solution changes. Fixed skeletal preps were imaged on a Leica M165 FC stereomicroscope.

Regeneration assay and fin morphometrics

Adult zebrafish were anaesthetized in 0.6 mM tricaine (MS222, Syndel) in system water and fins amputated with a straight-edge razor blade in between the 1st and 2nd procurrent ray, or approximate corollary when those landmarks were absent in *fras1*$^{-/-}$ mutants. Fish immediately were imaged on a Nikon T*i*-E inverted widefield microscope and returned to fresh system water and care. Fish were re-anesthetized at 3, 7, 14 (data not shown), and 28 dpa. Individual *fras1*$^{-/-}$ mutants were tracked by co-housing with controls in low tank density (n = 4-5 mutants with n = 3 controls per tank). Fin skeletal morphometrics were measured using Fiji ImageJ (NIH). Ray lengths were measured from the first discernable proximal joint to the most distal bony segment.

Immunostaining

Regenerating fins were amputated with a straight razor blade and tissue collected at 3 or 4 dpa, fixed, decalcified, and paraffin embedded as described (Stewart et al., 2014a). 7 μm sections were cut using a Leica RM255 microtome. Sections were dehydrated and deparaffinized, rehydrated, and antigen retrieved in 0.05% citranonic anhydride (ImmunoSaver, Electron Microscopy Science) for 5 min on high using a pre-heated pressure cooker. After 5 min, the pressure cooker was turned off and allowed to slowly depressurize for 30 min before the slides were transferred to 1x PBS. Sections were blocked in 1%BSA/1%DMSO/1%NGS/1%FBS in PBS+0.1% Tween-20 (PBST). An anti-FRAS1 human antibody with 76% immunogen identity with zebrafish Fras1 including part of a highly conserved Calx-beta domain (Bethyl Labs, Cat #A305-622A) and anti-FREM2 human antibody with 77% immunogen identity with zebrafish Frem2a/b (Invitrogen PA5-55986) were used. Both primary antibodies were used 1:250 in block solution and incubated overnight at 4°C in a humidified chamber. The next day, sections were washed 3 x 10 min in a high-salt solution of 500 mM NaCl in PBST, followed by 1x PBS rinse.

Secondary-conjugated AlexaFluor antibodies (Invitrogen) were used at 1:1000 in PBST for 1 hour protected from light. Slides were washed 3x 5 min in PBS, followed by 1:1500 Hoechst stain (stock 10 mg/mL, Invitrogen) for 5 min, slides washed, and mounted in SlowFade Gold (Invitrogen). Slides were imaged on a Nikon T*i*-E inverted microscope with a Yokogawa CSU-W1 spinning disc confocal attachment.

In situ hybridization

mRNA transcripts were visualized using the above described 7 μm paraffin sections of regenerating zebrafish fins. mRNA probes for zebrafish *frem2a* and *frem2b* were obtained and visualized using ViewRNA Tissue Assay technology (Invitrogen, #19942) according to manufacturer's instructions. After probe hybridization and amplification, nuclei were stained with 1:1500 Hoechst stain (Invitrogen), mounted in SlowFade Gold (Invitrogen), and imaged as described above.

Transcriptomic Analysis

Single Cell RNA-seq expression profiling used a previously assembled and validated dataset comprised of regenerating fin tissue collected at 3- and 7-days post amputation (Lewis et al., 2022). The "choose_cells" function was used to reduce the extended dataset to only include epidermal, fibroblast and osteoblast lineages. Uniform Manifold Approximation and Projection (UMAP) plots detailing the cell-type clustering and expression profiles of Frasier complex genes were generated in Monocle3 using the "Plot_cells" function with otherwise default parameters.

Shh/Ptch2 reporter line assessment

For Shh ligand expression, adult fins of *shha:GFP* hets were amputated as described above and imaged with a Nikon T*i*-E inverted widefield microscope with metal halide fluorescence capacity at 4 (not shown), 8, 14 (not shown), and 30 dpa. Developing *shha:GFP* 6 wpf juveniles were imaged with a Nikon T*i*-E inverted widefield microscope using a Yokogawa CSU-W1 spinning disc attachment. *ptch2:Kaede* adults and juveniles had dorsal portions of their caudal fins photoconverted to red emission with images acquired by CSU before photoconversion (all green, not shown), immediately after photoconversion (all red), and 24 hours after conversion (newly produced Kaede is green). Photoconversion used a 20x confocal objective set to 100% 405 λ laser for 1 min (juveniles) or 2 min (regenerating adult). Fish were anesthetized as described for imaging and then returned to standard care.

Hematoxylin and Eosin Histology

7 μm paraffin sections were collected as described above and deparaffinized with xylenes. Slides were stained with Hematoxylin (Ricca Chemical CAT#3530-16) and Eosin (Sigma-Aldrich REF#HT110132) according to the manufacturer's protocol with the durations: filtered hematoxylin 1 minute, eosin 4 minutes. Slides were then dehydrated and mounted using Permount Mounting Media (Electron Microscopy Sciences CAT#17986). Brightfield images were acquired on a Leica DM4000B widefield microscope and confocal Eosin images were taken using a Nikon T*i*-E with a Yokogawa W1-CSU confocal unit.

Statistical Analyses

Fin morphometric data was collected using Fiji ImageJ (NIH) and organized in Microsoft Excel. Fin width was measured from the most proximal distinguishable joint segement. Ray length was

measured starting at the same location. Number of principal rays was quantified prior to ray branching, if present. Statistical analyses were performed and graphs generated using GraphPad Prism v9.

REFERENCES

Armstrong, B.E., Henner, A., Stewart, S., Stankunas, K., 2017. Shh promotes direct interactions between epidermal cells and osteoblast progenitors to shape regenerated zebrafish bone. Development (Cambridge) 144, 1165–1176. https://doi.org/10.1242/dev.143792

Arratia, G., Schultze, H.-P., Wilson, M.V.H., 2008. Actinopterygian postcranial skeleton with special reference to the diversity of fin ray elements, and the problem of identifying homologies, in: Mesozoic Fishes 4 – Homology and Phylogeny. pp. 49–101.

Bensimon-Brito, A., Cardeira, J., Dionísio, G., Huysseune, A., Cancela, M.L., Witten, P.E., 2016. Revisiting in vivo staining with alizarin red S - A valuable approach to analyse zebrafish skeletal mineralization during development and regeneration. BMC Dev Biol 16. https://doi.org/10.1186/s12861-016-0102-4

Boisvert, C.A., Mark-Kurik, E., Ahlberg, P.E., 2008. The pectoral fin of Panderichthys and the origin of digits. Nature 456, 636–638. https://doi.org/10.1038/nature07339

Braunstein, J.A., Robbins, A.E., Stewart, S., Stankunas, K., 2021. Basal epidermis collective migration and local Sonic hedgehog signaling promote skeletal branching morphogenesis in zebrafish fins. Dev Biol 477, 177–190. https://doi.org/10.1016/j.ydbio.2021.04.010

Butt, J.B.Y., Qureshi, T.M., Khan, M.T., Ahmad, A.-H., 2014. Cryptophthalmos Syndrome: A Case Report. Pakistan Journal of Ophthalmology 30, 172–174.

Cardeira-da-Silva, J., Bensimon-Brito, A., Tarasco, M., Brandão, A.S., Rosa, J.T., Borbinha, J., Almeida, P.J., Jacinto, A., Cancela, M.L., Gavaia, P.J., Stainier, D.Y.R., Laizé, V., 2022. Fin ray branching is defined by TRAP + osteolytic tubules in zebrafish. Proceedings of the National Academy of Sciences 119. https://doi.org/10.1073/pnas.2209231119

Carney, T.J., Feitosa, N.M., Sonntag, C., Slanchev, K., Kluger, J., 2010. Genetic Analysis of Fin Development in Zebrafish Identifies Furin and Hemicentin1 as Potential Novel Fraser Syndrome Disease Genes. PLoS Genet 6, 1000907. https://doi.org/10.1371/journal.pgen.1000907

Chen, C.H., Merriman, A.F., Savage, J., Willer, J., Wahlig, T., Katsanis, N., Yin, V.P., Poss, K.D., 2015. Transient laminin beta 1a Induction Defines the Wound Epidermis during Zebrafish Fin Regeneration. PLoS Genet 11, 1–21. https://doi.org/10.1371/journal.pgen.1005437

Coates, M.I., 1994. The origin of vertebrate limbs. Development 120, 169–180. https://doi.org/10.1242/dev.1994.supplement.169

Dalezios, Y., Papasozomenos, B., Petrou, P., Chalepakis, G., 2007. Ultrastructural localization of Fras1 in the sublamina densa of embryonic epithelial basement membranes. Arch Dermatol Res 299, 337–343. https://doi.org/10.1007/s00403-007-0763-8

Desvignes, T., Carey, A., Postlethwait, J.H., 2018. Evolution of caudal fin ray development and caudal fin hypural diastema complex in spotted gar, teleosts, and other neopterygian fishes. Developmental Dynamics 247, 832–853. https://doi.org/10.1002/dvdy.24630

Desvignes, T., Robbins, A.E., Carey, A.Z., Bailon-Zambrano, R., Nichols, J.T., Postlethwait, J.H., Stankunas, K., 2022. Coordinated patterning of zebrafish caudal fin symmetry by a central and two peripheral organizers. Developmental Dynamics 1306–1321. https://doi.org/10.1002/dvdy.475

Divya, K., Shreedhara, A.K., Amitha, S., 2014. Fraser Syndrome. Muller Journal of Medical Sciences and Research 5, 85.

Ertzer, R., Müller, F., Hadzhiev, Y., Rathnam, S., Fischer, N., Rastegar, S., Strähle, U., 2007. Cooperation of sonic hedgehog enhancers in midline expression. Dev Biol 301, 578–589. https://doi.org/10.1016/j.ydbio.2006.11.004

Freitas, R., Gómez-Marín, C., Wilson, J.M., Casares, F., Gómez-Skarmeta, J.L., 2012. Hoxd13 Contribution to the Evolution of Vertebrate Appendages. Dev Cell 23, 1219–1229. https://doi.org/10.1016/j.devcel.2012.10.015

Gautier, P., Naranjo-Golborne, C., Taylor, M.S., Jackson, I.J., Smyth, I., 2008. Expression of the fras1/frem gene family during zebrafish development and fin morphogenesis. Developmental Dynamics 237, 3295–3304. https://doi.org/10.1002/dvdy.21729

Hines, E.A., Verheyden, J.M., Lashua, A.J., Larson, S.C., Branchfield, K., Domyan, E.T., Gao, J., Harvey, J.F., Herriges, J.C., Hu, L., Mcculley, D.J., Throckmorton, K., Yokoyama, S., Ikeda, A., Xu, G., Sun, X., 2016. Syndactyly in a novel Fras1rdf mutant results from interruption of signals for interdigital apoptosis. Developmental Dynamics 245, 497–507. https://doi.org/10.1002/dvdy.24389

Huang, P., Xiong, F., Megason, S.G., Schier, A.F., 2012. Attenuation of Notch and hedgehog signaling is required for fate specification in the spinal cord. PLoS Genet 8. https://doi.org/10.1371/journal.pgen.1002762

Impallomeni, M., Subramanian, D., Mahmood, N., Joseph, I., 2006. Fraser syndrome in a 96-year-old female. Age Ageing 35, 642–643. https://doi.org/10.1093/AGEING/AFL109

Jadeja, S., Smyth, I., Pitera, J.E., Taylor, M.S., Van Haelst, M., Bentley, E., McGregor, L., Hopkins, J., Chalepakis, G., Philip, N., Aytes, A.P., Watt, F.M., Darling, S.M., Jackson, I., Woolf, A.S., Scambler, P.J., 2005. Identification of a new gene mutated in Fraser syndrome and mouse myelencephalic blebs. Nat Genet 37, 520–525. https://doi.org/10.1038/ng1549

Kashgari, G., Meinecke, L., Gordon, W., Ruiz, B., Yang, J., Ma, A.L., Xie, Y., Ho, H., Plikus, M. V., Nie, Q., Jester, J. V., Andersen, B., 2020. Epithelial Migration and Non-adhesive Periderm Are Required for Digit Separation during Mammalian Development. Dev Cell 52, 764-778.e4. https://doi.org/10.1016/j.devcel.2020.01.032

Kimmel, C.B., Wind, A.L., Oliva, W., Ahlquist, S.D., Walker, C., Dowd, J., Blanco-Sánchez, B., Titus, T.A., Batzel, P., Talbot, J.C., Postlethwait, J.H., Nichols, J.T., 2021. Transgene-mediated skeletal phenotypic variation in zebrafish. J Fish Biol 98, 956–970. https://doi.org/10.1111/jfb.14300

Kiyozumi, D., Sugimoto, N., Sekiguchi, K., 2006. Breakdown of the reciprocal stabilization of QBRICK/Frem1, Fras1, and Frem2 at the basement membrane provokes Fraser syndrome-like defects. Proc Natl Acad Sci U S A 103, 11981–11986. https://doi.org/10.1073/pnas.0601011103

Letelier, J., de La Calle-Mustienes, E., Pieretti, J., Naranjo, S., Maeso, I., Nakamura, T., Pascual-Anaya, J., Shubin, N.H., Schneider, I., Martinez-Morales, J.R., Gómez-Skarmeta, J.L., 2018. A conserved Shh cis-regulatory module highlights a common developmental origin of unpaired and paired fins. Nat Genet. https://doi.org/10.1038/s41588-018-0080-5

Lewis VM, Le Bleu HK, Henner AL, Markovic H, Robbins AE, Stewart S, Stankunas K. Insulin-like growth factor receptor / mTOR signaling elevates global translation to accelerate zebrafish fin regenerative outgrowth. Dev Biol. 2023 Jun 6:S0012-1606(23)00092-1. doi: 10.1016/j.ydbio.2023.05.008.

Mahadevan, B., Bhat, B.V., Sastri, A.T., Rao, S., Kusre, G., 2002. Fraser Syndrome With Unusual Features-A Case Report. J Anat Soc India 51, 59–60.

Martínez-Frías, M.L., Bermejo, E., Sánchez Otero, T., Urioste, M., Morena, E., Cruz, E., 1994. Sclerocornea, hypertelorism, syndactyly, and ambiguous genitalia. Am J Med Genet 49, 195–197. https://doi.org/https://doi.org/10.1002/ajmg.1320490206

McGregor, L., Makela, V., Darling, S.M., Vrontou, S., Chalepakis, G., Roberts, C., Smart, N., Rutland, P., Prescott, N., Hopkins, J., Bentley, E., Shaw, A., Roberts, E., Mueller, R., Jadeja, S., Philip, N., Nelson, J., Francannet, C., Perez-Aytes, A., Megarbane, A., Kerr, B., Wainwright, B., Woolf, A.S., Winter, R.M., Scambler, P.J., 2003. Fraser syndrome and mouse blebbed phenotype caused by mutations in FRAS1/Fras1 encoding a putative extracellular matrix protein. Nat Genet 34, 203–208. https://doi.org/10.1038/ng1142

Miller, K.A., Gordon, C.T., Welfare, M.F., Caruana, G., Bertram, J.F., Bateman, J.F., Farlie, P.G., 2013. bfb, a Novel ENU-Induced blebs Mutant Resulting from a Missense Mutation in Fras1. PLoS One 8. https://doi.org/10.1371/journal.pone.0076342

Nakamura, T., Gehrke, A.R., Lemberg, J., Szymaszek, J., Shubin, N.H., 2016. Digits and fin rays share common developmental histories. Nature 537, 225–228. https://doi.org/10.1038/nature19322

Nauroy, P., Guiraud, A., Chlasta, J., Malbouyres, M., Gillet, B., Hughes, S., Lambert, E., Ruggiero, F., 2019. Gene profile of zebrafish fin regeneration offers clues to kinetics, organization and biomechanics of basement membrane. Matrix Biology 75–76, 82–101. https://doi.org/10.1016/j.matbio.2018.07.005

Pasu, S., Dhir, L., Mackenzie, S., Thompson, G., 2011. Fraser Syndrome: Case Report with Review of Literature. Open J Ophthalmol 01, 1–3. https://doi.org/10.4236/ojoph.2011.11001

Petrou, P., Pavlakis, E., Dalezios, Y., Chalepakis, G., 2007. Basement membrane localization of Frem3 is independent of the Fras1/Frem1/Frem2 protein complex within the sublamina densa. Matrix Biology 26, 652–658. https://doi.org/10.1016/J.MATBIO.2007.05.008

Quint, E., Smith, A., Avaron, F., Laforest, L., Miles, J., Gaffield, W., Akimenko, M.-A., 2002. Bone patterning is altered in the regenerating zebrafish caudal fin after ectopic expression of sonic hedgehog and bmp2b or exposure to cyclopamine. Proceedings of the National Academy of Sciences 99, 8713–8718. https://doi.org/10.1073/pnas.122571799

Sehring, I.M., Weidinger, G., 2020. Recent advancements in understanding fin regeneration in zebrafish. Wiley Interdiscip Rev Dev Biol 9, 1–16. https://doi.org/10.1002/wdev.367

Shubin, N., Tabin, C., Carroll, S., 2009. Deep homology and the origins of evolutionary novelty. Nature 457, 818–823. https://doi.org/10.1038/nature07891

Shubin, N.H., Daeschler, E.B., Jenkins, F.A., 2006. The pectoral fin of Tiktaalik roseae and the origin of the tetrapod limb. Nature 440, 764–771. https://doi.org/10.1038/nature04637

Slavotinek, A.M., Tifft, C.J., 2002. Fraser syndrome and cryptophthalmos: Review of the diagnostic criteria and evidence for phenotypic modules in complex malformation syndromes. J Med Genet 39, 623–633. https://doi.org/10.1136/JMG.39.9.623

Smyth, I., Du, X., Taylor, M.S., Justice, M.J., Beutler, B., Jackson, I.J., 2004. The extracellular matrix gene Frem1 is essential for the normal adhesion of the embryonic epidermis. Proc Natl Acad Sci U S A 101, 13560–13565. https://doi.org/10.1073/pnas.0402760101

Smyth, I., Scambler, P., 2005. The genetics of Fraser syndrome and the blebs mouse mutants. Hum Mol Genet 14, R269–R274. https://doi.org/10.1093/hmg/ddi262

Sordlno, P., Hoeven, F. van der, Duboule, D., 1995. Hox gene expression in origin of vertebrate digits. Nature 375, 678–681.

Stewart, S., Gomez, A.W., Armstrong, B.E., Henner, A., Stankunas, K., 2014. Sequential and Opposing Activities of Wnt and BMP Coordinate Zebrafish Bone Regeneration. Cell Rep 6, 482–498. https://doi.org/10.1016/j.celrep.2014.01.010

Takamiya, K., Kostourou, V., Adams, S., Jadeja, S., Chalepakis, G., Scambler, P.J., Huganir, R.L., Adams, R.H., 2004. A direct functional link between the multi-PDZ domain protein GRIP1 and the Fraser syndrome protein Fras1. Nat Genet 36, 172–177. https://doi.org/10.1038/ng1292

Talbot, J.C., Nichols, J.T., Yan, Y.L., Leonard, I.F., BreMiller, R.A., Amacher, S.L., Postlethwait, J.H., Kimmel, C.B., 2016. Pharyngeal morphogenesis requires fras1-itga8-dependent epithelial-mesenchymal interaction. Dev Biol 416, 136–148. https://doi.org/10.1016/j.ydbio.2016.05.035

Talbot, J.C., Walker, M.B., Carney, T.J., Huycke, T.R., Yan, Y.L., BreMiller, R.A., Gai, L., Delaurier, A., Postlethwait, J.H., Hammerschmidt, M., Kimmel, C.B., 2012. Fras1 Shapes Endodermal Pouch 1 and Stabilizes Zebrafish Pharyngeal Skeletal Development. Development 139, 2804–2813. https://doi.org/10.1242/dev.074906

Thomas, I.T., Frias, J.L., Felix, V., Sanchez de Leon, L., Hernandez, R.A., Jones, M.C., 1986. Isolated and syndromic cryptophthalmos. Am J Med Genet 25, 85–98. https://doi.org/10.1002/ajmg.1320250111

van Haelst, M.M., Maiburg, M., Baujat, G., Jadeja, S., Monti, E., Bland, E., Pearce, K., Hennekam, R.C., Scambler, P.J., Al-Gazali, L., Aytes, P., Bonato, A., Chitayat, D., Dobbie, A., Donnai, D., Elmslie, F., Ferreira, J., Francannet, C., Gilbert, B., Graham, J., Hennekam, R., Holder, S., Kerr, B., Maas, S., Megarbane, A., Meinecke, P., Melancon, S., Midro, A., Nelson, J., Philip, N., Reardon, W., Reutter, H., Santos, H., Scambler, P., Thauvin, C., Todos, E., Tolmie, J., Van Essen, T., Van Haelst, M., Wilkie, A., Wilson, L., 2008. Molecular study of 33 families with Fraser syndrome new data and mutation review. Am J Med Genet A 146, 2252–2257. https://doi.org/10.1002/ajmg.a.32440

Vrontou, S., Petrou, P., Meyer, B.I., Galanopoulos, V.K., Imai, K., Yanagi, M., Chowdhury, K., Scambler, P.J., Chalepakis, G., 2003. Fras1 deficiency results in cryptophthalmos, renal agenesis and blebbed phenotype in mice. Nat Genet 34, 209–214. https://doi.org/10.1038/ng1168

Walker, M.B., Kimmel, C.B., 2007. A two-color acid-free cartilage and bone stain for zebrafish larvae. Biotechnic and Histochemistry 82, 23–28. https://doi.org/10.1080/10520290701333558

Woltering, J.M., Noordermeer, D., Leleu, M., Duboule, D., 2014. Conservation and Divergence of Regulatory Strategies at Hox Loci and the Origin of Tetrapod Digits. PLoS Biol 12. https://doi.org/10.1371/journal.pbio.1001773

Zhang, J., Jeradi, S., Strähle, U., Akimenko, M.A., 2012. Laser ablation of the sonic hedgehog-a-expressing cells during fin regeneration affects ray branching morphogenesis. Dev Biol 365, 424–433. https://doi.org/10.1016/j.ydbio.2012.03.008

FIGURES

Figures 4.1 – 4.8
Figures S4.1 – S4.3

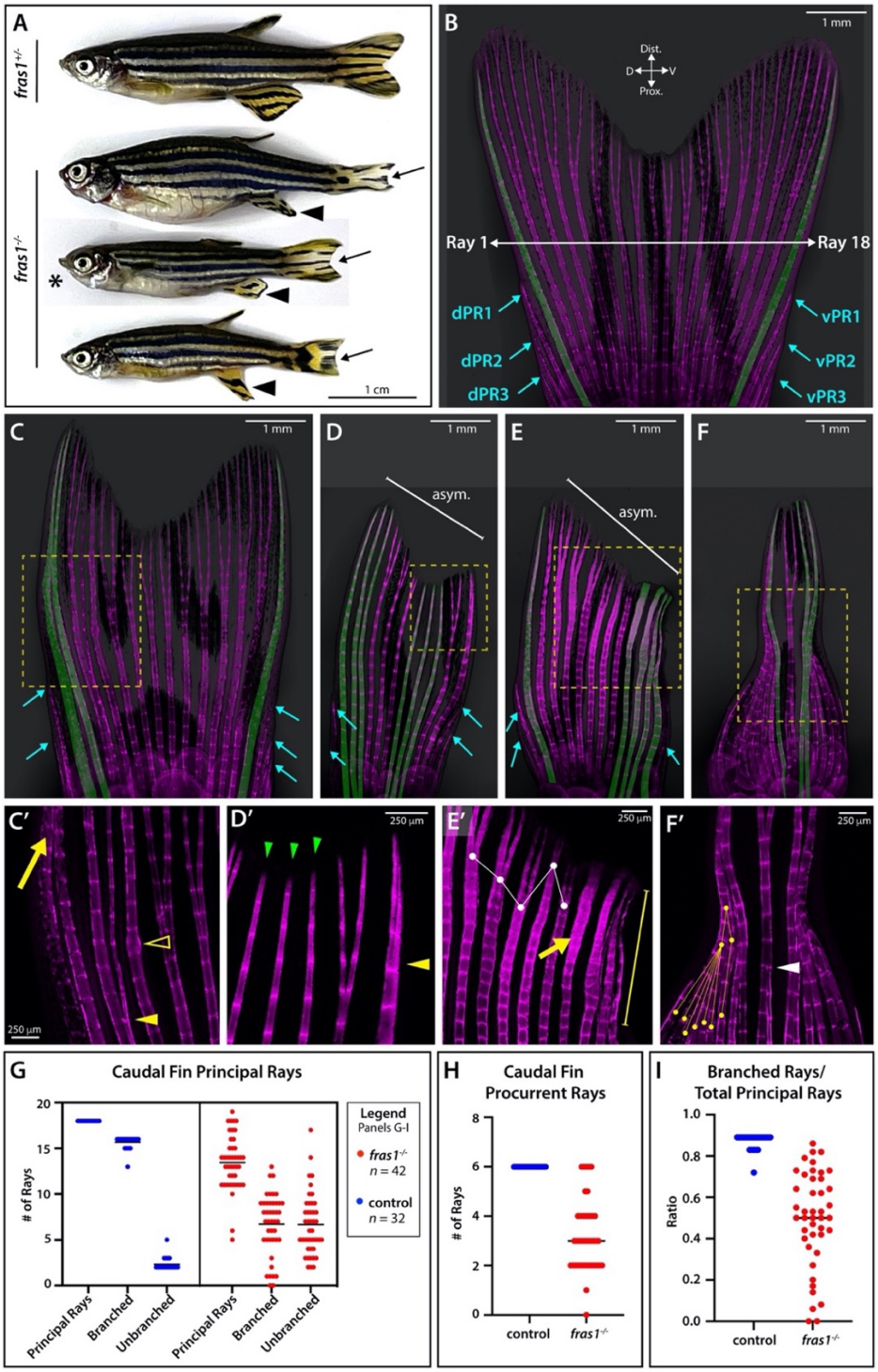

Figure 4.1. Fras1 promotes robust patterning of the caudal fin skeleton including bony ray number and branching.

Figure 4.1. Fras1 promotes robust patterning of the caudal fin skeleton including the number of bony rays and ray branching.

(A) Whole-mount imaged adult zebrafish representing three homozygous *fras1*$^{-/-}$ mutants and a heterozygous sibling. *fras1*$^{-/-}$ fish are variably runted with gross abnormalities including caudal fin pigment pattern defects (black arrows), misshapen anal fins (black arrowheads), and lower jaw protrusions (black asterisk). (B-F) Representative Alizarin Red-stained caudal fins of (B) control and (C-F) *fras1*$^{-/-}$ adult siblings. Unbranched rays are shaded green as a visual aid. Dorsal and ventral procurrent rays (dPR and vPR) are labeled with cyan arrows. Asymmetrical fins (D, E) are indicated by white "asym." brackets. (C'-F') Various skeletal patterning abnormalities highlighted by zoomed in regions shown by yellow dashed boxes in (C-F) and noted below. (C') Fused peripheral rays (yellow arrow), ectopic branching (yellow arrowhead), and fracture scar (yellow open arrowhead). (D') Three unbranched rays (green arrowheads) followed by a branched ray followed by ectopic partially branched peripheral ray (yellow arrowhead). (E') Uneven branch points (white connected dots), poorly articulated joints (yellow arrow), wavy misaligned rays (yellow bracket). (F') Numerous rays fusing (yellow connected dots) and reverse branching (white arrowhead). (G) Caudal fin principal ray quantification. (H) Caudal fin procurrent ray quantification. (I) Caudal fin ray branching expressed as a ratio of total principal rays.

Figure 4. 1 Panel	# Principal Rays	# Procurrent Rays	Branched/Total Principal Rays
B (het)	18	6	16/18 (88.89%)
C (*fras1*$^{-/-}$)	14	5	11/14 (78.57%)
D (*fras1*$^{-/-}$)	11	4	6/11 (54.54%)
E (*fras1*$^{-/-}$)	12	3	5/12 (41.67%)
F (*fras1*$^{-/-}$)	4	N/A	1/4 (25.00%)

Table 4.1. Fin morphometrics associated with Figure 4.1.

Quantification of principal rays, procurrent rays, and ratio of branched over total principal rays for adult caudal fins from the indicated Figure 4.1 panels.

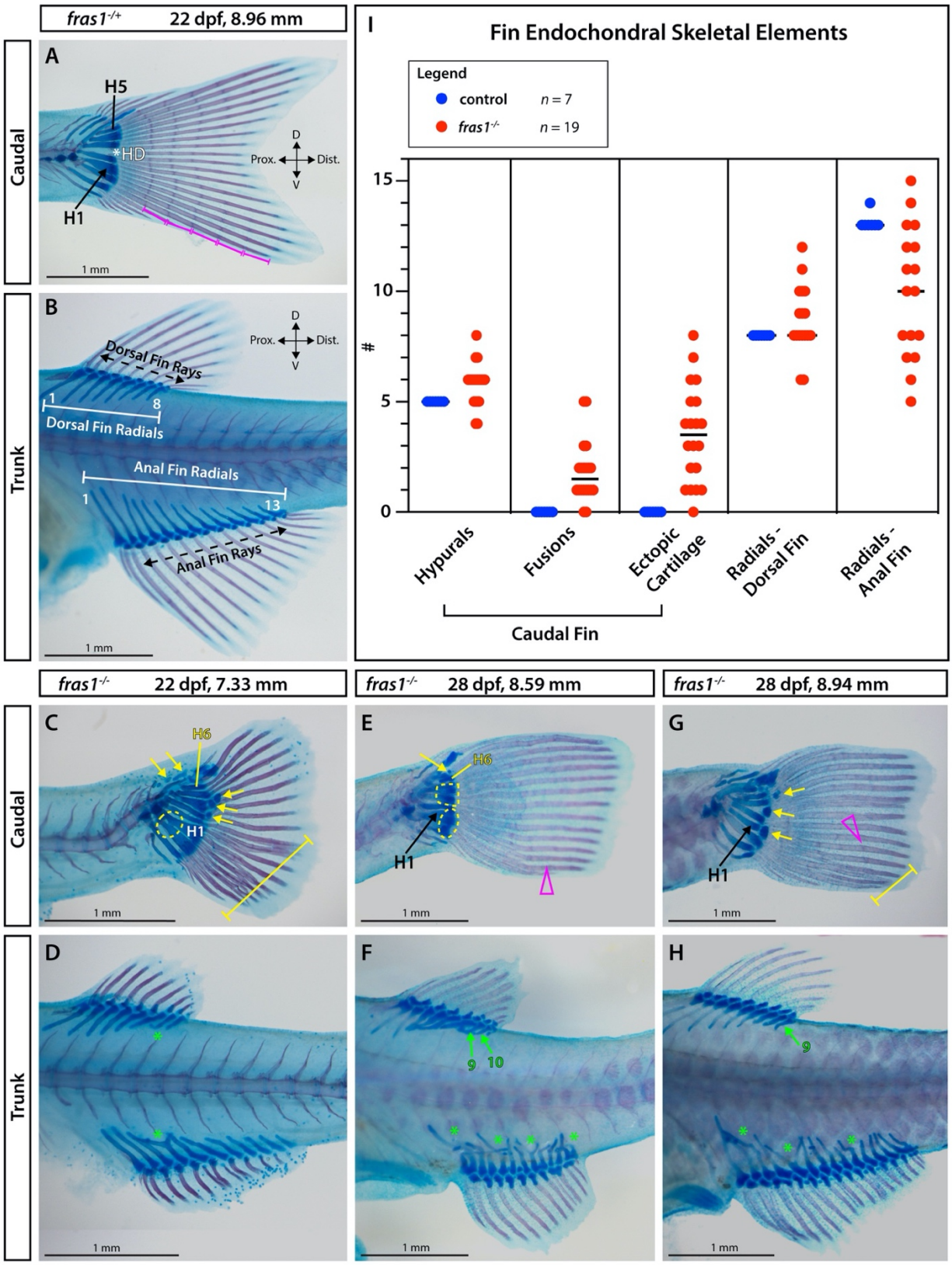

Figure 4.2. Fras1 contributes to both dermal and endochondral appendicular skeletal patterning.

Figure 4.2. Fras1 contributes to both dermal and endochondral appendicular skeletal patterning.

(A-H) Representative whole mount imaging of Alcian Blue (cartilage) and Alizarin Red (calcified bone) stained zebrafish of indicated *fras1* genotypes and ages. (A) Late larval *fras1*$^{+/-}$ control caudal fin. H1, hypural 1 and H5, hypural 5. Magenta brackets denote joint segmentation. (B) Trunk region of the same control larvae. Dorsal and anal fin radials are marked by white brackets and rays are marked by black dashed arrows. (C-H) Images of sibling *fras1*$^{-/-}$ late larvae age-matched (C, D) or size-matched (E-H) to control for frequent developmental delays, with highlighted defects described below. (C, E, G) Caudal fin endoskeletons (blue) are disorganized, often with a sixth hypural (H6, yellow), fused elements (yellow dashed lines), and ectopic cartilaginous structures (yellow arrows). (E) Caudal fin dermal rays (magenta) are variably misaligned (C, G yellow brackets) and (E, G) have delayed joint development (magenta open arrowheads) even when size-matched to (A) younger controls. (D, F, H) Dorsal and anal fin endoskeletons (blue) have variably mispatterned radials (green asterisks), with dorsal fins often having extra radials (green arrows). Scale bars are 1 mm. (I) Quantification of fin skeletal elements in *fras1*$^{-/-}$ mutants and control siblings.

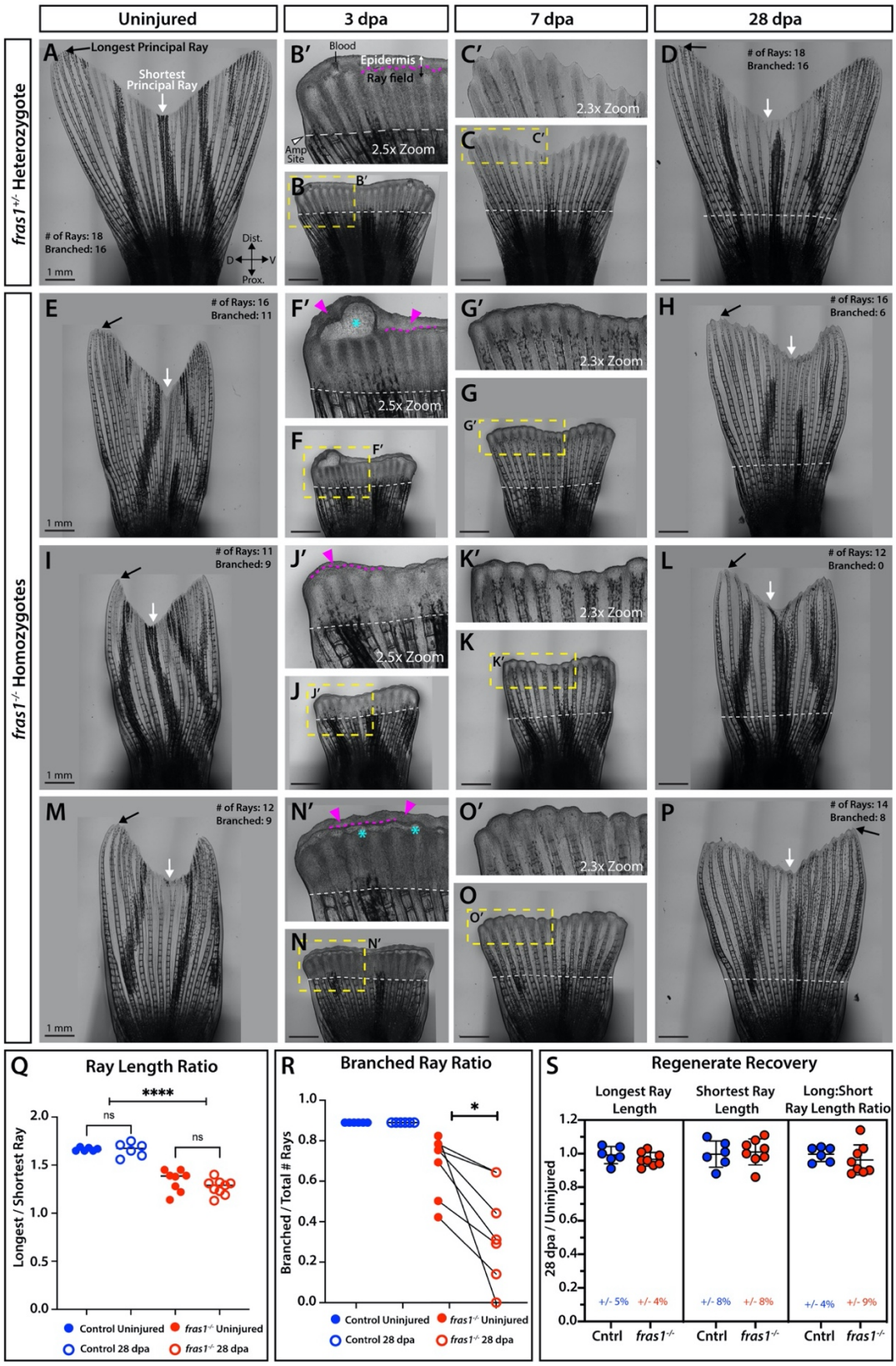

Figure 4.3. Fras1 robustly restores skeletal pattern including ray branching during adult caudal fin regeneration.

Figure 4.3. Fras1 robustly restores skeletal pattern including ray branching during adult caudal fin regeneration.

(A-D) Images of representative *fras1*$^{+/-}$ heterozygote control adult caudal fins before injury (A, uninjured) and at 3 (B), 7 (C), and 28 (D) days post amputation (dpa). (B', C') Zoom insets of the yellow boxed regions in B and C. (B') Black arrows (A) indicate the longest principal ray and white arrows indicate the shortest. Magenta dashed line denotes the approximate boundary between the outgrowing ray field and distal epidermis. White dashed lines indicate the plane of amputation. (E-P) Three representative *fras1*$^{-/-}$ homozygote siblings at the same regenerative time points as (A-D) highlighting defects noted below. At 3 dpa, mutants exhibit blistering (cyan asterisk, F', N') and extended epidermal tissue distal to the ray field (magenta arrowheads, F', J', N'). (G, G', K, K', O, O') Blistering subsides by 7 dpa. (H-P) Fully regenerated mutant fins have (H) fewer branched rays, (L) no branched rays, or more equal ray length ratios (i.e., less pronounced V-shape) (C) compared to their uninjured states. Scale bar lengths are indicated. (Q) Quantification of longest/shortest principal rays before injury (solid circles) or 28 dpa (unfilled circles) time points. (R) Quantification of the # of branched/ total # of principal rays. Connecting lines indicate the same fish assessed before injury and at 28 dpa. (S) Quantification of regenerative outgrowth for the longest and shortest principal rays and their respective ratios.

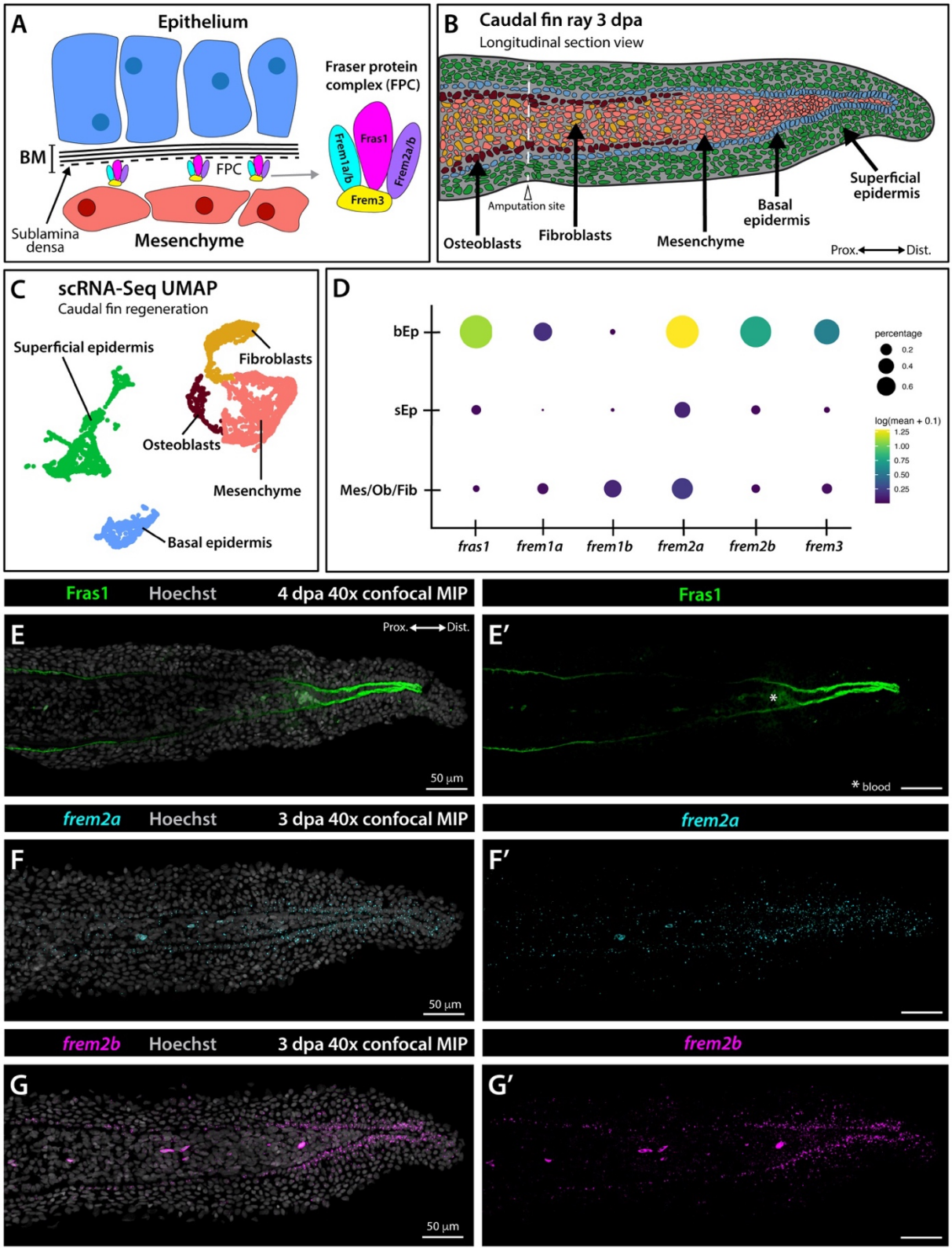

Figure 4.4. Fraser Complex transcripts and Fras1 protein are basal epidermal-expressed and distally-enriched in regenerating fins.

Figure 4.4. Fraser Complex transcripts and Fras1 protein are basal epidermal-expressed and distally-enriched in regenerating fins.

(A) Schematic of epithelial (blue cells) and mesenchymal (pink cells) tissue layers separated by basement membrane (BM, black lines). The Fraser Complex (FPC, multicolored) localizes to the innermost BM layer (sublamina densa, dashed black line) and comprises Fras1 (magenta), Frem1a/b (cyan), Frem2a/b (purple), and Frem3 (yellow). (B) Longitudinal section schematic of tissue organization in a 3 day post amputation (dpa) regenerating caudal fin. (C) Single cell RNA-Seq clustering of regenerating 3 and 7 dpa zebrafish fin tissue shows unique clusters for basal epidermis (blue), superficial epidermis (green), and mixed mesenchyme/osteoblast/fibroblast lineages (dark red, pink, yellow) in UMAP space. (D) Bubble plot of FPC transcript expression in the basal epidermis, superficial epidermis (sEp), and mixed mesenchyme/osteoblast/fibroblast (Mes/Ob/Fib) clusters. (E-G) 40x confocal maximum intensity projections of regenerating fin longitudinal sections stained as follows: (E) Fras1 immunostaining (green) at 4 dpa, (F) ViewRNA fluorescent *in situ* hybridization for *frem2a* (cyan) at 3 dpa, and (G) ViewRNA fluorescent *in situ* hybridization for *frem2b* (magenta) at 3 dpa. Hoechst-stained nuclei are grey. (E'-G') Single channel fluorescence images of (E-G). Scale bars are 50 mm.

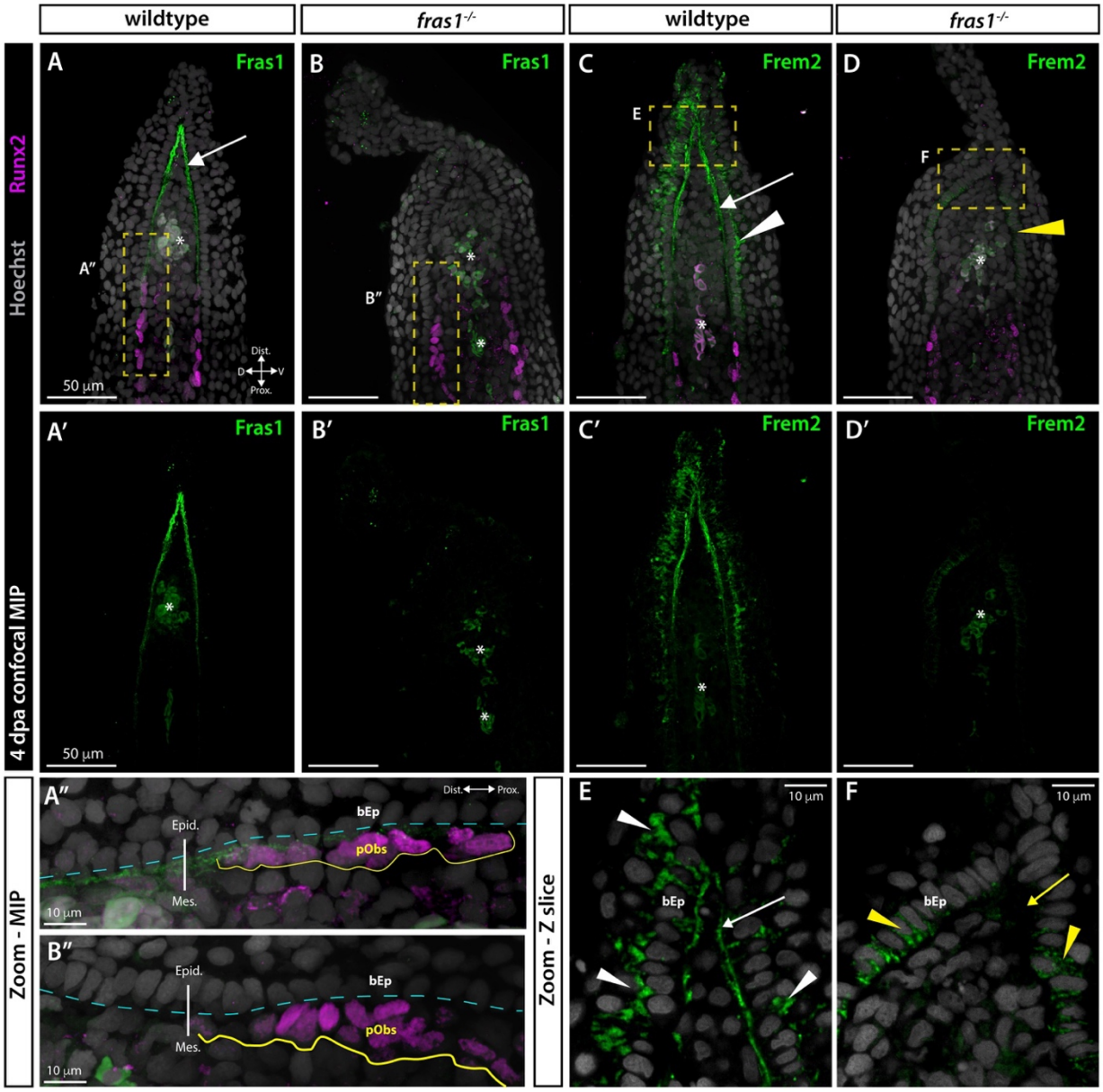

Figure 4.5. Fras1 promotes Fraser Complex subunit processing and pre-osteoblast organization during fin regeneration.

Figure 4.5. Fras1 promotes Fraser Complex assembly and pre-osteoblast organization during fin regeneration.

(A-D) Confocal images of immunofluorescent stained paraffin sections of 4-day post amputation (4 dpa) regenerating caudal fins. Hoechst (gray) stains nuclei and anti-Runx2 antibody staining (magenta) marks pre-osteoblasts. Asterisks indicate blood autofluorescence. (A-D) Maximum intensity projection 3-channel overlays. (A'-D') Single channel showing Fras1 or Frem2 immunostaining (green). (A", B") Maximum intensity projection zoomed views of the yellow boxed regions in (A-B). (E, F) Single optical slice zooms of the yellow boxed regions in (C-D). (A, A') Fras1 (green) in wildtype fins is strongly expressed in the distal basement membrane with diminishing expression extending proximally. (A") Fras1 is expressed between Runx2+ pre-osteoblasts (yellow outline) and epidermal cells. Epid, epidermis; Mes., mesenchyme. The cyan dashed line indicates the approximate basement membrane position. (B-B") Fras1 (green) is lost and pre-osteoblasts are disorganized in *fras1*$^{-/-}$ mutants. (C, C', C") Frem2 (green) is expressed in the distal basement membrane (white arrow) and in the extracellular space around basal epidermal cells (bEp, white arrowheads, C"). (D-D") Frem2 expression (green) in *fras1*$^{-/-}$ mutants is absent from distal basement membrane (yellow arrow) and the remaining protein appears intracellular within basal epidermal cells (yellow arrowheads). Scale bar lengths are indicated.

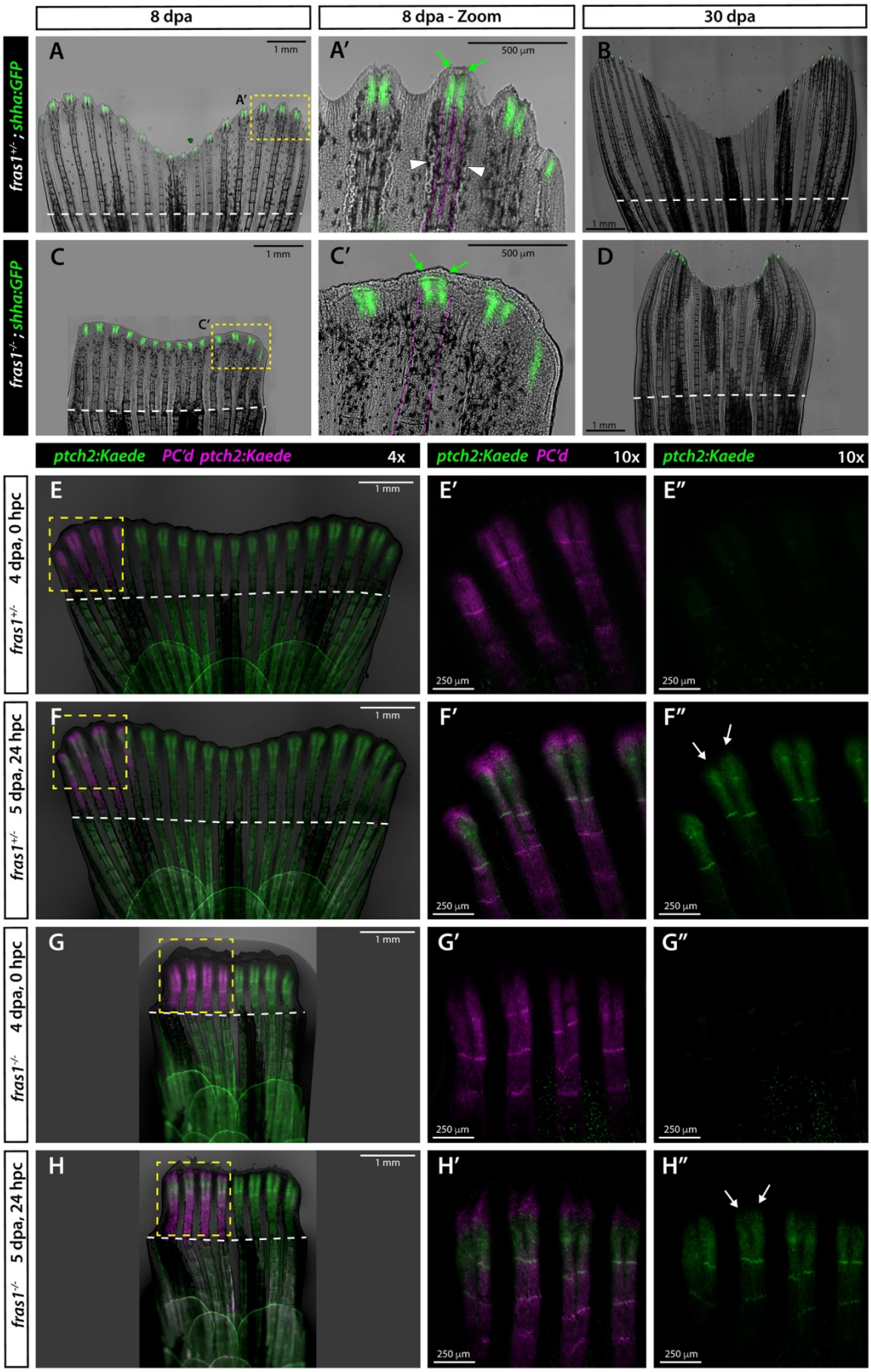

Figure 4.6. The Fraser Complex is not essential for Sonic hedgehog/Smoothened signal transduction during fin regeneration.

Figure 4.6. The Fraser Complex is not essential for Sonic hedgehog/Smoothened signal transduction during fin regeneration.

(A-D) Whole mount images of regenerating caudal fins of (A-B) *fras1*$^{+/-}$ control sibling and (C-D) *fras1*$^{-/-}$ mutant zebrafish carrying the *shha:GFP* reporter. (A) At 8 dpa, *shha:GFP* is expressed in basal epidermal cells overlying the distal outgrowth zone of each ray. (A') Zoom of ventral ray regions showing GFP domain splitting (green arrows) associated with a branched ray (magenta dashed outline). (C, C') A *fras1*$^{-/-}$ mutant at 8 dpa with split distal GFP domains (C', green arrows) even while the underlying rays fail to branch (magenta dashed outline). (B, D) Regeneration is complete at 30 dpa, with only residual distal GFP. The *fras1*$^{-/-}$ mutant (D) fails to regenerate branched rays. White dashed lines indicate the amputation site. (E-H) Whole mount images of regenerating caudal fins from *ptch2:Kaede* sibling zebrafish of indicated *fras1* genotype. (E, G) 4 dpa fins imaged immediately after *ptch2:Kaede* is photoconverted from green to red (shown in magenta) fluorescence in the marked field (yellow dashed boxes, 0 hours-post-conversion hpc). (F, H) The same fins imaged 24 hours later (at 5 dpa, 24 hpc) showing newly produced green Kaede domains in both genotypes (F", H" white arrows). (E'-H') Double fluorescent and (E"-H") single fluorescence channels. Scale bar lengths are indicated.

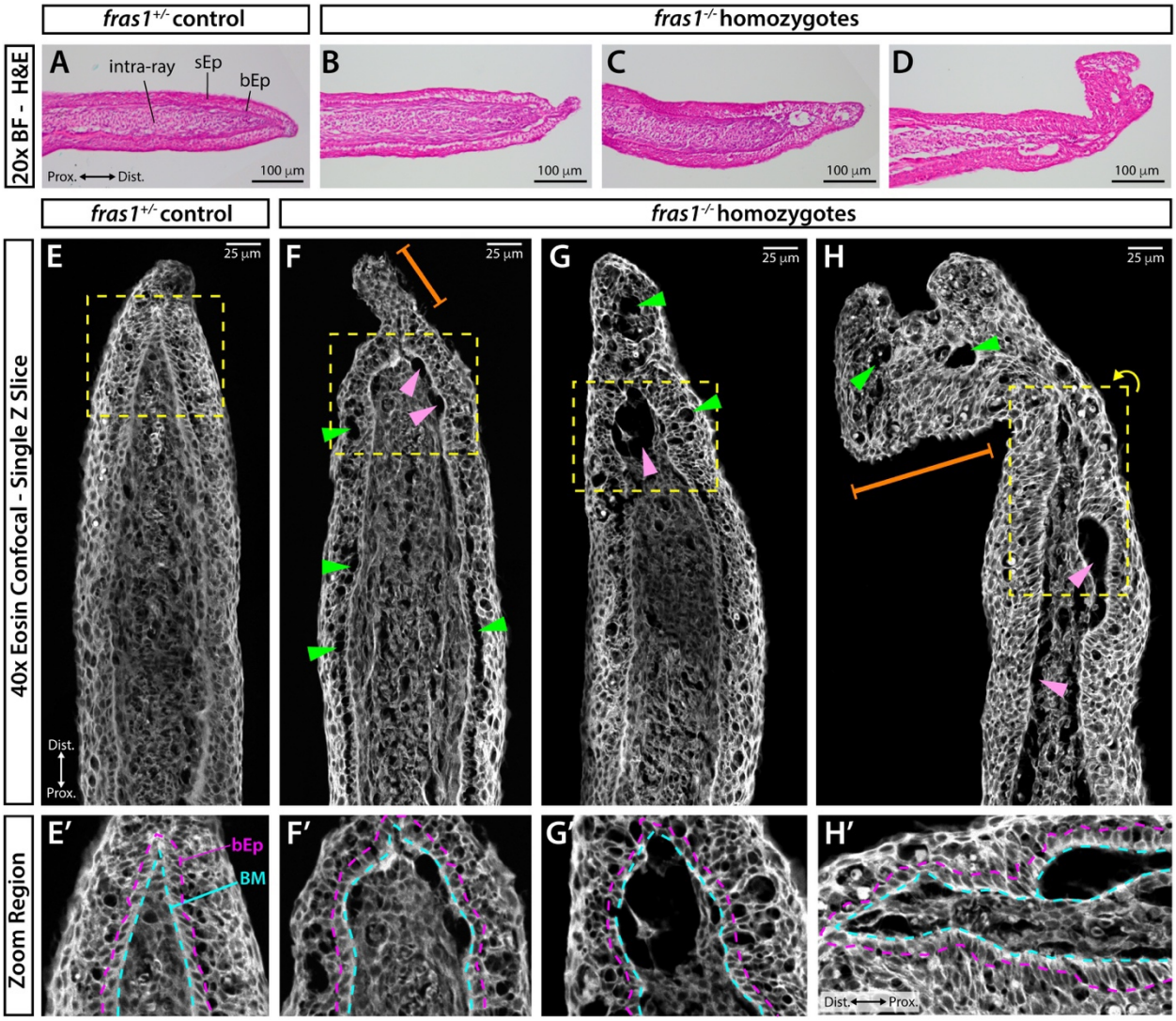

Figure 4.7. The Fraser complex maintains distal epithelial-mesenchymal tissue layering during fin regeneration.

Figure 4.7. The Fraser complex maintains distal epithelial-mesenchymal tissue layering during fin regeneration.

(A-H') Hematoxylin and eosin-stained longitudinal sections of 4 day post amputation (4 dpa) regenerating caudal fins from *fras1*$^{+/-}$ control and *fras1*$^{-/-}$ adult zebrafish. (A-D) Brightfield images with hematoxylin-marked nuclei (purple) and eosin-marked cytoplasm and ECM (pink). Representative *fras*$^{+/-}$ control (A) and *fras1*$^{-/-}$ mutants (B-D) are shown. sEp, superficial epidermis; bEp, basal epidermis; Mes., mesenchyme. (E-H) Confocal optical slices of fluorescent eosin from the samples in (A-D). Green arrowheads indicate epidermal blistering. Pink arrowheads indicate mesenchymal blistering. Orange brackets indicate excess epidermal tissue. (E'-H') Zoom regions of yellow dashed boxes in (E-H) with approximate boundaries of the distal-most forming basement membrane (BM, cyan dashed line) and basal epidermis (bEp, magenta dashed line).

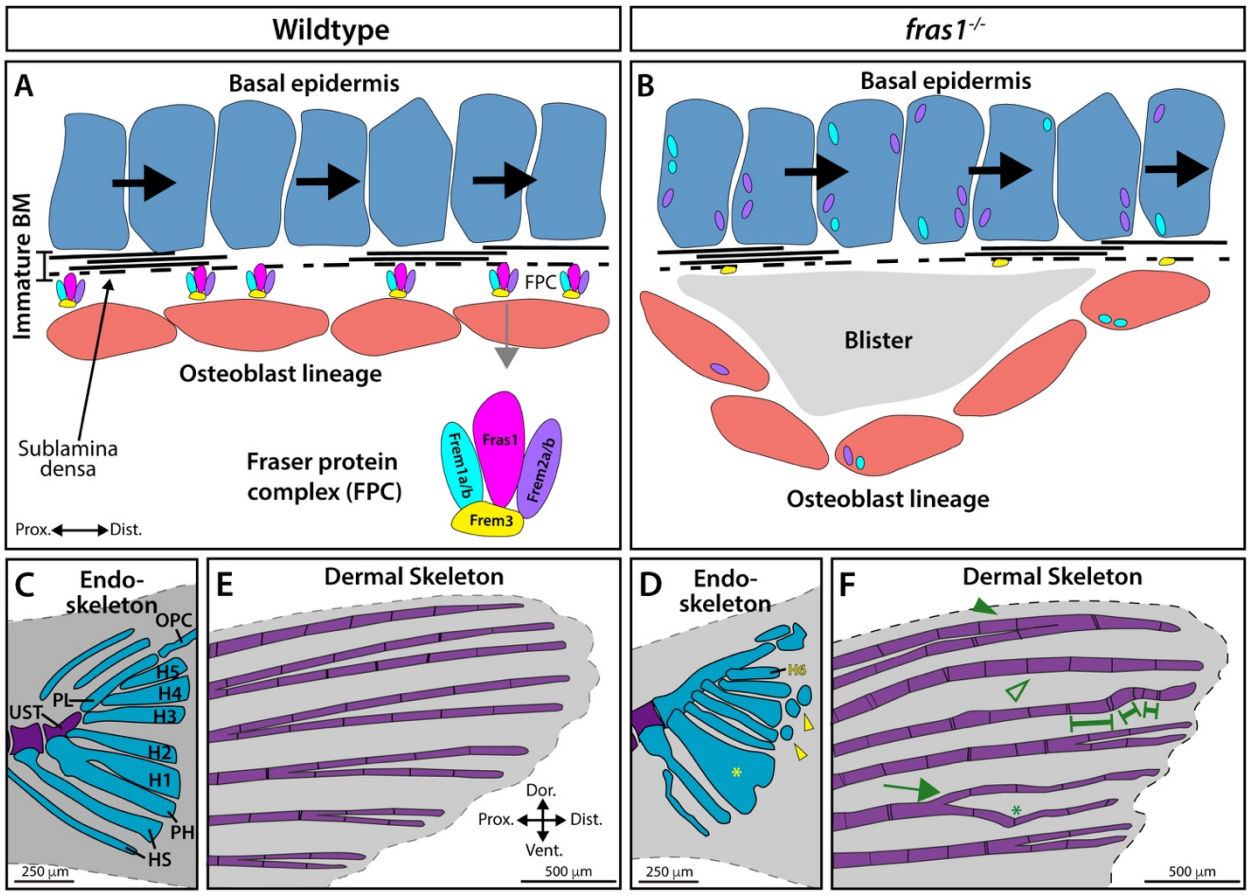

Figure 4.8. The Fraser Complex promotes growth zone epidermal – mesenchymal tissue connectivity enabling robust fin skeletal development and regeneration.

(A, B) Schematic of epithelial (basal epidermis, blue cells) and mesenchymal-derived (osteoblast lineage, salmon cells) tissue organization separated by an immature basement membrane (BM, black dashed lines) in the distal developing or regenerating fin ray. (A) The Fraser Complex (FPC) adheres epidermal and mesenchymal tissue layers to support osteoblast organization and therefore skeletal patterning. (B) In *fras1*$^{-/-}$ mutants, Fraser Complex components cannot translocate to the sublamina densa basement membrane layer and blisters form between tissue layers. (C) Wildtype developing caudal endoskeleton with blue and purple representing cartilage and calcified bone, respectively. Abbreviations: UST, urostyle; PL, pleurostyle; OPC, opisthural cartilage; H1-H5, hypurals 1-5; PH, parhypural; HS, hemal spine. (D) Example of *fras1*$^{-/-}$ caudal endoskeleton, including ectopic cartilaginous structures (yellow arrowheads), an additional hypural (H6, yellow), fusions between elements (yellow asterisk), and general poor articulation. (E) Wildtype caudal fin dermal skeleton (fin rays) anatomy. (F) Example of *fras1*$^{-/-}$ fin ray patterning defects. Abnormalities include ray fusions (green arrowhead), absent branching (open green arrowhead), uneven joints (green brackets), precocious branching (green arrow), and wavy rays (green asterisk).

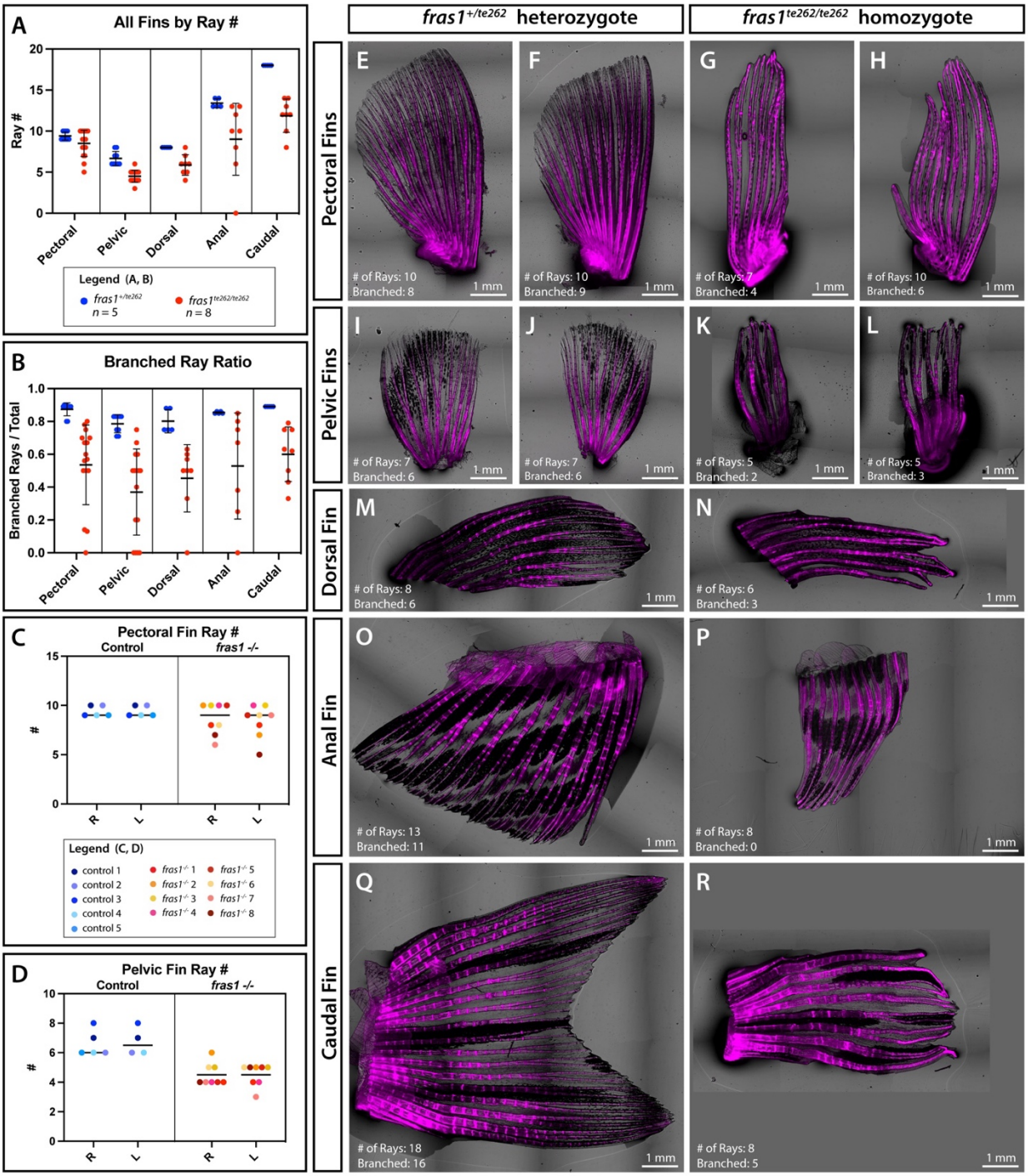

Figure S4.1. Variable expressivity of *fras1*$^{-/-}$ skeletal patterning abnormalities across all fins.

Figure S4.1. Variable expressivity of *fras1*$^{-/-}$ skeletal patterning abnormalities across all fins.

(A) Fin ray scoring for all 7 zebrafish adult fins for $n = 5$ *fras1*$^{+/-}$ heterozygote controls and $n = 8$ *fras1*$^{-/-}$ homozygote mutants. The paired pectoral and pelvic fins have two data points per fish. (B) Ratio of branched fin rays over total fin rays per fin. The paired pectoral and pelvic fins have two data points per fish. (C) Pectoral fin ray number and (D) Pelvic fin ray number for right (R) and left (L) fins with individual control fish marked in the blue spectrum and individual *fras1*$^{-/-}$ mutants marked in the red spectrum. (E-R) Representative adult Alizarin Red-stained fins overlayed with brightfield for (E, F, I, J, M, O, Q) controls and (G, H, K, L, N, P, R) *fras1*$^{-/-}$ mutants. (E-H) Pectoral and (I-L) pelvic fins are from the same animal to highlight left-right asymmetry in *fras1*$^{-/-}$ mutants. Number of rays, branched rays, and scale bars are as marked.

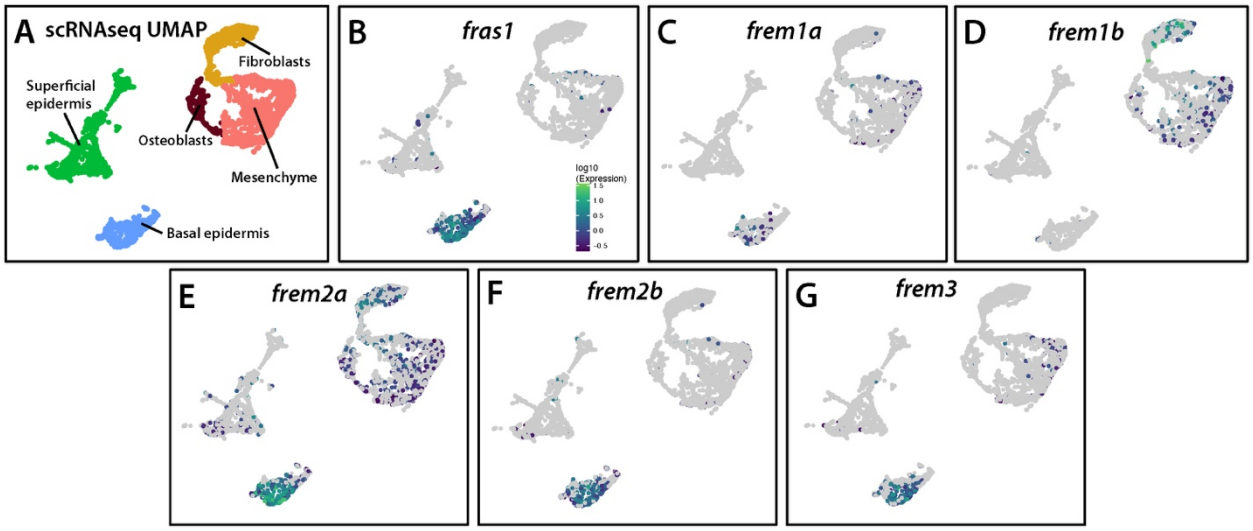

Figure S4.2. Single cell-resolved gene expression profiles show Fraser Complex transcripts are basal epidermal-enriched during fin regeneration.

(A) UMAP cluster analysis from single cell transcriptomes of 3- and 7-days post amputation (dpa) zebrafish fin tissue identifying unique clusters for basal epidermis (blue), superficial epidermis (green), and mixed mesenchyme/osteoblast/fibroblast lineages (dark red, pink, yellow) in UMAP space. (B-G) Individual UMAP plots for Fraser Complex components *fras1*, *frem1a*, *frem1b*, *frem2a*, *frem2b*, and *frem3*, respectively. *fras1* is the most highly enriched basal epidermal marker of all captured transcripts.

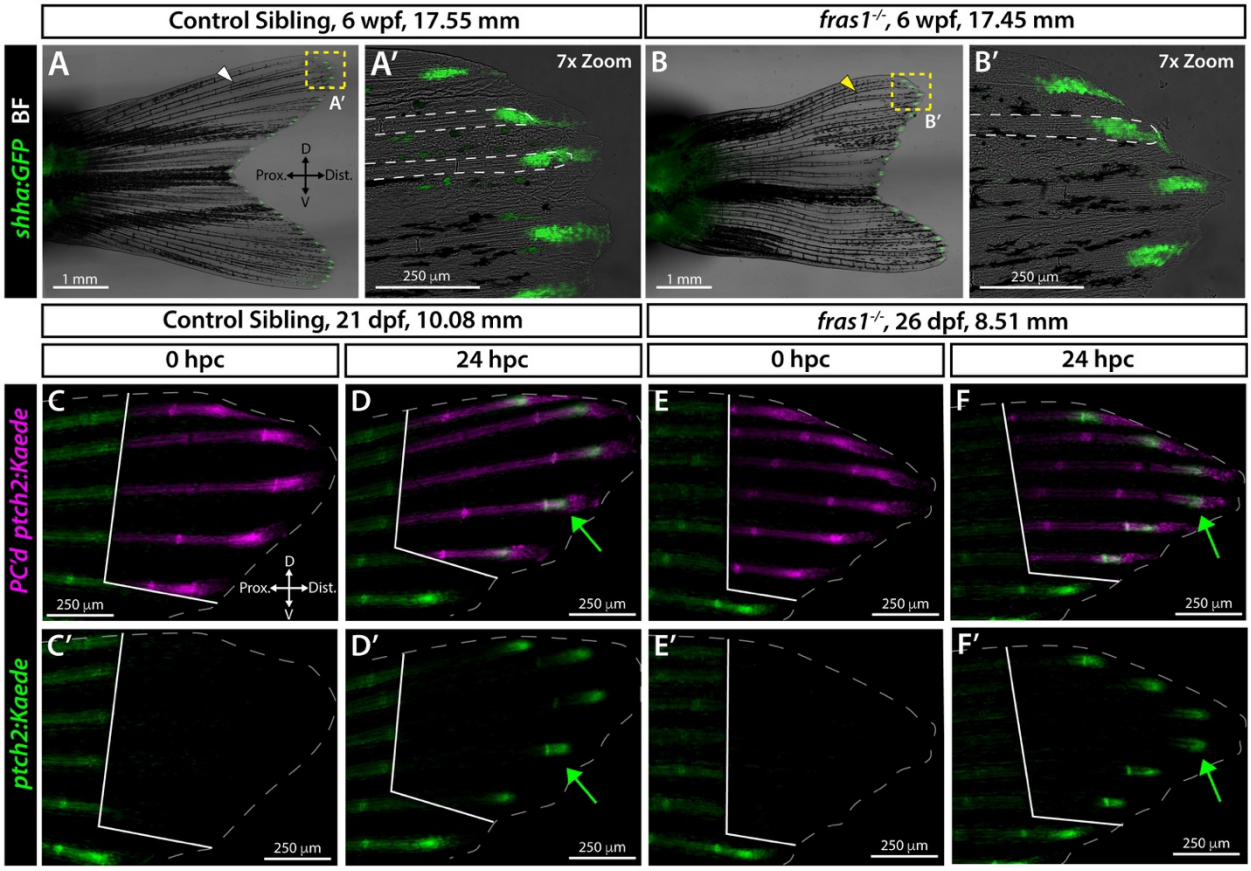

Figure S4.3. Loss of Fras1 does not impair Shh/Smo signaling during fin development.

(A, B) Whole mount caudal fin images of representative (A) *shha:GFP* control (n = 4) and (B) *shha:GFP; fras1*$^{-/-}$ mutant (n = 6) siblings at six weeks post fertilization (wpf). (A', B') Zoom insets of the dorsal tip of the caudal fins. Dorsal ray 2 (dashed white outline) is branched in (A') but unbranched in (B'). (C-F') Confocal fluorescence images of the dorsal lobe of developing caudal fins from a *ptch2:Kaede* control and stage-matched *fras1*$^{-/-}$ mutant sibling (n = 3 controls, n = 8 mutants). (C, E) White outlined regions shows complete conversion of Kaede from green to red emission at 0 hours-post-conversion (hpc) following UV light exposure (single channel panels C', E'). (D, F) At 24 hpc, the same fish express small domains of green Kaede protein (green arrows) newly produced in the photoconverted region (white lines), indicating active Shh/Smo signaling. Dashed gray lines indicate fin boundaries.

BRIDGE TO CHAPTER V

In this chapter, we demonstrate the extracellular environment plays a permissive role to stabilize fin skeletal patterning, including but not limited to ray branching. We use a zebrafish model of Fraser Syndrome, *fras1*^{te262}, and demonstrate the line which was previously thought to be homozygous lethal can be reared to adulthood with 10% viability. We therefore establish the first adult Fraser Syndrome model in zebrafish and characterize a variety of fin ray patterning abnormalities similar to the digit abnormalities of Fraser Syndrome patients and mouse models. Using both developmental and regenerative models, we show the Fraser Complex maintains epithelial-mesenchymal associations during fin morphogenesis. Importantly, we found Fraser Complex promotes skeletal patterning independently of Shh/Smo signaling. In Chapters V and VI, we return to investigating how Shh signaling is activated to regulate ray branching upstream.

CHAPTER V: WNT10A PROMOTES ZEBRAFISH MEDIAN FIN DEVELOPMENT AND CAUDAL FIN REGENERATION

In preparation (style of *Developmental Biology*)

Co-authored material to be published as Robbins, A.E.; O'Hara-Smith, J; Square, T.A; Miller, C. T; Stewart, S; and Stankunas, K.

AUTHOR CONTRIBUTIONS

Amy E. Robbins[1, 2] conceived of the study and performed the majority of experiments. Johnathan O'Hara-Smith assisted with experiments and mutant husbandry[1, 2.] Tyler A. Square[3] and Craig T. Miller[3] generated the inducible transgenic wnt10a line. Kryn Stankunas[1, 2] supervised the project with support from Scott Stewart[1]. Amy E. Robbins wrote the manuscript with editing by Kryn Stankunas.

[1]Institute of Molecular Biology
[2]Department of Biology
University of Oregon
273 Onyx Bridge
1318 Franklin Blvd
Eugene, OR 97403-1229
Office: (541) 346-7416
Fax: (541) 346-4854

[3]Department of Molecular & Cell Biology
University of California, Berkeley

INTRODUCTION

Zebrafish fin appendages robustly regenerate, unlike human limbs. Following amputation, fins will completely return to their pre-injury size and shape, including an elaborate bony ray skeleton. Innately regenerative animals like the zebrafish primarily re-deploy developmental mechanisms to restore tissue after injury. Despite the vast differences between fish and humans, fin and limb appendage development are governed by many of the same genetic mechanisms (Cass et al., 2021; Crotwell and Mabee, 2007; Shubin et al., 2009, 1997). Identifying conservation in the molecular signals that direct fin development and regeneration could provide insights for treating congenital limb abnormalities and developing regenerative bone therapies.

The zebrafish caudal fin is a leading model of appendage regeneration. The stereotyped skeletal pattern, powerful genetic and molecular toolkit, and amenability to live imaging has made the caudal fin an ideal model for dissecting the role of myriad signaling pathways during regeneration (Gemberling et al., 2013; Sehring and Weidinger, 2020). The zebrafish caudal fin joins the trunk posterior to the distal-most vertebrae. A proximal endoskeleton of hypural and ural bones supports an intricate arrangement of distal dermal bony rays, or lepidotrichia (Arratia et al., 2008; Desvignes et al., 2022). The dermal skeleton of the zebrafish caudal fin usually comprises 18 rays, each consisting of two curved hemi-rays lined by bony matrix-expositing osteoblasts surrounding inter-ray fibroblasts and all encompassed by a stratified epidermis. After injury, a wound epidermis forms to seal the fin and initiate the regenerative program. Between 1-3 days post-amputation (dpa), the regenerative blastema is formed, followed by the outgrowth phase that completely restores the fin to its original size and shape (~21-28 dpa) (Nechiporuk and Keating, 2002; Stoick-Cooper et al., 2007; Tornini et al., 2016).

Wnt ligands represent a highly conserved family of secreted signaling proteins that function throughout development to promote proliferation, fate specification, and differentiation activities (Clevers and Nusse, 2012; Logan and Nusse, 2004). Wnt/β-catenin functions upstream of many signaling pathways to robustly coordinate fin growth and patterning during both development and regeneration (Stewart et al., 2014; Stoick-Cooper et al., 2007; Wehner et al., 2014). During blastema formation, osteoblasts dedifferentiate to a mesenchymal pre-osteoblast (pOb) state. Distal Wnt/β-catenin signaling promotes and sustains pOb proliferation and opposes BMP-dependent redifferentiation activity (Stewart et al., 2014). Consistently, inhibition of Wnt/β-catenin signaling completely arrests fin regeneration, at least in part by disrupting pObs maintenance and subsequent bone maturation (Stewart et al., 2014, Stoick-Cooper et al., 2007; Wehner et al., 2014). However, specific roles for individual Wnt/β-catenin ligands during development and regeneration remain poorly understood.

A RNA-Seq analysis showed *wnt10a* as the most highly expressed Wnt/β-catenin ligand during regeneration. Further, *wnt10a* transcripts are expressed in the distal blastema of regenerating fins (Grotek et al., 2013; Stewart et al., 2019; Stoick-Cooper et al., 2007). Additionally, mammalian Wnt10a has been shown to support bone mineralization, trabeculation, and wound healing (Cawthorn et al., 2012; Tsukamoto et al., 2019; Wang et al., 2018). Therefore, *wnt10a* is a strong candidate regulator of fin ray growth, patterning, and/or maturation. However, no zebrafish *wnt10a* genetic loss-of-function studies have been conducted. We mutagenized *wnt10a* using CRISPR/Cas9 to generate three stable, adult-viable alleles (*wnt10a*$^{b1423\text{-}b1425}$). Two of these

alleles were predicted loss-of-function (*wnt10a*^{b1423} and *wnt10a*^{b1424}) and exhibited severe fin loss phenotypes.

We used the *wnt10a*^{b1423} allele to evaluate Wnt10a contributions to zebrafish fin development. *wnt10a*^{b1423} homozygous mutants exhibited a complete loss of dorsal and anal fins. The caudal fin endoskeleton was variably reduced while fin rays ranged from absent to forming partial caudal fins. We tracked fin deficiencies to reductions of the medial fin fold as early as two days-post-fertilization (dpf). We found the severity of fin fold reduction correlated with the severity of defects in caudal fin morphology during juvenile development by following the development of individual larvae during fin ontogeny. We used the heat-shock inducible transgenic line *Tg(hsp70l:mCherry-2A-wnt10a)*^{bk409Tg} to identify when *wnt10a* is required for fin fold development. Heat shock induction of *wnt10a* from 1-2 dpf rescued fin fold size in *wnt10a*^{b1423} mutant larvae and partially rescued median fin development assayed at 28 dpf. Fin rescue was further improved with additional heat shock inductions through 15 dpf. We next assessed the adult caudal skeleton and found a minority of *wnt10a*^{b1423} mutants developed partial caudal fins. A regenerative assay of partial caudal fins revealed variable phenotypes; some fins regenerated to approximately pre-amputation levels, some had intermediate regenerative capabilities, and a final subset showed no regenerative capability. Further, heat shock stress during regeneration completely abrogated the regenerative capacity of *wnt10a*^{b1423} mutants. Finally, heat shock induction of *wnt10a* at the time of injury rescued the regenerative potential of *wnt10a*^{b1423} mutants. Collectively, we identify *wnt10a* as critical for zebrafish median fin development and supportive for caudal fin regeneration.

RESULTS

Wnt10a is necessary for fin development

We mutagenized *wnt10a* using CRISPR/Cas9 technology to determine its specific requirement during fin development and regeneration (Figure 1). We selected targets in exon 2 near pan-Wnt conserved domains and generated three homozygous alleles termed *wnt10a*$^{b1423\text{-}5}$ (Figure 5.1A, B). Two of these alleles (*b1423* and *b1424*) had severe fin loss phenotypes (Figure 5.1A, D, E), while the third (*b1425*) appeared wildtype (Figure 5.1A, C, F). DNA sequencing and protein alignments revealed *wnt10a*^{b1423} is a 6-base pair in-frame deletion, *wnt10a*^{b1424} is a frameshift mutation leading to an early stop in exon 3, and *wnt10a*^{b1454} has two in-frame insertions (Figure 5.1B, Table 5.1). Protein folding software revealed Wnt10a^{b1423} protein was predicted to be structurally similar to wildtype and the deleted residues (p.Q136_F137del) were located on the end of an α-helix reported to form a stabilizing disulfide bond and containing a pan-Wnt conserved sequence (ECQHQFR) required for Frizzled receptor recognition (Bateman et al., 2023; Logan and Nusse, 2004; Willert et al., 2003) (Figure 5.1G, H). Wnt10a^{b1424} protein was expectedly severely truncated compared to wildtype (Figure 5.1I) while insertions to Wnt10a^{b1425} appeared to only affect disordered protein regions (Figure 5.1J). We conclude the *wnt10a*^{b1423} and *wnt10a*^{b124} alleles, which have no observable phenotypic differences, are nulls or severe hypomorphs, and the *wnt10a*^{b1425} allele is an isomorph. We chose the *wnt10a*^{b1423} allele for subsequent investigation to avoid the possibility of nonsense-mediated decay in the truncated *wnt10a*^{b1424} allele. Henceforth, *wnt10a*$^{+/-}$ and *wnt10a*$^{-/-}$ refer to *wnt10a*$^{+/b1423}$ and *wnt10a*$^{b1423/b1423}$, respectively.

Wnt10a is required fin endoskeleton and dermal skeleton

We first sought to characterize the striking developmental fin loss phenotypes in *wnt10a* mutants. Whole-mount Alizarin Red staining for calcified bone revealed adult homozygous mutants lack dorsal and anal dermal fin rays with minimal fin elements visible for pectoral, pelvic, and caudal fins (Figure 5.2B, $n = 8$) compared to heterozygote controls, which appear wildtype (Figure 5.2A, $n = 5$). We additionally noted the ectodermal bony scales appeared unaffected in *wnt10a* mutants (Figure 5.2B), though Wnt/β-catenin signaling is known to be required for scale development (Aman et al., 2018). Alizarin Red staining of 1 month-post-fertilization (mpf) juvenile fish with skin and soft tissue removed revealed fin loss extended to the dorsal and anal endochondral radials (Figure 5.2D, E, $n = 4$). The paired pectoral and pelvic fins, while diminished relative to controls (Figure 5.2C, $n = 4$) were still present. The spine and craniofacial skeleton appeared superficially unaffected in mutants (Figure 5.2D, E). We additionally noted the caudal fin reduction in *wnt10a* mutants to be variable, whereby some mutants had partial caudal fins including extended rays complete with joints (Figure 5.2D) and others had no fin rays akin to a stump (Figure 5.2E). On closer examination (Figure 5.2C'-E'), the endochondral caudal skeletal appeared relatively well articulated, with defined hypurals (H1-H5), a urostyle (UST), and preural centrum (PU). However, the ventral elements such as the parhypural (PH) and haemal spines were reduced. Nonetheless, considering the severity of the caudal fin phenotype, the endoskeleton was relatively intact, with no obvious differences between mutants with partial caudal fins (Figure 5.2D') and those with stumps (Figure 5.2E'). We conclude *wnt10a* is required for the development of all fins but with variable expressivity.

We next questioned when *wnt10a* was required during fin ontogeny. Alcian Blue and Alizarin Red staining for cartilage and calcified bone, respectively, demonstrated the absence of dorsal and anal fins, including radials, by the mid-larval stage (13-14 dpf, SL ~6 mm) (Figure 5.2F, G, H) while developing pectoral fins appeared unaffected (Figure 5.2I, J) (Walker and Kimmel, 2007). We again noted variable reduction of the caudal fin, even between clutch mates (Figure 5.2F). Confocal imaging of fluorescent Alizarin Red overlayed with DIC confirmed developing control fins (Figure 5.2K, $n = 12$) have two ray fields of 9 rays each that originate from a central gap between hypurals 2 and 3 (the hypural diastema) and go on to form the dorsal and ventral lobes of the caudal fin (Desvignes et al., 2022). In *wnt10a* mutants, hypural numbers ranged from 2-5 and fin ray numbers from 0-11 despite no significant difference in standard length (SL) with control siblings (Figure 5.2L, M, N). Interestingly, mutants that had a field of caudal fin rays (Figure 5.2L) appeared comparable in their size and endoskeleton to mutants with no fin rays at all (Figure 5.2M). These findings demonstrate *wnt10a* requirements during fin establishment occur prior to the mid-larval stage. Moreover, the absence of fin rays does not occur from an absent endoskeleton but likely is another variably expressed trait from the loss of *wnt10a*.

The larval fin fold establishes caudal fin pattern

We assayed earlier developmental timepoints to identify when *wnt10a* is required for fin development. Larval 6 dpf (~3.30 mm) fish do not yet have fins but rather a median fin fold (MFF) from which the unpaired median caudal, anal, and dorsal fins emerge (Figure 5.3A). This thin, primarily epidermal structure is supported by actinotrichia fibrils and becomes populated by

migratory mesenchymal cells that condense prior to fin ray emergence (Cadete et al., 2023; Crotwell and Mabee, 2007; Ka et al., 2020; Kimmel et al., 1995; Miyamoto et al., 2022; Parichy et al., 2009; Van Den Boogaart et al., 2012). We used Alcian Blue to stain acidic polysaccharides present in the epidermis and actinotrichia and visualize the boundaries of developing fin tissue (Lalonde and Akimenko, 2018; Walker and Kimmel, 2007). We found *wnt10a* mutants have no dorsal or ventral fin fold tissue. However, the MFF around the caudal region remained intact (Figure 5.3A, B). We did not observe any obvious deficiencies to the developing pectoral fins (Figure 5.3C, D). Altogether, the MFF was significantly reduced in *wnt10a* mutants (Figure 5.3E).

We were able to identify MFF deficiencies by eye as early as 2 dpf (~ 3.00 mm) in just-hatched larvae (Figure 5.3F-H). At this stage, the trunk of *wnt10a* mutants was not completely exposed as in 6 dpf larvae but rather the amount of tissue surrounding the trunk was reduced. Quantification confirmed variable expressivity in the reduction of MFF even between sibling homozygote mutants (Figure 5.3G, H, I). We wondered if the variable reduction in MFF corresponded to the variability observed in juvenile and adult caudal fin morphology (i.e., partial caudal fins vs stumps). We therefore individually tracked *in vitro* fertilization (IVF)-generated larvae of known genotype (n = 6 heterozygous controls and n = 12 *wnt10a* $^{-/-}$) and imaged them at 2 dpf (early larvae), 20 dpf (late larvae), and 30 dpf (juvenile onset) (Figure 5.3F-H, F'-H', F"-H"). We divided *wnt10a* $^{-/-}$ caudal fin phenotypes into two categories: partial fins, in which the length of the longest ray must be at least 30% of the length of the longest ray in matched controls, and stumps, in which there are no rays or rays are shorter than 30% of the length of the longest rays in matched controls. 2 dpf MFF normalized area was significantly lower in fish that developed

stumps by 20 dpf vs partial caudal fins (Figure 5.3J). Linear regression of 2 dpf normalized fin fold area against 20 dpf normalized caudal fin area revealed an expected separation between controls and mutants (Figure 5.3K), while mutants alone (Figure 5.3L) separated out into stumps vs partial caudal fins. These data demonstrate the severity of *wnt10a* mutant caudal fin phenotypes is determined early in development. Further, decreased MFF size as early as 2 dpf is correlated with defects in later-arising caudal fin morphology.

Larval *wnt10a* rescues the median fin fold and partial median fin development

We next sought to map the timing of when *wnt10a* expression was required for MFF development. We used a new heat shock-inducible *wnt10a* overexpression line, *Tg(hsp70l:mCherry-2A-wnt10a)*^{bk409Tg}, henceforth referred to as *hs:wnt10a* (Square et al., 2022) . We crossed *hs:wnt10a* to *wnt10a*$^{-/-}$*; shha:GFP* where Sonic hedgehog a (Shha) expression as marked by GFP is used as a visual guide for fin emergence (Crotwell and Mabee 2007; Hadzhiev 2007; Braunstein 2021). We generated *wnt10a* heterozygous controls and homozygous mutants with and without the hs*:wnt10a* transgene. Heat shock from 1-2 dpf during the period directly prior to first observation of MFF deficiencies in *wnt10a* mutants. We found normalized MFF area between control (- *hs:wnt10a*) and *wnt10a* overexpression larvae (+*hs:wnt10a)* were not significantly different in *wnt10a*$^{+/-}$ heterozygotes (Figure5.4B, D, N), indicating additional *wnt10a* expression does not make control fin folds grow excessively large. Expectedly, *wnt10a*$^{-/-}$ (without *hs:wnt10a*) MFFs were smaller compared to both controls (Figure 5.4C, N). In contrast, heat-shocked *wnt10a*$^{-/-}$ mutants with *hs:wnt10a* largely restored MFF area (Figure 5.4E, N).

These data demonstrate 1-2 dpf is the critical window for Wnt10a-dependent MFF establishment.

Given the robust rescue in fin fold tissue, we wondered if ubiquitous *wnt10a* induction would also rescue median fin development. We reasoned that *wnt10a* may be required only for finfold initiation, and therefore 1-2 dpf would be sufficient to rescue median fin development. Alternatively, *wnt10a* may be active during fin initiation and expansion, in which case *wnt10a* would be required throughout median fin morphogenesis. To discriminate between these hypotheses, we split the remaining larvae heat-shocked from 1-2 dpf into two groups: the first, we monitored without any additional heat shock treatments ("short-term" group, Figure S5.1) and the second, we conducted a heat shock regiment of 4 hours every other day until 15 dpf when the caudal fin ray pattern is largely established ("sustained" group, Figure 5.4A). We imaged both groups at 16 dpf (mid-larval) and 28 dpf (juvenile onset). Remarkably, both groups of *wnt10a*$^{-/-}$*; shha:GFP; hs:wnt10a* larvae demonstrated variable but significant rescue of developing fin tissue compared to *wnt10a*$^{-/-}$*; shha:GFP* mutants (Figure 5.4F-G, O, P; Figure S5.1B-D). Mesenchymal *shha* expression as marked by GFP surrounds the radials of developing dorsal and anal fins (Crotwell and Mabee 2007). In *wnt10a*$^{-/-}$*; shha:GFP* mutants, we observed GFP around the caudal endoskeleton but no GFP dorsoventrally (Figure 5.4G; Figure S5.1C), matching skeletal preps which demonstrated *wnt10a* mutants have no dorsal or anal radials (Figure 5.2D, E, F, H). Notably, GFP expression was restored in some dorsal and anal fin regions for both short-term and sustained heat shock groups in *wnt10a*$^{-/-}$*; shha:GFP; hs:wnt10a* 16 dpf mid-larvae, indicating partial rescue of radials (Figure 5.4I, Figure S5.1D). We noted mCherry expression was visible throughout the bodies of the "sustained" group but not for the "short

term" group, which corresponds with perduring mCherry from the final heat shock of the "sustained" group at 15 dpf whereas the "short-term" group had not been exposed to 38°C for two weeks. Finally, we assessed again fish at the 28 dpf onset of the juvenile stage, when all temporary effects of heat shock would have ceased (Figure 5.4J-M; Figure S5.1E-G). We scored fins on a rescue scale of 0-4 where 0 indicates no fin and 4 indicated a wildtype fin (Figure 5.4 Q, Figure S5.1H, I). Both "short-term" and "sustained" *wnt10a*$^{-/-}$*; shha:GFP; hs:wnt10a* groups had caudal fins closer to wildtype than matched *wnt10a*$^{-/-}$ groups without *hs:wnt10a* (sustained average score 2.53, short-term 2.88) . Both *wnt10a*$^{-/-}$*; shha:GFP; hs:wnt10a* groups also partially rescued the anal fin, although the "sustained" group had a higher rescue score compared to "short term" (2.13 vs 1.35). Interestingly, only the "sustained" group significantly rescued the dorsal fin (1.27 vs 0.18), and the level of rescue was the lowest of the three median fins. We conclude *wnt10a* expression is required during early larval fin initiation for all median fins and may additionally support fin expansion during larval morphogenesis.

Wnt10a promotes caudal fin development and regenerative robustness

Having probed the timing and function of developmental *wnt10a,* we returned to our original question of how *wnt10a* contributes to adult caudal fin regeneration. We first characterized caudal fin phenotypes of *wnt10a*$^{-/-}$ mutants. We scored $n = 421$ mutants across nine clutches of various transgenic backgrounds, excluding any with *hs:wnt10a* background to control for the possibility of environmental or stress-triggered ectopic *wnt10a* production. We found a majority *wnt10a*$^{-/-}$ mutants have a caudal stump (60%, $n = 232/421$) and a minority have partial caudal fins (40%, $n = 139/421$), using our previously defined metric wherein the length of the longest

ray of a partial caudal fin must be at least 30% of the length of the longest ray of a matched control. We more closely examined the partial fins of two clutches totaling n = 18 heterozygous sibling controls and n = 96 mutants (Figure 5.5). We found *wnt10a* mutants with partial caudal fins have significantly fewer caudal fin rays (n =1-8) versus controls (n = 17-18), despite no significant difference in standard length (SL) (Figure 5.5A-D, I, J). We amputated the caudal fins and allowed regeneration to progress to 28 days-post-amputation (dpa) when regeneration has completed in wildtype fins. While all controls regenerated as expected, we found three distinct phenotypes in *wnt10a*$^{-/-}$ regenerates: all rays regenerated (47%, n = 45), some rays regenerated (35%, n = 34), or no rays regenerated (18%, n = 17) (Figure 5.5E-H, K, L). To determine if rays competent to regenerate restored their original size, we individually tracked an experimental subset of clutch mates (n = 8 *wnt10a*$^{+/-}$ and n = 46 *wnt10a*$^{-/-}$). We measured uninjured and 28 dpa caudal fin area. For controls, regenerated caudal fins were 9% larger than uninjured, indicating the growth of the fish over one month (Figure 5.5M). For *wnt10a* mutants, regenerated caudal fins were 14% smaller than in their uninjured state (Figure 5.5N). However, when the data are split into groups of mutants that regenerated all, some, or no rays, we found differences of +7%, -15%, and -39%, respectively (Figure 5.5O). These data indicate that Wnt10a promotes robust regeneration such that not all rays regenerate, but those that do are able to grow back to their uninjured size.

Finally, we assayed whether induction of *wnt10a* expression could rescue the regenerative deficiencies observed in *wnt10a*$^{-/-}$ mutants (Figure 5.6). We imaged *wnt10a*$^{+/-}$ controls and *wnt10a*$^{-/-}$ mutants with partial caudal fins with and without the *hs:wnt10a* transgene. We then amputated the caudal fins and began a 30-day heat shock regiment (Figure 5.6A). At 14 dpa,

when regeneration should be well into its outgrowth phase, we found that none of the *wnt10a*$^{-/-}$ mutant caudal fins had regenerated (*n* = 0/10). In contrast, a majority (*n* = 9/11) of *wnt10a*$^{-/-}$*; hs:wnt10a* mutants regenerated their caudal fins. All *wnt10a*$^{+/-}$ controls (*n* = 14/14) regenerated their caudal fins whether carrying the *hs:wnt10a* transgene or not. We surmise heat shock stress decreases the capacity of *wnt10a*$^{-/-}$ partial caudal fins to regenerate, while heat shock-induced *wnt10a* expression rescues regenerative potential. These data suggest environmental stress affects regenerative capacity in *wnt10a* mutants, which may partially explain the variability of regenerative capacity of *wnt10a*$^{-/-}$ partial caudal fins or even the variable development of caudal fin rays. Given the capacity of *wnt10a*$^{-/-}$ partial caudal fins to regenerate at all, which is bolstered by ectopic *wnt10a* induction, we conclude *wnt10a* is not a key instructive signal required for regeneration but rather acts as a developmental buffer.

DISCUSSION

In this study, we sought to determine *wnt10a* requirements for zebrafish caudal fin development and regeneration. We generated three stable and homozygous viable *wnt10a* alleles and chose the *wnt10a*^{b1423} allele, which contains an in-frame deletion of two amino acids (p.Q136_F137del) for further investigation. We found the deleted residues in the *wnt10a*^{b1423} mutant are highly conserved across Wnts and contain a Frizzled recognition sequence (Bateman et al., 2023; Logan and Nusse, 2004; Willert et al., 2003). The *wnt10a*^{b1424} frameshift early stop mutation produced homozygous mutants indistinguishable from *wnt10a*^{b1423}. We conclude p.Q136_F137 residues are likely necessary for the function of numerous Wnts including *Wnt10a*.

The Wnt/β-catenin pathway is fundamental through numerous developmental events and adult tissue homeostasis such that perturbations to the pathways are linked to a plethora of congenital disorders and human disease states (Clevers and Nusse, 2012; Logan and Nusse, 2004). It was therefore surprising that *wnt10a*$^{b1423\text{-}4}$ homozygous mutants were adult-viable, needing no special care, and did not differ in standard length from their wildtype or heterozygous siblings. Also surprising was that only the fins appeared to be affected; other bony elements known to be regulated by Wnt/β-catenin signaling such as the craniofacial skeleton, spine, and scales were intact, suggesting alternative Wnt/β-catenin ligands are expressed during the ontogeny of these structures (Aman et al., 2018; Cawthorn et al., 2012; Doolan et al., 2021; Watson et al., 2022; Yuan et al., 2017) .The limitation of aberrant phenotypes to the median fins is consistent with expectations suggested by a recent transcriptional dataset from 3-120 hpf showing *wnt10a* transcripts are primarily expressed in fin epithelia and fin mesenchyme starting at 14-21 hpf (Farrell et al., 2018; Sur et al., 2023).

We found *wnt10a* is required for development of all three median fins. The dorsal and anal fin endoskeleton and dermal fins rays were absent in *wnt10a* mutants with 100% penetrance. However, the caudal fin exhibited variable penetrance ranging from an endoskeletal stump with no rays to partial caudal fins. We traced fin abnormalities to 2 days-post-fertilization (dpf) reductions in the median fin fold (MFF) and found the level of larval MFF reduction correlated to juvenile caudal fin phenotypes. We tested the necessity of *wnt10a* during fin development and identified 1-2 dpf as a critical window for MFF development. Additional *wnt10a* expression induction from 3-15 dpf improved the level of median fin rescue. This result could indicate sustained *wnt10a* supports robust median fin development. Alternatively, there may be one or

more additional “critical windows” between 3-15 dpf that cannot be resolved by the current experimental design. The dorsal fin proved the least successful median fin to rescue; taken in consideration with transcriptional data indicating robust *wnt10a* expression may begin as early as 14 hpf, it is probable that our heat shock regiment beginning at 24 hpf was too late in development for dorsal fin recovery (Farrell et al., 2018; Sur et al., 2023). It is also possible that pre-24 hpf induction of *wnt10a* would improve anal and caudal fin rescue. Future studies could theoretically identify fin-specific critical windows, as the emergence of median fins is staggered (Kimmel et al., 1995; Parichy et al., 2009).

We found MFF size at 2 dpf corresponds to later-arising caudal fin phenotypes followed up to 28 dpf. Intriguingly, a previous study using genetically induced fin fold mesenchymal ablation from 72 hpf to 30 dpf was associated with targeted collapse of the fin fold and even varied reduction in pectoral fin ray number (Lalonde and Akimenko, 2018). The caudal fin was not similarly affected. We interpret this study as further evidence for associated fin fold size with proper fin development. We surmise the lack of a caudal fin phenotype in this study may be due to the ablation start time of 72 hpf, as we found 24-48 hpf to be the critical window of *wnt10a*-promoted median fin fold establishment and hypothesize even earlier timepoints may involved. We find the referenced study to further reinforce that different fins are spatiotemporally distinct in their development.

All fins undergo similar stages of morphogenesis from larval fin fold to mature fin appendage. Therefore, the concept that fin fold mesenchyme is a critical component of fin fold structure and fin emergence may also apply to the median fins. In rodents, mesenchymal and epithelial

Wnt10a/b support bone development, mineralization, mass, and maintenance of adult bone progenitors (Bennett et al., 2007, 2005; Cawthorn et al., 2012; Liu et al., 2020; Stevens et al., 2010; Zhou et al., 2008). A convenient hypothesis is that mesenchymal *wnt10a* expressed in the fin fold promotes the formation of mesenchymal condensates from which rays later emerge (Crotwell and Mabee, 2007; Miyamoto et al., 2022; Parichy et al., 2009). Alternatively, epidermal *wnt10a* could be supporting the fin fold by promoting collagen or actinotrichia production (Van Den Boogaart et al., 2012b; Wang et al., 2018). Future expression studies will help discriminate between these hypotheses.

Finally, heat shock induction of *wnt10a* following amputation of partial caudal fins resulted in a majority of *wnt10a*$^{-/-}$*; hs:wnt10a* transgenic fish regenerating their rays. While this experiment is complicated by the environmental stress of heat shock, the stark contrast between no *wnt10a*$^{-/-}$ partial caudal fins regenerating versus the majority of their *wnt10a*$^{-/-}$*; hs:wnt10a* clutch mates at least suggests a supportive role in regenerative capacity. This result suggests an unknown shared mechanism between fin development is re-deployed during regeneration. Given *wnt10a* transcripts are highly expressed in intra-ray and pre-osteoblast regions during fin regeneration (Grotek et al., 2013; Stoick-Cooper et al., 2007; Wehner et al., 2014), we therefore propose *wnt10a* maintains mesenchymal progenitor cells during median fin development and regeneration. This model is also consistent with known functions of Wnt/β-catenin signaling in fin regeneration as well as in mammalian bone homeostasis (Cawthorn et al., 2012; McGowan et al., 2021; Rudnicki and Williams, 2015; Stewart et al., 2014; Wehner et al., 2014). Variable expressivity of fin development and regeneration could be a result of genetic redundancy, for example by other Wnt/β-catenin signals, or as a result of developmental buffering. In conclusion,

our present study uncovers a fin-specific role for *wnt10a* during median fin development and regeneration. Further, we provide new avenues of study towards identifying shared mechanisms between median fin development and regeneration.

MATERIALS & METHODS

Zebrafish

Danio rerio zebrafish were reared and maintained at the University of Oregon Aquatic Animal Care Services (UO AqACS) fish facility under previously described conditions (Braunstein et al., 2021). All animal protocols were approved by the University of Oregon Institutional Animal Care and Use Committee (IACUC). We used the following lines: wildtype AB, *Tg(-2.4shha:gfp:ABC)*^{sb15} (Ertzer et al., 2007b), *Tg(RUNX2:mCherry)* (Barske et al., 2020), and *Tg(hsp70l:mCherry-2A-wnt10a)*^{bk409Tg} (Square et al., 2022).

CRISPR/Cas9 mutagenesis and allele identification

We generated *wnt10a*^{b1423}, *wnt10a*^{b1424}, and *wnt10a*^{b1425} mutants by mutagenizing a conserved region in exon 2. We identified this region using CHOPCHOP target searches and CDSEARCH. We used the following gRNA protospacer: 5' AGTGCCAGCATCAGTTCCGA 3'

Single-cell embryos were injected with 200 ng gRNA and 500 ng Cas9 protein. F_0 animals were fin clipped and a 589 bp region of exon 2 containing the target site was isolated by PCR using the following primers (in 5'-3'):

F: CTGTTCAGGAAACTGCTCA

R: TGCATACGGCCAACAATCA

PCR products were sequenced and fish with mutations in the target site outcrossed. We subsequently reared, fin clipped, performed PCR, and sequenced F_1 animals and identified the mutations in *wnt10a*^{b1423}, *wnt10a*^{b1424}, and *wnt10a*^{b1425} (Figure 1, Table 1). Fish with like mutations were incrossed to generate homozygous mutants. Alignment, protein sequences, and predicated protein structures were generated using Benching software integrated with AlphaFold2. PyMol was used to generate images of predicted protein structures in similar positions with highlighted residues.

Alcian Blue Alizarin Red Staining

Alcian Blue Alizarin Red staining was performed as previously described for larval stages between 6-14 dpf (Desvignes et al., 2022; Walker and Kimmel, 2007) or with the following modifications: For adults and juveniles, fish euthanized in MS-222 (Syndel) were fixed in 4% PFA overnight at 4°C. Next day, fish were skinned using microdissection scissors and fine forceps and internal organs removed. Following a dehydration series, fish were stained overnight as described (Desvignes et al., 2022).

Live Alizarin Red staining was performed on intact adults by swimming fish in 0.02% Alizarin Red S (Sigma Aldrich) in fish facility water for 15 minutes, followed by three 5-minute washes in fish facility water.

Microscopy

Alcian Blue Alizarin Red color images were acquired on a Leica M165 FC stereomicroscope equipped with a Leica DFC425 C camera. Fluorescent Alizarin images overlayed with DIC were acquired on a Nikon Eclipse T*i*-E inverted microscope with a Yokogawa CSU-W1 spinning disk

confocal attachment. Brightfield or DIC images of larvae immobilized by MS-222 anesthetization were imaged on a Nikon Eclipse T*i*-E inverted microscope. Following live imaging experiments, fish were euthanized or returned standard housing. ImageJ Fiji or Adobe Photoshop were used to adjust levels with identical image acquisition and processing settings for a given experiment.

Larval Tracking

To follow the development of individual larvae, clutches were generated via *in vitro* fertilization (IVF) from fish of known genotypes to generate *wnt10a*$^{+/-}$ or *wnt10a*$^{-/-}$ groups. Larvae were imaged as early as 2 dpf using the methods described above. Following imaging, larva were placed in individual petri dishes until 6 dpf and then moved to 250 mL beakers until 30 dpf. Fish received the standard larval diet (Westerfield, 2007) provided by UO fish facility professionals and regular water changes.

Heat shock regiments

For larval heat shock treatment, *hsp70l:mCherry-2A-wnt10a*^{bk409Tg}*; shha:GFP*$^{+/-}$*; wnt10a*$^{-/-}$ were crossed via IVF to wildtype or *wnt10a*$^{-/-}$ mutants. Groups of n = 25 larvae in petri dishes were placed in a 38°C incubator for up to 24 hours (from 1-2 dpf) or for 4 hours every other day until 15 dpf. As above, at 6 dpf larvae were moved to 250 mL beakers until 28 dpf at the culmination of the experiment. For adult heat shock treatments, adult fish were placed in a standard care tank equipped with a programmable heating element and plugged into a timer outlet. Fish were heat shocked to 38°C for 2 hours 3x daily. Fish were health checked daily and water temperature max and min was recorded by an external probe.

Fin morphometrics and data analysis

Fin morphometrics (i.e., fin fold size, ray length, standard length) were measured using ImageJ Fiji and data collected in Microsoft Excel. Graphs were generated using GraphPad Prism V9.

REFERENCES

Aman, A.J., Fulbright, A.N., Parichy, D.M., 2018. Wnt/β-catenin regulates an ancient signaling network during zebrafish scale development. Elife 7, e37001. https://doi.org/10.7554/elife.37001

Arratia, G., Schultze, H.-P., Wilson, M.V.H., 2008. Actinopterygian postcranial skeleton with special reference to the diversity of fin ray elements, and the problem of identifying homologies, in: Mesozoic Fishes 4 – Homology and Phylogeny. pp. 49–101.

Avaron, F., Smith, A., Akimenko, M.A., 2006. Sonic Hedgehog Signaling in the Developing and Regenerating Fins of Zebrafish [WWW Document]. Madame Curie Bioscience Database [Internet]. URL http://www.ncbi.nlm.nih.gov/books/NBK6368/

Barske, L., Fabian, P., Hirschberger, C., Jandzik, D., Square, T., Xu, P., Nelson, N., Yu, H.V., Medeiros, D.M., Gillis, J.A., Crump, J.G., 2020. Evolution of vertebrate gill covers via shifts in an ancient Pou3f3 enhancer. Proceedings of the National Academy of Sciences 117, 24876–24884. https://doi.org/10.1073/pnas.2011531117

Bateman, A., Martin, M.-J., Orchard, S., Magrane, M., Ahmad, S., Alpi, E., Bowler-Barnett, E.H., Britto, R., Bye-A-Jee, H., Cukura, A., Denny, P., Dogan, T., Ebenezer, T., Fan, J., Garmiri, P., da Costa Gonzales, L.J., Hatton-Ellis, E., Hussein, A., Ignatchenko, A., Insana, G., Ishtiaq, R., Joshi, V., Jyothi, D., Kandasaamy, S., Lock, A., Luciani, A., Lugaric, M., Luo, J., Lussi, Y., MacDougall, A., Madeira, F., Mahmoudy, M., Mishra, A., Moulang, K., Nightingale, A., Pundir, S., Qi, G., Raj, S., Raposo, P., Rice, D.L., Saidi, R., Santos, R., Speretta, E., Stephenson, J., Totoo, P., Turner, E., Tyagi, N., Vasudev, P., Warner, K., Watkins, X., Zaru, R., Zellner, H., Bridge, A.J., Aimo, L., Argoud-Puy, G., Auchincloss, A.H., Axelsen, K.B., Bansal, P., Baratin, D., Batista Neto, T.M., Blatter, M.-C., Bolleman, J.T., Boutet, E., Breuza, L., Gil, B.C., Casals-Casas, C., Echioukh, K.C., Coudert, E., Cuche, B., de Castro, E., Estreicher, A., Famiglietti, M.L., Feuermann, M., Gasteiger, E., Gaudet, P., Gehant, S., Gerritsen, V., Gos, A., Gruaz, N., Hulo, C., Hyka-Nouspikel, N., Jungo, F., Kerhornou, A., Le Mercier, P., Lieberherr, D., Masson, P., Morgat, A., Muthukrishnan, V., Paesano, S., Pedruzzi, I., Pilbout, S., Pourcel, L., Poux, S., Pozzato, M., Pruess, M., Redaschi, N., Rivoire, C., Sigrist, C.J.A., Sonesson, K., Sundaram, S., Wu, C.H., Arighi, C.N., Arminski, L., Chen, C., Chen, Y., Huang, H., Laiho, K., McGarvey, P., Natale, D.A., Ross, K., Vinayaka, C.R., Wang, Q., Wang, Y., Zhang, J., 2023. UniProt: the Universal Protein Knowledgebase in 2023. Nucleic Acids Res 51, D523–D531. https://doi.org/10.1093/nar/gkac1052

Bennett, C.N., Longo, K.A., Wright, W.S., Suva, L.J., Lane, T.F., Hankenson, K.D., MacDougald, O.A., 2005. Regulation of osteoblastogenesis and bone mass by Wnt10b. Proc Natl Acad Sci U S A 102, 3324–3329. https://doi.org/10.1073/pnas.0408742102

Bennett, C.N., Ouyang, H., Ma, Y.L., Zeng, Q., Gerin, I., Sousa, K.M., Lane, T.F., Krishnan, V., Hankenson, K.D., MacDougald, O.A., 2007. Wnt10b increases postnatal bone formation by enhancing osteoblast differentiation. Journal of Bone and Mineral Research 22, 1924–1932. https://doi.org/10.1359/jbmr.070810

Braunstein, J.A., Robbins, A.E., Stewart, S., Stankunas, K., 2021. Basal epidermis collective migration and local Sonic hedgehog signaling promote skeletal branching morphogenesis in zebrafish fins. Dev Biol 477, 177–190. https://doi.org/10.1016/J.YDBIO.2021.04.010

Cadete, F., Francisco, M., Freitas, R., 2023. Bmp-signaling and the finfold size in zebrafish: implications for the fin-to-limb transition. Evolution (N Y) 77, 1262–1271. https://doi.org/10.1093/evolut/qpad043

Cass, A.N., Elias, A., Fudala, M.L., Knick, B.D., Davis, M.C., 2021. Conserved mechanisms, novel anatomies: The developmental basis of fin evolution and the origin of limbs. Diversity (Basel) 13, 1–17. https://doi.org/10.3390/d13080384

Cawthorn, W.P., Bree, A.J., Yao, Y., Du, B., Hemati, N., Martinez-Santibañez, G., MacDougald, O.A., 2012. Wnt6, Wnt10a and Wnt10b inhibit adipogenesis and stimulate osteoblastogenesis through a β-catenin-dependent mechanism. Bone 50, 477–489. https://doi.org/10.1016/J.BONE.2011.08.010

Clevers, H., Nusse, R., 2012. Wnt/β-catenin signaling and disease. Cell 149, 1192–1205. https://doi.org/10.1016/j.cell.2012.05.012

Crotwell, P.L., Mabee, P.M., 2007. Gene expression patterns underlying proximal-distal skeletal segmentation in late-stage zebrafish, Danio rerio. Developmental Dynamics 236, 3111–3128. https://doi.org/10.1002/dvdy.21352

Desvignes, T., Robbins, A.E., Carey, A.Z., Bailon-Zambrano, R., Nichols, J.T., Postlethwait, J.H., Stankunas, K., 2022. Coordinated patterning of zebrafish caudal fin symmetry by a central and two peripheral organizers. Developmental Dynamics 1306–1321. https://doi.org/10.1002/dvdy.475

Doolan, B.J., Onoufriadis, A., Kantaputra, P., McGrath, J.A., 2021. WNT10A, dermatology and dentistry. British Journal of Dermatology 185, 1105–1111. https://doi.org/10.1111/bjd.20601

Ertzer, R., Müller, F., Hadzhiev, Y., Rathnam, S., Fischer, N., Rastegar, S., Strähle, U., 2007. Cooperation of sonic hedgehog enhancers in midline expression. Dev Biol 301, 578–589. https://doi.org/10.1016/j.ydbio.2006.11.004

Farrell, J.A., Wang, Y., Riesenfeld, S.J., Shekhar, K., Regev, A., Schier, A.F., 2018. Single-cell reconstruction of developmental trajectories during zebrafish embryogenesis. Science (1979) 360. https://doi.org/10.1126/science.aar3131

Gemberling, M., Bailey, T.J., Hyde, D.R., Poss, K.D., 2013. The zebrafish as a model for complex tissue regeneration. Trends in Genetics 29, 611–620. https://doi.org/10.1016/j.tig.2013.07.003

Grotek, B., Weidinger, G., Wehner, D., 2013. Notch signaling coordinates cellular proliferation with differentiation during zebrafish fin regeneration. Development 140, 1412–1423. https://doi.org/10.1242/dev.087452

Ka, J., Kim, J.D., Pak, B., Han, O., Choi, W., Kim, H., Jin, S.W., 2020. Bone Morphogenetic Protein Signaling Restricts Proximodistal Extension of the Ventral Fin Fold. Front Cell Dev Biol 8, 1–10. https://doi.org/10.3389/fcell.2020.603306

Kimmel, C.B., Ballard, W.W., Kimmel, S.R., Ullmann, B., Schilling, T.F., 1995. Stages of embryonic development of the zebrafish. Developmental Dynamics 203, 253–310. https://doi.org/10.1002/aja.1002030302

Lalonde, R.L., Akimenko, M.A., 2018. Effects of fin fold mesenchyme ablation on fin development in zebrafish. PLoS One 13, 1–25. https://doi.org/10.1371/journal.pone.0192500

Liu, Y., Fang, J., Zhang, Q., Zhang, X., Cao, Y., Chen, W., Shao, Z., Yang, S., Wu, D., Hung, M., Zhang, Y., Tong, W., Tian, H., 2020. Wnt10b-overexpressing umbilical cord mesenchymal stem cells promote critical size rat calvarial defect healing by enhanced osteogenesis and VEGF-mediated angiogenesis. J Orthop Translat 23, 29–37. https://doi.org/10.1016/j.jot.2020.02.009

Logan, C.Y., Nusse, R., 2004. The Wnt signaling pathway in development and disease. Annu Rev Cell Dev Biol 20, 781–810. https://doi.org/10.1146/annurev.cellbio.20.010403.113126

McGowan, L.M., Kague, E., Vorster, A., Newham, E., Cross, S., Hammond, C.L., 2021. Wnt16 Elicits a Protective Effect Against Fractures and Supports Bone Repair in Zebrafish. JBMR Plus 5, 1–14. https://doi.org/10.1002/jbm4.10461

Miyamoto, K., Kawakami, K., Tamura, K., Abe, G., 2022. Developmental independence of median fins from the larval fin fold revises their evolutionary origin. Sci Rep 12, 1–13. https://doi.org/10.1038/s41598-022-11180-1

Nechiporuk, A., Keating, M.T., 2002. A proliferation gradient between proximal and msxb - expressing distal blastema directs zebrafish fin regeneration. Development 129, 2607–2617. https://doi.org/10.1242/dev.129.11.2607

Parichy, D.M., Elizondo, M.R., Mills, M.G., Gordon, T.N., Engeszer, R.E., 2009. Normal table of postembryonic zebrafish development: staging by externally visible anatomy of the living fish. Dev Dyn 238, 2975–3015. https://doi.org/10.1002/dvdy.22113

Poss, K.D., Shen, J., Nechiporuk, A., McMahon, G., Thisse, B., Thisse, C., Keating, M.T., 2000. Roles for Fgf signaling during zebrafish fin regeneration. Dev Biol 222, 347–358. https://doi.org/10.1006/dbio.2000.9722

Rudnicki, M.A., Williams, B.O., 2015. Wnt signaling in bone and muscle. Bone 80, 60–66. https://doi.org/10.1016/J.BONE.2015.02.009

Sehring, I.M., Weidinger, G., 2020. Recent advancements in understanding fin regeneration in zebrafish. Wiley Interdiscip Rev Dev Biol 9, 1–16. https://doi.org/10.1002/wdev.367

Shubin, N., Tabin, C., Carroll, S., 2009. Deep homology and the origins of evolutionary novelty. Nature 457, 818–823. https://doi.org/10.1038/nature07891

Shubin, N., Tabin, C., Carroll, S., 1997. Fossils, genes and the evolution of animal limbs. Nature 388, 639–648. https://doi.org/10.1038/41710

Singh, S.P., Holdway, J.E., Poss, K.D., 2012. Regeneration of Amputated Zebrafish Fin Rays from De Novo Osteoblasts. Dev Cell 22, 879–886. https://doi.org/10.1016/j.devcel.2012.03.006

Square, T.A., Mackey, E.J., Chen, Z.Z., Sundaram, S., Miller, C.T., 2022. Modulation of tooth regeneration through opposing responses to Wnt and BMP signals in teleosts. bioRxiv.

Stevens, J.R., Miranda-Carboni, G.A., Singer, M.A., Brugger, S.M., Lyons, K.M., Lane, T.F., 2010. Wnt10b deficiency results in age-dependent loss of bone mass and progressive reduction of mesenchymal progenitor cells. Journal of Bone and Mineral Research 25, 2138–2147. https://doi.org/10.1002/jbmr.118

Stewart, S., Gomez, A.W., Armstrong, B.E., Henner, A., Stankunas, K., 2014. Sequential and Opposing Activities of Wnt and BMP Coordinate Zebrafish Bone Regeneration. Cell Rep 6, 482–498. https://doi.org/10.1016/j.celrep.2014.01.010

Stewart, S., Stankunas, K., 2012. Limited dedifferentiation provides replacement tissue during zebrafish fin regeneration. Dev Biol 365, 339–349. https://doi.org/10.1016/j.ydbio.2012.02.031

Stewart, S., Yette, G.A., Le Bleu, H.K., Henner, A.L., Braunstein, J.A., Chehab, J.W., Harms, M.J., Stankunas, K., 2019. Skeletal geometry and niche transitions restore organ size and shape during zebrafish fin regeneration. bioRxiv. https://doi.org/https://doi.org/10.1101/606970

Stoick-Cooper, C.L., Weidinger, G., Riehle, K.J., Hubbert, C., Major, M.B., Fausto, N., Moon, R.T., 2007. Distinct Wnt signaling pathways have opposing roles in appendage regeneration. Development 134, 479–489. https://doi.org/10.1242/dev.001123

Sur, A., Wang, Y., Capar, P., Margolin, G., Farrell, J.A., 2023. Single-cell analysis of shared signatures and transcriptional diversity during zebrafish development. bioRxiv. https://doi.org/https://doi.org/10.1101/2023.03.20.533545

Tornini, V.A., Puliafito, A., Slota, L.A., Thompson, J.D., Nachtrab, G., Kaushik, A.L., Kapsimali, M., Primo, L., Di Talia, S., Poss, K.D., 2016. Live Monitoring of Blastemal Cell

Contributions during Appendage Regeneration. Current Biology 26, 2981–2991. https://doi.org/10.1016/j.cub.2016.08.072

Tsukamoto, M., Wang, K.Y., Tasaki, T., Murata, Y., Okada, Y., Yamanaka, Y., Nakamura, E., Yamada, S., Izumi, H., Zhou, Q., Azuma, K., Sasaguri, Y., Kohno, K., Sakai, A., 2019. Findings as a starting point to unravel the underlying mechanisms of in vivo interactions involving Wnt10a in bone, fat and muscle. Bone 120, 75–84. https://doi.org/10.1016/J.BONE.2018.10.009

Van Den Boogaart, J.G.M., Muller, M., Osse, J.W.M., 2012. Structure and function of the median finfold in larval teleosts. Journal of Experimental Biology 215, 2359–2368. https://doi.org/10.1242/jeb.065615

Walker, M.B., Kimmel, C.B., 2007. A two-color acid-free cartilage and bone stain for zebrafish larvae. Biotechnic and Histochemistry 82, 23–28. https://doi.org/10.1080/10520290701333558

Wang, K.Y., Yamada, S., Izumi, H., Tsukamoto, M., Nakashima, T., Tasaki, T., Guo, X., Uramoto, H., Sasaguri, Y., Kohno, K., 2018. Critical in vivo roles of WNT10A in wound healing by regulating collagen expression/ synthesis in WNT10A-deficient mice. PLoS One 13, 1–18. https://doi.org/10.1371/journal.pone.0195156

Watson, C.J., Joyce Tang, W., Rojas, M.F., Fiedler, I.A.K., de Oca, E.M.M., Cronrath, A.R., Callies, L.K., Swearer, A.A., Ahmed, A.R., Sethuraman, V., Addish, S., Farr, G.H., Gómez, A.E., Rai, J., Monstad-Rios, A.T., Gardiner, E.M., Karasik, D., Maves, L., Busse, B., Hsu, Y.H., Kwon, R.Y., 2022. Wnt16 Regulates Spine and Muscle Morphogenesis Through Parallel Signals From Notochord and Dermomyotome. PLoS Genet 18, 1–30. https://doi.org/10.1371/journal.pgen.1010496

Wehner, D., Cizelsky, W., Vasudevaro, M.D., Özhan, G., Haase, C., Kagermeier-Schenk, B., Röder, A., Dorsky, R.I., Moro, E., Argenton, F., Kühl, M., Weidinger, G., 2014. Wnt/β-Catenin Signaling Defines Organizing Centers that Orchestrate Growth and Differentiation of the Regenerating Zebrafish Caudal Fin. Cell Rep 6, 467–481. https://doi.org/10.1016/j.celrep.2013.12.036

Westerfield, M., 2007. The Zebrafish Book: A Guide for the Laboratory Use of Zebrafish (Danio rerio), 5th ed. University of Oregon Press, Eugene.

Willert, K., Brown, J.D., Danenberg, E., Duncan, A.W., Weissman, I.L., Reya, T., Yates, J.R., Nusse, R., 2003. Wnt proteins are lipid-modified and can act as stem cell growth factors. Nature 423, 448–452. https://doi.org/10.1038/nature01611

Yuan, Q., Zhao, M., Tandon, B., Maili, L., Liu, X., Zhang, A., Baugh, E.H., Tran, T., Silva, R.M., Hecht, J.T., Swindell, E.C., Wagner, D.S., Letra, A., 2017. Role of WNT10A in failure of tooth development in humans and zebrafish. Mol Genet Genomic Med 5, 730–741. https://doi.org/10.1002/mgg3.332

Zhou, H., Mak, W., Zheng, Y., Dunstan, C.R., Seibel, M.J., 2008. Osteoblasts directly control lineage commitment of mesenchymal progenitor cells through Wnt signaling. Journal of Biological Chemistry 283, 1936–1945. https://doi.org/10.1074/jbc.M702687200

FIGURES

Figures 5.1 – 5.6

Table 5.1, Figure S5.1

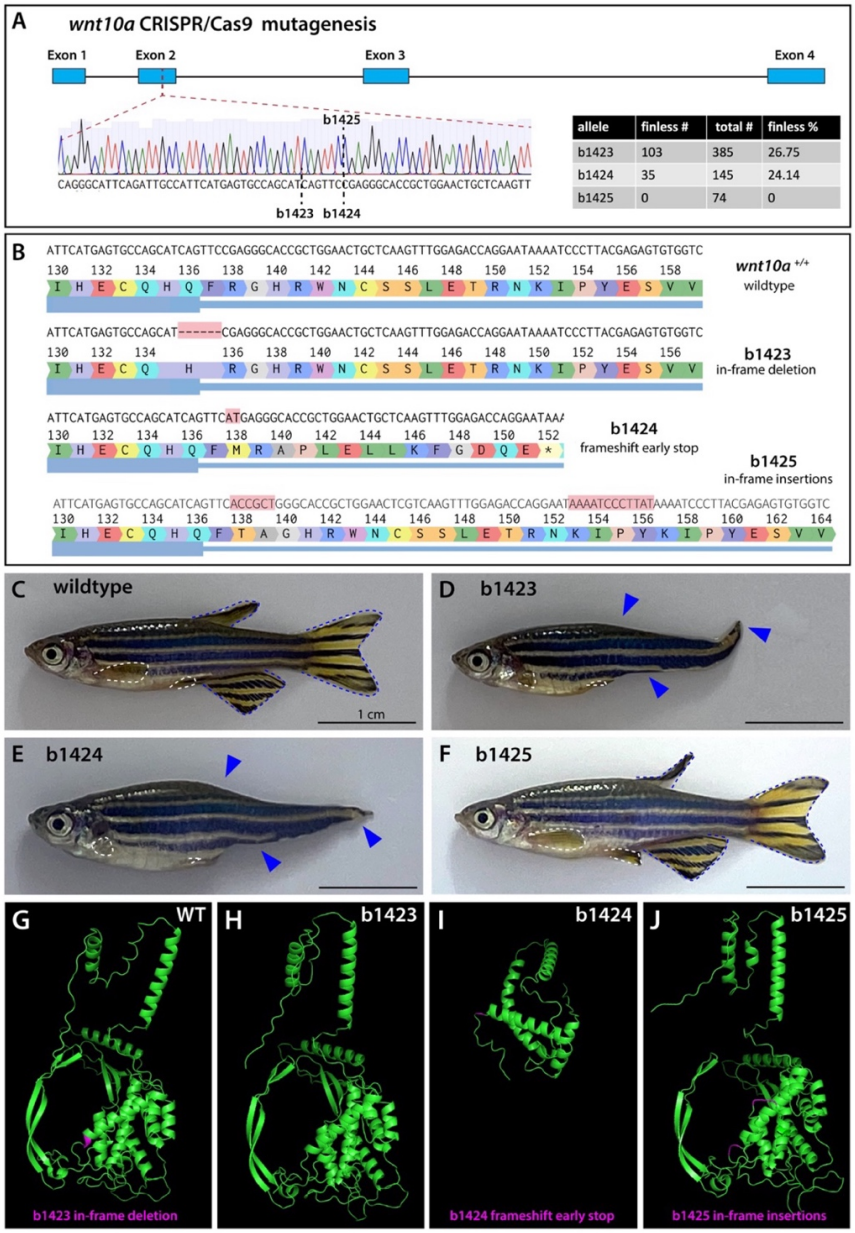

Figure 5.1. Wnt10a is necessary for fin development.

Figure 5.1. Wnt10a is necessary for fin development.

(A) CRISPR mutagenesis schematic for *wnt10a.* Exon 2 was targeted and three alleles generated exhibiting mendelian recessive (b1423, b1424) or no phenotype (b1425, table insert). (B) Exact mutations and amino acid sequences for each allele. (C) Wildtype adult and (D-F) representatives for b1423, b1424, and b1425, respectively. Blue dashed outlines, medial fins. White dashed outlines, paired fins. Blue arrowheads, absent medial fins. (G-J) Predicted protein structures (green) for each allele with mutagenized residues in magenta. (G) The two amino acids deleted in b1423 are highlighted in the wildtype structure as a visual aid as they are absent in (H).

Table 5.1. *wnt10a* alleles generated

Allele	Phenotype	Mutation	Predicted effect	Coding position	Amino acid position	Protein length (AA)
wnt10a $^{+/+}$	Wildtype					441
b1423	Severe fin-reduced	In-frame deletion	Deletion of last two AA in helix A	c.406_411delCAGTTC	p.Q136_F137del	439
b1424	Severe fin-reduced	Frameshift early stop	Truncated protein with early stop in exon 3 at AA152	c.412_413delinsAT	p.R138fs	151
b1425	Wildtype	In-frame insertions	Insertions in disordered region of protein	c.412_417delinsACCGCT c.477_489insAAAATCCCTTAT	p.R138TA p.K153_Y156dup	446

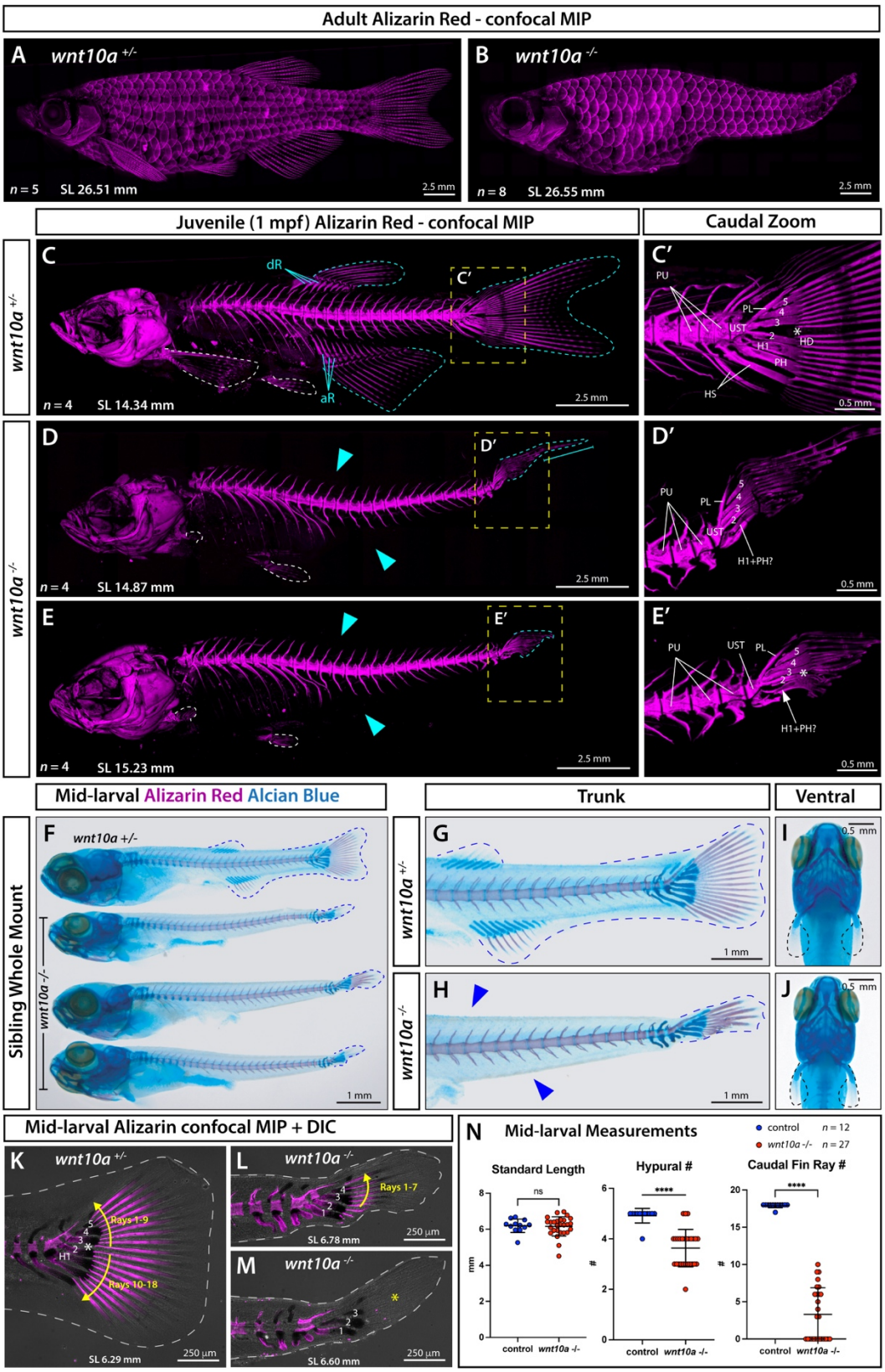

Figure 5.2. *wnt10a* is required for endochondral and dermal fin skeletal elements.

Figure 5.2. *wnt10a* is required for endochondral and dermal fin skeletal elements.

(A, B) Whole mount confocal MIP representative images for adult (A) *wnt10a* heterozygote control (*n* = 5) and (B) homozygous sibling (*n* = 8) representatives with calcified bony elements stained by Alizarin Red. (C-E) Whole mount Alizarin Red confocal MIP for juvenile (C) *wnt10a* heterozygote control (*n* = 3) and (D, E) homozygous sibling representatives (*n* = 3). White dashed lines, paired fins; cyan dashed lines, medial fins; dR, dorsal radials; aR, anal radials. (D) Cyan bracket indicates caudal fin rays. (D, E) Cyan arrowheads indicate absent medial fins and radials. (C'-E') Zoom insets of yellow dashed boxes in (C-E) with the caudal fin endochondral skeleton labeled. HD, hypural diastema (white asterisk); H1, hypural 1 (white arrow); 2-5, hypurals 2-5; PH, parhypural; HS, haemal spines; PL, pleurostyle; UST, urostyle; PU, preural centrum. (F-M) Mid-larval whole mount skeletal preps stained with Alizarin Red for calcified bone and Alcian Blue for cartilage. (F) One *wnt10a* heterozygote and three homozygote siblings with medial fins outlined in blue dashed line. (G, H) Trunk regions of two representatives. Blue arrowheads (H) indicate absent medial fins and radials. (I, J) Ventral view of two representatives with pectoral fin buds outlined in black dashed line. (K-M) Alizarin Red confocal MIP and DIC overlay for 14 dpf (K) heterozygote and (L, M) homozygote siblings. Gray dashed line outlines fin and trunk boundaries. Yellow asterisk (M) indicates absent fin rays. (N) Quantification of 13 and 14 dpf mid-larvae for standard length (SL), hypurals, and calcified fin rays.

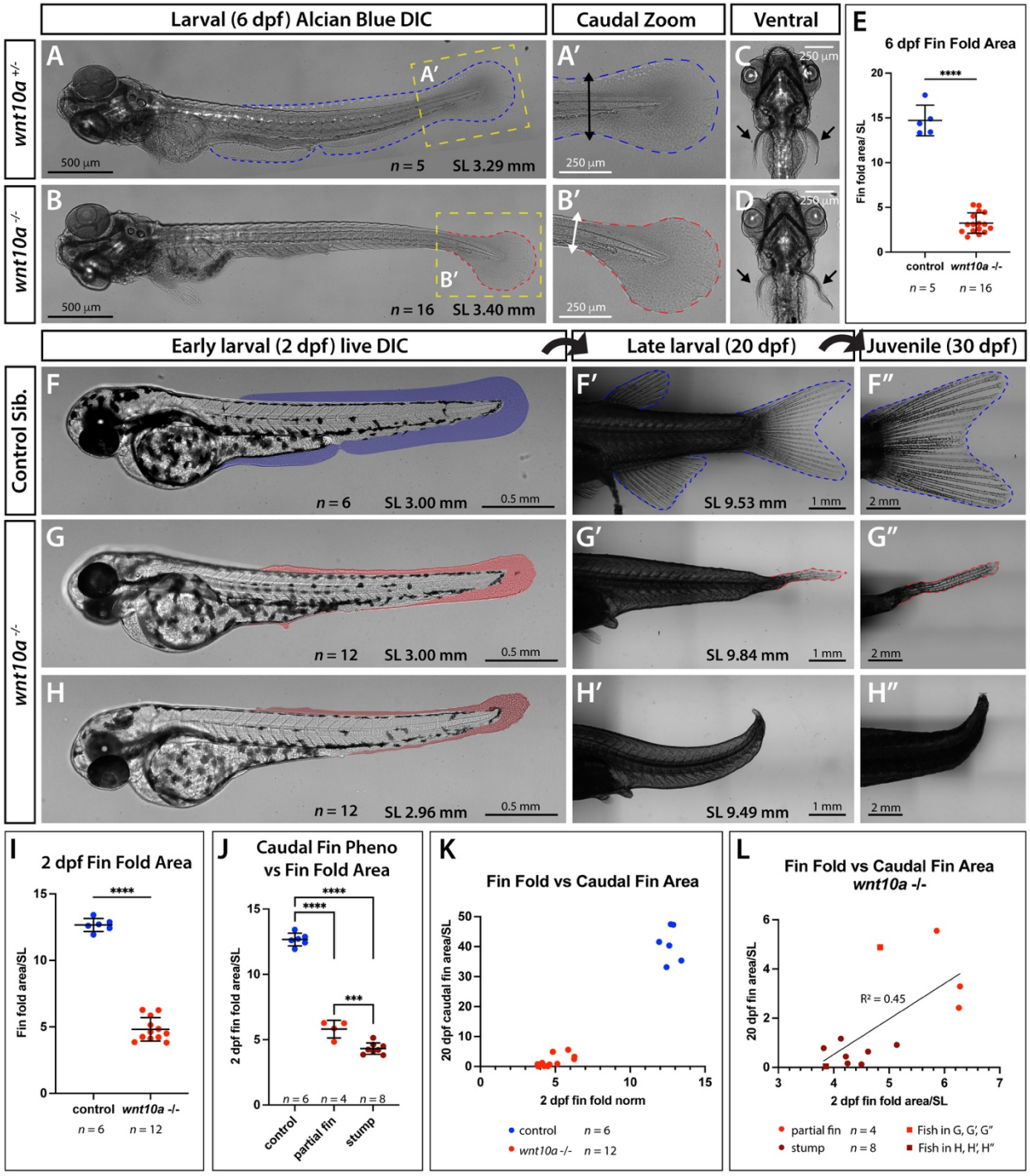

Figure 5.3. Wnt10a promotes larval fin fold formation preceding median fin emergence.

Figure 5.3. Wnt10a promotes larval fin fold formation preceding median fin emergence.

(A-D) 6 dpf fixed larval specimen stained with Alcian Blue for cartilage and imaged by DIC. (A) *wnt10a* heterozygote control (*n* = 5) with medial fin fold outlined in dashed blue and (B) homozygous representative (*n* = 16) with reduced fin fold outlined in red. (A', B') Zoom region of yellow dashed boxes in (A, B). (A') The fin fold extends on both sides of the notochord in controls (black arrows) but (B') tapers away in mutants (white arrows). (C, D) Ventral view shows no obvious difference in the developing pectoral fins (black arrows). (E) Quantification of fin fold normalized to standard length (SL). (F-H) Representative 2 dpf siblings (*n* = 6 control and *n* = 12 *wnt10a -/-*) live imaged by DIC and individually tracked to (F'-G') 20 dpf late larval stage and (F"-G") 30 dpf juvenile stage. Blue shading (F) indicates control fin fold area, red shading (G) indicates reduced fin fold area, and dark red shading (H) indicates severely reduced fin fold area. (F'-H") Blue dashed lines denote control medial fin area and red dashed lines denote partial caudal fin area. Black curved block arrows between age panels indicate the same individual fish tracked and re-imaged over time. (I) Quantification of 2 and 20 dpf fin fold area and caudal fin area, respectively, shown normalized to standard length (SL) and as a linear regression.

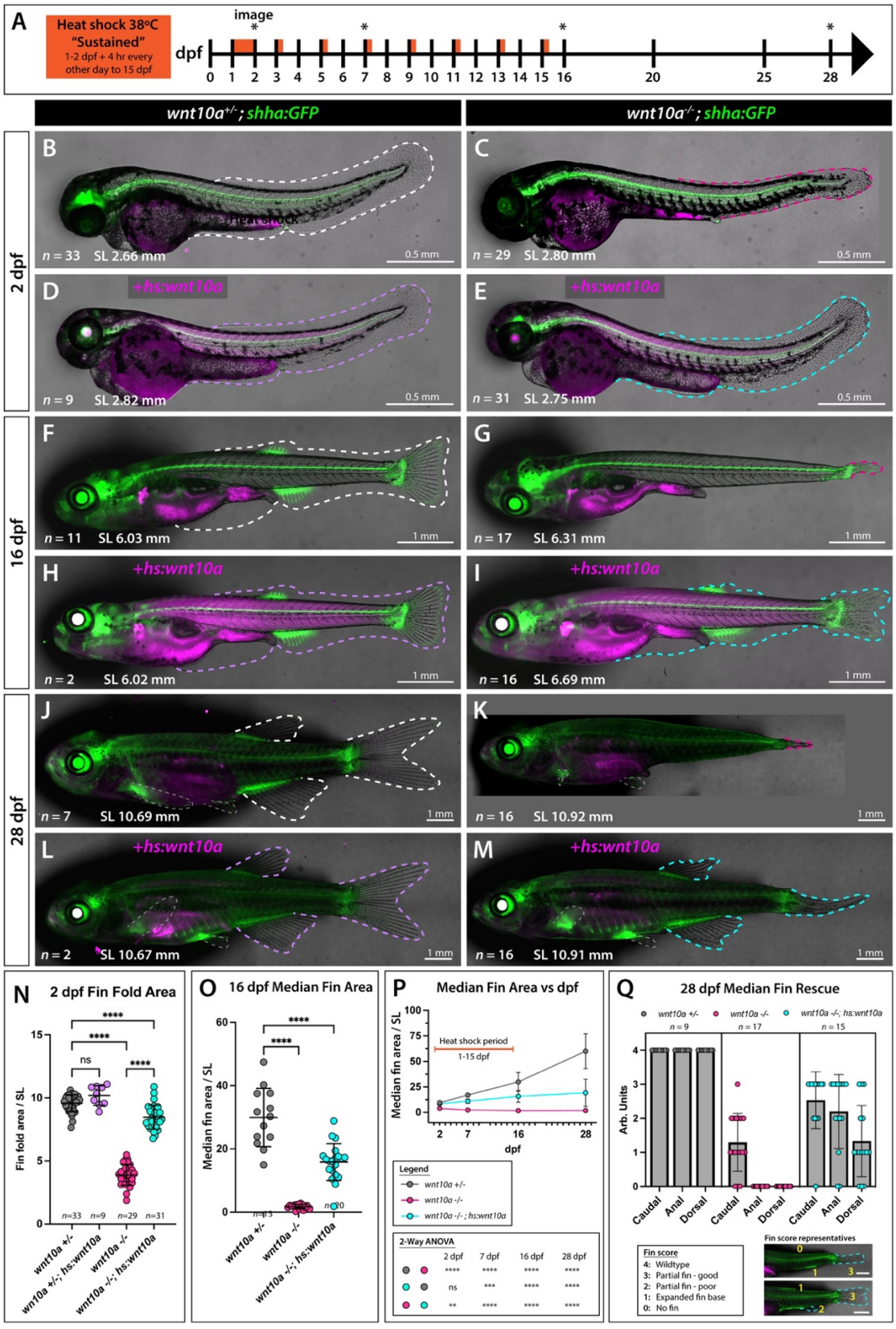

Figure 5.4. Embryonic *wnt10a* expression rescues fin fold and median fin development.

Figure 5.4. Embryonic *wnt10a* expression rescues fin fold and median fin development.

(A) Experimental schematic. IVF-derived clutches were heat shocked from 1-2 dpf and for 4 hours every other day until 15 dpf. Fish were imaged at 2, 7, 16, and 28 dpf. (B-E) Representative 2 dpf larvae for (B, D) *wnt10a* +/- controls or (C, E) *wnt10a* -/- mutants in the absence (B, C) or presence of *hs:wnt10a* (D, E) following 24 hours of heat shock at 38°C. (B) Wildtype fin fold outlined in dashed white. (C) Reduced fin fold outlined in dashed magenta. (D) Wildtype fin fold in *hs:wnt10a* background outlined in dashed lavender. (E) Rescued *wnt10a* -/- fin fold in *wnt10a* background outlined in dashed cyan. (F-I) Representative 16 dpf mid-larvae with the same dashed outline scheme. *shha:GFP* (green) marked emerging fin structures. (J-M) Representative 28 dpf juveniles with the same dashed outline scheme and paired fins outlined in thin dashed gray. (N) Quantification of fin fold area normalized to Standard Length (SL) at 2 dpf and at (O) 16 dpf with One-Way ANOVA significance denoted. (P) Longitudinal quantification of fin fold or median fin area normalized to SL over time with Two-Way ANOVA significance shown. Orange brackets indicate duration of heat shock. (Q) Characterization of fin rescue at 28 dpf.

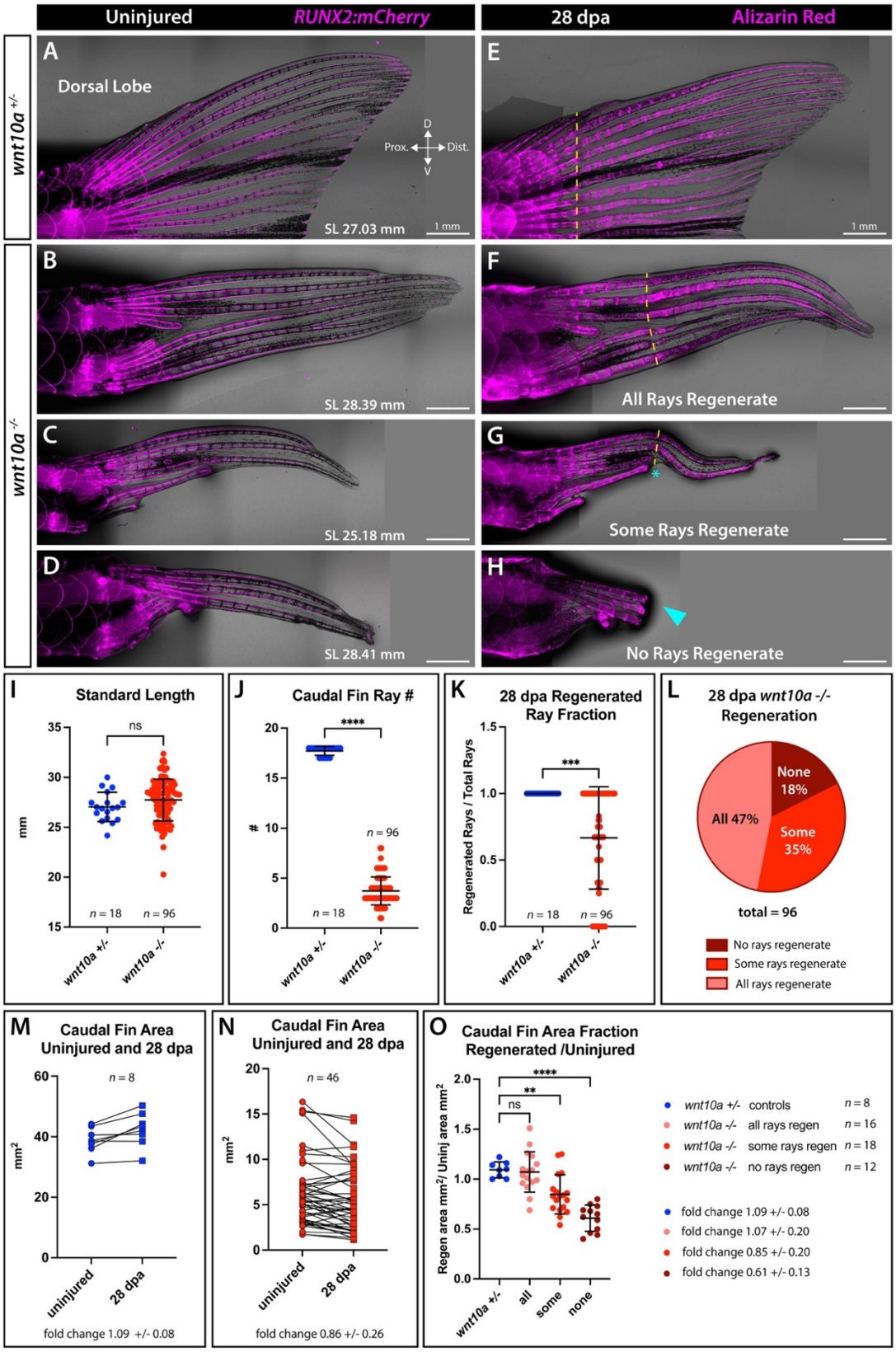

Figure 5.5. Variable regenerative capacity of *wnt10a* mutants.

Figure 5.5. Variable regenerative capacity of *wnt10a* mutants.

(A-D) Representative *wnt10a* heterozygote (A) and (B-D) homozygous mutant adult clutch mates in *RUNX2:mCherry* (magenta) transgenic background. Uninjured caudal fins are overlaid in brightfield. (E-H) The same fish shown in (A-D) at 28 dpa and stained with Alizarin Red (magenta) to visualize the skeleton in more detail. Yellow dashed lines indicate plane of amputation. Cyan asterisk (G) indicates a ray which did not regenerate. Cyan arrow (H) indicates failure of any rays to regenerate. (I) Standard length and (J) Caudal fin ray number for *wnt10a* heterozygotes (blue, $n = 18$) and homozygous mutants (red, $n = 96$). (K) Fraction of regenerated rays over total number of caudal fin rays. (L) Regenerative variability of *wnt10a -/-* mutants. Pink, red, and dark red indicate fish where all, some, or no caudal fin rays regenerated, respectively. (M-O) Quantification for a subset of fish ($n = 8$ heterozygotes and $n = 46$ *wnt10a -/-* mutants) that were individually tracked to 28 dpa. (M) Change in caudal fin area from uninjured heterozygotes controls (blue circles) to 28 dpa (blue squares). Lines connect data from individual fish. (N) Change in caudal fin area for *wnt10a -/-* mutants from uninjured (red circles) to 28 dpa (red squares) with lines connecting data from individual fish. (O) Fraction of 28 dpa regenerated caudal fin area divided by the uninjured caudal fin area for individual fish. Blue circles indicate *wnt10a* +/- controls ($n = 8$); pink circles indicate *wnt10a -/-* in which all rays regenerated ($n = 16$); red circles indicate *wnt10a -/-* in which some rays regenerated ($n = 18$); and dark red circles indicate *wnt10a -/-* in which no rays regenerated ($n = 12$).

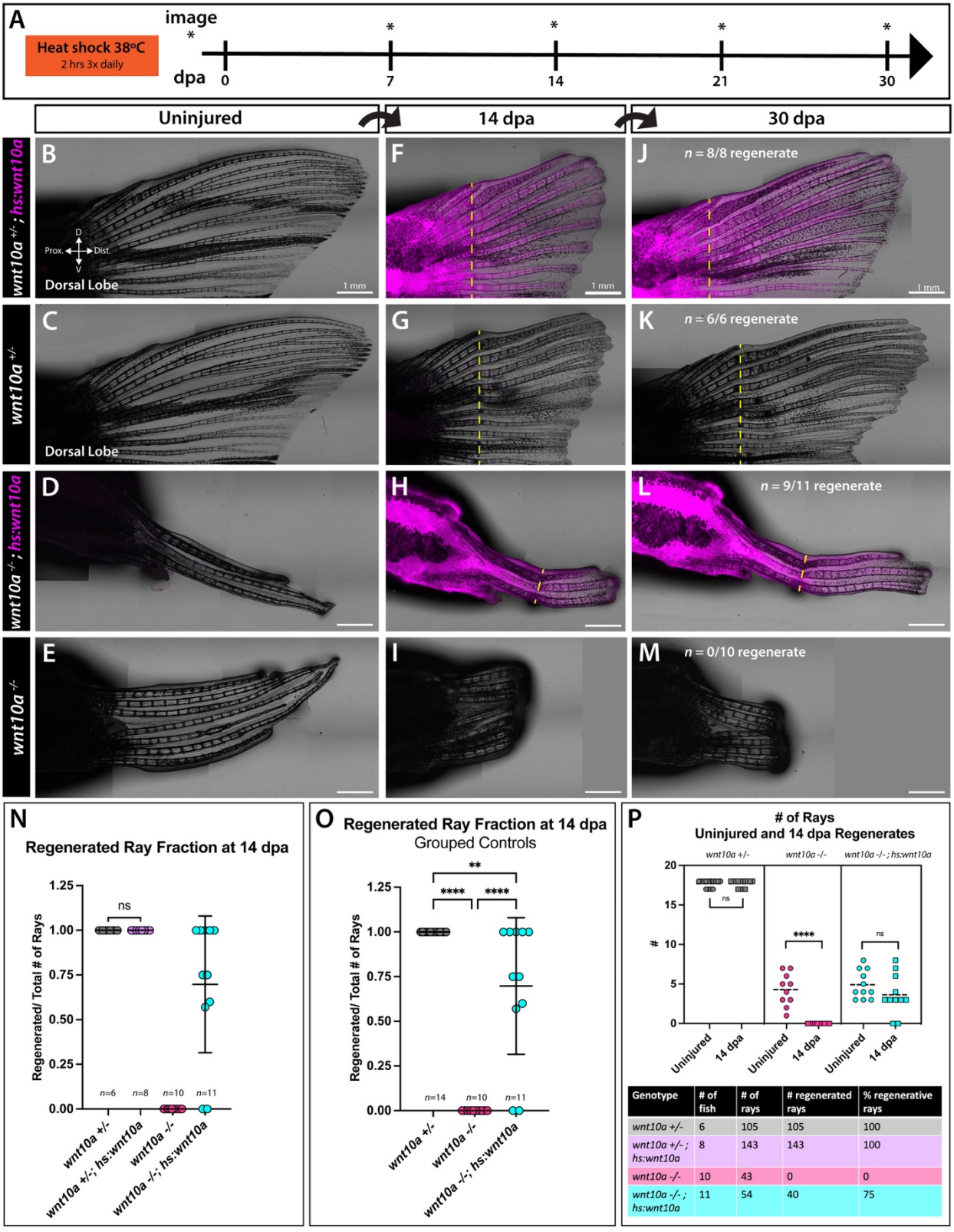

Genotype	# of fish	# of rays	# regenerated rays	% regenerative rays
wnt10a +/-	6	105	105	100
wnt10a +/- ; hs:wnt10a	8	143	143	100
wnt10a -/-	10	43	0	0
wnt10a -/- ; hs:wnt10a	11	54	40	75

Figure 5.6. *wnt10a* expression rescues fin regeneration deficiency.

Figure 5.6. *wnt10a* expression rescues fin regeneration deficiency.

(A) Experimental schematic. Caudal fins were amputated and fish heat shocked at 38°C for 2 hours 3x daily for 30 days. Images were acquired prior to amputation and weekly. (B-E) Representative clutch mate uninjured caudal fins for controls (B) *wnt10a*$^{+/-}$*; hs:wnt10a,* (C) *wnt10a*$^{+/-}$ and partial caudal fin *wnt10a* mutants (D) *wnt10a*$^{-/-}$*; hs:wnt10a,* (E) *wnt10a*$^{-/-}$. (F-I) The same fish in (B-E) imaged at 14 dpa. Yellow dashed lines indicate the plane of amputation. (J-M) The same fish in (B-E) and (F-I) imaged at 30 dpa. No *wnt10a*$^{-/-}$ partial caudal fins regenerated (M), whereas n = 9/11 *wnt10a*$^{-/-}$*; hs:wnt10a* partial caudal fins regenerated. (N) Regenerated ray fraction for all groups. Heterozygote *wnt10a* controls regenerate their rays with (n = 8) or without (n = 6) *hs:wnt10a.* Statistics are by one-way ANOVA. (O) Regenerated ray fraction with *wnt10a* heterozygote groups combined. Statistics are by one-way ANOVA. (P) Number of rays in uninjured fins (circles) and regenerated rays at 14 dpa (squares). Statistics are student's t-test. Table indicates how many rays were quantified per genotype and their regenerative %.

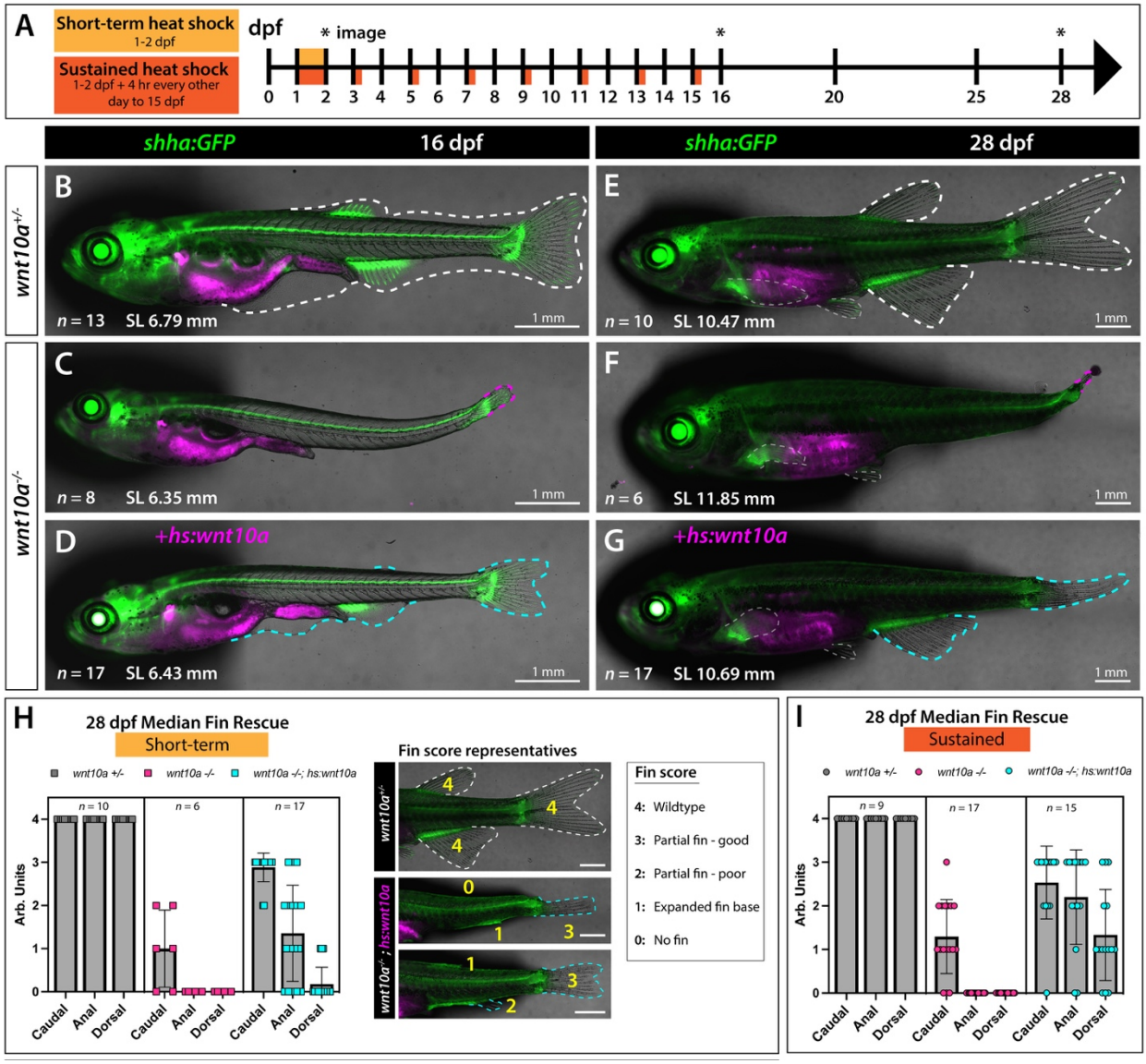

Figure S5.1. 1-2 dpf *wnt10a* expression is sufficient for partial fin rescue.

(A) Experimental schematic. Larvae were heat-shocked at 38°C for 24 hours from 1-2 dpf (this figure, light orange) or from 1-2 dpf + 4 hours every other day until 15 dpf (Figure 4, dark orange). Asterisks mark imaging timepoints of 2, 16 and 28 dpf. (B-G) Whole mount DIC overlay with *shha:GFP* (green) marking emerging fin structures and *hs:wnt10a* in magenta. Representative controls (B, E) heterozygous for *wnt10a* +/- or (C, D, F, G) homozygous for *wnt10a* -/- are shown at (B-D) 16 dpf mid-larval stage and (E-G) 28 dpf juvenile stage. Wildtype medial fin area outlined in (B, E) dashed white, reduced *wnt10a* -/- median fin area outlined in dashed magenta, and rescued *wnt10a* -/- medial fin area in *hs:wnt10a* background outlined in dashed cyan. (E-G) Paired fins outlined in thin dashed gray. (H) Median fin rescue at 28 dpf for 1-2 dpf heat shock group (squares). Examples of fin scoring included for reference with scores in yellow. (I) Median fin rescue at 28 dpf for 1-2 dpf heat shock + 4 hours every other day until 15 dpf group (circles).

BRIDGE TO CHAPTER VI

This chapter demonstrates *wnt10a* is separately required for median fin development and caudal fin regeneration. We found deleting two conserved amino acids implicated in Frizzled receptor binding (*wnt10a*^{b1423}) phenocopies an insertion-deletion frameshift early stop mutation (*wnt10a*^{b1424}). This finding may inform Wnt signaling mechanics in other contexts and organisms. *wnt10a* mutants completely lack median dorsal and anal fin endo- and dermal skeletons and have drastically reduced but variable caudal fin skeletons. We found median fin establishment could be traced to as early as 2 dpf defects in the median fin fold. Ubiquitous expression of *wnt10a* from 1-2 dpf using a heat shock inducible transgenic line rescued median fin fold area and partially rescues fin development. Separately, we found *wnt10a* mutants with partial caudal fins exhibited variable regenerative capabilities that were again rescued by heat shock *wnt10a* expression. These findings represent novel understanding of a specific canonical Wnt and may inform future understanding of shared mechanisms between fin development and regeneration. The next chapter examines the specific effects of *wnt10a* on *shha* expression and caudal fin ray branching.

CHAPTER VI: WNT10A ACTIVATES BASAL EPIDERMAL SONIC HEDGEHOG A EXPRESSION TO INITIATE ZEBRAFISH FIN RAY BRANCHING

In preparation (style of Developmental Biology)

Co-authored material to be published as Robbins, A.E[1,2].; Braunstein, J. A[1,2]; O'Hara-Smith, J[1,2]; Square, T.A[3]; Miller, C. T[3]; Stewart, S[1]; and Stankunas, K[1,2].

AUTHOR CONTRIBUTIONS

Amy E. Robbins[1,2] conceived of the study and performed all experiments. Joshua A. Braunstein[1,2] contributed intellectually during the study design and conducted preliminary experiments. Johnathan O'Hara-Smith[1,2] assisted with experiments and mutant husbandry. Tyler A. Square[3] and Craig T. Miller[3] generated the inducible transgenic *wnt10a* line. Scott J. Stewart[1] and Kryn Stankunas[1, 2] supervised the project. Amy E. Robbins wrote the manuscript with editorial assistance from Kryn Stankunas.

1Institute of Molecular Biology
2Department of Biology
University of Oregon
273 Onyx Bridge
1318 Franklin Blvd
Eugene, OR 97403-1229
Office: (541) 346-7416
Fax: (541) 346-4854

3Department of Molecular & Cell Biology
University of California, Berkeley

INTRODUCTION

The caudal fin of zebrafish (*Danio reiro)* is an accessible and tractable model to investigate mechanisms of appendage development and innate regeneration. Deep conservation of genetic and molecular pathways across vertebrates, including Sonic hedgehog (Shh) and Wnts, make basic research advances in studying zebrafish fins applicable to understanding developmental, disease, and injury states in humans (Goodrich et al., 1996; Marí-Beffa et al., 2007; Marigo et al., 1996; Shubin et al., 2009). Conversely, the evolutionary distance between teleost zebrafish and high-order mammals can reveal ancient regulatory mechanisms lost in tetrapods. For example, the caudal fin and paired pectoral fins share many of the same skeletal patterning mechanisms. Yet, the caudal fin is more ancestral than the paired fins, which are the evolutionary precursors to limbs (Letelier et al., 2021; Nakamura et al., 2016; Shubin et al., 1997). Therefore, the zebrafish caudal fin is a valuable model to uncover mechanisms of skeletal growth and regeneration and provide insight into how evolutionary cooption of conserved genetic modules functions between diverse species.

The zebrafish caudal skeleton comprises endochondral bones on the distal end of the body and associated dermal fin rays that are deposited as a secreted bony matrix. The fin rays sequentially emerge around a central organizer to form the homocercal dorsal and ventral lobes of the caudal fin (Desvignes et al., 2022; Marí-Beffa and Murciano, 2010). Each ray is formed of two hemi-cylindrical halves (hemi-rays) segmented by joints. Vasculature, nerves, and fibroblasts, osteoblasts populate the intra-ray space. The typically 18 caudal fin rays form a stereotyped branching pattern. While the principal peripheral rays (1 and 18) do not branch, the inner ray field undergoes staggered branching morphogenesis to support the growing fin. Unlike

mammalian skeletal appendage patterning which occurs early in development, fin ray branching begins at the onset of the juvenile stage around 30 days-post-fertilization (~ 15 mm standard length, SL) (Kimmel et al., 1995; Parichy et al., 2009). The long peripheral rays (2 and 17) are the first to branch, and the innermost, shortest medial rays (9 and 10) are the last. In regenerating adult fins, rays begin to form from a proliferative blastema between 2-4 days-post-amputation. Regenerated branch points can be observed around 5-10 dpa depending on the site of amputation and size of the fish. Regeneration slows between 14-21 dpa and the fin restores its original size, shape, and pattern by 28 dpa (Chen et al., 2015; Nechiporuk and Keating, 2002; Poss et al., 2000a; Shibata et al., 2018).

The Sonic hedgehog (Shh) signaling pathway is conserved across vertebrates and has long been associated with limb and digit specification (Chiang et al., 2001; Letelier et al., 2021; Marigo et al., 1996; Riddle et al., 1993). In the caudal fin, the zebrafish ortholog *shha* is expressed in discrete basal epidermal domains overlying pOb regions in the fin's distal outgrowth zone (Laforest et al., 1998; Quint et al., 2002). Our lab previously found Shha is specifically required for ray branching, but not fin outgrowth (Armstrong et al., 2017). Disrupting the Shh pathway by inhibiting its downstream target Smoothened (Smo) results in unbranched rays during development and regeneration. Moreover, we found Shh-mediated fin ray branching is conserved in all seven zebrafish fin appendages: the three median fins (caudal, anal, and dorsal) and four paired fins (pectoral and pelvic) (Braunstein et al., 2021). Finally, Shh-mediated ray branching occurs short-range between *shha*-expressing basal epidermal cells and underlying immature bone separated only by a thin basement membrane. Our model of *shha*-directed ray branching is in stark contrast to classical understanding of Shh acting as a long-range morphogen to specify

digits in limbs (Marigo et al., 1996; Riddle et al., 1993; Shubin and Alberch, 1986; Tickle, 2017). Therefore, we have identified a novel context to investigate skeletal patterning wherein Shha expressed in skin instructs the movement of underlying immature bone (pre-ostoblasts, pObs). However, the fundamental question of how *shha* is transiently activated in migratory basal epidermal cells as they near pObs is unresolved.

We questioned what molecule acts directly upstream of *shha* and therefore ray branching morphogenesis. *shha* is transcriptionally activated only when basal epidermal cells are in close proximity to pObs, thus we assessed what signals are active in pOb regions. The Wnt family of secreted proteins is highly active during fin regeneration and inhibition of Wnt signaling blocks regenerative outgrowth. Specifically, canonical Wnt/β-catenin signaling has been shown regulate numerous signaling pathways including Shh (Stewart et al., 2014; Stoick-Cooper et al., 2007; Wehner et al., 2014). We found low levels of Wnt inhibition induced skeletal pattering defects in regenerating fins including unbranched rays but did not perturb fin outgrowth. We next identified Wnt/β-catenin signaling in basal epidermal cells next to pObs. We identified *wnt10a* as a candidate *shha*-activating canonical Wnt due to its high expression in pOb regions of regenerating fins. Assessment of *shha* expression using the *Tg(-2.4shha:gfpABC)*^{sb15} reporter line (Ertzer et al., 2007; Zhang et al., 2012) in our previously generated *wnt10a*^{b1423} mutant (unpublished, see Chapter V) revealed Shha:GFP was expressed in various organs known to be patterned by Shh but was notably absent from caudal fin rays. We assessed the partial caudal fins of *wnt10a* mutants with the *shha:GFP* reporter line and found Shh:GFP to be mosaic or absent in distal fin ray regions. Correspondingly, *wnt10a* mutant fin rays almost never branched. The fraction of branched rays was further reduced in caudal fin regenerates. Ubiquitous *wnt10a*

expression induced by *Tg(hsp70l:mCherry-2A-wnt10a)*^{bk409Tg} (Square et al., 2022) in *wnt10a* mutants both rescued Shha:GFP expression and ray branching. We conclude *wnt10a* promotes basal epidermal *shha* expression to direct ray branching morphogenesis.

RESULTS

Wnt signaling contributes to caudal fin skeletal patterning

Wnt signaling is a master orchestrator of caudal fin regeneration and pan-Wnt inhibition fully arrests regeneration (Stoick-Cooper et al., 2007; Wehner et al., 2014). We previously noted low doses of the pan-Wnt secretion small molecule inhibitor Wnt-C59 (Proffitt et al., 2013) appear to allow regenerative outgrowth but show skeletal ray defects (Stewart et al., 2019). We therefore sought to isolate skeletal patterning specific effects of Wnt signaling through titration of Wnt-C59 inhibition. We treated regenerating caudal fins across a range of low-dose pan-Wnt inhibition (Wnt-C59 2-10 nM) from 2-14 days-post-amputation. Alizarin Red visualization of calcified bone (Walker and Kimmel, 2007) showed 8 nM Wnt-C59 as a dose inhibitory to ray branching morphogenesis yet fully permissive to regenerative outgrowth (n = 9) (Figure 6.1A, B). Typical (100 nM Wnt-C59) treatment over the same 2-14 dpa timeline completely inhibited outgrowth (n = 6; Fig 6.1C), and we observed no significant difference in the length of representative dorsal rays 1, 3, and 9 relative to DMSO controls (n = 6; Figure 6.1D; expanded data in Figure S6.1). Fin ray abnormalities in 8 nM Wnt-C59 treated fins included unbranched rays, disrupted branching in rays and curved medial rays (Figure 6.1B, B'; expanded data in S6.1). Thus, we conclude low levels of Wnt inhibition disrupt skeletal pattern independent of Wnt contributions to regenerative outgrowth.

Wnt/β-catenin signaling is active in the basal epidermis

Wnt/β-catenin signaling acts upstream of *shha* during fin regeneration, but which Wnts(s) are involved have not been elucidated (Wehner et al., 2014). After we confirmed independent roles for Wnt signaling during regenerative outgrowth and fin skeletal patterning, we next sought to identify specific Wnts functioning upstream of Shh expression and thus skeletal patterning. We first confirmed Wnt/β-catenin activity in the distal blastema through RNAscope visualization of the downstream activity marker *axin2.* This showed strong expression in the intra-ray mesenchyme, pre-osteoblasts (pOb) and basal epidermis in 4 dpa regenerating fin sections (Figure 6.2A, A'). Additionally, immunostaining showed nuclear localization of β-catenin in basal epidermal cells adjacent to pObs that was lost following 4-hour 300 nM Wnt-C59 treatment (n = 3; Figure 6.2B, C). These data indicate Wnt/β-catenin is active in a subset of basal epidermal cells in the distal blastema.

We next aimed to visualize putative *shha*-activating canonical Wnts in a *shha* and *runx2* double reporter background. The *Tg(-2.4shha:gfpABC)*^{sb15} line, hereafter referred to as *shha:GFP,* recapitulates endogenous *shha* expression (Armstrong et al., 2017; Ertzer et al., 2007; Zhang et al., 2012) while the *Tg(RUNX2:mCherry)* line marks *runx2*-expressing pObs (Barske et al., 2020). We selected *wnt10a* as a strong candidate due to previously reported expression data in the distal regenerating fin (Grotek et al., 2013; Stoick-Cooper et al., 2007; Takayama et al., 2018) and our own RNAseq analysis which identified *wnt10a* as the highest expressed predicted Wnt/ β-catenin ligand in distal fin regenerates (Stewart et al., 2019) . RNAscope *in situ* hybridization showed *wnt10a* mRNA prominently expressed in pObs regions adjacent to Shh+

basal epidermal cells, although *wnt10a* puncta were not exclusive to this region (Figure 6.2D). This suggests *wnt10a* expressed by pObs may activate *shha* in neighboring basal epidermal cells as they migrate through the distal outgrowth region.

Shha is downstream of Wnt/β-catenin signaling

Our data and prior studies indicate Wnt/β-catenin signaling modulates Shh expression during regeneration (Stewart et al., 2014; Stoick-Cooper et al., 2007; Wehner et al., 2014). We therefore tested if modifying Wnt/β-catenin signaling during fin regeneration *in vivo* impacted *shha:GFP* expression. We first tested the sufficiency of Wnt/β-catenin signaling to upregulate *shha:GFP* expression lithium chloride (LiCl) treatment, a well-characterized GSK3β agonist in zebrafish (Clément-Lacroix et al., 2005; Klein and Meltont, 1996; Ross and Bonner, 2012; Siebel et al., 2014; Xia et al., 2017; Zhong et al., 2009). 24-hour treatment with 25 mM LiCl from 4-5 dpa in *shha:GFP;RUNX2:mCherry* fish (n = 7) showed expanded GFP domains relative to 25 mM NaCl controls (n = 7) (Figure 6.3A, B). We quantified the number of GFP+ cells in Dorsal Ray 3 using IMARIS confocal reconstruction which confirmed LiCl treatment expanded Shha:GFP-expressing cell domains (Figure 6.3E, F, I).

We next inhibited Wnt/β-catenin activity through heat shock overexpression of *dickkopf WNT signaling pathway inhibitor 1b* (*dkk1b*) using the *Tg(hsp70l:dkk1b-GFP)*^{w32} line (hereafter referred to as *hs:dkk1b*) (Stewart et al., 2014; Stoick-Cooper et al., 2007). Heat shock treatment in the triple transgenic background (*shha:GFP;RUNX2:mCherry;hs:dkk1b)* from 4-5 dpa showed severely reduced domains of GFP+ cells (n = 5) relative to *hs:dkk1b*- clutch mate controls (n = 4) (Figure 6.3C, D, C', D'). Correspondingly, quantifying the number of GFP+

cells in Dorsal Ray 3 demonstrated *hs:dkk1b+* had significantly fewer GFP+ cells compared to control animals. Collectively, this demonstrates *shha:GFP* expression is activated by and dependent upon Wnt/β-catenin signaling.

wnt10a contributes to _shha_ expression in the caudal fin and ray branching

We recently generated the zebrafish *wnt10a*^{b1423} allele which exhibits a dramatic reduction of the median fins in a homozygous recessive manner. The majority (60%) of *wnt10a*^{b1423} mutants (henceforth *wnt10a*$^{-/-}$) do not form caudal fins, but a minority (40%, n = 139/421) form partial caudal fins with up to 8 rays (unpublished data, Chapter V). We crossed *wnt10a*$^{-/-}$ to the *shha:GFP* reporter line to determine effects of *wnt10a* on *shha* expression. At late larval stages (21 dpf, SL ~ 8 mm) when fish are semi-transparent, *shha:GFP* was visible in both *wnt10a*$^{+/-}$ control siblings (n = 5) and *wnt10a*$^{-/-}$ mutants in various organs known to be patterned by Shh including the eye, forebrain, and spine (Figure S6.2 A-C) (Ertzer et al., 2007; Reimer et al., 2009; Shkumatava et al., 2004; Wullimann and Umeasalugo, 2020). However, *wnt10a*$^{-/-}$ partial caudal fins predominantly lacked *shha:GFP* expression (Figure S6.2 D-F) consistent with our prediction that *wnt10a* activates Shh expression in the fin. Interestingly, we did observe the majority of *wnt10a*$^{-/-}$ mutants showed some GFP expression in the pectoral fins (n = 7/10), although reduced compared to heterozygote controls (Figure S6.2 A-C). From this we conclude *wnt10a* is required for caudal fin-specific *shha* expression and contributes to *shha* expression in paired fins as well.

We next examined caudal fins from a single clutch of *shha:GFP* two month-post-fertilization (mpf) adults. Out of n = 111 *wnt10a*$^{-/-}$ mutants, n = 50 (45%) had partial caudal fins, defined as

the length of the longest fin ray in mutants being at least 30% the length of the longest ray of sibling controls. We examined these 50 partial caudal fins along with $n = 10$ *wnt10a*$^{+/-}$ control siblings. Controls had an average of 18 caudal fin rays with Shha:GFP domains at the end of each ray (Figure 6.4A, J, K). (Braunstein et al., 2021; Laforest et al., 1998; Marí-Beffa and Murciano, 2010; Murciano et al., 2001; Zhang et al., 2012). Partial caudal fins of *wnt10a*$^{-/-}$ mutants had an average of 4 rays and exhibited sporadic, diminished Shha:GFP expression (Figure 6.4B, C, K). Finally, only 11% (n = 50) *wnt10a*$^{-/-}$ caudal fin rays branched relative to 75% (n = 10) in heterozygous controls at 2 mpf (Figure 6.4B, C, L, O).

Adult caudal fins have comparatively few *shha*-expressing cells in distal ray regions as fin outgrowth has slowed. To better understand how *wnt10a* affects *shha* expression, we amputated control caudal fins ($n = 10$) and *wnt10a*$^{-/-}$ partial caudal fins ($n = 50$) to visualize *shha:GFP* expression during regeneration. At 3 dpa, Shha:GFP domains in the distal regenerate split immediately prior to the onset of ray branching (Figure 6.4D, D') (Armstrong et al., 2017; Laforest et al., 1998; Zhang et al., 2012). However, *wnt10a*$^{-/-}$ regenerating fins exhibited mosaic Shha:GFP similar to their non-regenerative expression profiles (Figure 6.4E, E', F, F'). At 28 dpa, control fins fully regenerated (Figure 6.4G) with all rays ending in Shha:GFP domains and an average of 15 branched rays (87%) (Figure 6.4M,N, O). We interpret the increase in the fraction of branched rays due to the growth of the fish between 2-3 mpf. However, only 3% of *wnt10a*$^{-/-}$ partial caudal fins branched ($n = 5/162$) during regeneration in contrast to 11% during development (Figure 6.4H, I, M, N, P). These results demonstrate *wnt10a* promotes caudal fin ray *shha* expression and downstream ray branching.

Caudal fin rays of *wnt10a*$^{-/-}$ mutants are competent to express *shha* and branch

We next questioned if the compounded regenerative defects to *shha* expression could be ameliorated by ectopic addition of *wnt10a*. We assessed this using a new *Tg(hsp70l:mCherry-2A-wnt10a)*^{bk409Tg} line which conditionally expresses *wnt10a* and mCherry upon heat shock (herafter *hs:wnt10a*) (Square et al., 2022). We evaluated a clutch of *shha:GFP* adults of either *wnt10a*$^{+/-}$ or *wnt10a*$^{-/-}$ genotype, with and without the *hs:wnt10a* transgene (Figure 5). Uninjured caudal fins of *wnt10a*$^{+/-}$*; shha:GFP; hs:wnt10a* controls (*n* = 7) had an average of 18 total rays and 15 branched (Figure 6.5A), as did their *wnt10a*$^{+/-}$*; shha:GFP* siblings (*n* = 3) (Figure 6.5G; Table 6.1). All *wnt10a*$^{+/-}$ controls expressed small Shha:GFP domains at the distal end of each ray (Figure 6.5A, G; Table 6.1). Mutant *wnt10a*$^{-/-}$*; shha:GFP; hs:wnt10a* caudal fins (*n* = 7, Figure 6.5B, C) had an average of 6 rays, none of which branched or expressed Shha:GFP (Figure 6.5, Table 6.1). Again this was consistent with their *wnt10a*$^{-/-}$*; shha:GFP* siblings (Figure 6.5H; Table 6.1), confirming the presence of the *hs:wnt10a* transgene does not affect caudal skeletal development in the absence of heat shock induction. Somewhat unexpectedly, following amputation and 30-day heat shock induction both *hs:wnt10a*+ (*n* = 6, avg. 10/18 branched rays, 56%) (Figure 6.5D, K; Table 6.2) and *hs:wnt10a*- non-mutant animals (Figure 6.5I, K) regenerated all their rays yet with fewer branch points (*n* = 3 avg. 13/18 branched rays, 74%) (Figure 6.5D, K; Table 6.2). Interestingly, we observed rays that seemed to branch but the daughter rays stayed close together instead of separating laterally (Figure 6.5D', D"). This suggests heat shock stress and/or reduced speed of water flow in our system may induce skeletal patterning defects alone.

Regardless, we observed a dramatic response to heat shock in *wnt10a*$^{-/-}$ mutants. Mutants without the *hs:wnt10a* transgene completely failed to regenerate any caudal fin rays (n = 5/5) (Figure 6.5 J; Table 6.2). However, *wnt10a*$^{-/-}$*; shha:GFP; hs:wnt10a* mutants (n = 5/5) all regenerated. 15/19 rays expressed Shha:GFP (79%) (Figure 6.5E, F, E', F'; Table 6.2) and 11/19 (58%) had fully or partially branched (e.g., rays bifurcated and then re-fused) (Figure 6.5E', F", K; Table 6.2). Notably, we observed a ray with both primary and secondary bifurcations at 30 dpa where the uninjured fin had none (Figure 6.5C, F-F"). These data indicate that while heat shock stress destabilizes skeletal pattern for control fish, sustained ubiquitous *wnt10a* expression in *wnt10a*$^{-/-}$ mutants promotes *shha* activity and ray branching.

DISCUSSION

In the present study, we investigated how *shha* is transcriptionally activated in basal epidermal cells to facilitate zebrafish fin ray branching. Previous studies indicate Wnt/β-catenin signaling, a master regulator of fin regeneration, functions upstream of Shha signaling and likely ray branching (Stoick-Cooper et al., 2007; Wehner et al., 2014). Although Wnt/β-catenin signaling is described as active only in intra-ray regions, we suspected basal epidermal activity from the correlation between expression patterns of *shha* and the downstream effector *lef1* (Grotek et al., 2013; Poss et al., 2000a). We suspect our visualization of low levels of *axin2* mRNA and nuclear β-catenin protein in basal epidermal regenerating fin regions may have previously gone unnoticed as high-sensitivity RNAscope probes allow for better resolution than colorimetric *in situs*. Additionally, we found Shha:GFP domain size is sensitive to direct perturbations in Wnt/β-

catenin pathway *in vivo*. We are therefore confident that Wnt/β-catenin signaling is active in a subset of basal epidermal cells to activate Shha.

We selected *wnt10a* as the most promising putative *shha* transcriptional activator due to previously reported expression patterns (Grotek et al., 2013; Stoick-Cooper et al., 2007; Wehner et al., 2014) and confirmed expression in regenerative pObs among other regenerative lineages. The profound loss of Shha:GFP in partial caudal fins of *wnt10a*$^{-/-}$ mutants supports our hypothesis that *wnt10a* in pObs activates *shha* in the neighboring basal epidermis. However, *wnt10a*$^{-/-}$ mutants (Chapter V) typically fail to generate complete caudal fins. Thus, one caveat to our analysis is that partial caudal fins may not behave like full-sized caudal fins. Future efforts, likely involving conditional knock out or lineage-restricted overexpression of *wnt10a* in pObs during fin regeneration, would help clarify our results. A requirement for Wnt10a in ray patterning is further supported by the dramatic absence of branched rays in *wnt10a*$^{-/-}$ partial caudal fins.

Regeneration re-activates developmental patterning mechanisms, and our data demonstrate the loss of *wnt10a* destabilizes branching morphogenesis resulting in even fewer branched rays. Similarly, we show ectopic *wnt10a* during regeneration rescues Shha:GFP expression and branching in partial fin rays. Unexpectedly, our heat shock regiment over 30 days reduced the fraction of branched rays in control *wnt10a*$^{+/-}$ clutch mates with or without the *hs:wnt10a* transgene. We hypothesize the stress of heat shock may destabilize the robustness of regeneration, however, further studies would improve our understanding in this area. It is intriguing to think optimizing long-term heat shock experiments may also improve branching in

wnt10a$^{-/-}$ regenerates, as we cannot currently discriminate between genetic or environmental causes of the incomplete branched rays we observed.

Our results identify *wnt10a* as a central driver of fin-specific *shha* expression and ray branching. Our previous study found *shha* is required for ray branching in all zebrafish fins (Braunstein et al., 2021); therefore, it is likely *wnt10a* promotes *shha* in those contexts as well. However, variable penetrance of ray branching and regenerative Shha:GFP expression in *wnt10a*$^{-/-}$ partial caudal fins suggest *wnt10a* may be acting in combination with other signals. Future studies investigating the role of other Wnt/β-catenin ligands, for example *wnt16*, which has been implicated in supporting zebrafish bone repair, would likely improve our understanding of Wnt-regulated skeletal patterning in development and regeneration (McGowan et al., 2021; Watson et al., 2022). Finally, the interplay between Wnt/β-catenin signaling and other interacting signaling networks involved in skeletal patterning (e.g., *fgfs, eda, nf-κb, etc.)* offer exciting mechanisms for future exploration (Grotek et al., 2013; Harris et al., 2008; Logan and Nusse, 2004; Poss et al., 2000; Rudnicki and Williams, 2015; Sehring et al., 2022; Stewart et al., 2014).

MATERIALS & METHODS

Zebrafish

All zebrafish experimental protocols were approved by the University of Oregon Institutional Animal Care and Use Committee (IACUC). Zebrafish were reared and maintained as previously described at the University of Oregon Aquatic Animal Care Services (UO AqACS) fish facility (Braunstein et al., 2021; Stewart et al., 2014). We used wildtype AB, *Tg(-2.4shha:gfp:ABC)*^{sb15}

(Ertzer et al., 2007b), *Tg(RUNX2:mCherry)* (Barske et al., 2020), *Tg(hsp70l:dkk1b-GFP)*^{w32} (Stoick-Cooper et al., 2007), and *Tg(hsp70l:mCherry-2A-wnt10a)*^{bk409Tg} (Square et al., 2022) zebrafish lines.

Drug Treatments

Wnt-C59 (BioVision) was diluted to a 3 mM stock in DMSO and further diluted to 8, 100, or 300 nM in 1 L fish facility water as needed. Lithium Chloride (7.5 M stock, Invitrogen) was diluted to 25 mM in fish facility water. DMSO or sodium chloride control tanks were treated in parallel to Wnt-C59 or LiCl groups, respectively.

Drug treated fish were kept in 1.5 L breeding tanks with a maximum density of one fish per 200 mL water as previously described. Drug and water were changed every other day until the completion of the experiment, and fish were promptly euthanized with MS-222 (Syndel).

Alizarin Red staining

Live Alizarin Red staining was performed on intact adults by swimming fish in 0.02% Alizarin Red S (Sigma Aldrich) in fish facility water for 15 minutes, followed by three 5-minute washes in fish facility water. Fluorescent Alizarin images overlayed with DIC were acquired on a Nikon Eclipse T*i*-E inverted microscope with a Yokogawa CSU-W1 spinning disk confocal attachment.

Histology

4 dpa fin regenerates were processed as described (Armstrong et al., 2017; Braunstein et al., 2021; Stewart et al., 2014). Briefly, fins were collected, fixed overnight in 4% PFA/1xPBS, decalcified in 0.5M EDTA for 4 days with daily solution changes, dehydrated overnight, tissue cleared

embedded in paraffin and cut to 7 μm sections on a Leica RM255 Microtome. Immunostaining and RNAscope mRNA detection was performed as previously described (Stewart et al., 2021, 2014) using the following key reagents:

Primary antibodies: anti-GFP (1:3000; AVES, GFP-1020), anti-mCherry (1:50; SicGen Ab008-500)anti-β catenin (1:250; Cell Signaling, #8480).

RNAscope probes (ACDBio): *axin2*-C1, *wnt10a*-C3

Sections were imaged on a Nikon Eclipse T*i*-E inverted microscope Yokogawa CSU-W1 spinning disk confocal attachment or on a Zeiss LSM-880.

Fin morphometrics and data analysis

Fin morphometrics (i.e., fin fold size, ray length, standard length) were measured using ImageJ Fiji and data collected in Microsoft Excel. For measuring Shha:GFP domains, we confocal imaged fins and used Imaris software to reconstruct and count GFP-expressing cells in representative Dorsal Ray 3. Graphs were generated using GraphPad Prism V9.

Heat shock treatments

For short-ter larval heat shock treatment, *hsp70l:mCherry-2A-wnt10a*^{bk409Tg}*; shha:GFP*$^{+/-}$*; wnt10a*$^{-/-}$ were crossed via IVF to wildtype or *wnt10a*$^{-/-}$ mutants. Groups of $n = 25$ larvae in petri dishes were placed in a 38°C incubator for up to 24 hours (from 1-2 dpf) or for 4 hours every other day until 15 dpf. As above, at 6 dpf larvae were moved to 250 mL beakers until 28 dpf at the culmination of the experiment.

For adult heat shock treatments, adult fish were placed in a standard care tank equipped with a programmable heating element and plugged into a timer outlet. Fish were heat shocked to 38°C for 2 hours 3x daily and health checked daily. Water temperature max and min was recorded by an external probe. *Tg(hsp70l:dkk1b-GFP)*^{w32} fish were treated from 4-5 dpa. *Tg(hsp70l:mCherry-2A-wnt10a*^{bk409Tg}*)* fish were treated from 0-30 dpa.

REFERENCES

Armstrong, B.E., Henner, A., Stewart, S., Stankunas, K., 2017. Shh promotes direct interactions between epidermal cells and osteoblast progenitors to shape regenerated zebrafish bone. Development 144, 1165–1176. https://doi.org/10.1242/dev.143792

Barske, L., Fabian, P., Hirschberger, C., Jandzik, D., Square, T., Xu, P., Nelson, N., Yu, H.V., Medeiros, D.M., Gillis, J.A., Crump, J.G., 2020. Evolution of vertebrate gill covers via shifts in an ancient Pou3f3 enhancer. Proceedings of the National Academy of Sciences 117, 24876–24884. https://doi.org/10.1073/pnas.2011531117

Braunstein, J.A., Robbins, A.E., Stewart, S., Stankunas, K., 2021. Basal epidermis collective migration and local Sonic hedgehog signaling promote skeletal branching morphogenesis in zebrafish fins. Dev Biol 477, 177–190. https://doi.org/10.1016/J.YDBIO.2021.04.010

Chen, C.H., Merriman, A.F., Savage, J., Willer, J., Wahlig, T., Katsanis, N., Yin, V.P., Poss, K.D., 2015. Transient laminin beta 1a Induction Defines the Wound Epidermis during Zebrafish Fin Regeneration. PLoS Genet 11, 1–21. https://doi.org/10.1371/journal.pgen.1005437

Chiang, C., Litingtung, Y., Harris, M.P., Simandl, B.K., Li, Y., Beachy, P.A., Fallon, J.F., 2001. Manifestation of the Limb Prepattern: Limb Development in the Absence of Sonic Hedgehog Function. Dev Biol 236, 421–435. https://doi.org/10.1006/dbio.2001.0346

Clément-Lacroix, P., Ai, M., Morvan, F., Roman-Roman, S., Vayssière, B., Belleville, C., Estrera, K., Warman, M.L., Baron, R., Rawadi, G., 2005. Lrp5-independent activation of Wnt signaling by lithium chloride increases bone formation and bone mass in mice. Proc Natl Acad Sci U S A 102, 17406–17411. https://doi.org/10.1073/pnas.0505259102

Desvignes, T., Robbins, A.E., Carey, A.Z., Bailon-Zambrano, R., Nichols, J.T., Postlethwait, J.H., Stankunas, K., 2022. Coordinated patterning of zebrafish caudal fin symmetry by a central and two peripheral organizers. Developmental Dynamics 1306–1321. https://doi.org/10.1002/dvdy.475

Ertzer, R., Müller, F., Hadzhiev, Y., Rathnam, S., Fischer, N., Rastegar, S., Strähle, U., 2007. Cooperation of sonic hedgehog enhancers in midline expression. Dev Biol 301, 578–589. https://doi.org/10.1016/j.ydbio.2006.11.004

Goodrich, L. V, Johnson, R.L., Milenkovic, L., McMahon, J.A., Scott, M.P., 1996. Conservation of the hedgehog/patched signaling pathway from flies to mice: induction of a mouse patched gene by Hedgehog. Genes Dev 10, 301–312. https://doi.org/10.1101/gad.10.3.301

Grotek, B., Weidinger, G., Wehner, D., 2013. Notch signaling coordinates cellular proliferation with differentiation during zebrafish fin regeneration. Development 140, 1412–1423. https://doi.org/10.1242/dev.087452

Harris, M.P., Rohner, N., Schwarz, H., Perathoner, S., Konstantinidis, P., Nüsslein-Volhard, C., 2008. Zebrafish eda and edar mutants reveal conserved and ancestral roles of ectodysplasin signaling in vertebrates. PLoS Genet 4. https://doi.org/10.1371/journal.pgen.1000206

Kimmel, C.B., Ballard, W.W., Kimmel, S.R., Ullmann, B., Schilling, T.F., 1995. Stages of embryonic development of the zebrafish. Developmental Dynamics 203, 253–310. https://doi.org/10.1002/aja.1002030302

Klein, P.S., Meltont, D.A., 1996. A Molecular Mechanism for the Effect of Lithium on Development. PNAS 93, 8455–8459.

Laforest, L., Brown, C.W., Poleo, G., Géraudie, J., Tada, M., Ekker, M., Akimenko, M.A., 1998. Involvement of the sonic hedgehog, patched 1 and bmp2 genes in patterning of the zebrafish dermal fin rays. Development 125, 4175–4184.

Letelier, J., Naranjo, S., Sospedra-Arrufat, I., Ramon Martinez-Morales, J., Lopez-Rios, J., Shubin, N., Gomez-Skarmeta, J.L., 2021. The Shh/Gli3 gene regulatory network precedes the origin of paired fins and reveals the deep homology between distal fins and digits. Proc Natl Acad Sci U S A 118, 1–7. https://doi.org/10.1073/pnas.2100575118

Logan, C.Y., Nusse, R., 2004. The Wnt signaling pathway in development and disease. Annu Rev Cell Dev Biol 20, 781–810. https://doi.org/10.1146/annurev.cellbio.20.010403.113126

Marí-Beffa, M., Murciano, C., 2010. Dermoskeleton morphogenesis in zebrafish fins. Developmental Dynamics 239, 2779–2794. https://doi.org/10.1002/dvdy.22444

Marí-Beffa, M., Santamaría, J.A., Murciano, C., Santos-Ruiz, L., Andrades, J.A., Guerado, E., Becerra, J., 2007. Zebrafish fins as a model system for skeletal human studies. ScientificWorldJournal 7, 1114–1127. https://doi.org/10.1100/tsw.2007.190

Marigo, V., Scott, M.P., Johnson, R.L., Goodrich, L. V, Tabin, C.J., 1996. Conservation in hedgehog signaling: induction of a chicken patched homolog by Sonic hedgehog in the developing limb. Development 122, 1225–1233.

McGowan, L.M., Kague, E., Vorster, A., Newham, E., Cross, S., Hammond, C.L., 2021. Wnt16 Elicits a Protective Effect Against Fractures and Supports Bone Repair in Zebrafish. JBMR Plus 5, 1–14. https://doi.org/10.1002/jbm4.10461

Murciano, C., Ruiz, J., Maseda, D., Fernández, T.D., Durán, I., Marín-Girón, F., Becerra, J., Marí-Beffa, M., 2001. Ray and inter-ray blastemas interact to control bifurcations of Danio rerio fin rays. International Journal of Developmental Biology 45, 129–130.

Nakamura, T., Gehrke, A.R., Lemberg, J., Szymaszek, J., Shubin, N.H., 2016. Digits and fin rays share common developmental histories. Nature 537, 225. https://doi.org/10.1038/nature19322

Nechiporuk, A., Keating, M.T., 2002. A proliferation gradient between proximal and msxb - expressing distal blastema directs zebrafish fin regeneration. Development 129, 2607–2617. https://doi.org/10.1242/dev.129.11.2607

Parichy, D.M., Elizondo, M.R., Mills, M.G., Gordon, T.N., Engeszer, R.E., 2009. Normal table of postembryonic zebrafish development: staging by externally visible anatomy of the living fish. Dev Dyn 238, 2975–3015. https://doi.org/10.1002/dvdy.22113

Poss, K.D., Shen, J., Keating, M.T., 2000a. Induction of lef1 during zebrafish fin regeneration. Developmental Dynamics 219, 282–286. https://doi.org/10.1002/1097-0177(2000)9999:9999<::AID-DVDY1045>3.3.CO;2-3

Poss, K.D., Shen, J., Nechiporuk, A., McMahon, G., Thisse, B., Thisse, C., Keating, M.T., 2000b. Roles for Fgf signaling during zebrafish fin regeneration. Dev Biol 222, 347–358. https://doi.org/10.1006/dbio.2000.9722

Proffitt, K.D., Madan, B., Ke, Z., Pendharkar, V., Ding, L., Lee, M.A., Hannoush, R.N., Virshup, D.M., 2013. Pharmacological inhibition of the Wnt acyltransferase PORCN prevents growth of WNT-driven mammary cancer. Cancer Res 73, 502–507. https://doi.org/10.1158/0008-5472.CAN-12-2258

Quint, E., Smith, A., Avaron, F., Laforest, L., Miles, J., Gaffield, W., Akimenko, M.-A., 2002. Bone patterning is altered in the regenerating zebrafish caudal fin after ectopic expression of sonic hedgehog and bmp2b or exposure to cyclopamine. Proceedings of the National Academy of Sciences 99, 8713–8718. https://doi.org/10.1073/pnas.122571799

Reimer, M.M., Kuscha, V., Wyatt, C., Sörensen, I., Frank, R.E., Knüwer, M., Becker, T., Becker, C.G., 2009. Sonic hedgehog is a polarized signal for motor neuron regeneration in adult zebrafish. Journal of Neuroscience 29, 15073–15082. https://doi.org/10.1523/JNEUROSCI.4748-09.2009

Riddle, R.D., Johnson, R.L., Laufer, E., Tabin, C.J., 1993. Sonic hedgehog mediates the polarizing activity of the ZPA. Cell 75, 1401–1416.

Ross, A.W., Bonner, J., 2012. Activation of Wnt signaling using lithium chloride: Inquiry-based undergraduate laboratory exercises. Zebrafish 9, 220–225. https://doi.org/10.1089/zeb.2012.0739

Rudnicki, M.A., Williams, B.O., 2015. Wnt signaling in bone and muscle. Bone 80, 60–66. https://doi.org/10.1016/J.BONE.2015.02.009

Sehring, I., Mohammadi, H.F., Haffner-Luntzer, M., Ignatius, A., Huber-Lang, M., Weidinger, G., 2022. Zebrafish fin regeneration involvgeneric and regeneration-specifiosteoblast injury responses. Elife 11, 1–28. https://doi.org/10.7554/eLife.77614

Shibata, E., Ando, K., Murase, E., Kawakami, A., 2018. Heterogeneous fates and dynamic rearrangement of regenerative epidermis-derived cells during zebrafish fin regeneration. Development 145, dev.162016. https://doi.org/10.1242/dev.162016

Shkumatava, A., Fischer, S., Müller, F., Strahle, U., Neumann, C.J., 2004. Sonic hedgehog, secreted by amacrine cells, acts as a short-range signal to direct differentiation and lamination in the zebrafish retina. Development 131, 3849–3858. https://doi.org/10.1242/dev.01247

Shubin, N., Tabin, C., Carroll, S., 2009. Deep homology and the origins of evolutionary novelty. Nature 457, 818–823. https://doi.org/10.1038/nature07891

Shubin, N., Tabin, C., Carroll, S., 1997. Fossils, genes and the evolution of animal limbs. Nature 388, 639–648. https://doi.org/10.1038/41710

Shubin, N.H., Alberch, P., 1986. A morphogenetic approach to the origin and basic organization of the tetrapod limb. Evol Biol 319–387. https://doi.org/10.1007/978-1-4615-6983-1_6

Siebel, A.M., Vianna, M.R., Bonan, C.D., 2014. Pharmacological and Toxicological Effects of Lithium in Zebrafish. ACS Chem Neurosci 5, 468–476. https://doi.org/10.1021/cn500046h

Square, T.A., Mackey, E.J., Chen, Z.Z., Sundaram, S., Miller, C.T., 2022. Modulation of tooth regeneration through opposing responses to Wnt and BMP signals in teleosts. bioRxiv.

Stewart, S., Gomez, A.W., Armstrong, B.E., Henner, A., Stankunas, K., 2014a. Sequential and Opposing Activities of Wnt and BMP Coordinate Zebrafish Bone Regeneration. Cell Rep 6, 482–498. https://doi.org/10.1016/j.celrep.2014.01.010

Stewart, S., Gomez, A.W., Armstrong, B.E., Henner, A., Stankunas, K., 2014b. Sequential and Opposing Activities of Wnt and BMP Coordinate Zebrafish Bone Regeneration. Cell Rep 6, 482–498. https://doi.org/10.1016/j.celrep.2014.01.010

Stewart, S., Yette, G.A., Le Bleu, H.K., Henner, A.L., Braunstein, J.A., Chehab, J.W., Harms, M.J., Stankunas, K., 2019. Skeletal geometry and niche transitions restore organ size and shape during zebrafish fin regeneration. bioRxiv. https://doi.org/https://doi.org/10.1101/606970

Stoick-Cooper, C.L., Weidinger, G., Riehle, K.J., Hubbert, C., Major, M.B., Fausto, N., Moon, R.T., 2007a. Distinct Wnt signaling pathways have opposing roles in appendage regeneration. Development 134, 479–489. https://doi.org/10.1242/dev.001123

Takayama, K., Muto, A., Kikuchi, Y., 2018. Leucine/glutamine and v-Atpase/lysosomal acidification via mTORC1 activation are required for position-dependent regeneration. Sci Rep 8, 1–13. https://doi.org/10.1038/s41598-018-26664-2

Tickle, C., 2017. An historical perspective on the pioneering experiments of John Saunders. Dev Biol 429, 374–381. https://doi.org/10.1016/j.ydbio.2017.05.028

Walker, M.B., Kimmel, C.B., 2007. A two-color acid-free cartilage and bone stain for zebrafish larvae. Biotechnic and Histochemistry 82, 23–28. https://doi.org/10.1080/10520290701333558

Watson, C.J., Joyce Tang, W., Rojas, M.F., Fiedler, I.A.K., de Oca, E.M.M., Cronrath, A.R., Callies, L.K., Swearer, A.A., Ahmed, A.R., Sethuraman, V., Addish, S., Farr, G.H., Gómez, A.E., Rai, J., Monstad-Rios, A.T., Gardiner, E.M., Karasik, D., Maves, L., Busse, B., Hsu, Y.H., Kwon, R.Y., 2022. Wnt16 Regulates Spine and Muscle Morphogenesis Through Parallel Signals From Notochord and Dermomyotome. PLoS Genet 18, 1–30. https://doi.org/10.1371/journal.pgen.1010496

Wehner, D., Cizelsky, W., Vasudevaro, M.D., Özhan, G., Haase, C., Kagermeier-Schenk, B., Röder, A., Dorsky, R.I., Moro, E., Argenton, F., Kühl, M., Weidinger, G., 2014. Wnt/β-Catenin Signaling Defines Organizing Centers that Orchestrate Growth and Differentiation of the Regenerating Zebrafish Caudal Fin. Cell Rep 6, 467–481. https://doi.org/10.1016/j.celrep.2013.12.036

Wullimann, M.F., Umeasalugo, K.E., 2020. Sonic hedgehog expression in zebrafish forebrain identifies the teleostean pallidal signaling center and shows preglomerular complex and posterior tubercular dopamine cells to arise from shh cells. Journal of Comparative Neurology 528, 1321–1348. https://doi.org/10.1002/cne.24825

Xia, M.Y., Zhao, X.Y., Huang, Q.L., Sun, H.Y., Sun, C., Yuan, J., He, C., Sun, Y., Huang, X., Kong, W., Kong, W.J., 2017. Activation of Wnt/β-catenin signaling by lithium chloride attenuates d-galactose-induced neurodegeneration in the auditory cortex of a rat model of aging. FEBS Open Bio 7, 759–776. https://doi.org/10.1002/2211-5463.12220

Zhang, J., Jeradi, S., Strähle, U., Akimenko, M.-A., 2012. Laser ablation of the sonic hedgehog-a-expressing cells during fin regeneration affects ray branching morphogenesis. Dev Biol 365, 424–433. https://doi.org/10.1016/j.ydbio.2012.03.008

Zhong, H., Zou, H., Semenov, M. V., Moshinsky, D., He, X., Huang, H., Li, S., Quan, J., Yang, Z., Lin, S., 2009. Characterization and development of novel small-molecules inhibiting GSK3 and activating Wnt signaling. Mol Biosyst 5, 1356–1360. https://doi.org/10.1039/b905752h

FIGURES

Figures 6.1 – 6.5

Figures S6.1 – S 6.2

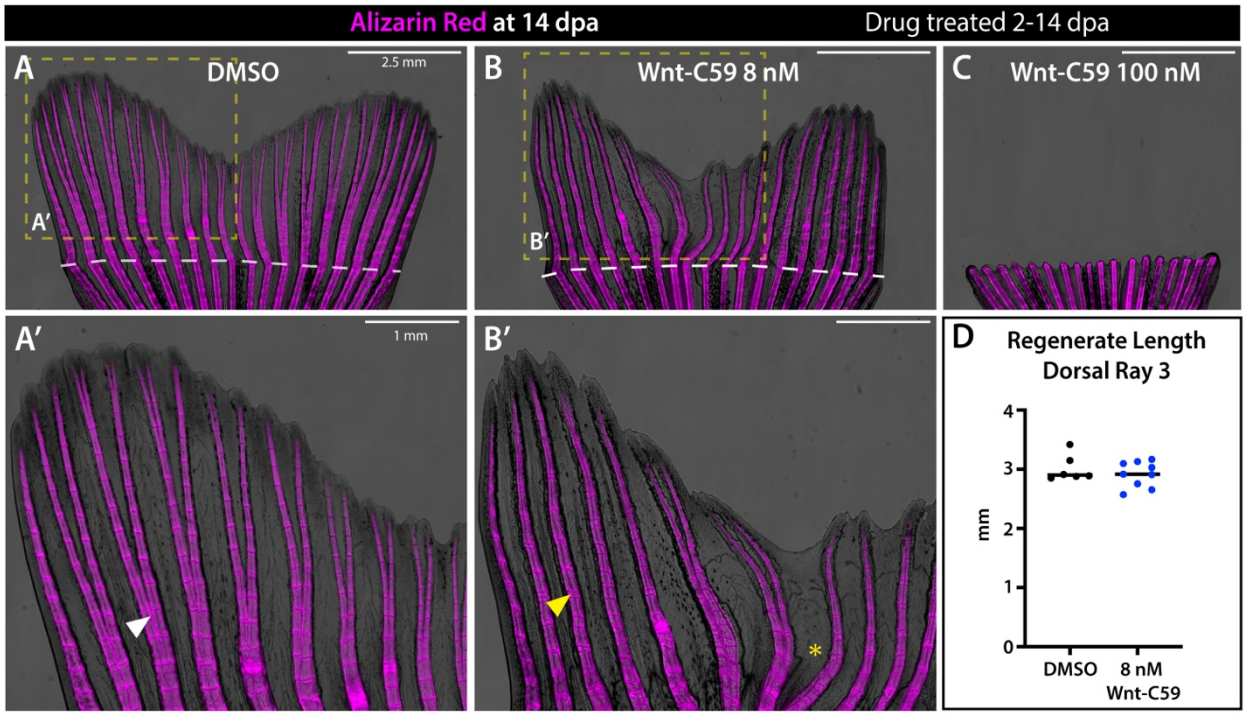

Figure 6.1. Low levels of Wnt inhibition disrupt skeletal pattern but not regenerative outgrowth.

Wildtype fins were amputated and treated with (A, A') DMSO control (n = 6), (B, B') 8 nM Wnt-C59 (n = 9), or (C) 100 nM Wnt-C59 (n = 6) from 2-14 dpa and stained with Alizarin Red. White dashed lines indicate plane of amputation. Yellow dashed boxes denote zoom regions in (A', B'). (A') White arrowhead denotes a branch point on representative Dorsal Ray 3. (B') Yellow arrowhead denotes an absent branch point on Dorsal Ray 3. Yellow asterisk indicates abnormal curvature of a medial ray. (D) Regenerated length of Dorsal Ray 3 is not significantly different between DMSO and 8 nM Wnt-C59.

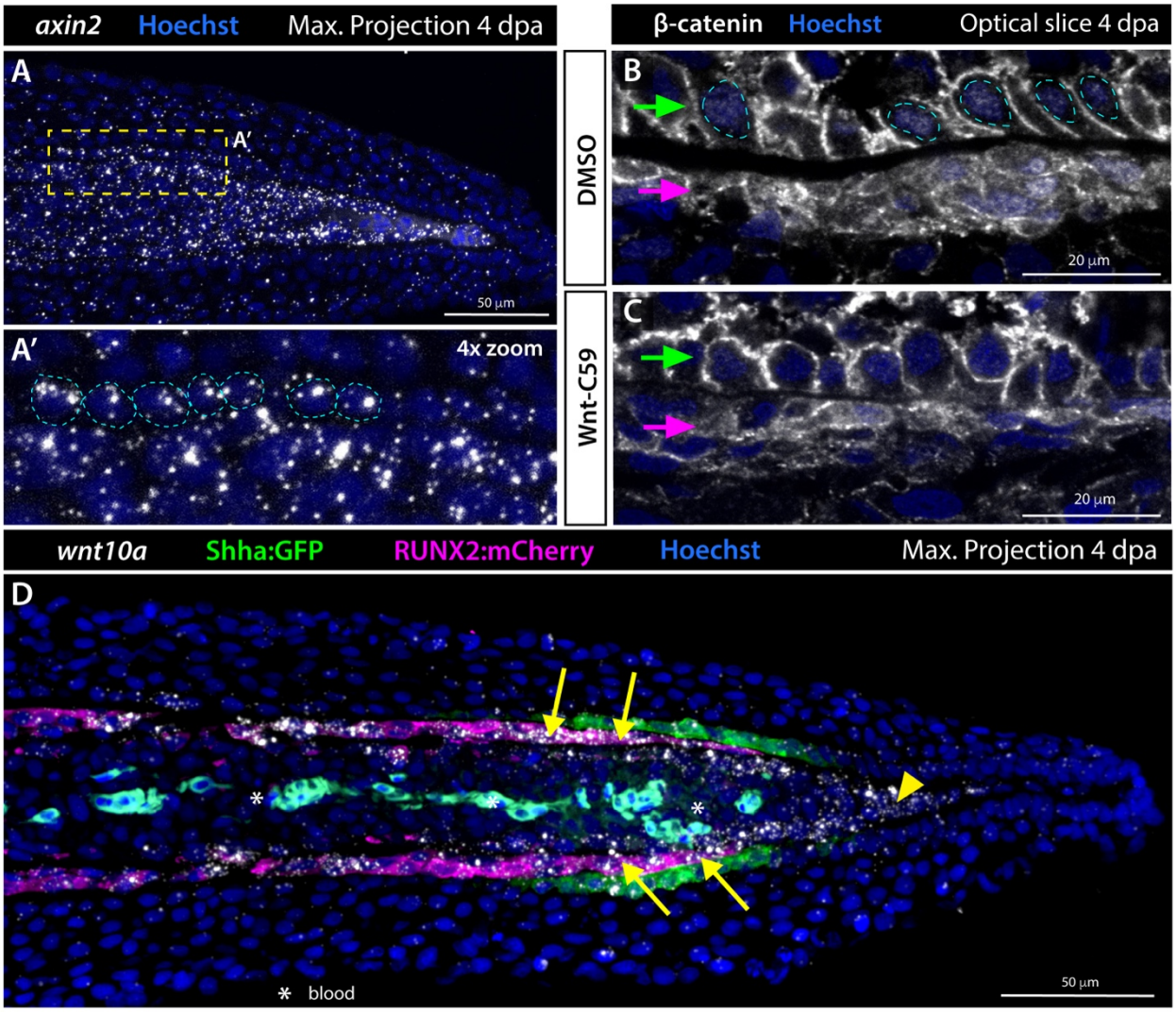

Figure 6.2. Histological expression of Wnt/β-catenin signaling in regenerating rays.

(A) RNAscope mRNA for *axin2* (white) in a 4 dpa longitudinal section (n = 3). Nuclei are stained with Hoechst (blue). Yellow dashed box indicates zoom region in (A'). Cyan dashed circles denote basal epidermal cells containing *axin2* mRNA puncta. (B, C) Longitudinal sections showing one hemi-ray with basal epidermal layer indicated by green arrows and pre-osteoblast regions indicated by magenta arrows. β-catenin antibody stain is in white. Nuclei are stained with Hoechst (blue). 4 dpa fish were treated with a (B) DMSO control or (C) 300 nM Wnt-C59 4 hours prior to tissue harvest (n = 3 per group). (B) Cyan dashed circles indicate nuclear β-catenin in basal epidermal cells which is absent (C) upon Wnt-C59 treatment. (D) 4 dpa longitudinal section of a *shha:GFP; RUNX2:mCherry* double transgenic regenerating fin (n = 5). Antibody staining for GFP (green) and mCherry (magenta) show Shha and RUNX2 expression, respectively. RNAscope for *wnt10a* is in white. Yellow arrows indicate mRNA puncta located in mCherry+ pre-osteoblasts. Yellow arrowhead indicates *wnt10a* expression in the far distal mesenchyme. Hoechst-stained nuclei are in blue.

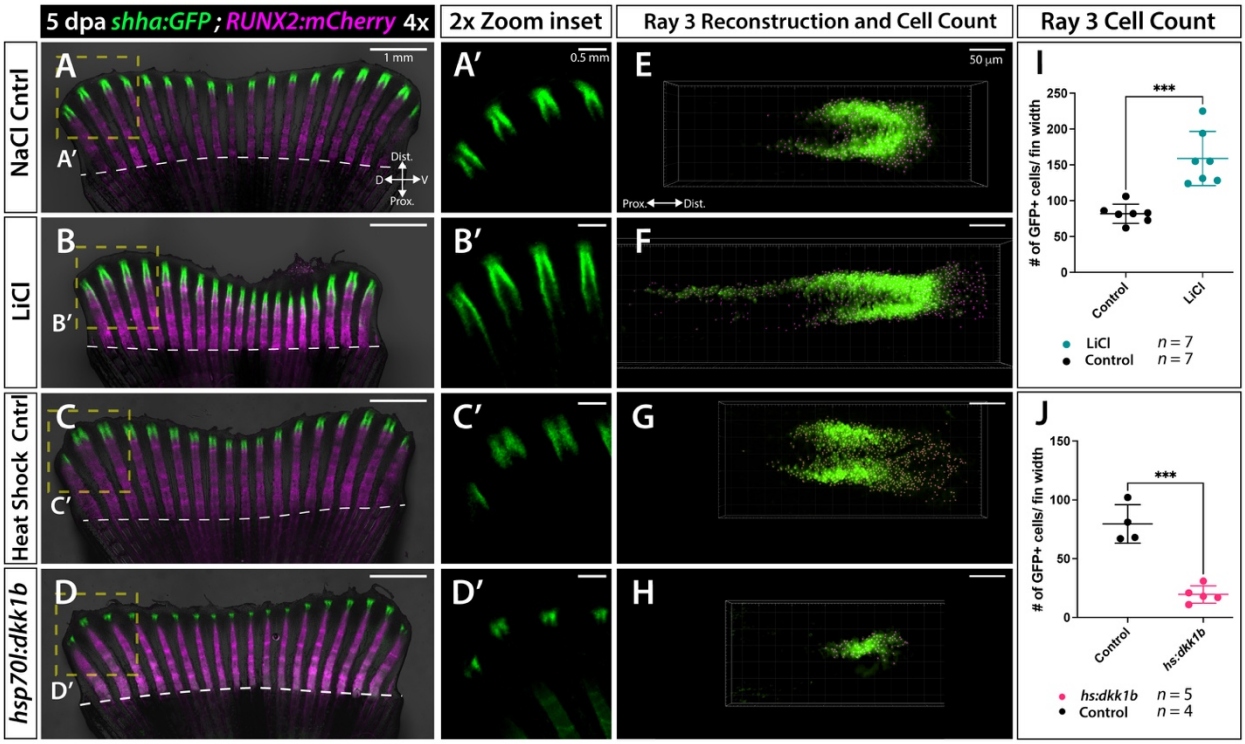

Figure 6.3. Shha domains are responsive to Wnt/β-catenin gain and loss-of-function.

(A-D) 5 dpa *in vivo* fin regenerates. *shha:GFP; RUNX2:mCherry* fish were amputated and treated from 4-5 dpa with (A) sodium chloride control 25 mM (n = 7) or (B) lithium chloride 25 mM (n = 7). Separately, *shha:GFP; RUNX2:mCherry* fish were amputated and heat shocked from 4-5 dpa (C) without (n = 4) and (D) with the *hsp70l:dkk1b-GFP* transgene (n = 5). (A'-D') Zoom regions of the yellow dashed boxes in (A-D)/ (E-H) 3D reconstruction of Shha:GFP domains in representative Dorsal Ray 3 with cells marked by magenta spheres. (I) Quantification Ray 3 Shh+ cells for NaCl and LiCl groups. (J) Quantification Ray 3 Shh+ cells for heat shock groups.

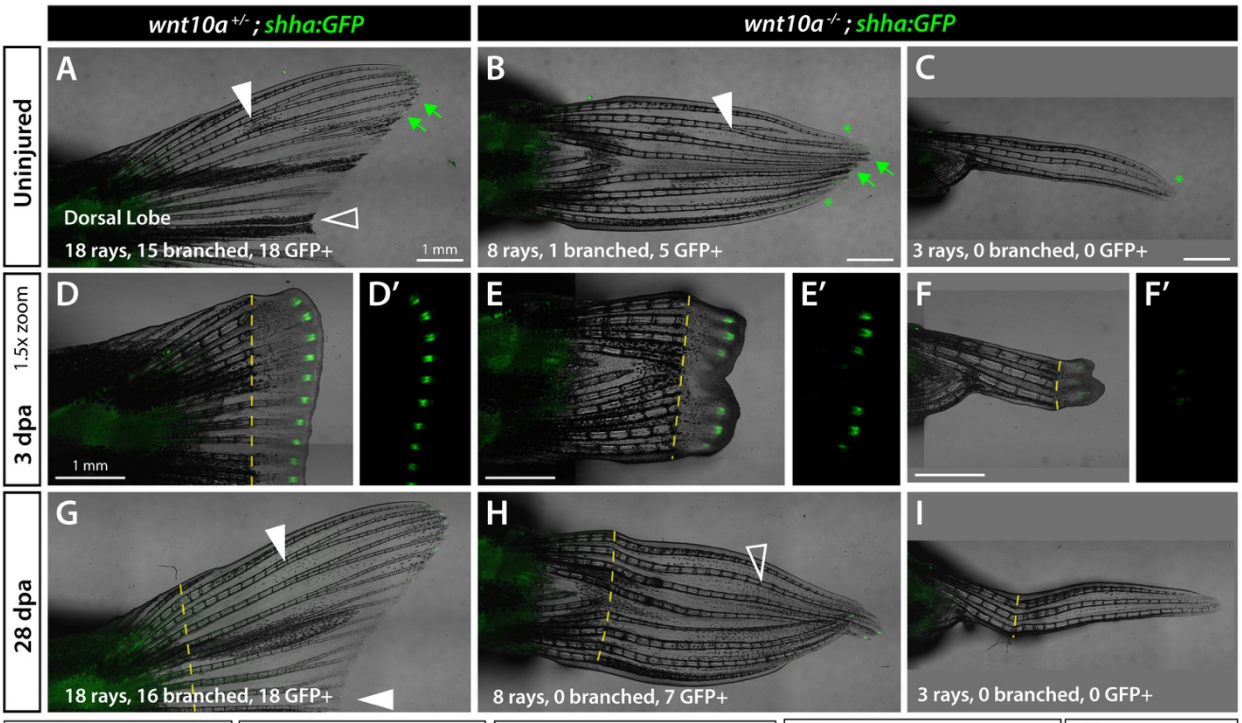

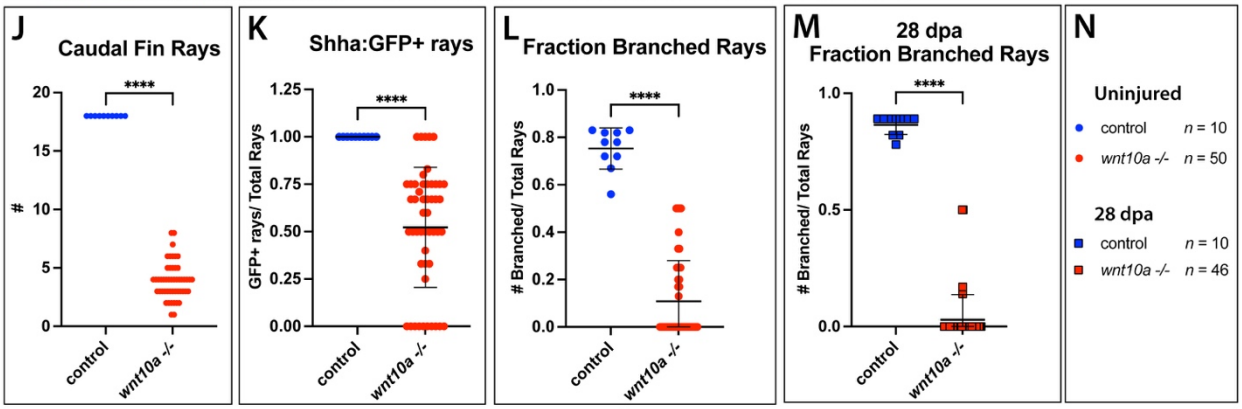

O Uninjured

Genotype	# of fish	# of rays	# branched rays	% branched rays
wnt10a +/-	10	178	134	75%
wnt10a -/-	50	195	22	11%

P 28 dpa

Genotype	# of fish	# of rays	# branched rays	% branched rays
wnt10a +/-	10	178	154	87%
wnt10a -/-	46	162	5	3%

Figure 6.4. Shh expression and ray branching of *wnt10a*$^{-/-}$ partial caudal fins.

Figure 6.4. Shh expression and ray branching of *wnt10a*$^{-/-}$ partial caudal fins.

(A-C) Uninjured caudal fins of young adult (2 mpf) *shha:GFP* clutch mates. (A) Dorsal lobe of the caudal fin of a representative *wnt10a*$^{+/-}$ control (n = 10). Green arrows indicate small GFP domains at the distal end of each ray. White arrowhead indicates a typical branch point. Open arrowhead indicates an unbranched medial ray. (B, C) *wnt10a*$^{-/-}$ siblings with variable caudal fin skeletal patterning. Green asterisks mark rays without GFP domains. (D-F) The same representative fish in (A-C) imaged at 3 dpa. (D) Shha:GFP domains are robustly expressed in control fins but (E) variably or (F) not expressed in *wnt10a*$^{-/-}$ mutants. (D'-F') Single channel GFP of the caudal fin regenerate regions. (G-I) Fully regenerated caudal fins at 28 dpa. Quantification of uninjured (J) caudal fin ray number, (K) number of rays expressing Shha:GFP, and (L) fraction of branched rays per animal. (M) Fraction of branched rays per animal at 28 dpa. (N) Legends for (J-M). (O) Data on clutch sample size, number of rays counted, and fraction of branched rays in uninjured and (P) 28 dpa.

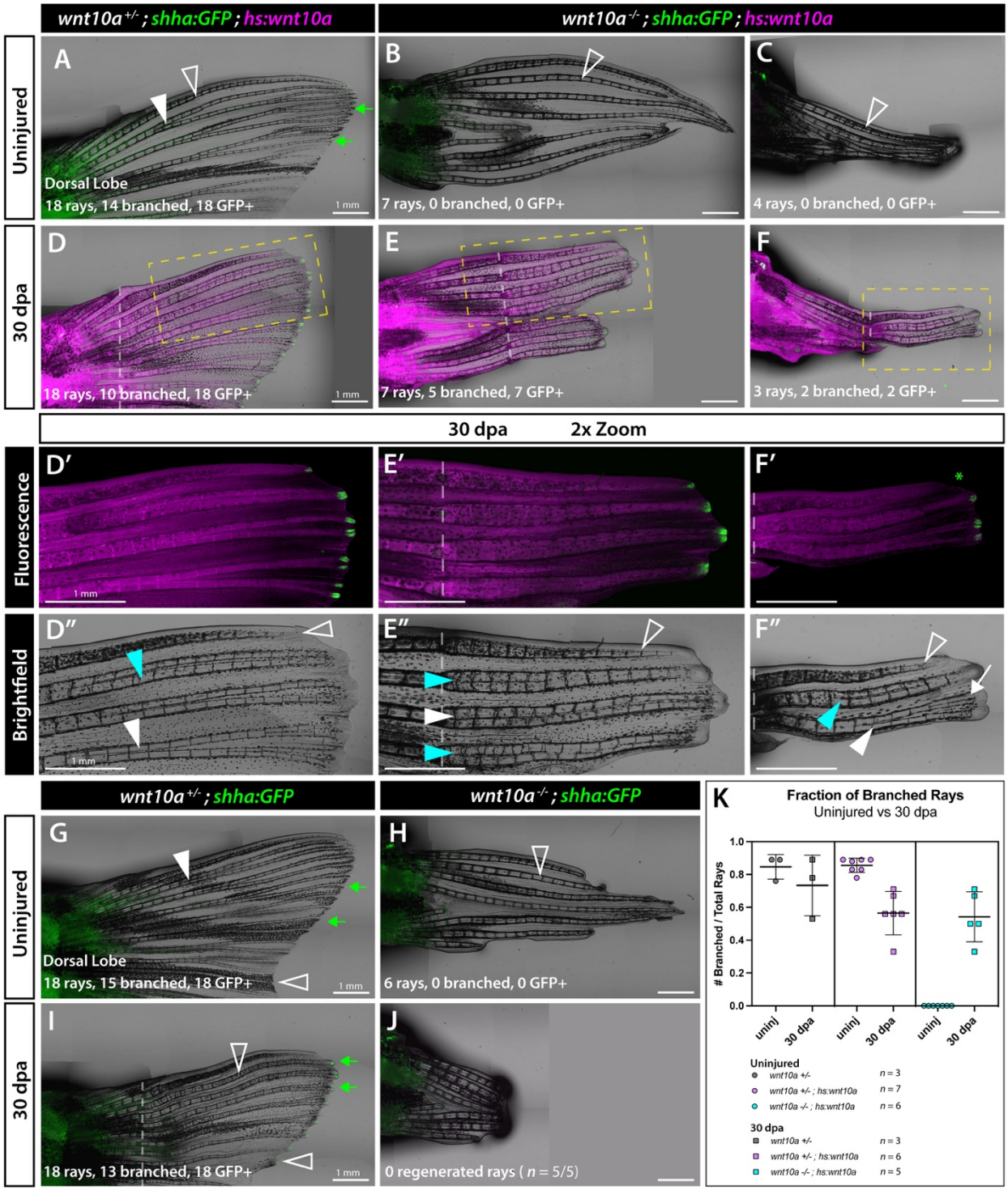

Figure 6.5. Ubiquitous *wnt10a* restores *shha* expression and branching in regenerating *wnt10a*$^{-/-}$ partial caudal fins.

Figure 6.5. Ubiquitous *wnt10a* restores *shha* expression and branching in regenerating *wnt10a*$^{-/-}$ partial caudal fins.

Representative live images from a single clutch of adult fish subjected to 30 days of heat shock following caudal fin amputation. (A) Dorsal lobe of a control *wnt10a*$^{+/-}$*; shha:GFP; hs:wnt10a* uninjured caudal fin. White arrowhead denotes typical ray branching. Green arrows indicate small GFP+ domains on the distal end of each ray. (B, C) Uninjured *wnt10a*$^{-/-}$*; shha:GFP; hs:wnt10a* partoal caudal fins. Open arrow heads indicate a lack of ray branching. (D-F) The same fish in (A-C) imaged at 30 dpa. White dashed lines indicate site of amputation. Yellow dashed boxes indicate 2x zoom regions in (D'-F"). (D'-F') 2-channel fluorescent zooms. All regenerates express mCherry and all rays have distal GFP domains expect one ray in (F') indicated by a green asterisk. (D"-F") Brightfield zoom regions of (D'-F'). (D") Control regenerates form some typical branch points (white arrowheads) but also sporadically unbranched rays or branched rays that do not separate as expected (cyan arrowhead). (E") Representative *wnt10a*$^{-/-}$*; shha:GFP; hs:wnt10a* regenerate with a combination of full branchpoints (white arrowhead) and abnormal ray branching (cyan arrowheads). (F") Representative *wnt10a*$^{-/-}$*; shha:GFP; hs:wnt10a* regenerate exhibiting 3 regenerated rays out of 4 in the uninjured state, where the dorsal ray does not branch (open arrowhead), middle ray branches but re-fuses (cyan arrowhead), and the ventral ray exhibits both primary (white arrowhead) and premature secondary branchpoints (white arrow). (G) Dorsal lobe of a control *wnt10a*$^{+/-}$*; shha:GFP* and (H) *wnt10a*$^{-/-}$*; shha:GFP* caudal fins. (I) 30 dpa regenerate of the control caudal fin in (G) with branching defects marked by open arrowheads. (J) *wnt10a*$^{-/-}$*; shha:GFP* caudal fin in (H) at 30 dpa. No rays regenerated. (K) Quanitifcation of fraction branched rays in uninjured and 30 dpa caudal fins. The *wnt10a*$^{-/-}$*; shha:GFP* group is excluded because n = 5/5 fins did not regenerate any rays.

Table 6.1. Uninjured data from Figure 6.5

Genotype	# of fish	# of rays	# branched rays	% branched rays	# of Shh+ rays	% Shh+ rays
wnt10a +/-; shha:GFP	3	53	45	85%	53	100%
wnt10a +/- ; shha:GFP ; hs:wnt10a	7	125	107	86%	125	100%
wnt10a -/- ; shha:GFP	6	33	0	0%	0	0%
wnt10a -/- ; shha:GFP ; hs:wnt10a	7	31	0	0%	0	0%

Table 6.2. 30 dpa from Figure 6.5

Genotype	# of fish	# of regenerated rays	# branched rays	% branched rays	# of Shh+ rays	% Shh+ rays
wnt10a +/-; shha:GFP	3	53	39	74%	53	100%
wnt10a +/- ; shha:GFP ; hs:wnt10a	6	107	60	56%	125	100%
wnt10a -/- ; shha:GFP	5	0	0	0%	0	0%
wnt10a -/- ; shha:GFP ; hs:wnt10a	5	19	11	58%	15	79%

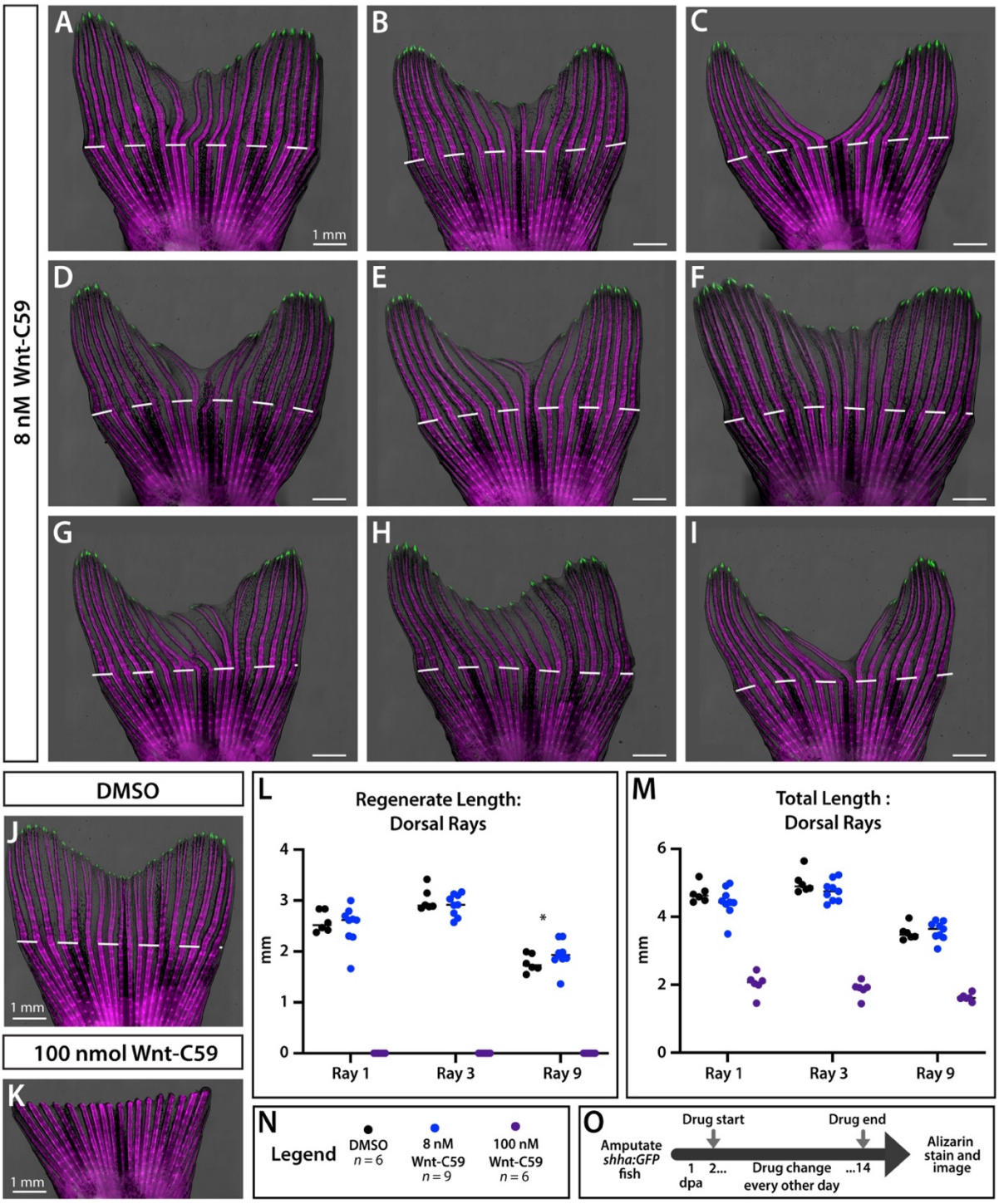

Figure S6.1: Expanded data from Figure 1.

Expanded data from experiment in Figure 1 showing 14 dpa Alizarin Red stain with *shha:GFP* transgenic background. (A-I) All fish treated with 8 nM Wnt-C59. (J) Representative DMSO-treated control and (K) 100 nM Wnt-C59 treated fish. (L) Quantification of regenerate length and (M) total ray length for representative Dorsal Rays 1, 3, and 9. (N) Legend for (L, M). (O) Experimental schematic.

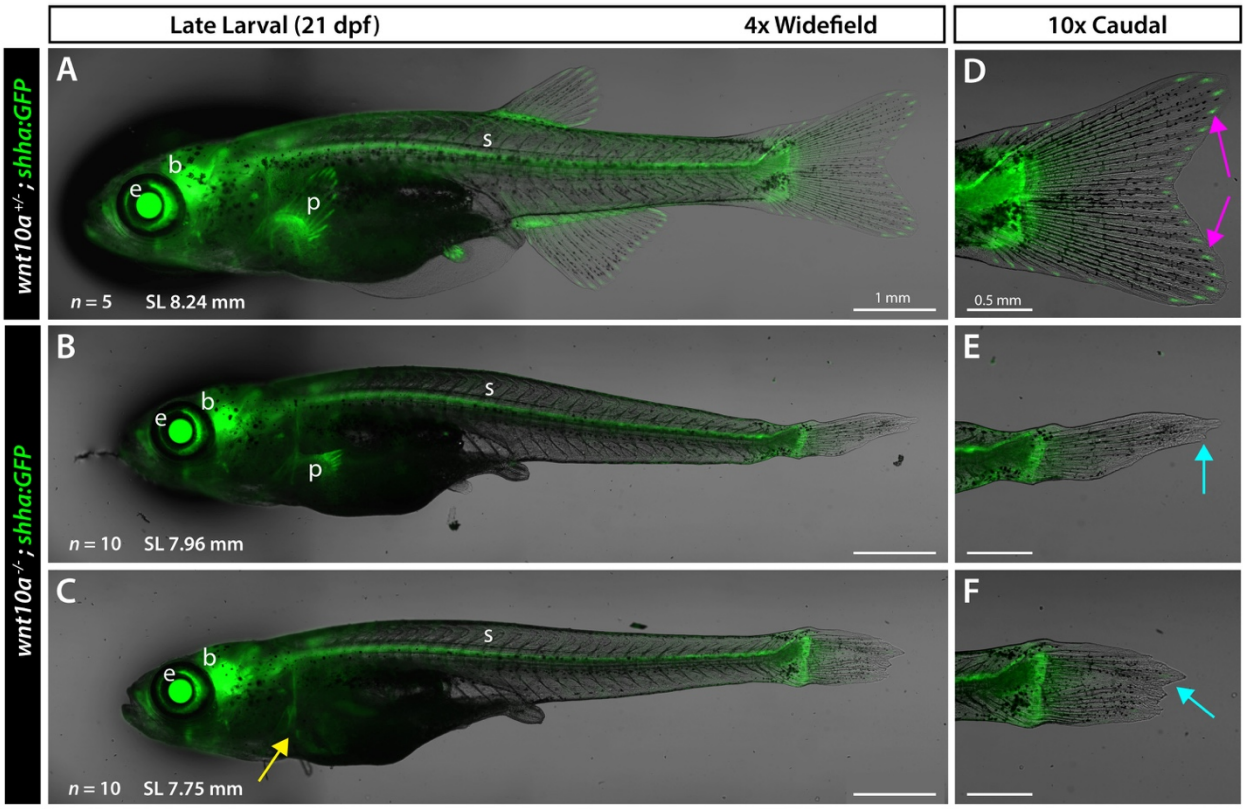

Figure S6.2. Developmental *shha* expression in *wnt10a*$^{-/-}$ mutants.

Whole mount live imaging of 21 dpf (A) *wnt10a*$^{+/-}$*; shha:GFP* control (*n* = 5) and (B, C) *wnt10a*$^{-/-}$*; shha:GFP* mutant clutch mates (*n* = 10). The *shha:GFP* transgene is expressed in the eye (e), brain (b), and spine (s) in all controls and mutants. Pectoral fins (p) showed GFP expression in (A) all controls and (B) 7/10 *wnt10a* mutants but not in (C) 3/10 *wnt10a* mutants. (D-F) 10x zoom on the caudal fin. (D) *shha:GFP* expression in control developing fin rays (magenta arrows). (E-F) Cyan arrows indicate a lack of *shha:GFP* in the partial caudal fins of *wnt10a* mutants.

CHAPTER VII: CONCLUDING REMARKS

INTRODUCTION

The zebrafish fin skeleton is a powerful model to uncover molecular mechanisms coordinating appendage development and regeneration relevant to human disease, hopefully informing the rational development of new therapeutics (Reviewed in Marí-Beffa et al., 2007). This dissertation primarily investigates how the key conserved signaling pathways Sonic hedgehog (Shh) and Wingless/Integrated (Wnt) interact in the environment of a growing fin ray, while also segueing into related areas of zebrafish caudal fin biology relevant to skeletal patterning. We first confirmed Shh-mediated ray branching is shared between development and regeneration and generated new insights into the cell behaviors between Shh-expressing basal epidermis and pre-osteoblasts (pObs) using novel live imaging techniques (Chapter II). We next extensively detailed the emergence of caudal fin ray ontogeny (Chapter III). Returning to components of growing fin rays, we considered how the extracellular environment separating Shha-expressing basal epidermal cells from the intra-ray regions contributes to fin morphogenesis. This resulted in the development and characterization of an adult zebrafish model for Fraser Syndrome, which has defective basement membrane adhesion causing diverse epithelial-mesenchymal tissue junction defects including a spectrum of fin ray patterning abnormities (Chapter IV). We then refocused our investigations on Shha by seeking to identify an upstream transcriptional activator. This identified *wnt10a* as a promising candidate, and *wnt10a* mutants generated by CRISPR/Cas9 exhibit extreme fin loss or reduction despite otherwise being healthy and viable. This enabled us to detail the spatiotemporal requirement of *wnt10a* during median fin emergence

and caudal fin regeneration (Chapter V). Finally, we provide evidence that *wnt10a* contributes to fin-specific shha expression and promotes regeneration in the caudal fin (Chapter VI).

REVISITING THE SONIC HEDGEHOG PATHWAY: NOT JUST A MORPHOGEN

We found Shha acts at short-range between basal epidermal cells and neighboring pre-osteoblasts (pObs) to restrain basal epidermal collective cell migration and ultimately position pObs into branch points (Chapter II) (Armstrong et al., 2017; Braunstein et al., 2021). This model differs fundamentally from Shh's frequently cited role as a long-range secreted morphogen in limb buds (Chiang et al., 2001; Marigo et al., 1996; Riddle et al., 1993). However, short range and even juxtacrine signaling has been identified in other contexts. Hedgehog famously mediates interactions between directly adjacent cells through wingless as a segment polarity gene during Drosophila embryogenesis (Ingham 1993). Additionally, during mammalian development Epithelial Shh expression shapes directly underlying dermal mesenchyme facilitating hair follicle development (Millar, 2002; Sato et al., 1999; Woo et al., 2012). Shh is retained on lengthy cytoplasmic projections (cytonemes) to activate signal transduction in receiving cells during avian limb patterning (Sanders et al., 2013). Similar examples are also found in zebrafish specifically as wildtype cells transplanted into the retina of shha mutant embryos only rescues Müller glia differentiation in neighboring cells (Shkumatava et al., 2004), consistent with exclusive short range signaling. Finally, during scale morphogenesis, shha+ epidermal cells mediate folding in adjacent Hh-responsive cells by collective cell migration to provide a 'pocket' for ossified tissue during scale extension (Aman et al., 2018). These studies and ours collectively highlight the versatility of Shh signaling mechanisms, acting at short or long ranges as needed to promote morphogenesis.

FIN RAY ONTOGENY INFORMS MOLECULAR COORDINATION AND EVOLUTIONARY SPECIFICATION

Fish fins are an established research model, capturing the interest of developmental biologists for hundreds of years (Broussonet, 1786; Morgan, 1900; Nabrit, 1929). Detailed insights into the anatomy and patterning of the ray-finned actinopterygian fishes, including zebrafish, have mostly used fossil records and 'ancient' fishes to map phylogenetic and morphological changes through evolution (Arratia, 2000; Betancur et al., 2017; Desvignes et al., 2018; Schultze and Arratia, 1986; Wright et al., 2012; Written and Hall, 2016). The evolutionary origin of the fin skeleton—and how changes to this skeleton facilitated the fin-to-limb transition— remain a particularly intriguing area of study in the field (Cass et al., 2021; Coates, 1994; Nakamura et al., 2016a; Oster et al., 1988; Shubin et al., 1997; Zhang et al., 2010). In Chapter III, I collaborated with interdisciplinary fish scientists to identify molecular coordination of fin ray ontogeny. We described a new subtype of principal caudal fin rays that are distinct in their spatiotemporal emergence, musculoskeletal connections, and patterning. Our work proposed a central fin ray organizer in the hypural diastema gap between hypurals 2 and 3 pattern the central principal rays, while two peripheral organizers pattern the peripheral principal rays (Desvignes et al., 2022). Excitedly, this suggests future experiments through ablation of the proposed organizer regions. Further, the ancestral and homocercal caudal fin is uniquely bi-lobed, whereas more derived paired fins have one ray field. It would be interesting to learn if the caudal fin's peripheral organizers were lost, or if a central and peripheral organizer were lost to create one ray field. As the paired fins represent the evolutionary progenitor to limbs (Ahn and Ho, 2008; Grandel and Schulte-Merker, 1998), such studies likely have broader implications for understanding the molecular dynamics of the fin-to-limb transition.

SKIN AND THE EXTRACELLULAR ENVIRONMENT IN FIN AND LIMB SKELETAL MORPHOGENESIS

Initial studies of fin ray branching have shown the fin ray epidermis, particularly the basal epidermis, is a major signaling center during outgrowth which directs skeletal patterning (Armstrong et al., 2017; Braunstein et al., 2021; Poss et al., 2000). This phenomenon is not unique to fin rays or fish. During limb development, polarized adhesion of the stratified epidermis and directed apoptosis specify digits (Hines et al., 2016; Kashgari et al., 2020). In the zebrafish craniofacial skeleton, maintenance of epithelial-mesenchymal junctions including by the basement-membrane localized Fraser Complex robustly pattern the lower jaw (Kimmel et al., 2021; Talbot et al., 2016, 2012). However, the variable expressivity of fras1 fin ray defects compounded by the multi-systemic and often lethal effects of Fraser Syndrome indicate that the Fraser complex (or basement membrane-mediated adhesion more broadly) does not act alone in creating a permissive environment for fin ray morphogenesis (Chapter IV). Our findings are further supported by studies demonstrating the loss of the structurally supportive actinotrichia result in fras1mutant-like unbranched rays (König et al., 2018; Nakagawa et al., 2022). We surmise that not a single factor, but rather a complex extracellular environment including the Fraser Complex promotes skeletal patterning. Functional redundancy and environmental modulation may further improve the robustness of fin ray, and limb, pattering. Ongoing research in the lab investigates the function of other extracellular components in dictating proper osteoblast coordination, including how these components interact with major signaling networks indisputably essential for fin regeneration (Stewart et al., 2014a; Stewart and Stankunas, 2012; Stoick-Cooper et al., 2007a; Wehner et al., 2014). Expanding our knowledge of how the

extracellular environment supports skeletal patterning will provide a more nuanced understanding of skeletal robustness.

WNT10A, SHH, AND HOW TO BUILD A FIN

We hypothesized *wnt10a* expressed in pre-osteoblasts activate *shha* in adjacent basal epidermal cells to regulate branching morphogenesis upstream. While we did associate *wnt10a* expression with shha expression in fin rays and branching (Chapter VI), we also uncovered a fundamental and earlier role for *wnt10a* in patterning of the median fins (Chapter V). The wnt10ab1423-4 mutants are the most severe fin loss mutants documented as they lose both endochondral and dermal fin elements. This differs from the zebrafish *finless* (*fls*) and medaka *allfinless* (*afls*) *ectodysplasin* and receptor (*eda/edar*) mutants, which lack all fins but retain fin endochondral elements (Harris et al., 2008; Iida et al., 2014). Our finding that *wnt10a* promotes median fin fold development from 1-2 dpf which is required for median fin development is a leap forward in understanding the spatiotemporal initiation of fin development. It is curious that the median fins were more severely impacted than the paired fins in *wnt10a* mutants. This result suggests alternative signals – perhaps additional Wnts, or even other regulatory modules that evolved after the median fins – direct paired fin development. Given the *eda/edar* mutants lack all fins, we hypothesize *wnt10a* may interact with *eda* and *shha* to robustly develop and pattern fins. This hypothesis is supported by documented interactions between Eda, Wnt, and Shh in other contexts. For example, Shh/Wnt/Eda signaling interplay pattern zebrafish scale and tooth development (Adaimy et al., 2007; Aman et al., 2018; Dassule et al., 2000; Square et al., 2022; Yuan et al., 2017), and Shh/Wnt/Eda coordinate the development of Merkel cells, sweat glands, and salivary gland branching morphogenesis in mice (Cui et al., 2014; Häärä et al., 2011; Jaskoll

et al., 2004; Xiao et al., 2016). Of relevance, diseases states such as weakened bone, reduced wound healing, ectodermal dysplasia, tooth agenesis, and cancers have also been associated with these pathways (Adaimy et al., 2007; Doolan et al., 2021; Hanna and Shevde, 2016; Tsukamoto et al., 2019; Wang et al., 2018; Xu et al., 2017). Taken together, our findings that *wnt10a* promotes median fin development, regeneration, and *shha*-mediated fin ray branching open the way to explore more exciting questions centered around a *wnt10a-shha* skeletal patterning module.

REFERENCES

Adaimy, L., Chouery, E., Mégarbané, H., Mroueh, S., Delague, V., Nicolas, E., Belguith, H., De Mazancourt, P., Mégarbané, A., 2007. Mutation in WNT10A is associated with an autosomal recessive ectodermal dysplasia: The odonto-onycho-dermal dysplasia. Am J Hum Genet 81, 821–828. https://doi.org/10.1086/520064

Ahn, D., Ho, R.K., 2008. Tri-phasic expression of posterior Hox genes during development of pectoral fins in zebrafish: Implications for the evolution of vertebrate paired appendages. Dev Biol 322, 220–233. https://doi.org/10.1016/j.ydbio.2008.06.032

Aman, A.J., Fulbright, A.N., Parichy, D.M., 2018. Wnt/β-catenin regulates an ancient signaling network during zebrafish scale development. Elife 7, e37001. https://doi.org/10.7554/elife.37001

Armstrong, B.E., Henner, A., Stewart, S., Stankunas, K., 2017. Shh promotes direct interactions between epidermal cells and osteoblast progenitors to shape regenerated zebrafish bone. Development 144, 1165–1176. https://doi.org/10.1242/dev.143792

Arratia, G., 2000. Phylogenetic Relationships of Teleostei. Past and Present Relaciones Filogenéticas De Teleostei: Pasado Y Presente. Estud. Oceanol 19–51.

Betancur, R.R., Wiley, E.O., Arratia, G., Acero, A., Bailly, N., Miya, M., Lecointre, G., Ortí, G., 2017. Phylogenetic classification of bony fishes. BMC Evol Biol 17, 1–40. https://doi.org/10.1186/s12862-017-0958-3

Braunstein, J.A., Robbins, A.E., Stewart, S., Stankunas, K., 2021. Basal epidermis collective migration and local Sonic hedgehog signaling promote skeletal branching morphogenesis in zebrafish fins. Dev Biol 477, 177–190. https://doi.org/10.1016/J.YDBIO.2021.04.010

Broussonet, M., 1786. Observations sur la régénération de quelques parties du corps des poissons. Histoire de lAcadémie Royale des Sciences 684–688.

Cass, A.N., Elias, A., Fudala, M.L., Knick, B.D., Davis, M.C., 2021. Conserved mechanisms, novel anatomies: The developmental basis of fin evolution and the origin of limbs. Diversity (Basel) 13, 1–17. https://doi.org/10.3390/d13080384

Chiang, C., Litingtung, Y., Harris, M.P., Simandl, B.K., Li, Y., Beachy, P.A., Fallon, J.F., 2001. Manifestation of the Limb Prepattern: Limb Development in the Absence of Sonic Hedgehog Function. Dev Biol 236, 421–435. https://doi.org/10.1006/dbio.2001.0346

Coates, M.I., 1994. The origin of vertebrate limbs. Development 120, 169–180. https://doi.org/10.1242/dev.1994.supplement.169

Cui, C.Y., Yin, M., Sima, J., Childress, V., Michel, M., Piao, Y., Schlessinger, D., 2014. Involvement of Wnt, Eda and Shh at defined stages of sweat gland development. Development (Cambridge) 141, 3752–3760. https://doi.org/10.1242/dev.109231

Dassule, H.R., Lewis, P., Bei, M., Maas, R., McMahon, A.P., 2000. Sonic hedgehog regulates growth and morphogenesis of the tooth. Development 127, 4775–4785.

Desvignes, T., Carey, A., Braasch, I., Enright, T., Postlethwait, J.H., 2018. Skeletal development in the heterocercal caudal fin of spotted gar (lepisosteus oculatus) and other lepisosteiformes. Developmental Dynamics 247, 724–740. https://doi.org/10.1002/dvdy.24617

Desvignes, T., Robbins, A.E., Carey, A.Z., Bailon-Zambrano, R., Nichols, J.T., Postlethwait, J.H., Stankunas, K., 2022. Coordinated patterning of zebrafish caudal fin symmetry by a central and two peripheral organizers. Developmental Dynamics 1306–1321. https://doi.org/10.1002/dvdy.475

Doolan, B.J., Onoufriadis, A., Kantaputra, P., McGrath, J.A., 2021. WNT10A, dermatology and dentistry. British Journal of Dermatology 185, 1105–1111. https://doi.org/10.1111/bjd.20601

Grandel, H., Schulte-Merker, S., 1998. The development of the paired fins in the zebrafish (Danio rerio). Mech Dev 79, 99–120. https://doi.org/10.1016/S0925-4773(98)00176-2

Häärä, O., Fujimori, S., Schmidt-Ullrich, R., Hartmann, C., Thesleff, I., Mikkola, M.L., 2011. Ectodysplasin and Wnt pathways are required for salivary gland branching morphogenesis. Development 138, 2681–2691. https://doi.org/10.1242/dev.057711

Hanna, A., Shevde, L.A., 2016. Hedgehog signaling: modulation of cancer properies and tumor mircroenvironment. Mol Cancer 15, 24. https://doi.org/10.1186/s12943-016-0509-3

Harris, M.P., Rohner, N., Schwarz, H., Perathoner, S., Konstantinidis, P., Nüsslein-Volhard, C., 2008. Zebrafish eda and edar mutants reveal conserved and ancestral roles of ectodysplasin signaling in vertebrates. PLoS Genet 4. https://doi.org/10.1371/journal.pgen.1000206

Hines, E.A., Verheyden, J.M., Lashua, A.J., Larson, S.C., Branchfield, K., Domyan, E.T., Gao, J., Harvey, J.F., Herriges, J.C., Hu, L., Mcculley, D.J., Throckmorton, K., Yokoyama, S., Ikeda, A., Xu, G., Sun, X., 2016. Syndactyly in a novel Fras1rdf mutant results from interruption of signals for interdigital apoptosis. Developmental Dynamics 245, 497–507. https://doi.org/10.1002/dvdy.24389

Iida, Y., Hibiya, K., Inohaya, K., Kudo, A., 2014. Eda/Edar signaling guides fin ray formation with preceding osteoblast differentiation, as revealed by analyses of the medaka all-fin less mutant afl. Developmental Dynamics 243, 765–777. https://doi.org/10.1002/dvdy.24120

Jaskoll, T., Leo, T., Witcher, D., Ormestad, M., Astorga, J., Bringas, P., Carlsson, P., Melnick, M., 2004. Sonic hedgehog signaling plays an essential role during embryonic salivary gland epithelial branching morphogenesis. Developmental Dynamics 229, 722–732. https://doi.org/10.1002/dvdy.10472

Kashgari, G., Meinecke, L., Gordon, W., Ruiz, B., Yang, J., Ma, A.L., Xie, Y., Ho, H., Plikus, M. V., Nie, Q., Jester, J. V., Andersen, B., 2020. Epithelial Migration and Non-adhesive Periderm Are Required for Digit Separation during Mammalian Development. Dev Cell 52, 764-778.e4. https://doi.org/10.1016/j.devcel.2020.01.032

Kimmel, C.B., Wind, A.L., Oliva, W., Ahlquist, S.D., Walker, C., Dowd, J., Blanco-Sánchez, B., Titus, T.A., Batzel, P., Talbot, J.C., Postlethwait, J.H., Nichols, J.T., 2021. Transgene-mediated skeletal phenotypic variation in zebrafish. J Fish Biol 98, 956–970. https://doi.org/10.1111/jfb.14300

König, D., Page, L., Chassot, B., Jaźwińska, A., 2018. Dynamics of actinotrichia regeneration in the adult zebrafish fin. Dev Biol 433, 416–432. https://doi.org/10.1016/j.ydbio.2017.07.024

Marí-Beffa, M., Santamaría, J.A., Murciano, C., Santos-Ruiz, L., Andrades, J.A., Guerado, E., Becerra, J., 2007. Zebrafish fins as a model system for skeletal human studies. ScientificWorldJournal 7, 1114–1127. https://doi.org/10.1100/tsw.2007.190

Marigo, V., Scott, M.P., Johnson, R.L., Goodrich, L. V, Tabin, C.J., 1996. Conservation in hedgehog signaling: induction of a chicken patched homolog by Sonic hedgehog in the developing limb. Development 122, 1225–1233.

Millar, S.E., 2002. Molecular Mechanisms Regulating Hair Follicle Development. Journal of Investigative Dermatology 118, 216–225. https://doi.org/10.1046/j.0022-202x.2001.01670.x

Morgan, T.H., 1900. Regeneration in teleosts. Arch Entwicklmech Org.

Nabrit, S.M., 1929. The role of the fin rays in the regeneration in the tail-fins of fishes. Biological Bulletin LVI.

Nakagawa, H., Kuroda, J., Aramaki, T., Kondo, S., 2022. Mechanical role of actinotrichia in shaping the caudal fin of zebrafish. Dev Biol 481, 52–63. https://doi.org/10.1016/j.ydbio.2021.09.003

Nakamura, T., Gehrke, A.R., Lemberg, J., Szymaszek, J., Shubin, N.H., 2016. Digits and fin rays share common developmental histories. Nature 537, 225–228. https://doi.org/10.1038/nature19322

Oster, G.F., Shubin, N., Murray, J.D., Alberch, P., 1988. EVOLUTION AND MORPHOGENETIC RULES: THE SHAPE OF THE VERTEBRATE LIMB IN ONTOGENY AND PHYLOGENY. Evolution (N Y) 42, 862–884. https://doi.org/10.1111/j.1558-5646.1988.tb02508.x

Poss, K.D., Shen, J., Keating, M.T., 2000. Induction of lef1 during zebrafish fin regeneration. Developmental Dynamics 219, 282–286. https://doi.org/10.1002/1097-0177(2000)9999:9999<::AID-DVDY1045>3.3.CO;2-3

Riddle, R.D., Johnson, R.L., Laufer, E., Tabin, C.J., 1993. Sonic hedgehog mediates the polarizing activity of the ZPA. Cell 75, 1401–1416.

Sanders, T.A., Llagostera, E., Barna, M., 2013. Specialized filopodia direct long-range transport of SHH during vertebrate tissue patterning. Nature 497, 628. https://doi.org/10.1038/nature12157

Sato, N., Leopold, P.L., Crystal, R.G., 1999. Induction of the hair growth phase in postnatal mice by localized transient expression of Sonic hedgehog. Journal of Clinical Investigation 104, 855–864. https://doi.org/10.1172/jci7691

Schultze, H.-P., Arratia, G., 1986. Reevaluation of the caudal skeleton of actinopterygian fishes: I. Lepisosteus and Amia. J Morphol 190, 215–241. https://doi.org/10.1002/jmor.1051900206

Shkumatava, A., Fischer, S., Müller, F., Strahle, U., Neumann, C.J., 2004. Sonic hedgehog, secreted by amacrine cells, acts as a short-range signal to direct differentiation and lamination in the zebrafish retina. Development 131, 3849–3858. https://doi.org/10.1242/dev.01247

Shubin, N., Tabin, C., Carroll, S., 1997. Fossils, genes and the evolution of animal limbs. Nature 388, 639–648. https://doi.org/10.1038/41710

Square, T.A., Mackey, E.J., Chen, Z.Z., Sundaram, S., Miller, C.T., 2022. Modulation of tooth regeneration through opposing responses to Wnt and BMP signals in teleosts. bioRxiv.

Stewart, S., Gomez, A.W., Armstrong, B.E., Henner, A., Stankunas, K., 2014. Sequential and Opposing Activities of Wnt and BMP Coordinate Zebrafish Bone Regeneration. Cell Rep 6, 482–498. https://doi.org/10.1016/j.celrep.2014.01.010

Stewart, S., Stankunas, K., 2012. Limited dedifferentiation provides replacement tissue during zebrafish fin regeneration. Dev Biol 365, 339–349. https://doi.org/10.1016/j.ydbio.2012.02.031

Stoick-Cooper, C.L., Weidinger, G., Riehle, K.J., Hubbert, C., Major, M.B., Fausto, N., Moon, R.T., 2007. Distinct Wnt signaling pathways have opposing roles in appendage regeneration. Development 134, 479–489. https://doi.org/10.1242/dev.001123

Talbot, J.C., Nichols, J.T., Yan, Y.L., Leonard, I.F., BreMiller, R.A., Amacher, S.L., Postlethwait, J.H., Kimmel, C.B., 2016. Pharyngeal morphogenesis requires fras1-itga8-dependent epithelial-mesenchymal interaction. Dev Biol 416, 136–148. https://doi.org/10.1016/j.ydbio.2016.05.035

Talbot, J.C., Walker, M.B., Carney, T.J., Huycke, T.R., Yan, Y.L., BreMiller, R.A., Gai, L., Delaurier, A., Postlethwait, J.H., Hammerschmidt, M., Kimmel, C.B., 2012. Fras1 Shapes Endodermal Pouch 1 and Stabilizes Zebrafish Pharyngeal Skeletal Development. Development 139, 2804–2813. https://doi.org/10.1242/dev.074906

Tsukamoto, M., Wang, K.Y., Tasaki, T., Murata, Y., Okada, Y., Yamanaka, Y., Nakamura, E., Yamada, S., Izumi, H., Zhou, Q., Azuma, K., Sasaguri, Y., Kohno, K., Sakai, A., 2019. Findings as a starting point to unravel the underlying mechanisms of in vivo interactions involving Wnt10a in bone, fat and muscle. Bone 120, 75–84. https://doi.org/10.1016/J.BONE.2018.10.009

Wang, K.Y., Yamada, S., Izumi, H., Tsukamoto, M., Nakashima, T., Tasaki, T., Guo, X., Uramoto, H., Sasaguri, Y., Kohno, K., 2018. Critical in vivo roles of WNT10A in wound healing by regulating collagen expression/ synthesis in WNT10A-deficient mice. PLoS One 13, 1–18. https://doi.org/10.1371/journal.pone.0195156

Wehner, D., Cizelsky, W., Vasudevaro, M.D., Özhan, G., Haase, C., Kagermeier-Schenk, B., Röder, A., Dorsky, R.I., Moro, E., Argenton, F., Kühl, M., Weidinger, G., 2014. Wnt/β-Catenin Signaling Defines Organizing Centers that Orchestrate Growth and Differentiation of the Regenerating Zebrafish Caudal Fin. Cell Rep 6, 467–481. https://doi.org/10.1016/j.celrep.2013.12.036

Woo, W.-M., Zhen, H.H., Oro, A.E., 2012. Shh maintains dermal papilla identity and hair morphogenesis via a Noggin–Shh regulatory loop. Genes Dev 26, 1235–1246. https://doi.org/10.1101/gad.187401.112

Wright, J.J., David, S.R., Near, T.J., 2012. Gene trees, species trees, and morphology converge on a similar phylogeny of living gars (Actinopterygii: Holostei: Lepisosteidae), an ancient

clade of ray-finned fishes. Mol Phylogenet Evol 63, 848–856. https://doi.org/10.1016/j.ympev.2012.02.033

Written, P.E., Hall, B.K., 2016. Teleost Skeletal Plasticity: Modulation, Adaptation, and Remodelling. Copeia 103, 727–739. https://doi.org/10.1643/CG-14-140

Xiao, Y., Thoresen, D.T., Miao, L., Williams, J.S., Wang, C., Atit, R.P., Wong, S.Y., Brownell, I., 2016. A Cascade of Wnt, Eda, and Shh Signaling Is Essential for Touch Dome Merkel Cell Development. PLoS Genet 12, 1–19. https://doi.org/10.1371/journal.pgen.1006150

Xu, M., Horrell, J., Snitow, M., Cui, J., Gochnauer, H., Syrett, C.M., Kallish, S., Seykora, J.T., Liu, Fei, Gaillard, D., Katz, J.P., Kaestner, K.H., Levin, B., Mansfield, C., Douglas, J.E., Cowart, B.J., Tordoff, M., Liu, Fang, Zhu, X., Barlow, L.A., Rubin, A.I., McGrath, J.A., Morrisey, E.E., Chu, E.Y., Millar, S.E., 2017. WNT10A mutation causes ectodermal dysplasia by impairing progenitor cell proliferation and KLF4-mediated differentiation. Nat Commun 8. https://doi.org/10.1038/ncomms15397

Yuan, Q., Zhao, M., Tandon, B., Maili, L., Liu, X., Zhang, A., Baugh, E.H., Tran, T., Silva, R.M., Hecht, J.T., Swindell, E.C., Wagner, D.S., Letra, A., 2017. Role of WNT10A in failure of tooth development in humans and zebrafish. Mol Genet Genomic Med 5, 730–741. https://doi.org/10.1002/mgg3.332

Zhang, J., Wagh, P., Guay, D., Sanchez-Pulido, L., Padhi, B.K., Korzh, V., Andrade-Navarro, M.A., Akimenko, M.A., 2010. Loss of fish actinotrichia proteins and the fin-to-limb transition. Nature 466, 234–237. https://doi.org/10.1038/nature09137